The erodibility of fine sediment deposits in lowland chalk streams

Grabowski, Robert Carl

The erodibility of fine sediment deposits in lowland chalk streams

Robert Carl Grabowski

A thesis presented for the degree of

Doctor of Philosophy

in Geography

Queen Mary, University of London

2010

I hereby declare that the work presented in this thesis is my own and has not been submitted elsewhere for any award.

…….

Robert C. Grabowski

Abstract

Lowland chalk streams in the UK are experiencing increased deposition of fine sediment due to changes in land-use practices, channel modifications, and groundwater abstraction. The fine sediment is linked to benthic habitat degradation, the obstruction of surface-groundwater flow, and the storage of contaminants, such as nutrients and pesticides. Whilst research has been conducted on the provenance, transport, deposition, and storage of fine sediment in chalk streams, none has expressly investigated erosion. To help fill this gap in knowledge, a yearlong field survey was conducted in two reaches of the Frome-Piddle Catchment (Dorset) to quantify the erodibility of surficial fine sediment deposits. Sediment erodibility was measured in the field using a cohesive strength meter (CSM) and a shear vane. These measurements were paired with sediment cores for analysis of the physical, chemical and biological properties of the sediment. The large environmental dataset was analysed using a comprehensive suite of modern analytical techniques, including regression trees, linear regression, and mixed effects modelling. The results indicate that the erodibility of fine sediment varies significantly over time and within a stream reach due to variations in hydraulic conditions and sediment properties. Effective particle size and chlorophyll-a content were identified as the major sediment properties influencing CSM-derived erodibility, whereas root density was key for shear vane-derived strength. To date, the erosion thresholds generated by CSMs have been largely restricted to relative uses, and a calibration based on cohesive sediment is needed to permit their future incorporation into sediment transport models. This study developed an empirical calibration using laboratory experiments that estimated critical shear stress from CSM-derived erosion thresholds. By quantifying the erodibility of fine sediment deposits in chalk streams, and representing the erosion thresholds as critical shear stress, we can better gauge their local environmental impacts and help to inform models of fine sediment transport.

For Olivier, Sue and Dennis

Acknowledgements

First and foremost, I would like to thank my supervisors for their guidance over the past three years. Geraldene Wharton has been a model supervisor. She was always willing to bounce ideas back and forth, review endless drafts, and gently nudge me back on track when I became distracted by interesting side projects. I greatly appreciate the time Prof. Roger Wotton spent with me discussing chalk streams, field survey design and the wonders of EPS. I am also grateful to Ian Droppo for his advice and support. He offered the use of his CSM unit for the duration of the project, and supplied laboratory space, material, and expert technicians for the 2 months of calibration trials in Canada.

Practically, the project would never have been completed without the help of several individuals. Fieldwork would have been impossible without Grieg Davies. We were twinned together on the Frome and Piddle, and neither one of us will forget the days spent knee & elbow deep in freezing water to collect sediment samples. Laura Shotbolt was invaluable in the development of laboratory procedures, and Simon Dobinson made it all possible by chasing up suppliers and deliveries for me. Plus, they made the Physical Geography Labs a welcoming and friendly place to work. Ed Oliver made my figures look good, and never complained when asked to tweak them 2 or 3 times. Lindsay Smith and Niall Lehane assisted with fieldwork in the middle of winter, and Chris Jaskot, Brian Trapp, and Katrina Bernal spent days assisting with laboratory flume experiments at the National Water Research Institute, Environment Canada.

Several members of staff in the Department of Geography deserve special mention for their advice during the PhD. Kate Spencer, Kate Heppell, Prof. Jaap van der Meer, and Lisa Belyea were all willing to sit down with me for hours to chat about various aspects

of my project, from theoretical discussions of cohesive sediment erodibility to the practicalities of survey design and statistical analysis.

Finally, thanks to all of the Geography postgrads, but particularly my officemates in Room 224. What would a PhD be like without tea breaks, second breakfasts, cheeky pints, and more tea breaks?

Table of Contents

List of Tables

List of Figures

Chapter 1: Introduction

Historically, chalk streams in the UK were characterised by crystal clear waters and clean gravel beds. These systems supported diverse aquatic communities and productive salmonid fisheries (Berrie 1992, Bickerton et al. 1993). Many chalk streams, though, are experiencing increased deposition of fine sediment onto and into their gravel beds, which is attributed to changes in land-use practices, channel modifications, and groundwater abstraction (Walling & Amos 1999, Wood & Armitage 1999). A shift in focus from grazing to tilled agriculture has increased run-off and left soils more vulnerable to erosion, whilst urbanisation has extended the coverage of impervious surfaces increasing run-off and contaminant input into surface waters (Sear et al. 1999, Environment Agency 2004, Collins & Walling 2007b). The augmentation of fine particle loads from allochthonous sources is exacerbated by diminished baseflows in streams, caused by an intensification of groundwater abstraction to meet increasing demands for potable water. Consequently, as lowland chalk streams are carrying greater quantities of fine particles, they have reduced capacities to transport them, and fine sediment is accumulating on channel beds.

Chalk streams are particularly prone to fine sediment deposition due to their distinctive hydrology (Berrie 1992, Griffiths et al. 2006). The streams flow over permeable chalk, and are predominantly groundwater fed. Whilst discharges increase in the winter due to seasonal recharge of the chalk aquifer, chalk streams display less variability in discharge than other streams in the UK. Discharges are not strongly impacted by storm-runoff, so they are less flashy than streams on less permeable geology. The relatively constant discharges combined with a high width:depth ratio means that stream power is generally low. Consequently, chalk streams are less able to transport fine sediment or erode it once it deposits on the channel bed.

Fine sediment deposition is linked to negative impacts on chalk stream ecology, hydrology, and anthropogenic use. The ingress of fine sediments and the formation of surficial sediment deposits reduce the permeability and porosity of riverbeds, choking salmonid nesting grounds (Acornley & Sear 1999), obstructing surface-ground water exchange (Boulton et al. 1998, Packman & Salehin 2003), altering interstitial communities and affecting nutrient processing in the hyporheic (Hancock 2002, Pretty et al. 2006). Contaminants (e.g. heavy metals, pesticides, nutrients and pathogenic bacteria) preferentially bind to suspended particles, and settle along with the particles to create concentrated stores that can pose a long-term threat to local and downstream habitats (Droppo et al. 2001, Bowes et al. 2005, Luoma & Rainbow 2008, Heppell et al. 2009)

In response to concerns about the ecological impacts, the UK government identified chalk streams as a priority habitat for conservation, outlining a Biological Action Plan to improve their ecological status (Environment Agency 2004). Further emphasis has been placed on stream health by the European Water Framework Directive, which requires member states to maintain and improve surface waters to "good status" by 2015, as defined by ecological, chemical and hydrological measures (European Parliament 2000).

Whilst numerous studies have been conducted in recent years on the provenance, transport, deposition and storage of fine sediment within these systems, to date no study has expressly investigated the erosion of fine sediment deposits. Therefore, a key step is missing in our understanding of fine sediment dynamics in chalk streams. In particular, we do not know how resistant the sediment is to erosion (i.e. erodibility), so we are unable to assess the stability of the fine sediment deposits. By identifying spatial and temporal patterns in erodibility, and understanding the factors that influence those variations, we will be better able to predict fine sediment dynamics and assess its impact on humans and the environment.

Chapter 2: Literature Review

This chapter reviews the current literature on the erosion of fine sediment in aquatic environments. The review begins with a definition of fine sediment and a general description of its inorganic and organic components (Section 2.1). A short summary of fine sediment transport dynamics in rivers follows, with special attention paid to research from chalk stream environments (Section 2.2). The next section introduces erodibility, discusses its importance to the dynamics of sediment transport, and presents a comprehensive review of the sediment properties that dictate erodibility (Section 2.3). Finally, the specific research questions of the study are outlined (Section 2.4). Significant portions of the literature review were submitted as part of a review paper to *Earth Science Reviews*. The manuscript, entitled "Cohesive sediment erodibility: the importance of sediment properties," is now being revised for resubmission (Grabowski et al. *In Revision*).

2.1 What is fine sediment?

The term 'fine sediment' is used in this thesis to describe sediments composed of small-sized particles (< 2 mm). It is used instead of the terms 'fine-grained' and 'cohesive' because it is a more general classification and more appropriate for this study. Fine-grained refers to sediment, or the fraction of the sediment, composed of particles less than 63 μm in diameter, whereas cohesive defines a mechanical property of the sediment (for more information, see Section 2.3.1). The focus of this study is the fraction of sediment finer than gravel-sized (2 mm), because this is the size that will influence the hydrology and ecology of gravel-bed chalk streams due to colmation and the formation of surficial deposits (e.g. Wood & Armitage 1997, Walling & Amos

1999, Heppell et al. 2009). So, in this thesis, fine sediment refers to mixtures of clay, silt and sands, in any proportion, which can be either granular or cohesive.

The fine sediment found in rivers is a heterogeneous, particulate, and porous material, composed of solid, liquid and gas phases (Fig. 2.1) (Hillel 1982, Winterwerp & Van Kesteren 2004). The solid phase consists of granular inorganic and organic material. The liquid phase is predominately water, which can occupy a significant proportion of the sediment. The quantity of water can often exceed that of the solids, particularly at the surface of unconsolidated sediment (e.g. Bale et al. 2007). Gases may be found in fine riverine sediment but are not as ubiquitous as in soils or estuarine sediment exposed to air at low tides. They form primarily as a result of the breakdown of organic matter within the sediment (e.g. methane) (Gebert et al. 2006, Sanders et al. 2007).

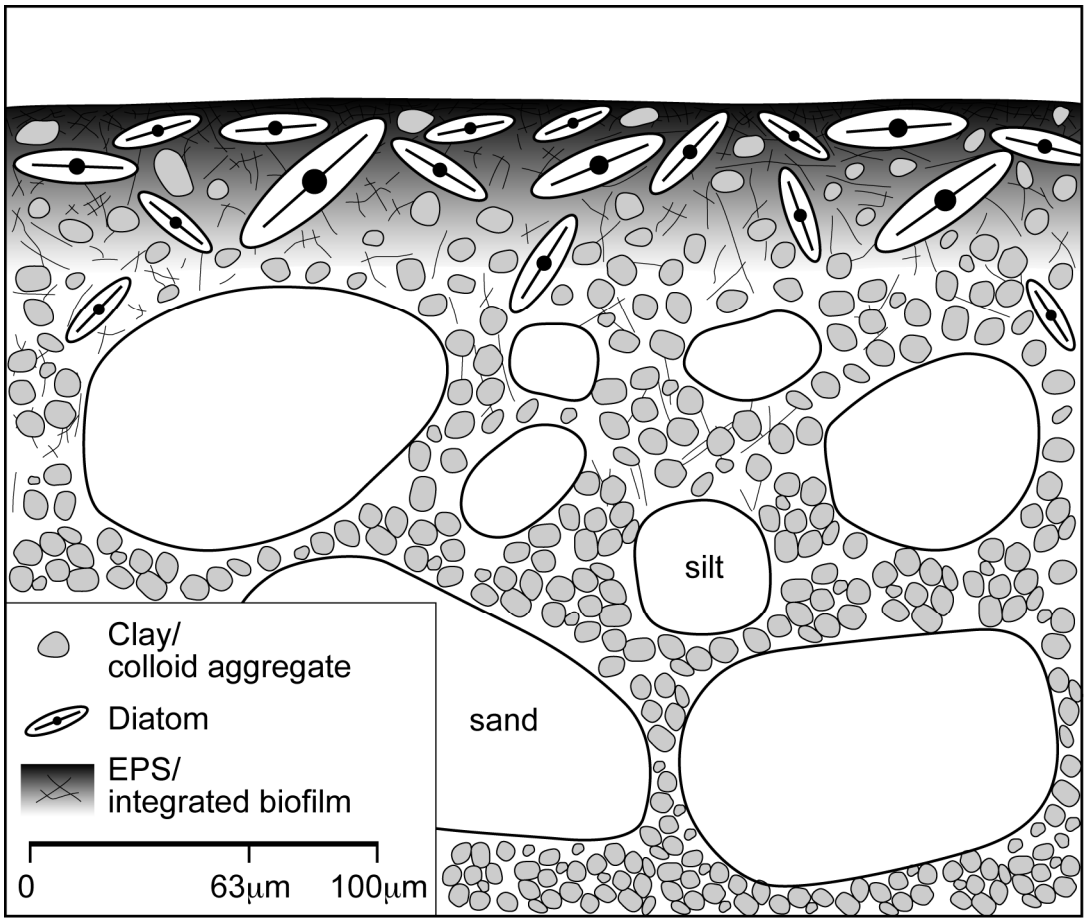

Figure 2.1. Diagrammatic representation of the microstructure of fine sediment, showing the matrices created by the abiotic and biotic components. Note: integrated biofilms are found primarily at the sediment surface, but the extracellular polymeric substances (EPS) that they are composed of can be found deeper in the sediment (After Gillott 1987).

The solid phase of fine sediment consists of primary and secondary mineral particles and a diversity of organic material. The inorganic fraction of the sediment is composed of mineral particles derived from chemical and physical weathering of bedrock, and includes clays, silts and sands (Hillel 1982, Leeder 1999, Brady & Weil 2001, Winterwerp & Van Kesteren 2004). Clay minerals are formed by the chemical weathering of primary minerals. They are typically less than 2 μm in diameter (Wentworth Scale), and are the most electro-chemically active portion of the sediment. They are largely responsible for the sticky, cohesive nature of mud (for more information see Section 2.3.1). Particles smaller than 0.1 μm represent the colloidal fraction of the clay minerals, and do not readily settle out of suspensions due to Brownian motion. Silt is an intermediate-sized inorganic particle, ranging from 2 μm to 63 μm. They are generated by the physical weathering of primary minerals, so are most commonly composed of quartz, but may also be feldspars or micas. Due to their small sizes, silt particles are commonly found along with clays in both suspended and bed sediment. The largest-sized inorganic particles in fine sediment are sands. They range in size from 63 μm to 2mm and are typically composed of the mineral quartz. The classification of inorganic particles by size, though, does not perfectly reflect patterns in mineralogy. Clay mineral particles can be larger than 2 μm and clay-sized particles can include other minerals, such as calcium carbonate and iron oxides, but primary minerals less than 2 μm are generally rare.

The organic components of the sediment include a wide variety of biogenic structures and compounds, including living organisms, detritus, faecal pellets, extracellular polymeric substances (EPS), and organic colloids. Organic matter ranges in size from colloidal dissolved organic matter (DOM) to large particulate organic matter (POM), such as leaf litter. Similar to the inorganic components, the smallest fraction of organic matter is the most electro-chemically active and has the most pronounced impact on the stability of aggregates and cohesive sediment erodibility (Winterwerp & Van Kesteren 2004).

2.2 Fine sediment in rivers

Fine sediment deposits are ubiquitous in aquatic systems, where they form as a result of weathering, transport and biological processes. The dynamics of fine sediments can be divided into 5 stages: (1) sediment input, (2) transport, (3) deposition, (4) storage, and

(5) erosion. These processes are discussed in the following subsections, with special attention paid to chalk stream environments in the UK.

2.2.1 Input

The fine sediment in lowland chalk rivers originates principally from four sources: (1) soil erosion, (2) bank erosion, (3) allochthonous organic matter input, and (4) autochthonous organic matter production. First, soil erosion is the most significant source of fine sediment in these systems. Using composite sediment fingerprinting, Collins and Walling (2007b) estimated that the majority of fine sediment on the beds of chalk rivers of the Pang and Lambourn catchment originated from pasture and cultivated land. For the Pang sub-catchment, pasture was the principal source (49%), whilst for Lambourn it was cultivated land (64%), reflecting patterns in agricultural practices and subcatchment topography. Second, bank erosion is a significant contributor to fine sediment load in lowland rivers in general (Knighton 1998, Simon et al. 2006). In chalk streams, though, bank erosion appears to be a minor source (18% for both the Pang and Lambourn sub-catchments) (Collins & Walling 2007b). This could be a result of low stream energies caused by the low gradients, a baseflow dominated flow, and an increased abstraction of groundwater from the chalk aquifer. Third, terrestrial inputs of organic matter (i.e. allochthonous) are the dominant source of organic matter in streams and rivers (Wetzel 2001). The material ranges from DOM originating from soils to POM in the form of detritus, such as leaves and tree branches. This material is essential to the functioning of stream ecosystems (Wetzel 2001), and can have significant impacts on stream hydrology and geomorphology, particularly large woody debris (Gurnell et al. 2002). Studies of the chalk streams in the Frome-Piddle catchment have generated evidence, in the form of C/N ratios and ^{15}N enrichment, to suggest that the organic matter in the fine sediment originates from agricultural soils (Walling & Amos 1999, Sanders et al. 2007). Finally, chalk streams support a diverse and abundant flora and fauna, which process allochthonous organic matter, and contribute to the organic matter in the sediment as living organisms (e.g. bacteria, diatoms, benthic invertebrates), detritus (e.g. plant debris), faecal products, or exuded organic matter (i.e. EPS) (Berrie 1992, Wotton 2005, Wharton et al. 2006, Joyce et al. 2007).

2.2.2 Transport

Fine sediment is transported within streams in three modes: the dissolved load, suspended load, and bedload (Knighton 1998). The dissolved load constitutes the dissolved material transported in the river (e.g. DOM and solutes). The suspended load is the fraction of the sediment that is carried in suspension in the flowing water, and typically includes clay and silt-sized material. Suspended sediment in nature is composed of complex aggregates of organic and inorganic material that forms as a result of particle cohesion and biological-induced adhesion (Droppo 2001) (for more information see Section 2.3.1). The bedload is the coarser-grained material that travels along the bed of a river. Whilst it is typically envisioned to be large inorganic minerals like sand and gravel, it can also include dense organic material. For example, in chalk streams, *Simulium* larvae ingest suspended material and repackage the wastes as dense faecal pellets that are typically transported as bedload (Joyce et al. 2007).

The capacity for a stream to transport sediment is dependent on its power. Stream power is an estimate of the energy of the flowing water per unit length of the channel, and is calculated based on stream discharge, channel slope and the density of the water (Knighton 1998). A stream with a high power can transport larger sediment grains than one with a lower power, because water velocity and turbulence are greater. Consequently, peak transport of suspended and bedload typically occurs during high discharge events, due to the resuspension of channel bed sediments as well as an increased input from run-off (Knighton 1998, Smith et al. 2003). Suspended sediment loads are lower in chalk streams than in other UK rivers, and are less impacted by storm events (Walling & Amos 1999, Heywood & Walling 2003). If stream power decreases below the minimum required to transport sediment, the material will settle onto the channel bed to form deposits.

2.2.3 Deposition within the channel

Fine sediment deposits form within river channels in areas and at times of reduced water velocity and turbulence. Within chalk streams, they are typically found in the following environments: (1) margins, (2) depressions in the bed topography, (3) within macrophyte stands, (4) downstream of obstructions (e.g. large wood), and (5) as fine laminae on the surface of the gravel bed (Wood & Armitage 1999). The location of these environments in relation to the patterns of flow in the stream will influence the

sediment composition. For example, a gradient from coarser to finer sediment exists from thalweg, the deepest part of the stream, to the margins because of a decrease in water velocities (Pye 1994, Leeder 1999).

Macrophytes play a dominant role in altering flow conditions and sedimentation patterns in rivers (Madsen & Warncke 1983, Sand-Jensen 1998, Madsen et al. 2001, Clarke 2002, Cotton, 2006 #158, Gurnell et al. 2006). The leaves and stems of dense macrophyte stands reduce flow velocities and turbulence within the stands and divert the main stream flow around the plants (Marshall & Westlake 1990, Sand-Jensen & Pedersen 1999, Green 2005, Wharton et al. 2006). Fine sediment accumulates within the macrophyte stands, though the exact mechanism by which this occurs is open to debate. The low flow, low turbulence environment may permit clay and silt sized particles, which would otherwise remain suspended, to settle out (Horvath 2004); see review in (Gacia et al. 1999). Conversely, net deposition may be unchanged, but erosion and resuspension rates may be reduced (Sand-Jensen 1998, James et al. 2004, Neumeier & Ciavola 2004). Or the macrophyte stands may act like sieves to physically retain sediment, suspended particles by the leaves and stems, and bedload by roots/rhizomes and stems (Sand-Jensen 1998, Horvath 2004, Sanders 2006). The density and morphology of the macrophyte does have an effect on the magnitude of the hydrodynamic effect. Sparse vegetation does not reduce the velocity and turbulence inside the stand as much as dense vegetation (e.g. Bouma et al. 2007, Luhar et al. 2008). Compact, bushy or branching macrophytes reduce flow within the stands more substantially than those with long, strap-like leaves (Sand-Jensen & Mebus 1996, Sand-Jensen & Pedersen 1999). However, Buoma et al. (2005) argue that, if morphology is constant, the most important attribute for sediment accretion in macrophyte stands is plant height. An emergent plant will accrete more sediment than a submerged one, because it has a larger surface area interacting with the flow. Research by Gurnell et al. (2006) supports this hypothesis; fine sediment deposition was higher in the emergent *Sparganium erectum* than the submergent *Ranunculus penicillatus* in a chalk stream. Furthermore, they argue that the stands of *Ranunculus* located in the channel centres diverted flow towards the margins, which increased the supply of suspended sediment to *S. erectum*.

Given the high biomass of macrophytes in chalk streams (0.5-5kg m^{-2}; Clarke 2002), and the significant effects it has on stream flow and fine sediment deposition (Cotton et

al. 2006, Gurnell et al. 2006, Wharton et al. 2006), they constitute a significant store of fine sediment.

2.2.4 Storage within the channel

River channel beds are not generally considered a major depositional environment over geologic time-scales (Leeder 1999). However, significant fine sediment deposits can form in areas where water velocities and turbulence decrease, either naturally (e.g. downstream fining, fluvial lakes) or due to anthropogenic influences (e.g. dams, reservoirs, and weirs). In these areas, sedimentation can pose a significant problem to navigation, the functioning of engineering structures, as well as environment/human health because of contaminants (Mehta et al. 1989b, Luoma & Rainbow 2008, Droppo et al. 2009). In small streams they can still represent a significant temporary sink/source of fine sediment over shorter time periods (i.e. months or years). Estimates for the amount of fine sediment stored within the gravel beds of chalk rivers are 920 g m^{-2} for the River Frome, 1290 g m^{-2} for the River Lambourn, 1590 g m^{-2} for the River Piddle, and 2390 g m^{-2} for the River Tern (Collins & Walling 2007a, b). These represent 19 - 57% of the rivers' annual fine sediment loads. When the deposits within aquatic macrophytes are included in the analysis, estimates of fine sediment storage increase significantly. Heppell et al. (2009) calculated fine sediment storage between 11.6 and 66.8 kg m^{-2} for the Bere Stream, and 0.9 and 23.5 kg m^{-2} in the River Frome. Storage was strongly correlated to the percent cover of macrophytes, and it is macrophyte cover which is responsible for the substantial temporal variations in fine sediment storage. For sediment stored within macrophytes, the permanence of the storage is tied to macrophyte stand dynamics. If the plants die back in the winter, leaving the sediment exposed to bed shear stress and turbulence, it will more likely to be transported away from the reach (Kleeberg et al. 2010). However, if macrophyte stands persist for greater than a year, deposition within the stands will have a more significant impact on sediment transport dynamics in these systems.

2.2.5 Erosion

The final stage in the transport and cycling of fine sediment within rivers is erosion. The likelihood of erosion for a sediment deposit in a river is dependent on the hydrodynamic conditions at its location (e.g. bed shear stress and turbulence) and the resistive forces within the sediment (i.e. erodibility). For example, all sediment is stable if no external

force is applied to it. Once a hydrodynamic shear stress is exerted on the sediment surface, though, it may or may not erode depending on the properties of the sediment.

Generally speaking, erosion occurs when hydrodynamic forces exceed the resistive forces of the sediment bed, causing particles or aggregates to be entrained in the flowing water. There are two basic modes of erosion depending on the mechanical properties of the sediment: granular and cohesive. Erosion in granular sediment is well-understood. It operates on individual particles, and occurs when lift and drag forces exceed the weight of the particle and the frictional forces between neighbouring grains (Knighton 1998, Leeder 1999). Drag force is caused by the velocity gradient experienced by the particle, or in other words, the magnitude of change in downstream velocity over the height of the particle. Lift is generated by the upward deflection of streamlines over an object. As streamlines merge on top of the particle, water velocity increases, and pressure decreases (i.e. Bernoulli's Principle), creating an upward acting force on the particle. The process is undoubtedly more complex in natural systems, not least due to the influence of biology. For example, organic colloids form coatings on the surfaces of sand grains, which induce cohesion between what are generally considered to be non-cohesive grains. (e.g. Lick et al. 2004) (for more information see Biofilms and EPS in Section 2.3.2).

For sediment with a high proportion of fine-grained particles and aggregates (< 63 μm), erosion becomes more complicated. Cohesion becomes the dominant resistive force (see Section 2.3.1). Particles bind strongly together, and erosion occurs at scales larger than individual particles. Several mechanisms for cohesive sediment erosion exist: (1) entrainment of fluid mud, (2) surface erosion, and (3) mass erosion (Mehta et al. 1989a, Winterwerp & Van Kesteren 2004). First, when mud is composed of a high volume of water, it is described as a fluid mud, and behaves as a viscous fluid. The fluid mud has little resistance to erosion, and the flow of turbulent water over the fluid mud will cause it to be entrained within the flow. Fluid mud exists at the surfaces of freshly deposited sediment, and can be formed in dense sediment by changes in overlying or pore water pressure (e.g. liquefaction by waves or fluidization by groundwater). In the second mode of erosion, individual aggregates are eroded from a solid sediment surface when the shear stress applied by the flowing water exceeds the strength of attraction between the aggregates/particles in the bed. Winterwerp and van Kesteren (2004) subdivide this mode further into floc and surface erosion. They apply the term floc erosion to the

minor erosion of aggregates from the bed surface, which occurs over short spatial and temporal scales (i.e. small bursts of erosion). They use surface erosion to describe the wide-spread erosion of aggregates from the surface that occurs at high bed shear stresses, which is tied to the influx of water into the sediment pore water. The third mode is mass erosion. Mass erosion occurs when water flows or wave-generated pressures exceed the bulk shear strength of the sediment, causing erosion of chunks of sediment. Simon et al. (2001) described a unique sediment detachment phenomenon for dense sediment in rivers associated with flood events. On the rising limb of a flood, the increased hydrostatic pressure of the fluid increases the pore water pressure in the sediment. When stage levels drop quickly, pore water pressure may not equilibrate rapidly enough resulting in a hydrostatic pressure gradient from the pore water to surface water. The upward force is sufficient to causes the detachment of aggregates or blocks from the sediment surface

Extensive research has been conducted on the hydrodynamic conditions that cause erosion, as well as the mechanism of granular sediment erosion (Leeder 1999, Winterwerp & Van Kesteren 2004). Much less is known about the mechanisms for erosion of cohesive sediment, particularly for surface and mass erosion. The major gap in knowledge in this area is the linkage between sediment properties and the forces in the sediment that resist erosion. What is lacking is a complete mechanistic understanding of erodibility.

2.3 Fine sediment erodibility

The term erodibility describes how readily a sediment deposit will erode under the force of flowing water. It is the propensity for erosion, so could be described as the inverse of resistance. Erodibility is often expressed as thresholds for erosion or erosion rates. Thresholds for erosion are the water velocity or bed shear stress that causes sediment to begin to erode, whilst erosion rates are the mass of sediment eroded once the threshold is exceeded (i.e. at an excess shear stress). So, highly erodible sediment has a low erosion threshold and/or high erosion rates at excess shear stress.

Erodibility is in essence a measure of the forces in the sediment that resist erosion by flowing water (e.g. gravity, friction, cohesion and adhesion). For granular sediment this is predominantly gravity and friction, which are well-understood from a theoretical

perspective. Erosion thresholds and rates for granular sediment beds can be predicted based on the behaviour of the water flow and on several key properties of the sediment, including particle size distribution, clast shape and degree of packing (Pye 1994, Leeder 1999). However, the strong inter-particle attractions found in cohesive sediment complicate the prediction of erosion thresholds from first principles, such as conservation of momentum (Black et al. 2002, Winterwerp & Van Kesteren 2004). Furthermore, empirical approaches to predict erodibility have been limited because cohesion is influenced by a large number of biogeochemical sediment properties that interact in complex ways.

Nevertheless, the erodibility of cohesive sediment is an important parameter in sediment dynamic models. The most widely used formulations for estimating sediment erosion rates require the critical shear stress for erosion to be determined (τ_c), a measure of erodibility represented as the threshold tangential force per unit area applied by the flowing water to the sediment surface in order to initiate erosion (Sanford & Maa 2001). Several variations exist depending on the nature of erosion, depth-limited erosion (Type I erosion) and uniform erosion (Type II erosion), however a general and widely-applied formulation is the Ariathurai-Partheniades stress-flux equation:

$$E = \alpha \left(\frac{\tau_b - \tau_c(z)}{\tau_c} \right)^{\beta} \tag{2.1}$$

where E is the erosion rate (mass of eroded sediment per unit area, per unit time), α is an empirical rate constant, τ_b is the shear stress applied to the sediment bed by the flowing water, $\tau_c(z)$ is a depth-dependent critical shear stress, and β is an empirical constant (Sanford & Maa 2001, Tolhurst et al. 2009). Since erodibility has yet to be accurately predicted for cohesive sediment, critical shear stress (τ_c) must be estimated or measured for the specific sediment in question.

The following sections present a review of recent erodibility research. The review starts with a summary of the major attractive forces in fine sediment, cohesion and adhesion (Section 2.3.1). Then, the major properties affecting erodibility are presented (Section 2.3.2). For each property, the mechanisms by which they affect erodibility are discussed first, then support is given from field and laboratory studies, and finally the property is discussed in relation to chalk streams. In the next section, recent research on spatial and

temporal variations in erodibility is summarised for fine riverine sediment (Section 2.3.3). The final section summarises the key findings from the review of erodibility (Section 2.3.4).

2.3.1 Cohesion vs. adhesion

Inter-particle attraction is a significant resistive force in fine sediment, and a clarification of the two principle forms of attraction, cohesion and adhesion, is essential to the discussion of erodibility. Cohesion occurs between similar particles or substances. The term cohesion is most commonly used to describe the attraction of clays and colloids by electro-chemical forces, such as van der Waals forces and electrostatic attraction (Pye 1994, Righetti & Lucarelli 2007). Adhesion occurs between dissimilar particles and substances. It can be used generally to describe, for example, the attachment of bacteria to a sediment grain. In terms of sediment erodibility research, though, adhesion is the binding of sediment components by an additional inter-particle substance, such as organic polymers or iron oxides, via cation bridging or polymerization. The aggregation of sediment particles in water by cohesion is termed coagulation, and by adhesion, flocculation (Johnson et al. 1994, Droppo et al. 2008).

Although quartz particles carry weak electro-chemical charges on their surfaces, it is the clay-fraction that is primarily responsible for cohesion. The small, thin, plate-like units of clays have high surface area to volume ratios, and their surfaces carry strong electro-chemical charges. The flat surfaces, or faces, of a clay particle generally carry permanent negative charges caused by the adsorption of anions and ionic substitutions in the clay mineral structure. The charges at the edges are caused by broken bonds and are highly dependent on mineralogy and water chemistry (Gillott 1987, Ravisangar et al. 2005). The strong net negative charges on the particle faces are counterbalanced by a layer of oppositely charged ions (i.e. cations) in the water, referred to as the electric double layer (Partheniades 2007). Clay particles experience net repulsive forces due to their similarly charged surfaces. However, inter-particle attraction can occur if the electric double layer is reduced. Positively charged cations dissolved in the water neutralize surface charges on the clay minerals, reducing the thickness of the electric double layer, allowing the particles to get close enough to attract by van der Waals forces. High valence cations, such as Ca^{2+}, are more effective at reducing the thickness of the electric double layer, so are more effective at coagulating clay minerals than

lower valence ones, namely Na^+ (Gillott 1987, Partheniades 2007). The electro-chemical activity of a clay mineral (i.e. surface charge density) is linked to the cation exchange capacity (CEC) and the particle size. CEC is a measure of the capacity of clay to adsorb cations in solution to the surface of the particles. A high CEC coupled with a small particle size results in an electro-chemically active clay with a high charge density.

Clay minerals rarely exist as individual, dispersed particles in nature. They coagulate at low ionic strengths (i.e. 0.3% salinity), forming an open, card-house arrangement, with particles interacting primarily edge-to-edge or edge-to-face (Keedwell 1984, Gillott 1987). At higher ionic strengths (e.g. in seawater), the positively charged cations neutralise the face charges on the minerals, allowing them to aggregate in a more stable face-face alignment (Partheniades 1971, Ravisangar et al. 2005). Organic compounds and bacteria adhere to these small, electro-chemically charged aggregates, which facilitates the development of larger aggregates through flocculation.

All sediment in aquatic environments has an organic component; even pure sand grains develop surface coatings of organic material. The coating consists of polysaccharides, proteins, and colloids that create a highly chemically active environment. Organic molecules can bind directly to sediment grains, and long polymers and polysaccharides can bind to more than one, adhering particles together (Winterwerp & Van Kesteren 2004). Organic colloids have cohesive and adhesive properties (Gillott 1987, Brady & Weil 2001). They can bind directly to sediment particles and other organic matter through ion exchange reactions and cation bridging (Dade et al. 1990). Similar to the inorganic colloids, they have strong electro-chemical charges that can be neutralized to permit coagulation by van der Waals forces. So non-cohesive sand grains can develop a coating of organic material that generates significant attractive forces between the grains.

2.3.2 Sediment properties that influence erodibility

Particle size distribution

Average particle size

Average particle size is arguably the most widely-used indicator of cohesiveness and erodibility for sediments. Early work by hydraulic engineers identified correlations

between particle sizes and the minimum water velocity needed to erode and transport sediment. The diagrams they created to illustrate their findings, namely the Hjulström and Postma plots, have subsequently become a standard reference tool because of their intuitive patterns (Fig. 2.2) (Dade et al. 1992). Boulders are more difficult to erode than sand, and cohesive mud is much more difficult to erode than silts or sand. Whilst it is tempting to use these figures to predict sediment erodibility, the patterns described for cohesive sediment should be restricted to illustrative purposes because: 1) the curves for particles < 100 μm were not based on empirical data, but rather observations by field engineers; and 2) they only consider the average particle size of the mineral fraction, ignoring the significant impacts of organic matter and other key sediment properties (Partheniades 1971, Dade et al. 1992).

Many laboratory studies have investigated how particle size affects erosion thresholds; however they have focused primarily on non-cohesive sediments to minimize the confounding effects of cohesion. These studies demonstrate that the erosion threshold is positively correlated to particle size (cf. Dade et al., 1992) (Fig. 2.3a). A notable exception, though, is Roberts et al. (1998) who report critical shear stress values for pure silica sand that mirror the Hjulström diagram (Fig. 2.3a). The thorough laboratory investigation noted a significant negative correlation between critical shear stress and particle size for fine particles < 100 μm, with the authors concluding that silt-sized quartz minerals behave in a cohesive fashion. However, it must be emphasized that the inter-particle attraction noted in the study is not caused by cohesion between the silt-sized quartz grains, but rather by attraction between organic coatings on the grains (Johnson et al. 1994, Lick et al. 2004). Whether this is due to cohesion between organic colloids or adhesion of sand grains by EPS is unclear. The long consolidation times used to increase bulk density (up to 124 days) would have been conducive to microbial growth and EPS production, which has been shown to increase the erosion thresholds of quartz grains (Dade et al., 1990) (for more information see the following Biofilms and EPS Section). Therefore, the patterns reported by Roberts et al. (1998) are more likely to represent the relationships between particle size and erosion threshold that would be observed in nature, inclusive of the effects of surface coatings and bacterial growth, than would be expected from particle size alone.

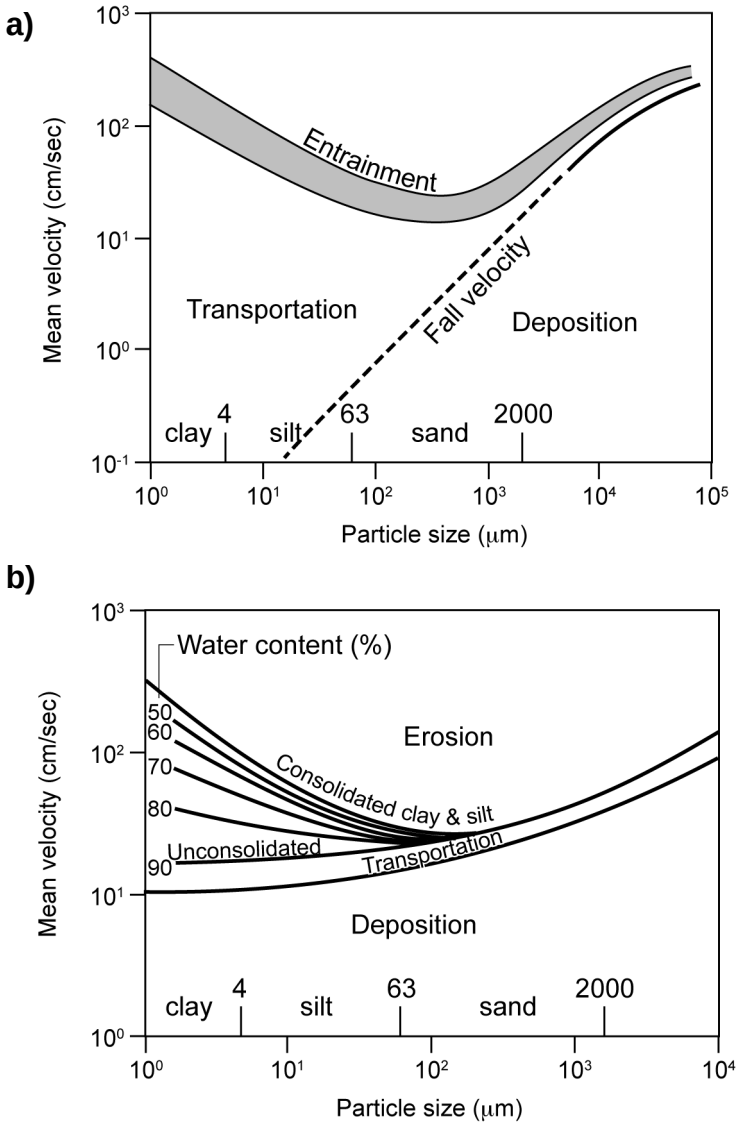

Figure 2.2. The (a) Hjulström and (b) Postma diagrams of threshold velocities for sediment entrainment and deposition based on particle size (Redrawn from Dade 1992).

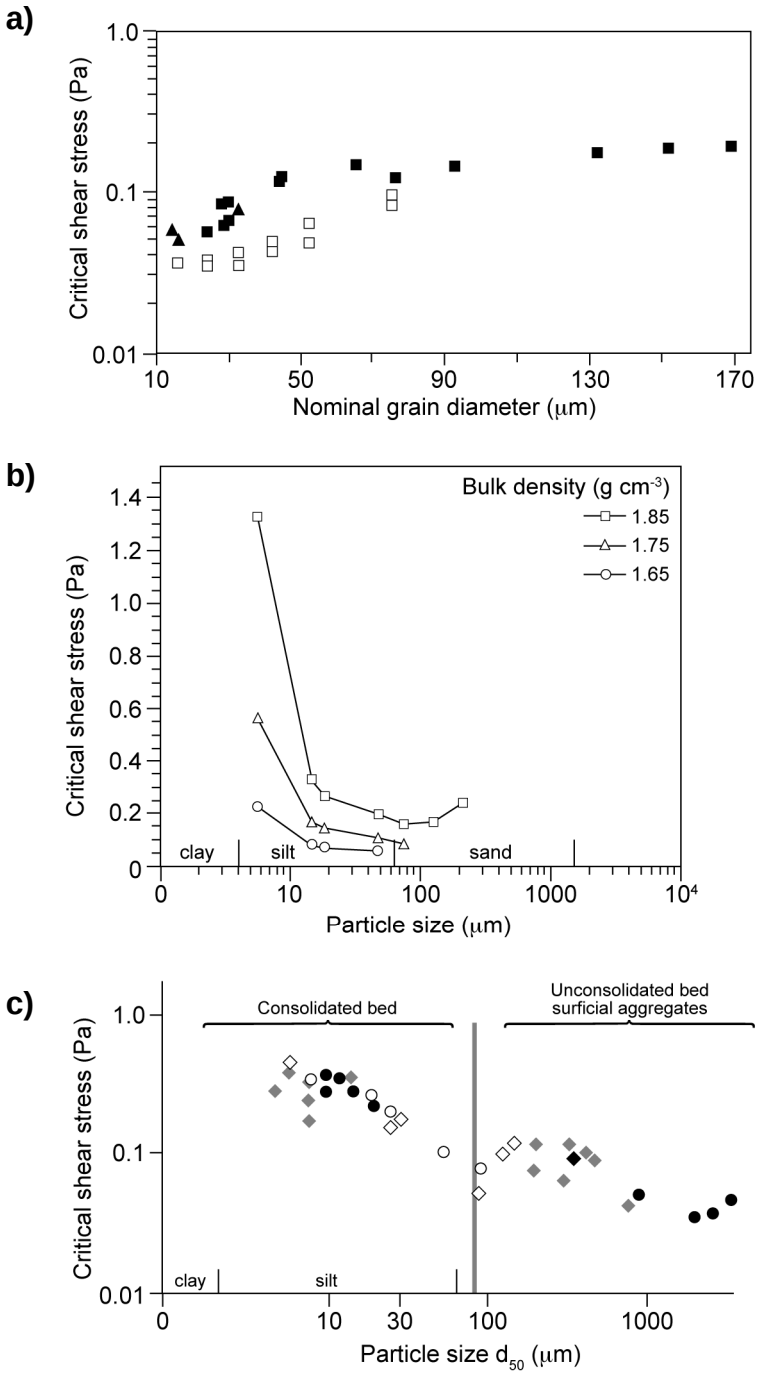

Figure 2.3. The influence of particle size on erosion threshold. (a) Critical shear stress for fine, non-cohesive sediment particles, including natural quartz grains (solid squares), crushed silica (solid triangles) and mica flakes (open squares) (After Dade et al. 1992). (b) Critical shear stress for sediment composed of non-cohesive silica particles, showing the importance of adhesion between organic coatings on silt-sized particles (After Roberts et al. 1998). (c) Critical shear stress vs. aggregate particle size (i.e. effective size) for marine sediment, including consolidated and unconsolidated sediment. Symbols represent different study sites (After Thomsen & Gust 2000).

Whilst sediment samples have been historically digested and disaggregated prior to particle size analysis, obtaining absolute particle size estimates, recent field studies have begun to focus on the natural size of sediment aggregates (i.e. effective particle size) (Walling & Amos 1999, Droppo 2001, Cotton et al. 2006, Heppell et al. 2009). The clearest demonstration of the importance of particle size from a field survey was provided by Thomsen and Gust (2000), who found a negative correlation between critical shear stress and median particle size for natural marine mud (Fig. 2.3c). The study included both consolidated and unconsolidated bed sediment (i.e. a surficial aggregate layer). Considering solely the consolidated sediment, the negative correlation mirrors that of the Hjulström and Postma diagrams (Fig. 2.2). The continual reduction in erosion threshold with particle size for the unconsolidated sediment likely corresponds with a decrease in the density of the aggregates, as porosity and organic content increase with aggregate size (Droppo et al. 2007a). However, in situations where particle size and floc density positively covary, we see marked increases in the stability of cohesive sediment with particle size. A good example of this phenomenon comes from laboratory studies on the impacts of antecedent flow conditions on cohesive sediment (Lau & Droppo 2000, Droppo et al. 2001). When suspended sediment is exposed to shear in the water column during deposition, it produces cohesive sediment beds that are more resistant to erosion than quiescently deposited beds. The aggregates that settle out under shear stress are larger and denser, and require higher critical shear stresses for erosion. So, effective particle size can be positively or negatively correlated with erodibility depending on the antecedent flow conditions.

The average particle size of the fine sediment in chalk streams will likely vary greatly within a reach, because of differences in sediment delivery and deposition between the channel and margins. Previous studies on chalk streams have shown that sediment in channel centres have larger median particle sizes than those in the margins (Heppell et al. 2009), and therefore, it would hypothesised that they would have greater erosion thresholds.

Clay/mud/sand content

Whilst it is convenient to describe sediment by a mean particle size, most natural cohesive sediment is composed of a range of particle sizes, and the relative proportions of these different sized particles can substantially affect sediment erodibility. The amount of clay in the sediment is a prime example. Adding clay or mud (i.e. clay & silt) to a sand bed makes it more resistant to erosion, up to a maximum erosion threshold at 30-50% clay (Mitchener & Torfs 1996, Panagiotopoulos et al. 1997) (Fig. 2.4). The increase in erosion threshold is caused by a combination of hydrodynamic smoothing, clay/sand adhesion and clay cohesion. At low clay contents, the small clay minerals fill in voids between sand grains, creating a smoother surface that is more difficult to erode. Also, experimental work by Lick et al. (2004) suggests that at low clay contents (2% for bentonite) clay particles coat silt and sand-sized quartz grains, adhering the non-cohesive particles together. At higher clay contents (4-10%), the structural framework of the sediment changes from a sand grain framework to a clay mineral framework, which corresponds to change from a non-cohesive to cohesive sediment (van Ledden et al. 2004, Winterwerp & Van Kesteren 2004). Above 30-50%, erosion thresholds are believed to decrease as the sediment mixtures approach pure clay, because of a decrease in bulk density. The stabilising effect of clay content on sandy beds appears to be universal, as the positive correlation with critical shear stress has been documented for a variety of pure clay minerals and natural muds. The nature of the response, though, does appear to be affected by clay mineralogy. In one study, montmorillonite added to sand produced cohesive sediment with lower critical shear stress than either kaolinite or natural marine mud (Torfs 1995).

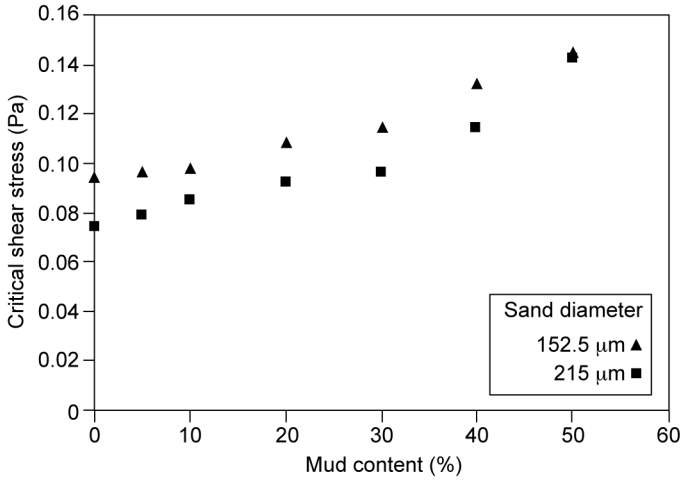

Figure 2.4. Critical shear stress as a function of mud content (% < 63 μm) for artificial sediment mixtures. Sieved natural estuarine mud was mixed with uniform sand of two particle sizes (After Panagiotopoulos et al. 1997).

Although most of the studies that have investigated the effects of particle size distributions on erodibility have been laboratory studies focusing on clay content, there has been some support from field studies. The clearest example is from Houwing (1999), who reported that erosion rates decrease by 2 orders of magnitude with increasing mud content (4 – 35%) for intertidal sediment. Other studies have found a negative correlation between critical shear stress and sand content (Gerbersdorf et al. 2005, 2007), and a negative correlation between the erosion coefficient β and mud content, meaning that less sediment was resuspended at excess shear stress at higher mud contents ($\beta = M/\rho_b$, where ρ_b is wet bulk density) (Debnath et al. 2007). These examples come predominately from riverine environments where distinct layers of sand are found at depth within the sediment, due to high flow events. The sand has a lower erosion threshold than the consolidated silts and clays, as is represented in the Postma Diagram (Fig. 2.2b). Aberle et al. (2004), though, found a positive correlation between β and mud content for riverine and estuarine sediment, which Debnath et al. (2007) suggest could be due to differences in particle size distributions.

In chalk streams, the mud content of the sediment increases from channel centres to the margins (Heppell et al. 2009). Therefore, it could be hypothesised that erosion thresholds would increase towards the margins as well. However, this would only be true if there was not a substantial decrease in bulk density.

Bulk properties

Bulk density and water content are measures of the proportion of solid:liquid states in the sediment (Rowell 1994, Avnimelech et al. 2001), whose roles in cohesive sediment erodibility have been intensively studied in laboratory and field studies. The measures are inversely related, and both give an indication of the degree of packing of the sediment grains, which for cohesive sediment indicates the level of consolidation.

The importance of bulk density to cohesive sediment erodibility is well supported in the literature. Bulk density is the overall density of the sediment (kg m^{-3}), and is dependent on particle density, the density and amount of water, and the presence of gas/air pockets. It can be calculated as wet bulk density, based on hydrated sediment mass, or dry bulk density, based on dry sediment mass. Bulk density is negatively correlated with erodibility, or in other words dense sediment beds have lower erosion rates, up to 100 times lower (Jepsen et al. 1997, Lick & McNeil 2001), and higher erosion thresholds, up to 5-8 times higher (Bale et al. 2006, Bale et al. 2007), than less dense beds. An empirical relationship between critical shear stress and wet bulk density was developed by Amos et al. (2004) for natural lacustrine, estuarine, and marine muds, defined as:

$$\tau_{cr} = 5.44 \times 10^{-4} (\rho_b) - 0.28 \qquad (2.2)$$

where τ_{cr} is critical shear stress (N m^{-2}) and ρ_b is the wet bulk density (kg m^{-3}), for wet bulk densities from 800 to 2000 kg m^{-3}. Caution must be exercised in extending this empirical relationship to sediments in more energetic environments, such as rivers, where sand layers can form within the sediment. Sand typically has a greater density than mud, but, as previously mentioned, it can have lower critical shear stresses (e.g. Gerbersdorf et al. 2005, 2007)

Several researchers have argued that it is actually water content that determines the erosive behaviour of cohesive sediment, not bulk density, as it directly affects the mechanical properties of clay (Gillott 1987, van Ledden et al. 2004, Winterwerp & Van Kesteren 2004). Water content is a gravimetric measure of the amount of water per unit mass of sediment. When clay is subjected to a stress, such as shear, it can respond in a variety of ways, most notably plastic deformation and viscous flow (Gillott 1987). Consolidated clays exhibit plastic deformation. The material is unresponsive to stress until the yield threshold is exceeded, above which the material will deform continuously

at a constant stress. Unconsolidated sediment is more akin to a viscous fluid, in which the rate of shear is directly proportional to the shear stress. The behaviour is not fixed for an individual clay sample, but can be changed by altering the water content. The Atterberg limits describe these transitions: the plastic (w_p) and liquid limits (w_l) define the minimum and maximum water content needed for plastic behaviour, respectively (Grim 1962). The liquidity index (I_L) is a measure of the actual water content (w) of the sediment in relation to the Atterberg limits, described as:

$$I_L = \frac{w - w_p}{w_l - w_p} \tag{2.3}$$

A liquidity index greater than 1 indicates that the sediment will behave in a viscous or visco-elastic manner, and less than 1, a plastic manner. This measure provides useful information on the erodibility of the sediment. Unconsolidated sediment, such as freshly deposited muds and surficial aggregate layers, have I_L >1 and are easily entrained; whereas heavily consolidated estuarine sediments typically have I_L <1 and are more resistant to erosion (Amaryan 1993). However, this generalisation may not hold for all natural fine sediments. Amos et al. (2003) recorded remarkably high erosion thresholds for lacustrine sediment with such high water contents (i.e. low wet bulk densities) that they would be described as fluid muds. A stationary fluid mud with a bulk density of 1100 kg m^{-3} should have little inherent resistance to erosion (c.f. Amos et al. 2004). However, Amos et al (2003) measured critical shear stresses as high as 0.5 Pa for lacustrine sediment with bulk densities of less than 1100 kg m^{-3} (Hamilton Harbour, ON, Canada). These high erosion thresholds are strong evidence of biogenic stabilisation of the sediment (i.e. biostabilisation) through the adhesion of sediment constituents by EPS (for more information, see the following section on Biofilms and EPS).

Other measures generated from the Atterberg limits, such as the plasticity index (w_l – w_p) and activity (w_p / clay content), provide additional information on the plastic behaviour of the sediment as a whole and on the clay fraction in the sediment, respectively (Grim 1962, Whitlow 1995). However, the utility of these measures for predicting the erodibility of surficial sediment is questionable (Partheniades 2007), as a plastic clay mineral can be more easily eroded under moving water depending on water chemistry.

Given the wide range of particle/aggregate sizes reported for chalk stream sediments (Heppell et al. 2009), bulk density and water contents are likely to vary greatly. One would expect bulk densities to be highest in the channel centres where the sediment has greater sand contents, and lower in the margins where mud contents are high.

Cations

Major cations (Ca^{2+}, Mg^{2+}, Na^{+})

The significant role of dissolved ions in determining erodibility has been well-supported in the soil science literature, but has only been investigated on a preliminary level for sediments. A key concern for soil scientists is the sodium absorption ration (SAR). SAR is the relative proportion of monovalent (Na^{+}) to divalent (Ca^{2+} and Mg^{2+}) cation concentrations in the soil. Soils with high SAR (> 13-15) are labelled sodic. Sodic soils present a serious management problem for agriculture, particularly when they contain high percentages of expansive, smectite clays. Smectite clays, such as montmorillonite, are the most plastic of the clay minerals, but are also the most easily erodible in soils (Morgan 2005). The clay mineral absorbs more water at high SAR than at low SAR, and this expansion and dispersion of the minerals results in a soil with high porosity, low permeability and high erodibility (Rowell 1994; Brady and Weil 2001).

In one of the few studies to address the role of water chemistry, Kandiah (1974) noted that sediment beds composed of montmorillonite have a lower critical shear stress than kaolinite, but only if the water used to create the sediments had a high SAR (Fig. 2.5) (cf. Winterwerp & Van Kesteren, 2004). The montmorillonite bed was more resistant to erosion than kaolinite at low SAR. In a separate study, Kandiah (1974) also demonstrated that critical shear stress was negatively correlated with SAR and positively correlated with total salinity for a pure illite sediment bed, a non-expansive clay (Fig. 2.6) (cf. Winterwerp & Van Kesteren, 2004). In other words, cohesive sediment is most resistant to erosion in environments with high total salinities (5 ‰), particularly with high concentrations of divalent cations.

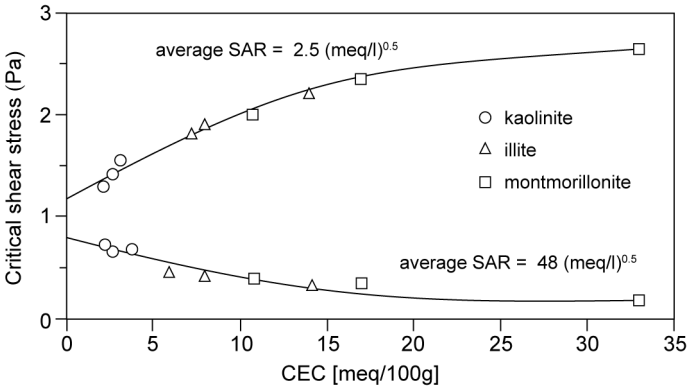

Figure 2.5. Critical shear stress as a function of sodium adsorption ratio (SAR) and cation exchange capacity (CEC) (Kandiah 1974, Redrawn from Winterwerp & Van Kesteren 2004).

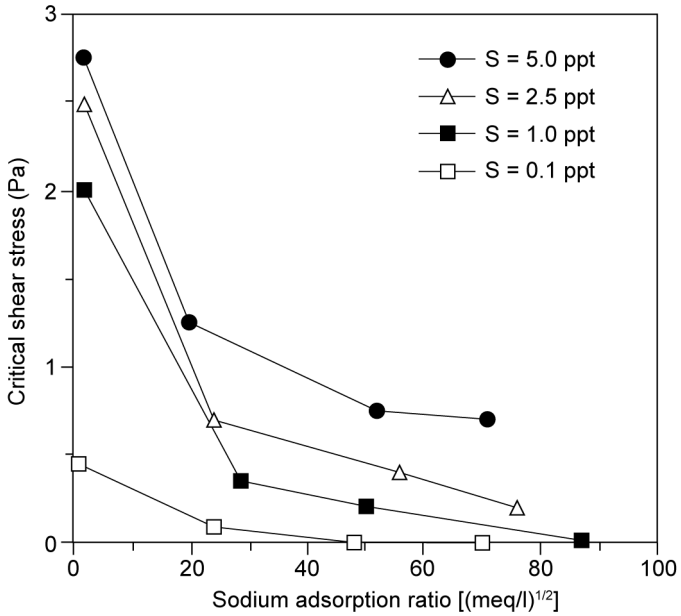

Figure 2.6. Critical shear stress for a pure illite clay sediment as a function of sodium absorption ratio (SAR) and total salinity (S) (Kandiah 1974, Redrawn from Winterwerp & Van Kesteren, 2004).

Cation concentrations also affect the mechanical properties of EPS. de Kerchove and Elimelech (2006) measured the attraction between alginate absorbed to a surface and in solution, using atomic force microscopy. Alginate is an important component of many biofilms, particularly in the gram-negative *Pseudomonas aeruginosa*. This study reports two interesting findings. First, in solutions of KCl, the force of attraction between alginate molecules increases with salinity, from ionic strengths of 3 to 300 mM. Second, the relationship changes when a set amount of calcium (1mM) is added to the solution. The force of attraction is highest at low ionic strength (3 mM), but with a high Ca:K (1:3). The force of attraction decreases with decreasing Ca:K ratio to 1:300, even though ionic strength increased from 3 to 300 mM (de Kerchove & Elimelech 2006). In a study of biofilm mechanical properties, Korstgens et al. (2001) found that high calcium concentrations increased the stiffness of a biofilm. They hypothesise that the calcium cations reinforced the EPS framework in biofilms, by increasing the cross-links between polymers.

Evidence from field studies on the effects of salinity on sediment erosion is less conclusive than the laboratory studies, due to covariance between salinity and other sediment properties. Debnath et al. (2007) showed that erosion parameter β, is correlated negatively with salinity for natural marine and freshwater muds, however Amos et al. (2003) found that erosion thresholds were similar for sediment from both environments at a given bulk density. Spears et al. (2008) report a significant increase in erosion thresholds across a salinity gradient (i.e. along a seaward transect in an estuary). They argued the EPS contents were high in riverine sediment, but that salinity levels were too low to stabilise the EPS framework. It should be noted, though, that salinity positively covaried with bulk density in their samples. SAR has been suggested to be an important control on the stability of salt marshes. Crooks and Pye (2000) found a positive correlation between calcium content and erosion threshold for salt marsh sediment, and suggest that actively eroding salt marshes of SE England are deficient in detrital calcium, as compared to the accreting salt marshes found elsewhere in England.

Total salinity and cation concentrations are high for chalk streams in comparisons to freshwaters on other geology types, such as granite or sandstone (Casey & Newton 1973, Wetzel 2001). Total salinity is on the order of 0.25 ppt, whilst the high calcium concentrations push SAR down to approximately 0.2. As divalent cations are better able to reduce the electric double layer around colloids and clays, they increase inter-particle

attraction, and should result in higher erosion thresholds than would be expect in other freshwater environments. Calcium concentrations may also be different between chalk streams due to differences in geology and hydrology. A chalk stream that is less dominated by baseflow could have lower calcium concentrations and a higher SAR, which may in turn affect erodibility.

Other metal cations (Fe, Al, and Mn)

Metals can potentially alter the erodibility of sediment through several mechanisms; however there is little empirical evidence at this time. First, soluble metals, particularly Fe, Al, and Mn, can reduce the double layer thickness of clay particles, theoretically increasing cohesion and reducing sediment erodibility (Winterwerp & Van Kesteren 2004). Second, divalent metal ions adsorbed to clays and organic matter can bind to metal ions on other particles, creating strong cation bridges (Dade et al. 1990). Soluble aluminium has been shown to increase the elastic strength of biofilms (Stoodley et al. 2001), and iron has been shown to increase their cohesive strength and resistance to detachment by shear stress (Mohle et al. 2007), due to increased cross-linking in the EPS matrix. Third, metals form insoluble complexes with oxides and carbonates, which act as cementing agents in soils (Brady and Weil 2001). The compounds carry a net positive charge that strongly attracts two negatively charged clay particles (Partheniades 2007). Finally, metal contamination may impact sediment stability through its toxic effect on infaunal communities. Sediment contamination with copper was shown to reduce the depth of erosion in flume experiments because of its toxic effect on bioturbating worms (Fernandes et al. 2009). In a field study, sediment erodibility, as measured by a shear vane, was negatively correlated to distance from a point source of industrial contaminants, as well as to bioturbation by the infaunal community (Mazik and Elliott 2000).

Dissolved metals are a natural component of aquatic systems, and their concentrations are dependent on the geology of the catchment and anthropogenic pollution (Forstner & Wittmann 1981, Luoma & Rainbow 2008). As stated above, they bind preferentially to clays and organic colloids, so the sediment can have significantly higher concentrations than the water. The author was unable to find studies on the effects of metals either on sediment erosion for rivers, or on metal distribution in chalk stream fine sediment.

Organic content

Organic content has long been recognized as a critical factor determining the erodibility of soils (for a review see Morgan 2005), and its stabilising role on cohesive sediment deposits has been preliminarily supported by field and laboratory studies. It is generally expressed as the quantity of organic material per unit mass of sediment, and is traditionally measured as the loss of weight on ignition (LOI) (4hrs at 550° C) for an air-dried sample (Rowell, 1994). So, estimates of organic content incorporate all forms of organic matter found in the sediment, such as living and dead organisms, faecal material, and EPS. Soil with less than 2% organic content is considered erodible, and erodibility is negatively correlated with organic content from 0-10% (Brady & Weil 2001, Morgan 2005).

A preliminary laboratory study of remoulded riverine sediment demonstrated that the removal of natural organic material changes how the sediment consolidates, altering both bulk density and erosion rates (Lick & McNeil 2001). In a recent laboratory study, natural dissolved organic matter (DOM) was shown to increase the stability of deposited kaolinite beds, but only when the pore water contained appreciable amounts of dissolved cations (Ravisangar et al. 2005). At a low ionic strength (0.004 M), DOM decreases both bulk density and erosion thresholds, as compared to a control. At a high ionic strength (0.14 M Na or Ca), bulk density still decreases but the critical shear stress increases by a factor of 2-3. The observed role of water chemistry on DOM is concurrent with the previous discussion on the effects of ionic strength/salinity on clay particle binding; dissolved cations increase sediment stability by decreasing the thickness of the double layers around colloid particles (Sections 2.3.1).

Field studies support the stabilising role of organic content on cohesive sediment. In a study of lacustrine sediment, Righetti and Lucarelli (2007) report a 5-fold increase in the critical Shields parameter with an increase in organic content from 8-25% (Fig. 2.7). A positive correlation between organic content and critical shear stress has also been reported for riverine sediment (Aberle et al. 2004, Gerbersdorf et al. 2007, Gerbersdorf et al. 2008a). Organic material is generally believed to operate as an adhesive between particles (Section 2.3.1). However, Aberle et al. (2004) suggest that layers of fibrous organic material act as a structural barrier in riverine sediment, preventing erosion of less stable sediment underneath. Finally, it is important to bear in mind that organic content has a significant positive correlation with water content, and a negative correlation with bulk density for natural sediments (Avnimelech et al. 2001), so its

effects on erodibility in field studies could be confounded by the bulk properties of the sediment.

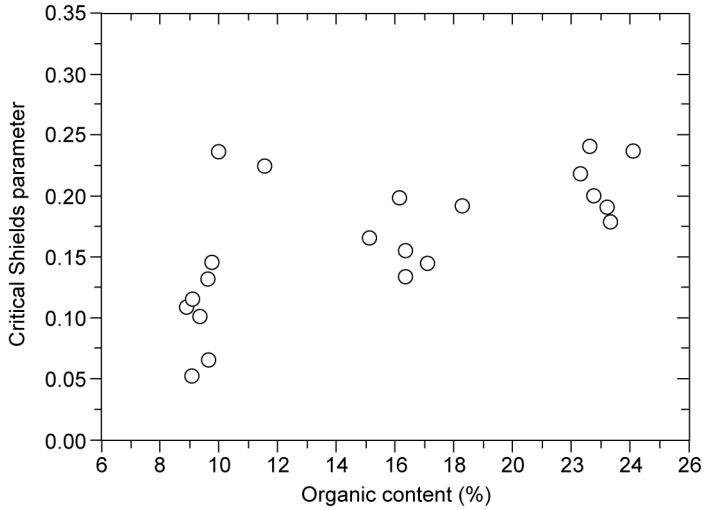

Figure 2.7. The effects of organic content on the critical Shields parameter, a non-dimensional erosion threshold, for littoral lacustrine sediment (After Righetti & Lucarelli 2007).

For chalk streams, Heppell et al. (2009) report that organic contents are substantially greater in the margins than in the channel centres. They also document temporal changes in organic content over time, with peaks occurring in summer and autumn.

Biofilms and extracellular polymeric substances (EPS)

Extracellular polymeric substances (EPS) is a general term for all polymers produced and exuded by organisms into their environment, and are the principal component of biofilms that form on and within the sediment (Fig 2.1). They are ubiquitous. EPS are produced by organisms of all sizes, unicellular to multicellular, bacteria to fishes, and are involved in a multitude of functions (Wotton 2005). They create the structural framework of biofilms, and function as lubricants for locomotion, anchors for attachment to substrata, buffers against the chemical environment, protection from the risk of desiccation, and deterrents from predators (Underwood et al. 1995, Paterson 1997, Sutherland et al. 1998a, Flemming & Wingender 2001, Wotton 2005, Flemming & Wingender 2010).

The stabilising influence of EPS on sediment has been widely reported in the literature over the last 20 years. Laboratory and field studies alike have demonstrated that EPS increase erosion thresholds and decrease erosion rates of both cohesive and non-

cohesive sediment, by physically binding sediment grains (i.e. adhesion), creating a pliant structural matrix, and reducing boundary layer roughness (see reviews in Paterson 1997, Black et al. 2002). This apparent consensus, though, belies the complexity and diversity of EPS molecules, the myriad of protocols to extract and quantify them, and equivocal results from field erodibility studies.

EPS are commonly defined as the high-weight polymer fraction of the exudates (8 - >1000 kDa), however they are a diverse grouping of compounds that vary in chemical composition, size, solubility in water, and structural properties. They are comprised of a range of organic molecules, including polysaccharides, proteins, nucleic acids and lipids (Decho 2000, Flemming & Wingender 2001, Sutherland 2001, Flemming & Wingender 2010). In the biofilm literature, EPS are often described generally as glycoconjugates, acknowledging that the molecular constituents can be bound to each other into more complex compounds, such as glycoproteins, peptidoglycans, and glycolipids (Mohle et al. 2007, Neu et al. 2010). The molecular composition of EPS varies between species, seasonally, or in response to changes in abiotic conditions (Sutherland 2001, Pamp et al. 2007, Flemming & Wingender 2010), and they are believed to exist in a variety of structural forms, including colloidal, capsular, slime-like, or fibrous (Decho 2000; Flemming & Wingender 2001).

With such diversity in chemical compounds, it is unsurprising that there is not a single technique that can extract all forms of EPS from a sediment sample, and that researchers use several different extraction methods to capture a range of EPS types (Frølund et al. 1996, Liu & Fang 2002). The most commonly-used technique employs a water extractration, and a quantification of EPS using a phenol-sulfuric acid assay, glucose standards, and calorimetric techniques (e.g. Underwood et al. 1995). This fraction is referred to as the total carbohydrate fraction if the entire sample is used to quantify EPS, and water-soluble, or colloidal, carbohydrate fraction if the sample is centrifuged and only the supernatant used. These carbohydrate fractions have been shown to be positively correlated to cohesive sediment stability in several studies (Gerbersdorf et al. 2005, Widdows et al. 2006, Droppo et al. 2007b, Gerbersdorf et al. 2007, Tolhurst et al. 2008), reducing erosion rates by 600% (Sutherland et al. 1998b) and increasing erosion thesholds by 120-900% (Friend et al. 2003, Tolhurst et al. 2003). Although the colloidal fraction may be easily removed from the sediment, high production rates may ensure a concentration sufficient enough to affect sediment erodibility (de Brouwer & Stal 2001,

Orvain et al. 2003). However, other studies do not consider this fraction to be EPS, a term they maintain exclusively for the high weight polymers, and which they isolate using filtration (e.g. Underwood et al. 1995, Yallop et al. 2000, de Brouwer & Stal 2001) or alcohol precipitation (e.g. Decho & Moriarty 1990, de Brouwer et al. 2002). Because of the difficulties in defining, extracting and quantifying EPS, as well as the considerable error and bias in some techniques (e.g. alcohol precipitation; Perkins et al. 2004), many studies continue to use the simpler extraction procedure outlined by Underwood et al. (1995). They operationally define the colloidal carbohydrate fraction as all of the oligomeric and polymeric carbohydrates extracted in the process (e.g. Gerbersdorf et al. 2009).

Visualizations of cohesive sediments using scanning electron microscopy show large EPS fibres adhered to sediment grains. These observations have led researchers to suggest that this bound EPS fraction may have a more significant influence on sediment erodibility than the colloidal fraction (Paterson 1989, Yallop et al. 1994, Droppo et al. 2007b). To quantify the bound fraction, various extraction techniques have been developed, such as EDTA, and cation exchange resin (CER) (Frølund et al. 1996, de Brouwer & Stal 2001, Liu & Fang 2002). However, few studies have reported statistically-significant correlations between these fractions and sediment erodibility. The complexing agent EDTA has been used to extract EPS from pure bacterial cultures, biofilms, and activated sludge (Decho & Moriarty 1990, Nielsen & Jahn 1999), but field studies have not found a correlation between the EDTA-extractable carbohydrate fraction and erosion threshold (Yallop et al. 2000, Friend et al. 2005). The CER approach appears to hold more promise (Frølund et al. 1996). Positive correlations between erosion thresholds and both colloidal carbohydrate and CER-extractable carbohydrates were found in recent field surveys of riverine sediment (Gerbersdorf et al. 2005, 2007). Further evidence comes from a recent laboratory experiment using natural cohesive sediments. Erosion thresholds were quantified for estuarine mud that was exposed to light/dark treatments and antibiotics to control diatom and bacterial growth (Lundkvist et al. 2007). The sediment had larger EPS fibres and higher critical shear stresses in sediments favouring diatom growth than those favouring bacteria (120% vs. 20% increases relative to a control).

Most studies have focused on the carbohydrate fraction, but evidence now suggests that EPS are composed of significant amounts of proteins and extracellular DNA (eDNA).

Proteins represent 15-30% (Liu & Fang 2002) and up to 60% of total EPS (Flemming & Wingender 2001). The role of the proteins is unclear; they may be part of bacterial capsules, function as adhesives to bind to surfaces (e.g. amyloids), act as structural components of the EPS matrix that strengthen polymer fibres (e.g. lectin), or exist as enzymes trapped within the matrix (Decho & Lopez 1993, Liu & Fang 2002, Gerbersdorf et al. 2009, Flemming & Wingender 2010). Flemming and Wingender (2001) report preliminary data to suggest that the proteins are relatively small in size (5-150 kDa) and are readily broken down by enzymatic activity in the EPS. Recent studies, though, have shown that proteins have a significant positive correlation with erosion threshold (Gerbersdorf et al. 2005, 2007, Gerbersdorf et al. 2008a, b). The presence of DNA in an EPS extraction was originally interpreted as a sign of cell lysis, but recent studies indicate otherwise (Flemming & Wingender 2010). It can be an abundant component of biofilms. An extracellular structure composed of eDNA has been identified in some biofilms, and, even more interestingly, bacterial cells have been observed migrating along them (c.f. Flemming & Wingender 2010).

In conclusion, the majority of recent studies find a correlation between cohesive sediment erodibility and at least one of the measures of EPS for freshwater and marine sediments. It should be noted, though, that several studies did not find a statistically significant correlation between erodibility and EPS (e.g. de Brouwer et al. 2000, Friend et al. 2005, Bale et al. 2006). Other studies find a stronger correlation between erodibility and chlorophyll-a, a proxy for the photoautotrophic microbial community abundance, which includes algae and cyanobacteria (Austen et al. 1999, Paterson & Black 2000, Tolhurst et al. 2003, Gerbersdorf et al. 2008a). The evidence strongly points to a stabilisation effect of EPS on cohesive sediment, and the equivocal results are probably caused by: (1) differences in polymer extraction techniques; (2) differences in sediment handling and storage; (3) inconsistent definitions of EPS; (4) inconsistent definitions of erodibility; and (5) spatial and temporal variability in the microbial community and EPS structure and mechanical properties (Widdows et al. 2007). Finally, it must be emphasised that our understanding of how EPS affects erodibility is based on, and limited by, the laboratory techniques for extraction and quantification. What we consider to be “gentle” extractions can still cause cell lysis, which contaminates the EPS sample with intracellular products. Chiovitti et al. (2004) found that extracellular glucans extracted using warm water primarily originated from inside

diatoms. Therefore, caution must be exercised when interpreting the results of an EPS extraction.

In hard waters like chalk streams, diatoms are the dominant member of the benthic algal community (Berrie 1992, Wetzel 2001). The polymer matrix of biofilms is stabilised by Ca^{2+}, so EPS produced by benthic diatoms in the calcium-rich chalk stream should increase the erosion threshold of the sediment, particularly during the benthic diatom blooms in spring (April-May) (Berrie 1992, Flynn et al. 2002).

Macrophyte roots and rhizomes

The stabilising effect of roots and rhizomes on sediment is well supported in the soil science literature. Root fibres are strong in tension, and a soil with fine fibrous roots is stronger than either the roots or soil separately (Morgan & Rickson 1995, Gyssels et al. 2005). A portion of the shear stress applied to a sediment with macrophyte roots is transferred to tensile strength in the roots (Simon et al. 2006). In addition to the structural network, roots and root hairs stabilise soil by increasing the organic content of the soil, supporting large microbial communities, and stabilising aggregates by the secretion of polyvalent cations and extracellular polymeric substances (Gyssels et al. 2005). Despite research that demonstrates the stabilising effects of plant roots on stream banks (Simon et al. 2006, Wynn & Mostaghimi 2006), and a classification of the rooting strengths of aquatic plants (Haslam 2006), to my knowledge, no study has explicitly measured the effects of aquatic plant roots and rhizomes on sediment erodibility.

As discussed earlier (Sections 2.2.3 & 2.2.4), aquatic macrophytes are abundant in many chalk streams, and deposition within macrophyte stands constitutes a significant store of fine sediment in these systems. Therefore, macrophyte roots have a significant potential to increase erosion thresholds in these systems.

2.3.3 Spatial and temporal variations in erodibility

Few studies have explicitly investigated the spatial and temporal variability in fine sediment erodibility for freshwater systems. Generally speaking, the most widely-accepted spatial variation for fine sediment is an increase in resistance to erosion with depth (Mehta et al. 1989a, Winterwerp & Van Kesteren 2004). At its simplest, it can be seen as a layer of unconsolidated aggregates (i.e. surface fluff) overlying a more erosion

resistant consolidated bed (e.g. Thomsen & Gust 2000, a marine example). However, it is often described as an increase in critical shear stress or decrease in erosion rates with depth, due to consolidation and a reduction in water content (e.g. McNeil et al. 1996, McNeil & Lick 2004). This has been widely observed in flume experiments, where it has been described as depth-limited (Type I) erosion. However, this is not a universal law. As mentioned earlier, erodibility of natural sediments can fluctuate, even increase, with depth, due to changes in particle size, organic content or the presence of gas (e.g. Jepsen et al. 2000, McNeil & Lick 2004).

Several studies have explored large-scale spatial variability in the erodibility of cohesive sediment in riverine systems. Hanson and Simon (2001) found that erodibility varied widely within and between streams flowing over loess soils. Critical shear stresses spanned six orders of magnitude, with the lowest values corresponding to sediment that originated from failed banks or deposited silt. These sediments were poorly consolidated and had higher water contents. McNeil and Lick (2004) identified significant spatial variations in sediment properties and erosion rates in a managed river. They found that where the river was faster flowing, the sediments were coarser-grained and denser (i.e. sandier), but had higher erosion rates. According to the authors, this was most evident when comparing sediment adjacent to an impoundment and sediment further upstream. Sediment from cores immediately upstream of an impoundment was finer-grained and had lower erosion rates, excluding the surficial fluff.

Whilst several studies of estuarine sediment have observed temporal variations in erodibility and sediment bed levels (e.g. Widdows et al. 2000, Amos et al. 2004) to my knowledge, none has reported them for fine riverine sediment. Gerbersdorf et al. (2005, 2008a) quantified the erodibility of riverine sediment cores over a full year, but did not report any seasonal patterns. They did present evidence to suggest that EPS is better able to stabilise the sediment in the spring than winter because of a change in EPS "quality" (Gerbersdorf et al. 2005).

2.3.4 Summary

Erodibility is a measure of the forces within the sediment that resist erosion. For fine sediment, which covers a range of particle sizes from clays to sands, these forces include gravity, friction, cohesion and adhesion. The significant inter-particle attractive

forces generated by cohesion and adhesion, though, have complicated the modelling of erodibility based on first principles. Consequently, researchers have turned to empirical studies to uncover the relationships between sediment properties and erodibility. According to numerous field and laboratory studies in freshwater and marine environments, particle size and bulk density appear to be the best overall predictors of erodibility over the fine sediment size range (< 2 mm). Biological stabilisation by macrophyte roots in soils and by benthic diatoms and bacteria in sediments, though, has been shown to significantly increase thresholds above the base levels dictated by the physical sediment properties. Therefore, one would expect that spatial and temporal patterns in the erodibility of fine sediment in chalk streams would be dependent on a combination of physical and biological sediment properties.

To date, few studies have investigated the erodibility of fine sediment in river channels, and none have specifically addressed chalk stream environments. To the best of my knowledge, no recent study has reported temporal variations for fine riverine sediment. Therefore, there is a significant gap in knowledge about how erodibility varies within these systems, and the sediment properties that influence erodibility.

2.4 Research questions

1) How does the erodibility of fine sediment vary spatially and temporally within a chalk stream reach?

   Question 1a: Are fine sediment deposits in the middle of the channel more stable than those in margins?

   Hypothesis: Sediment in the channel centres has higher erosion thresholds than in the margins. Sediment in the channel centre is exposed to higher shear stress and consequently is composed of larger and denser grains that are more resistant to erosion.

   Question 1b: Does sediment erodibility vary temporally?

   Hypothesis: Erodibility varies temporally in response to sediment loads and biological activity. Erosion thresholds will be highest in the summer and lowest in winter due to seasonal cycles of biological growth and decay. *Hypothesis*: An increase in the abundance in marginal macrophytes, in relation to channel macrophytes, will cause a decrease in average erosion thresholds due the lower particle sizes found in the margins.

2) What are the key sediment characteristics responsible for erodibility?

   Question 2a: Do macrophyte roots increase erosion thresholds?

   Hypothesis: Rooted aquatic macrophytes increase the bulk strength of the sediment during the growing season, due to the binding effects of roots and rhizomes, but bulk strength will decrease in the autumn as the roots decay.

   Question 2b: What is the effect of particle size, bulk density, organic content, cation concentrations, chlorophyll-a content and EPS content?

   Hypothesis: Particle size and bulk density will be responsible primarily for spatial variations in erodibility (e.g. channel centre vs. margin), but biological factors chlorophyll-a and EPS will be responsible for temporal variations.

Chapter 3: Survey methodology

This chapter outlines the methodology used to investigate the erodibility of fine sediment in lowland chalk streams. First, the criteria used to select field sites are discussed, and are followed by a detailed description of the geology, hydrology and ecology of each site. Second, the survey design used to select sampling locations in the reaches is presented, including the methods for characterisation of the environmental/ecological conditions of the stream reach and a discussion of the methods used to quantify erodibility. These erodibility measurements and environmental characteristics are used to examine the research questions on spatial and temporal variations in erodibility in Chapter 4 (Questions 1a and 1b, Section 2.4). Finally, the laboratory analyses used to quantify sediment properties are detailed. These sediment property data are used to examine research questions on the factors that influence erodibility in Chapter 5 (Questions 2a and 2b, Section 2.4). The statistical techniques used to analyse each research question are discussed in their respective results chapters (Chapters 4 & 5). The methodology for the cohesive strength meter calibration experiment is presented in Chapter 6.

3.1 Study sites

The stream reaches for this study were selected according to an *a priori* set of criteria based on bedrock geology, hydrology, and stream ecology. The reaches had to be located on chalk geology. They had to have a stable stream hydrograph, controlled predominantly by groundwater flow, as is characteristic for chalk streams (Berrie 1992, Sear et al. 1999). Sites with continuous flow or stage measurements were preferred, so that erodibility measurements could be taken in context with the hydrodynamic conditions of the streams. The sites had to have a recent history of siltation. In these

systems, siltation is principally associated with aquatic macrophyte stands (Heppell et al. 2009), so reaches had to have healthy macrophyte communities. Finally, the streams had to be shallow enough to permit year-round access by wading.

Two reaches were selected within the Frome-Piddle Catchment, Dorset, which satisfied these criteria: the Bere Stream at Snatford Bridge and the River Frome at Frome Vauchurch (Fig. 3.1).

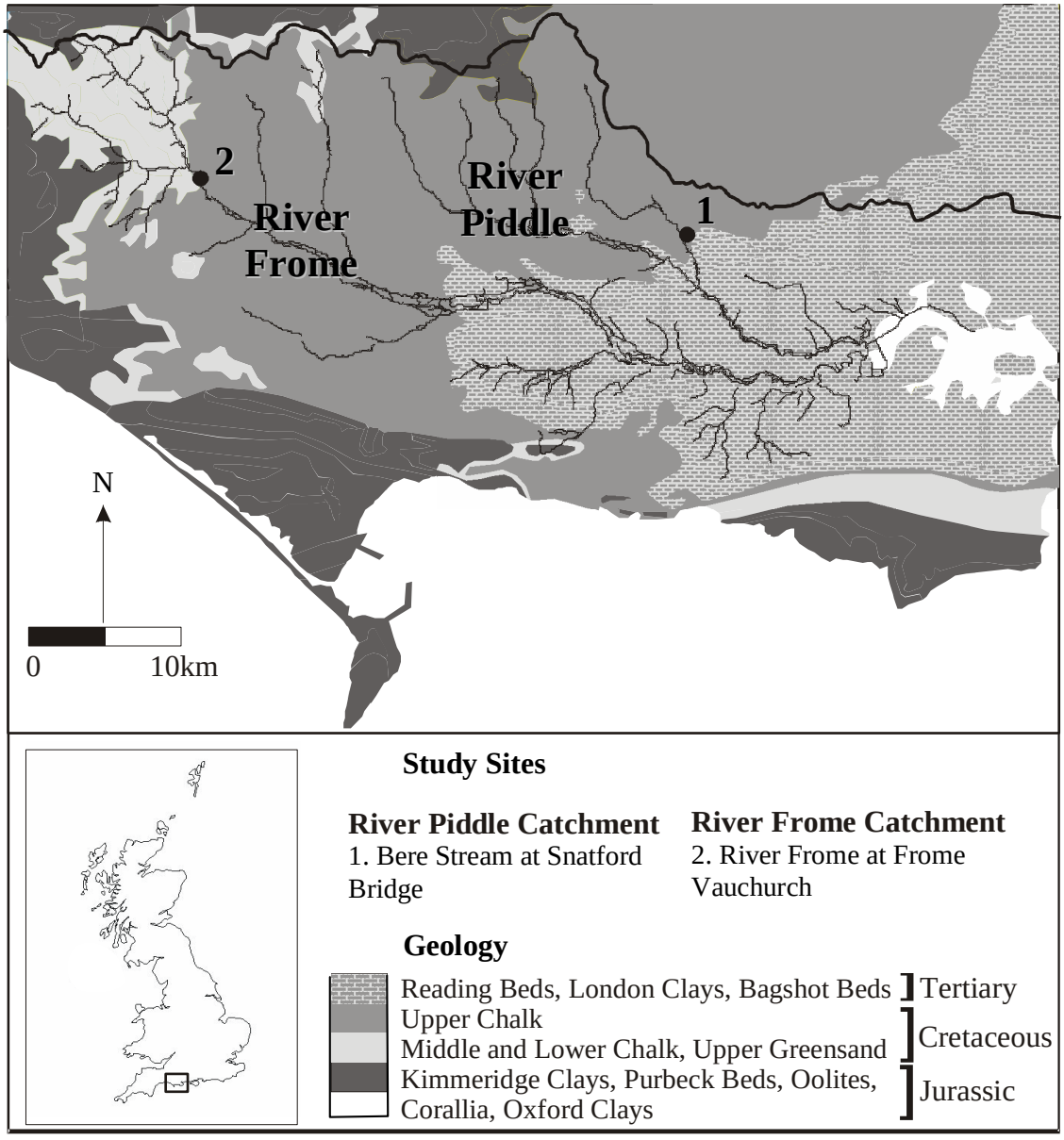

Figure 3.1. The study sites were located in the Frome-Piddle Catchment, Dorset, UK, and include the Bere Stream at Snatford Bridge and the River Frome at Frome Vauchurch (Wharton et al. 2006).

3.1.1 Bere Stream at Snatford Bridge

The Bere Stream is a first-order stream in the upper Piddle catchment (UK Grid Reference 385563, 93009) (Fig. 3.1). The Snatford Bridge site is located 2.3 km upstream of the confluence with the River Piddle, immediately upstream of Snatford Bridge, at the downstream end of a 150 m long straight section of the stream. The reach is located in a rural setting, between grazed and ungrazed pastures, but is downstream of a watercress farm and the town of Bere Regis, both of which are purported to be sources of fine sediment loads. The left bank rises steeply to a grazed pasture, and the riparian vegetation consists primarily of brambles, *Rubus fruticosus*. The right bank has a shallow gradient and is covered with herbaceous plants that extend into ungrazed, marshy pasture.

The bed is composed of flinty gravels with silts and fine sands found along the margins, beneath macrophyte stands, and within the gravel bed (Heppell et al. 2009). Fine sediment accumulation has been documented in this site over the past decade (Clarke et al. 2006, Cotton et al. 2006, Wharton et al. 2006, Heppell et al. 2009). This site has the most characteristic chalk stream hydrograph of the two sites, which means that the channel flows are relatively constant and only marginally affected by rainfall events (Table 3.1). Infrastructure for continuous discharge measurements was installed at the reach for the NERC LOCAR programme (Wheater & Peach 2004). Channel flows vary over the year primarily as a result of changes in the groundwater table, but are locally affected by channel morphology, bed topography, debris, and in-steam macrophytes.

The reach is unshaded by large trees permitting the growth of in-stream macrophytes, particularly *Ranunculus penicillatus* subsp. *pseudofluitans* (water crowfoot) and *Rorippa nasturtium-aquaticum* (watercress) (Heppell et al. 2009). *Ranunculus* is a submerged macrophyte that forms patches in the higher flow sections of the river. It is the dominant species in spring and early summer, but is gradually replaced by *Rorippa* over the summer. *Rorippa* is an emergent species that establishes along the margins in early summer and with time extends into the channel centre, becoming the dominant species by late summer.

Table 3.1. Channel dimensions and flow characteristics for the study sites on the Frome-Piddle Catchment.

	Bere Stream	Frome
National Grid Reference	385563,93009	359790,97427
Length of study reach (m)	30	30
Average Q ($m^3 s^{-1}$)[a]	0.93	1.07
Peak Q ($m^3 s^{-1}$)[a]	2.37	2.95
Peak Q / Average Q[a]	2.5	2.8
Average Width (m)	7.0	8.9
Average Depth (m)	0.30	0.42
Width: Depth Ratio	23	21
Bed Surface Slope	0.0087	0.0069

a – Based on flow measurements by G. Davies (Feb 2009 – Feb 2010).

3.1.2 River Frome at Frome Vauchurch

The River Frome is a third-order stream at the Frome Vauchurch site, located 500 m downstream of the confluence of the Rivers Hooke and Frome, in the upper Frome catchment (UK Grid Reference 359790, 97427) (Fig. 3.1). The study reach is located at the downstream end of a 350 m long straight section of the stream, 50 m downstream of the Frome Lane Bridge, in a rural setting at the edge of the village of Maiden Newton. The riparian vegetation on the left bank is predominately composed of woody shrubs, such as brambles, *Rubus*, and is shaded by large trees, beyond which is pasture. Frome Lane runs along the west side of the river, 5-10 metres from the right bank. Herbaceous perennials dominate along this stretch of land, however the bank is largely unvegetated at the margin. The right bank appears to be composed of old fill, possibly used in the construction or maintenance of the road, and is being actively undercut, particularly at the downstream end of the study reach.

The bed is composed of flint gravels, but fine sediment is found along the left-hand margin, beneath macrophyte patches, within the gravel bed, and as a surficial cover on the gravel bed during low flows in summer. The headwaters of the Rivers Frome and Hooke lie in Jurassic limestone, Upper Greensand and Gault clay formations, and, as a

result, the water flows in the study reach are more affected by storm flow than the Bere Stream (Heppell et al. 2009) (Table 3.1; Fig. 3.1). The annual hydrograph is still dominated by groundwater flow, but high-water events occur more frequently than in the Bere Stream. Storms can cause discharges to spike 2-3 times above base flow over short time spans (i.e. several days) (Heppell et al. 2009). The nearest Environment Agency gauging station was located 12 km downstream on the River Frome in Dorchester.

Rorippa is not found at this site, and *Ranunculus* is the dominant in-stream macrophyte year-round. The Frome is a Site of Special Scientific Interest, as described under the Wildlife and Countryside Act 1981, for its ecological significance.

3.1.3 Summary

The selected reaches (henceforth called the Bere Stream and River Frome) are representative of chalk streams in England, with groundwater-dominated hydrographs and high width:depth ratios (Table 3.1). Both reaches satisfy the criteria established for the study, but differ in several key characteristics as to make them good contrasting study sites. First, the River Frome experiences more frequent high water events than the Bere Steam (Heppell et al. 2009). This difference in hydrodynamic conditions could impact the properties of the fine sediment through differences in sediment delivery (e.g. particle size and allochthonous organic matter input). Second, the seasonal patterns in *Rorippa* growth at the Bere Stream cause significant changes in the hydrodynamic conditions over time, which could impact temporal patterns in sediment properties and erodibility (Cotton et al. 2006, Wharton et al. 2006). Finally, previous studies have demonstrated differences in sediment properties between the reaches. For example, fine sediment in the Bere Stream has greater mud contents than in the River Frome (Heppell et al. 2009). Using both streams for the survey should increase the variation in erodibility observed, and make the results more transferable to other chalk streams in the UK.

3.2 Field component

A routine field sampling programme was employed to quantify the erodibility of fine sediment deposits and identify the sediment properties responsible for erodibility (Fig. 3.2). Sediment cores and shear strength measurements were taken bimonthly in the 30 m study reaches in the Bere Stream and the River Frome, from September 2008 to September 2009.

3.2.1 Survey design and selection of sampling locations

For each bimonthly visit, a survey was first conducted to map fine sediment accumulation in the stream reach (Fig. 3.2). The survey formed the basis for a separate vegetation and sediment mapping project conducted by G. Davies (QMUL). A regular sampling strategy (i.e. grids) was used to ensure an even spatial resolution (Waite 2000, Quinn & Keough 2002). Transects were laid across the stream channel, at 1m intervals, and point estimates of sediment accumulation were recorded at 0.5 m intervals (Fig. 3.3). Next, the point estimate locations were stratified based on depth of fine sediment accumulation using a threshold of 5 cm. This depth was the minimum amount of sediment needed for the extraction of an intact core with an undisturbed sediment surface. Next, sampling locations for this study were chosen randomly from the >5 cm strata (n = 20). Finally, the locations were sorted by distance upstream, so that sampling progressed from the downstream to upstream, thereby minimising physical disturbance of the sediment.

The stratified random approach was selected for the survey because it offers the best compromise for statistical analyses and logistical concerns. Random sampling ensures that the samples (i.e. cores) are independent of each other and representative of the population (i.e. fine sediment deposits) (Waite 2000), which are essential criteria for subsequent statistical analysis (Quinn & Keough 2002). The approach is also flexible to spatial and temporal changes in sediment depositional patterns, and minimises the impact of sediment disruption associated with resampling at later time points. Stratification is advantageous for purely practical reasons; sampling effort is reduced by randomly sampling solely within surficial fine sediment deposits, which are the subject of the study, rather than the stream as a whole, without sacrificing the benefits of a random sampling programme.

3.2.2 Environmental variables

At each sampling location, the following environmental/ecological variables were recorded, channel depth, depth of surficial fine sediment, location within the stream channel and macrophyte species (Fig. 3.2). Two different measures of location within the stream channel were used: (1) classified as channel centre or margin, and (2) the relative distance across the channel, which is the distance from the nearest bank divided by the total distance, and ranges from 0 (bank) to 0.5 (mid-channel). Macrophyte species information was classified into five functional groups to facilitate data analysis, based on the two major macrophyte species, the macrophyte growth form and location within the channel: *Ranunculus*, *Rorippa*, Marginal, Riparian and Unvegetated. As stated earlier, *Ranunculus* is a submerged macrophyte that grows in the channel centre, and *Rorippa* is an emergent macrophyte found in both the channel centres and margins of Bere Stream. The Marginal group described sediment under emergent marginal species other than *Rorippa* that were rooted in the fine sediment. Riparian locations were located in the margins and were covered by the trailing stems and leaves of terrestrial macrophytes. Unvegetated locations were bare sediment without vegetative cover, and could be found in the channel or margin. Water velocity was measured using a Valeport Model 801 (Flat) EM flow meter at 60% of channel depth from the water surface (e.g. a velocity measurement at 0.16 m above the sediment surface if the water depth was 0.4 m) (Gordon et al. 2004). Three transects of water velocities were also conducted to estimate an average discharge based on cross-sectional area (Gordon et al. 2004).

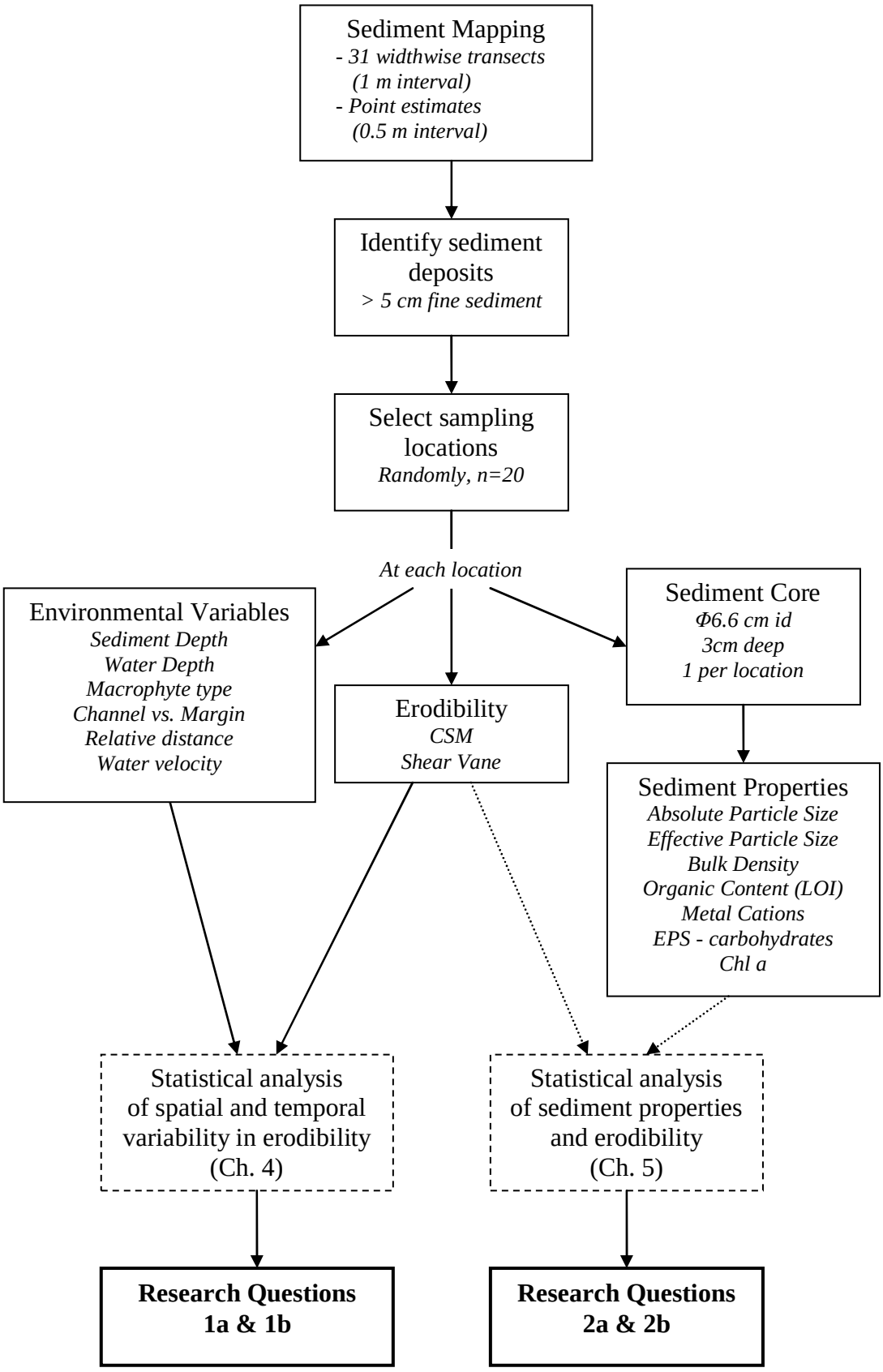

Figure 3.2. Diagrammatic representation of the field survey programme

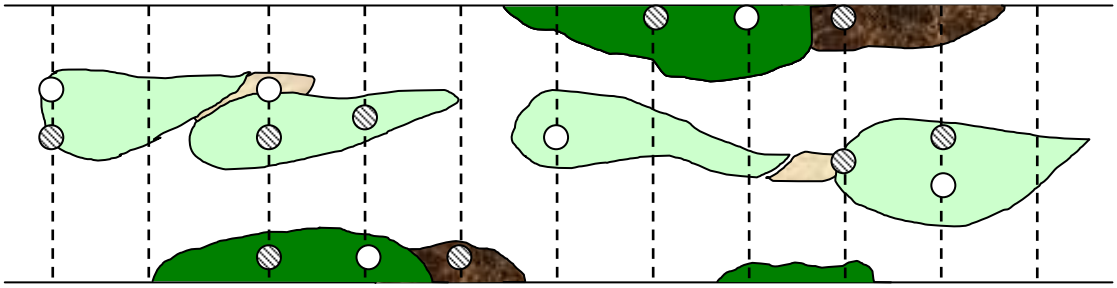

Figure 3.3. A representation of the stratified random sampling design for the field survey. Sampling locations (filled circles) for sediment cores and in situ erodibility measurements were selected randomly from the pool of locations with ≥ 5cm fine sediment depth (all circles).

3.2.3 Sediment erodibility measurements

Several methods exist to measure the erodibility of fine sediment. Laboratory approaches typically focus on flumes because they attempt to recreate, in a simplified form, the natural flow conditions found in the environment, be it unidirectional or oscillatory (e.g. Gerbersdorf et al. 2005, Droppo et al. 2007b, Lundkvist et al. 2007). Flumes use flowing water to apply horizontal shear forces and, at high velocities, turbulent energy to the sediment surface. By incrementally increasing flow velocities, researchers can describe the different modes of erosion occurring in the sediment sample, thereby pinpointing the velocity at which erosion occurs, allowing the calculation of critical shear stress. Erosion rates can also be estimated in flumes by measuring suspended sediment and bedload transport at excess shear stress. To quantify erosion in a laboratory flume, though, sediment must be removed from the bed and transported to the facility, where it is often stored prior to analysis. The physical disturbances and potential chemical alterations caused by sediment sampling, handling and storage have led researchers to develop several *in situ* techniques to quantify sediment stability, including shear vanes (e.g. Watts et al. 2003), field-deployable flumes (e.g. Widdows et al. 1998), the Gust erosion chamber (e.g. Thomsen & Gust 2000), the EROMES apparatus (e.g. Andersen et al. 2005), the *in situ* jet test (e.g. Hanson & Simon 2001), and the cohesive strength meter (CSM) (e.g. Paterson 1989). Of these methods, only two are both commercially available and have small enough footprints to be used in small, spatially heterogeneous vegetated streams: the cohesive strength meter (CSM) and the shear vane. The two devices measure different aspects of

sediment stability; the CSM provides an estimate of the surficial erodibility of the sediment, while the shear vane integrates over a greater depth (54 mm) providing a measure of bulk erodibility (Paterson 1989, Tolhurst et al. 1999, Mehta & Parchure 2000). In combination, the two techniques should provide a comprehensive assessment of sediment erodibility.

Cohesive Strength Meter (CSM)

The CSM is a small, portable device that measures the *in situ* erodibility of surficial sediments (Fig. 3.4) (Paterson 1989). Since its conception 20 years ago, the CSM has been increasingly used to measure *in situ* sediment erodibility, particularly in the estuarine environment (e.g. Yallop et al. 1994, Tolhurst et al. 2000c, Widdows et al. 2007), where it has formed the basis of several European sediment monitoring programs, including INTRMUD (EU MAS3-CT95-0022), F-ECTS (EU MAS3-CT97-0145), and BIOPTIS (EU MAS3- CT97-0158) (Friend et al. 2005).

Figure 3.4. The cohesive strength meter (CSM) being used in the Bere Stream. The yellow case is the main unit with computer and a water tank pressurised by the green air cylinder. The pressurised water is transported within the white tubing to the grey test unit within the core tube. A jet of pressurised water is fired downwards within the test unit towards the sediment surface, and resuspension is monitored by a transmissometer.

The CSM is a modern, portable version of the laboratory jet test used by soil scientists for over 50 years to measure the erodibility of clayey soil samples (cf. Paterson 1989). The device shoots a jet of water downward onto the sediment surface, incrementally increasing jet pressure and monitoring resuspension using an infrared transmissometer. The MK4 cohesive strength meter (Partrac, Glasgow) is factory-installed with 41 different routines that specify starting jet pressure and subsequent increments (PSI), as well as the duration of the pulse time (s) and interval between pulses. Before fieldwork commenced in the Frome-Piddle catchment, the routines were tested on refrigerated lacustrine sediment at the National Water Research Institute (NWRI), Environment Canada, Burlington, ON, Canada, in summer 2008. The Sand 1 routine was found to be the best routine for the range of sediment types likely encountered in the chalk streams; starting jet pressure is low (0.3 PSI), with a short jet pulse duration (0.3 s) and small pressure increments (0.3 PSI), suitable for fine muds, but with a high maximum jet pressure (12 PSI), allowing the test to be used on cohesive sands and consolidated muds. The Mud 1 routine has similar pressure settings, but the longer measurement times, 30 s at 1 s intervals, compared to 3 s at 0.1 s intervals for Sand 1, resulted in lower precision.

The CSM monitors erosion based on the resuspension of sediment. A transmissometer sensor is located at 1 cm above the sediment surface within the CSM test chamber. Erosion thresholds are defined by the manufacturer as the pressure at which average transmission within the test chamber drops below 90% of the maximum (Fig. 3.5). Average transmission is calculated for the 2^{nd} to 12^{th} data logged, which corresponds to 1 s for the Sand 1 routine. The CSM records the internal pressure (P_I) for each step in PSI, but the pressure of the impinging jet on the sediment surface (i.e. stagnation pressure (P_{stag})) is dependent on the specifics of the CSM model, the sampling routine, the length and diameter of tubing, and the height of the jet orifice above the sediment surface (Vardy et al. 2007). P_{stag} was calculated based on P_I for the specific CSM unit following the methods of Vardy et al. (2007) (n = 3). P_{stag} is reported in SI units for pressure (Pa) and for the MK4 CSM model is calculated according to the following equation,

$$P_{stag} = 3.71\ (6.89\ P_I)^{1.37} \qquad (R^2_{adj} = 0.94,\ p < 0.001) \qquad (3.1)$$

for P_I up to 4.8 PSI, for CSM measurements from September 2008 to May 2009. In July 2009, a different CSM MK 4 unit was used, whilst the usual unit was being serviced, and the calibration was,

$$P_{stag} = 1.23\ (6.89\ P_I)^{1.78} \qquad (R^2_{adj} = 0.93,\ p < 0.001) \qquad (3.2)$$

for P_I up to 4.8 PSI. The calculation of P_{stag} allows erosion thresholds to be compared between CSM models and individual units. At the moment, the CSM-derived erosion thresholds are relative because a calibration has not been successfully developed to convert the vertical forces generated by the CSM to horizontal shear stress (Vardy et al. 2007, Widdows et al. 2007). In Chapter 6, an empirical calibration is presented for the CSM, Sand 1 routine, based on a comparison of erosion thresholds from the CSM and a laboratory flume.

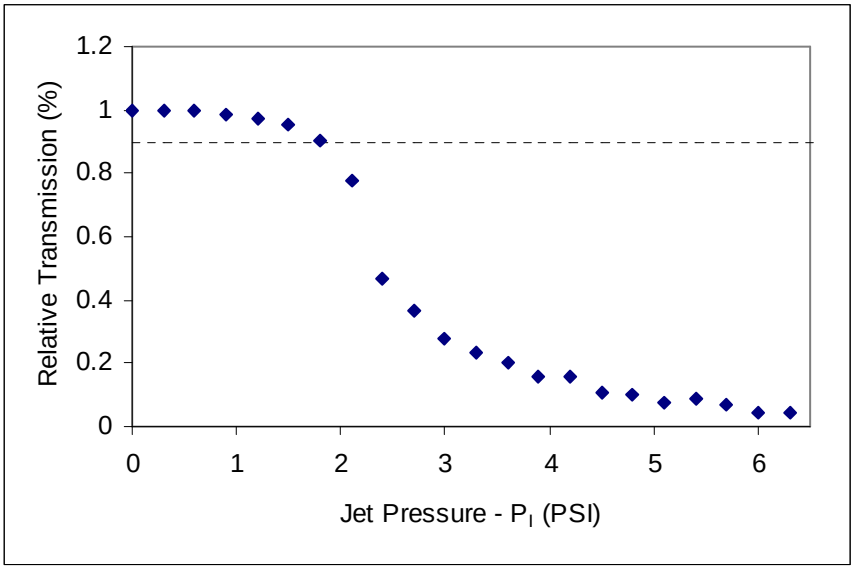

Figure 3.5. An example of a transmission curve from a cohesive strength meter run. The threshold for erosion is set at 90% transmission by the manufacturers, thus in this example, erosion is recorded to have occurred at a P_I of 2.1 Pa.

The sediment must contain a minimum mud content for CSM-derived erosion thresholds to be accurate. The reason for the minimum is that erosion thresholds are measured based on the resuspension of sediment in the CSM chamber. Pure sand would be entrained and transported as bedload at shear stress lower than what is necessary to suspend the sand grains to 1cm above the sediment surface, which is the height of the transmissometer sensor. In other words, the CSM overestimates erosion thresholds for

pure sand. When small amounts of clay or silt are added to the sand, the CSM-derived erosion thresholds decrease to a minimum, and then increase again due to the effects of cohesion (Fig. 3.6). For more detailed information on minimum clay/silt thresholds for the CSM, please see Chapter 6 on the calibration of CSM. For the field survey, sediment mixtures were prepared in the laboratory using sieved mud from the Bere Stream (<63 μm) and sand (d_{50} = 224 μm, Sibelco) at low water contents (25%) to ensure homogeneous mixtures. A range of mud contents were tested with the CSM, and a mud content of 5% (w/w) produced a minimum in erosion threshold (Fig. 3.6a). Particle size analysis was conducted on the sediment mixtures (see section 3.3.2 for more information on particle size analysis), and the 5% mud content threshold corresponded with a volumetric mud content of 8 % (v/v) (Fig. 3.6b). A threshold of 10% (v/v) was assigned, and the field survey dataset was filtered to remove all samples with less than the minimum clay content prior to data analysis.

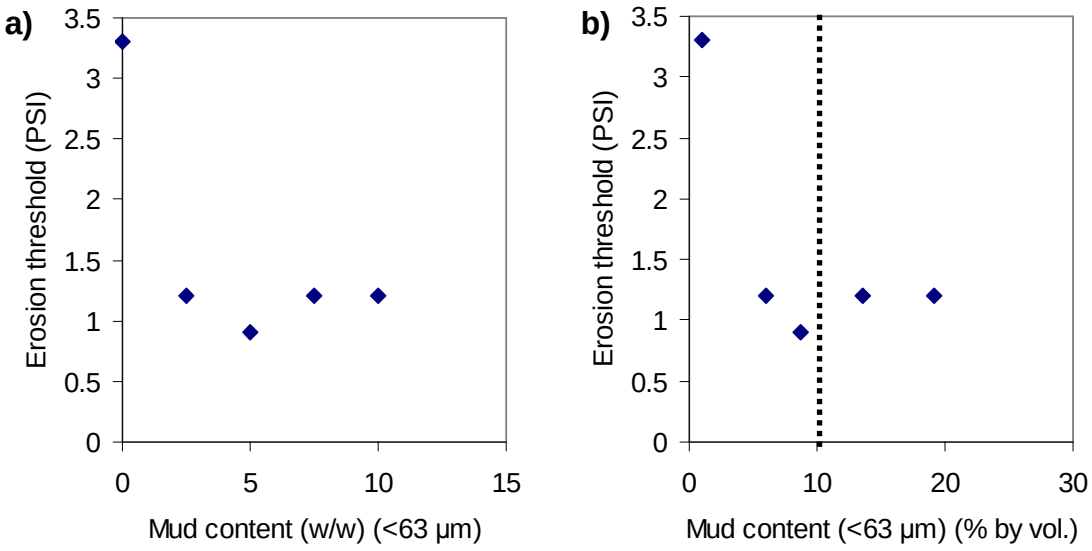

Figure 3.6. Erosion threshold as a function of (a) gravimetric or (b) volumetric mud content, using sieved Bere Stream mud (<63 μm). The minimum mud content was set at 10% by volume, and the data was filtered to remove samples with less than the minimum prior to analysis. Each data point represents the mean of 3 replicates. For more information, see Chapter 6 on the CSM calibration.

Shear Vane

The shear vane is a classic geomorphological device that measures the shear strength of soil (Serota & Jangle 1972, Goudie & Lewin 1990) (Fig. 3.7). It has also been recommended for the estimation of erodibility for sediments (Mehta & Parchure 2000). The Pilcon Hand Vane tester is a small handheld version equipped with two vanes, a small one (19 mm diam.) for consolidated samples and a wider one (33 mm diam.) for softer sediments (EDECO, England). To operate the tester, the vane is inserted into the sediment until just covered, and the dial is rotated at a constant rate (1 rev min^{-1}), until the sediment fails (i.e. the vane rotates freely in the sediment). Shear strength is indicated on the dial (kPa), and is a function of the torque applied at failure and the size of the vane.

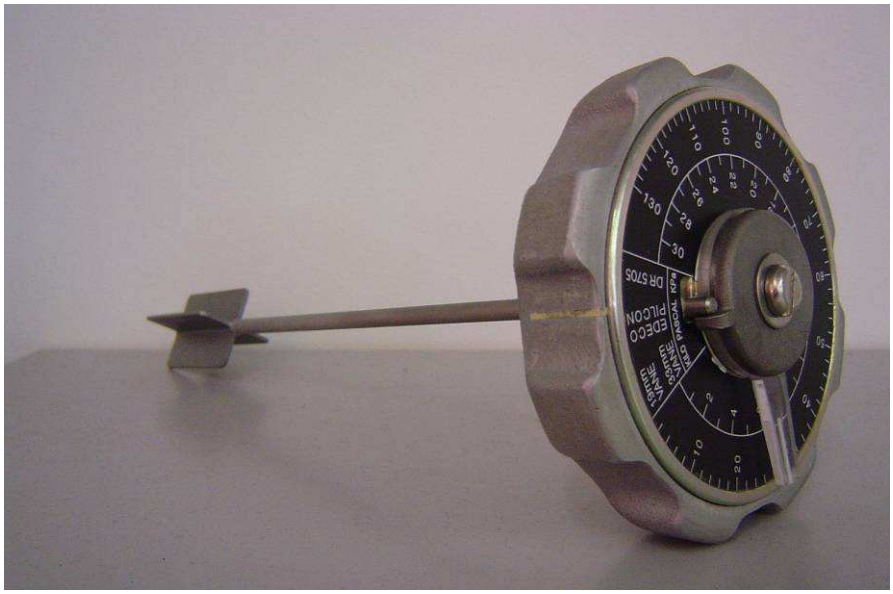

Figure 3.7. The Pilcon shear vane tester equipped with the wide, 33 mm diameter vane. The vane is inserted into the sediment, and the dial is rotated until the sediment fails, and the vane spins freely in the sediment.

3.2.4 Sediment coring and erodibility measurements in the field

At each sampling location, a large acrylic core tube (Φ 6.6 cm I.D.) was inserted into the sediment by hand, and the top sealed with a bung to stabilise the core (Fig. 3.8a). Shear vane measurements (n = 3) were taken adjacent to the core tube, within a 20 cm radius. The core tube was extracted from the sediment, a plunger (a rubber bung, Φ 6.6 cm O.D.) inserted at the base, and then sealed with a bung at the base (Fig. 3.8). If plant material was covering the surface of the sediment, it was cut or gently removed using tongs. The core tube was left to settle until CSM transmission levels exceed the 70% threshold (as established by the manufacturer), with a minimum wait time of 5 min and a maximum of 15 min. Care was taken to minimise sediment disturbance during extraction, and, in the majority of cases, the CSM could have been used immediately thereafter. Next, the CSM chamber was lowered into the core tube, and pressed into the sediment so that the flat base rested firmly on the sediment surface, which corresponded to a CSM jet height of 2 cm (Fig. 3.8b). After CSM analysis, the core was extruded upwards using the plunger and the top 3cm retained for laboratory analysis of sediment characteristics (Fig. 3.8c,d). The 3cm sediment core depth was selected as a compromise between the surface erodibility measurements of the CSM and the bulk erodibility of the shear vane. The sediment was stored on ice and transported back to the Physical Geography Laboratories at Queen Mary the same day. The sediment was stored at 4 ˚C for a maximum of 12 hours prior to laboratory analyses.

Figure 3.8. Field sampling in the Bere Stream, March 2009, (a) coring, (b) measuring erodibility with the CSM, (c) extruding the core using a plunger, and (d) collecting the top 3cm of sediment.

3.3 Laboratory component

Sediment samples were processed and analysed in the following order: (1) effective particle size analysis with fresh sediment, (2) samples were freeze-dried, (3) particle size analysis of very coarse sand and gravel fractions using sieves, and (4) retention of < 1mm fraction for the remaining laboratory analyses.

3.3.1 Sediment processing

Fresh sediment was used for effective particle size analysis and freeze-dried sediment for all other analyses. Sediment is commonly freeze-dried prior to laboratory analysis in sediment erodibility research (e.g. Underwood et al. 1995, Gerbersdorf et al. 2005). Dried sediments are precisely measurable in the laboratory, and the results from the analyses can be represented as a gravimetric content (e.g. g of chemical per g of sediment), or can be easily converted to concentrations based on dry bulk density. Freeze-drying was chosen over oven-drying because it produces dry, chemically stable samples, with minimal degradation to organic molecules like EPS (Underwood et al. 1995, Gerbersdorf et al. 2005).

The freeze-dried sediment samples were dry-sieved, and the mass of the gravel (> 2mm) and very coarse sand (1-2mm) fractions were recorded. Laboratory analyses focused on the < 1 mm fraction, for two reasons. First, preliminary trials showed that the inclusion of larger particles (1-2 mm diam.) caused an increase in the variation of laboratory measurements. This was particularly noticeable for particle size analysis with the laser diffraction size analyser, in which a few sand grains would substantially shift the particle size distribution. Second, sediment properties that influence cohesion and adhesion are primarily associated with silt and clay-sized particles (Section 2.3.1). However, dry sieving at 63 μm is not recommended for separating clays and silts from sands, and wet-sieving was ruled out to prevent dilution and alteration of chemical and biological properties (Rowell 1994). Therefore, a larger sieved size had to be used. Finally, processing sediment with a 1mm sieve has been used in previous studies in the Frome-Piddle catchment (Cotton et al. 2006, Heppell et al. 2009).The following is a summary of the laboratory methods used in this study, more complete methodologies can found in Appendix I.

3.3.2 Effective particle size

Fine particles rarely exist as individual mineral grains in natural sediment, and are more likely found combined into flocs and aggregates (Droppo 2001). Therefore, the diameter of natural aggregates (i.e. effective particle size) is increasingly being measured in sediment transport and erosion studies (Cotton et al. 2006, Heppell et al. 2009, Walling, & Amos 1999)

Effective particle size was analysed on fresh sediment cores, which were stored at 4 °C for less than 12 hours. The samples were gently mixed to homogenise the sediment, and a subsample was wet-sieved (1mm mesh size) directly into the test chamber of a Beckman Coulter LS 13 320 Laser Diffraction Particle Size Analyser. Effective particle size is reported as median diameter (d_{50}), based on sediment volume. Median particle size was corrected for the removal of 1-2 mm fraction, based on the dry mass of the fraction and converted to volume by using the particle density of sand, 2.65 g cm^{-3}. It was then recalculated using the Gradistat program (Blott & Pye 2001).

3.3.3 Absolute particle size

Particle sizes for sediment and soils are traditionally reported as absolute particle size, which is the diameter of the mineral fraction of the sediment (Rowell 1994). Absolute particle size is an important sedimentological characteristic because it describes the general mineralogy of the particles (i.e. clay, silt and sand) which has important implications for sediment erodibility (Sections 2.1 & 2.3.2)

Freeze-dried sediment was treated with hydrogen peroxide (30%) to remove organics and hexametaphosphate (i.e. Calgon) to disperse particles (Rowell 1994, Cotton et al. 2006). Particle size was measured with the Beckman Coulter LS 13 320 Laser Diffraction Particle Size Analyser. Absolute particle size is reported as median diameter (d_{50}), clay fraction (% < 4 μm), and mud fraction (% < 63 μm), based on sediment volume. Median particle size and the fractions were corrected for the removal of 1-2 mm fraction, based on the dry mass of the fraction and converted to volume by using the particle density of sand, 2.65 g cm^{-3}. The measures were then recalculated using the Gradistat program (Blott & Pye 2001)

3.3.4 Bulk properties

The bulk properties of the sediment are measures of the proportion of solid:liquid states in the sediment, and can be based on either volumetric or gravimetric approaches (Rowell 1994, Avnimelech et al. 2001). Bulk density is the overall density of the sediment (g cm^{-3}), and is dependent on both the particle density and the amount of water in a given volume of sediment (V_T). It can be calculated as wet bulk density (BD_W), based on hydrated sediment mass (M_{HS}), or dry bulk density (BD_D), based on dry sediment mass (M_{DS}), though the latter is more widely employed.

$$BD_w = \frac{M_{HS}}{V_T} \tag{3.3}$$

$$BD_D = \frac{M_{DS}}{V_T} \tag{3.4}$$

Porosity is the volume of pore space in the sediment, which for fully saturated sediment is equivalent to the volumetric water content. Gravimetric water content (WC) is a measure of the proportion of water (g) (M_W) to dry sediment (M_{DS}).

$$WC = \frac{M_W}{M_{DS}} \tag{3.5}$$

For this study, wet bulk density, dry bulk density and gravimetric water content are calculated based on the loss of water (g) due to freeze-drying. The samples were taken from the uppermost 3 cm of the core top (Φ 6.6 cm I.D.), so had a volume of 102.6 cm^3. Dry bulk density must be corrected for the small amount of the sample removed for effective particle size analysis (M_S), so equation 3.3 is modified as:

$$BD_D = \frac{M_{DS} + \frac{M_{DS}}{M_{HS}} * M_S}{V_T} \tag{3.6}$$

3.3.5 Cations

Water chemistry plays a prominent role in coagulation of clay minerals and the stabilisation of polymer networks (Sections 2.3.1 & 2.3.2). Thus, the chemical properties of the pore water have the potential to influence fine sediment stability, particularly molecules that reduce the electric double layer of clay minerals, such as Ca^{2+}, as well as those responsible for direct binding between particles (e.g. Fe and Mn). Water chemistry can vary longitudinally within a river or between rivers due to differences in catchment geology, terrestrial vegetation, and anthropogenic activity (e.g. Jarvie et al. 2005b).

A weak nitric acid digest is commonly used to extract the "reactive" (i.e. geochemically active) pool of metals from freshwater sediments (Tipping et al. 2003). Other techniques, such as aqua regia digestion, are more effective at extracting metals, but they liberate ions that are incorporated within the clay mineral lattices, which are unlikely to affect sediment erodibility.

Freeze-dried sediment (0.5 g) and 0.43 M HNO_3 (10 ml) were added to acid-washed centrifuge tubes (15 ml). The tubes were shaken for 2 hrs, centrifuged at 3000 RPM for 15 min, and the supernatant filtered through 0.2 μm PTFE filter. The supernatant was subsampled (0.5 ml) and diluted with HNO_3 by a factor of 10 (total 5ml), to reduce calcium concentrations to measurable levels and reduce the likelihood of matrix effects. Cation concentrations were measured using the Inductive Coupled Plasma – OES (ICP-OES), using matrix-matched multi-element standard spiked with calcium standard (Table 3.2). The specific sample dilution, standards and matrix-match selected for analysis were the result of a comprehensive trial conducted prior to the start of laboratory analysis.

Table 3.2. ICP standards using multi-element standard spiked with calcium

	Multi-element (ppm)	Calcium (ppm)
A	100	1000
B	50	500
C	25	250
D	10	100
E	5	50
F	2.5	25
G	1	10
H	0.1	1

Cation concentrations are reported as mass per unit volume of supernatant (e.g. PPM), and are converted to content (μg g^{-1} sediment) by multiplying them by the volume of HNO_3 added (0.01 L), by the dilution factor (10), and 1000 (to convert mg to μg) and dividing them by the dry mass of sediment used (ca. 0.5 g).

Sodium absorption ratio (SAR) is a non-dimensional measure of the proportion of monovalent to divalent cations in the sediment. Traditionally, it is calculated using cation concentrations (mmol/l) or milliequivalents (mEq). In this study, SAR was calculated from the cation contents using the following formula:

$$SAR = \frac{Na}{\sqrt{Ca + Mg}} \tag{3.7}$$

where cation contents (Ca, Mg, Na) are represented as molar content (mmol kg^{-1}), calculated by dividing cation contents by the atomic mass of the element (Rowell 1994). Another measure of relative monovalent:divalent cation concentration was also used, which was a simple ratio of cation contents (Na/(Ca + Mg)). Cations are principally associated with finest fraction of the sediment (< 63 um), which has the highest surface area-volume ratio, as well as the most electrochemically active surfaces. To correct for the strong correlation between grain size and cation content, a granulometric normalisation was also applied, in which cation contents were divided by the absolute mud content for the sample (Loring 1991, Luoma & Rainbow 2008).

3.3.6 Organic content

Natural sediment is always associated with organic compounds. The organic matter can be allochthonous or autochthonous, and can be in the form of living organisms (e.g. bacteria and meiofauna), EPS, detritus (e.g. leaf litter and humic compounds), or wastes (e.g. psuedofaeces and faecal pellets). Even in the coarsest sand beds, visibly devoid of organic material, each individual grain has a surface coating of organic polysaccharides, polymers and colloids (Johnson et al. 1994).

The quantification of organic matter is of importance for many areas of research, and as such several techniques are currently available. Loss on ignition (LOI) is the most commonly used method to approximate organic matter content (Aberle et al. 2006, Cotton et al. 2006, Heppell et al. 2009). In this technique, sediment samples are exposed to high temperatures (>325° C), and the loss of mass is a measure of organic content. It is an approximate measure, though, because the high temperatures used to burn off organic matter from a sample also cause clays and iron oxides to lose structural water. Consequently, LOI is not recommended for samples with high clay contents, particularly when they are low in organic contents. In general, sediments in the Frome-Piddle catchment have low clay contents (< 20%) (Heppell et al. 2009), so LOI was appropriate for the study.

Loss on ignition (LOI) was estimated according to the QMUL Geography 2006 protocol (Heiri et al. 2001). Freeze-dried sediment (5 g) was placed in a crucible, and incinerated at 550° C for 4 hours. Organic content (OC) is expressed as:

$$OC = \frac{M_{PS} - M_{IS}}{M_{PS}} \tag{3.8}$$

where M_{PS} is the pre-ignited freeze-dried sediment mass and M_{IS} is the mass after ignition.

3.3.7 Biofilms

Extracellular polymeric substances (EPS)

Extracellular polymeric substances (EPS) are compounds exuded into the sediment by infaunal organisms, particularly bacteria, diatoms, plants and meiofauna, during normal life functions (Underwood et al. 1995, Decho 2000). EPS is a diverse grouping of compounds that vary in chemical composition, size, solubility in water, and structural properties. Accordingly, there is no single technique that can extract all forms of EPS from a sediment sample.

In this study, the colloidal carbohydrate (i.e. water-soluble) EPS fraction was extracted and quantified according to Underwood et al. (1995). Freeze-dried sediment (100 mg) was placed in to 15 ml centrifuge tubes with 5 ml of deionised water. The centrifuge tubes were capped, placed horizontally on a flat-bed shaker, and allowed to mix for 15 min at room temperature. They were then centrifuged at 3500 g for 15 min. Next, 200 µl of the supernatant was pipetted into a clean centrifuge tube, along with 1 ml concentrated sulphuric acid and 200 µl 5% (w/v) phenol. The samples were left for 15 min at room temperature, transferred to cuvettes, and the absorbance was measured at 485 nm. A calibration curve was run with glucose standards (10, 20, 50, 100, 200, 500 g ml-1), and EPS contents are expressed as glucose equivalents (µg glucose g^{-1} sediment).

Comprehensive trials were conducted to develop a more general approach to the quantification of EPS. Alcian blue is a common histological dye that brightly stains polysaccharides, particularly acidic polysaccharides such as mucopolysaccharides (i.e. glycoproteins) (Gurr 1960). The stain has been used to visualise and quantify transparent extracellular polymers (TEP) in the open waters of lentic and marine environments for over 15 years (Alldredge et al. 1993, Logan et al. 1994, Passow 2002, Simon et al. 2002, Verdugo et al. 2004). TEP and EPS are the same material and the difference in name simply reflects historical differences in terminology between practitioners of pelagic and benthic research.

Freeze-dried sediment (100 mg) was hydrated with water (5ml), and then stained with an acidic solution of alcian blue (0.2 % alcian blue in 0.06% acetic acid) (Thornton et al. 2007). The sample was allowed the rest for 1 hr, then was centrifuged (10 min, 3000RPM), filtered through a 0.2 µm membrane filter, and the supernatant was measured colorimetrically (625nm). The colour of the supernatant was inversely

proportional to the amount of EPS retained by the filter. EPS content was calibrated using xanthan gum solution, so was expressed as equivalent xanthan gum (μg xanthan gum g^{-1} sediment).

Unfortunately, the operational range for the technique was too narrow. A given concentration of alcian blue produced a usable calibration curve for a range of 60-120 μg xanthan gum. This range was sufficient for the water samples studied in Thornton et al. (2007), but the sediment samples contained a much wider range of EPS contents. To resolve this problem, the amount of alcian blue solution added to the sediment was varied, from 0.1 to 1.2 ml. Every additional alcian blue amount necessitated a new calibration curve, making it impossible to run a calibration anew for each set of samples. Therefore, one master calibration was derived to correlate absorbance with xanthan gum content for each alcian blue amount. When the technique was implemented on the sediment samples from the survey, it quickly became apparent that the major problem with this approach was an inability to predict how much alcian blue to add to each sediment sample. Several solutions were attempted (e.g. incremental increases in alcian blue, and preliminary trials on subsamples along with a correlation to particle size), but were abandoned because of concerns about variable staining times and logistics. An alcian blue technique for the quantification of EPS in sediments has potential, but considerable more development work is needed.

Chlorophyll-a

Autotrophic microbial communities are a major producer of EPS in aquatic sediments, so have the potential to greatly impact sediment erodibility. Whilst any change in the species composition or activity of the community can potentially impact EPS quantities and forms (Sutherland 2001, Pamp et al. 2007), the overall abundance of the autotrophic community, as measured by chlorophyll-a content, has been shown in laboratory and field studies to have a significant positive correlation to EPS content (Sutherland et al. 1998b, Widdows et al. 2000, Gerbersdorf et al. 2005).

Chlorophyll-a is extracted from sediment samples using acetone, and can be quantified with a spectrophotometer or high pressure liquid chromatography. The US EPA method 446 for the spectrophotometer was used in this study (USEPA 1997). Freeze-dried sediment (100 mg) was placed into 10ml centrifuge tubes covered in aluminium foil, to which 4.5 ml of acetone was added. The centrifuge tubes were sealed and placed

horizontally on a flatbed shaker (120 rpm) for 1 hr. They were left overnight in a fridge (4˚ C), then centrifuged for 10 in at 3000 rpm. The supernatant was decanted into quartz cuvettes and chlorophyll-a was quantified using the spectrophotometer and the Lorenzen Pheopigment correction. Absorbance was measured at 750 nm for turbidity and 664 nm for chlorophyll-a. Then 0.09 ml of 0.1 N HCL was added and aspirated with a clean disposable pipette. After 90 seconds, absorbance was measured at 750 and 665 nm. Chlorophyll-a content (Chla) (μg g^{-1} sediment) is calculated as:

$$Chla = 26.7(A_{664} - A_{665}) * (\frac{0.0045}{S}) * 1000 \quad (3.9)$$

where A_{664} is the absorbance at 664 nm (minus absorbance at 750 nm) measured before acidification, A_{665} is the sample absorbance at 665 nm (minus absorbance at 750 nm) measured after acidification, and S is the sediment sample mass (g) (USEPA 1997).

3.3.8 Macrophyte roots and rhizomes

Macrophyte roots have been shown to increase the erosion resistance of soils (Gyssels et al. 2005, Simon et al. 2006). Whilst they are unlikely to affect the surface erodibility of the sediment as measured by the CSM, they could impact the bulk erodibility as measured by the shear vane. As no research has been conducted on the effects of roots on sediment erodibility (as opposed to hydrodynamic effects), a simple classification was proposed to quantify root density. Root index was an ordinal variable that classified the amount of roots in a sediment sample ranging from 0 to 4. A sample with no roots was designated 0; with very few roots, 1; with a moderate amount of roots, 2; with abundant roots, 3; and 4 was used when the sample was predominantly roots with a small amount of sediment.

3.4 Data Analysis

The large dataset of erodibility measurements, environmental variables and sediment properties was analysed using a range of multivariate statistical techniques. For research questions 1a and 1b, spatial and temporal patterns in erodibility were analysed by ANOVA and non-parametric equivalents, as well as regression trees. For research questions 2a and 2b, the sediment properties responsible for variations in sediment erodibility were analysed using correlations, regression trees, linear regression, and

mixed effects models. Analyses were conducted using the statistical software packages SPSS and R (R Core Development Team 2009). Full details of the analytical methods and justification for their use are described in the results and discussion chapters (Chapters 4 & 5).

Chapter 4: Spatial and temporal variations in erodibility

This chapter presents the fine sediment erodibility measurements collected during the field survey. The bimonthly, yearlong survey was conducted from July 08 to July 09 on two reaches in the Frome-Piddle catchment, the Bere Stream at Snatford Bridge and the River Frome at Frome Vauchurch. Paired sediment cores and sediment erodibility measurements (n = 20) were taken using a stratified random strategy within areas of fine sediment accumulation. These measurements were accompanied by ecological and environmental information for the sampling location, including macrophyte presence and species, water depth, and water velocity. First, a general description of the sediment is presented (Section 4.1). Then, the spatial and temporal patterns in erosion thresholds are reported (Sections 4.2 & 4.3). Within these sections, the environmental and sediment data are described first, then the cohesive strength meter (CSM)-derived erosion thresholds, and finally the vane-derived shear strength values. Next, results from regression tree analyses are presented that identify the key environmental variables responsible for the variations in erodibility (Section 4.4). Finally, the spatial and temporal patterns are summarised (Section 4.5).

4.1 General description of sediment

The sediment studied in the field survey ranged from medium sand to fine silt, reflecting the high spatial heterogeneity in sediment properties found within the reaches The sediments had high silt:clay ratios, and were predominantly classified as sandy silts and silty sands, according to Folk (1954) (Fig 4.1) (c.f. Blott & Pye 2001). Differences between channel and marginal sediment were visually apparent (Fig 4.2). Channel sediment had on average larger particle sizes and higher bulk density than marginal

sediment. Plasticity was not measured, but clay contents for most of the sediment samples were in excess of the minimum threshold needed for cohesion of sand-mud mixtures (Fig 4.3) (van Ledden et al. 2004). However, samples with high clay contents typically had low bulk densities, whilst high density samples had high sand contents and low clay contents (Fig. 4.4). van Ledden et al. (2004) developed a framework to predict whether sand-mud mixtures will erode in cohesive or non-cohesive manners. They estimated the threshold bulk density for cohesion for sediments with a range of clay contents and silt/clay ratios. Figure 4.4 displays the field survey data against the classification and plasticity data from van Ledden et al. (2004). Whilst the plasticity of the field survey sediment samples probably differs from the marine sediment tested in that study, Figure 4.4 suggests that the most of the sediment samples may erode in a non-cohesive manner. In the interest of an accurate description of the sediment, the term 'fine sediment' will continue to be used, as opposed to 'cohesive' or 'fine-grained' (Section 2.1).

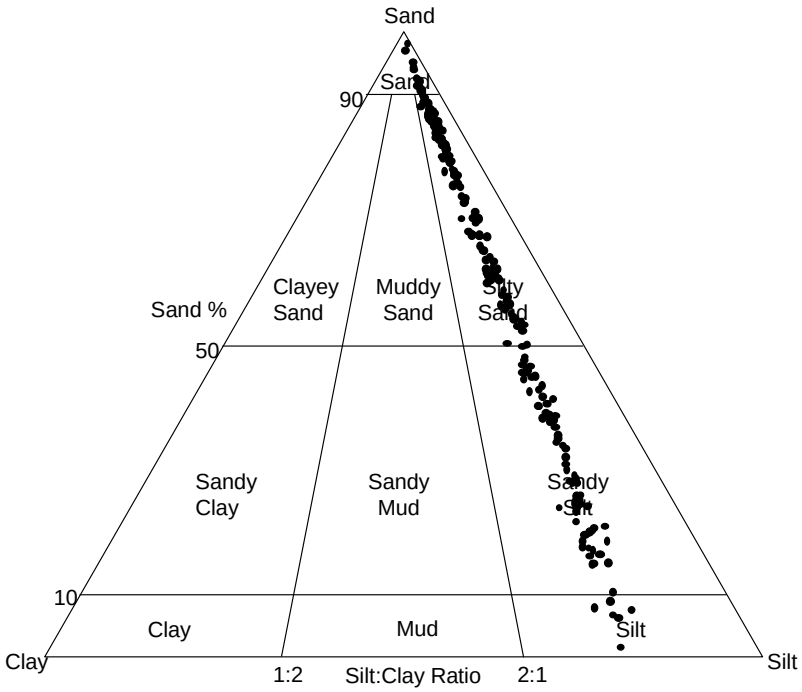

Figure 4.1. Sediment texture analysis for all sediment samples, according to Folk (1954) (c.f. Blott & Pye 2001).

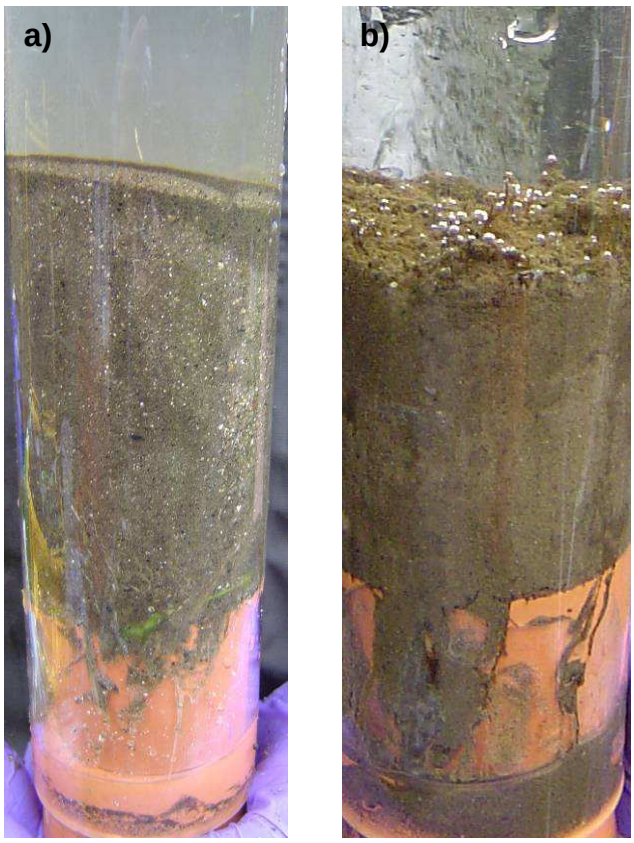

Figure 4.2. Examples of sediment cores taken from the (a) channel centre and (b) margin in the Bere Stream. Note: the channel sediment is sandier than the marginal sediment, and an abundant autotrophic microbial community is visible at the surface of the marginal sediment.

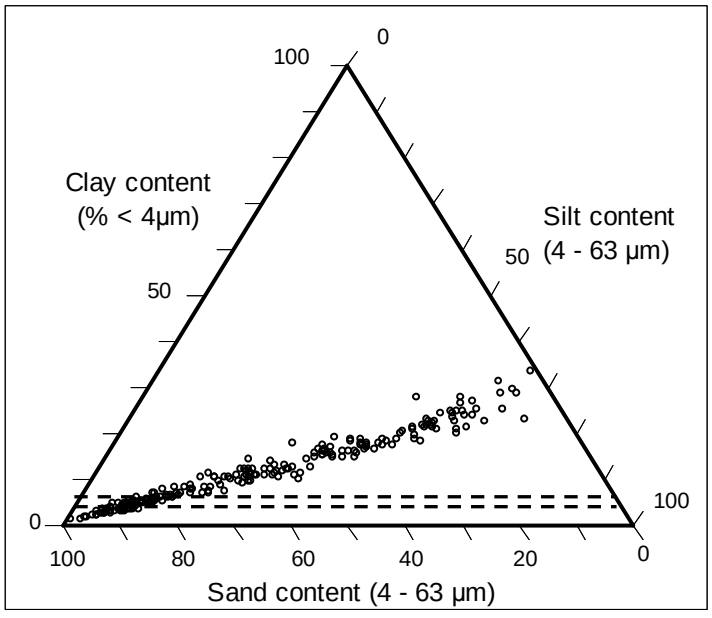

Figure 4.3. Tri-plot of clay, silt and sand contents for all sediment samples. The dashed lines indicate the minimum clay contents needed to produce cohesive sediment (4-7%) (van Ledden et al. 2004)

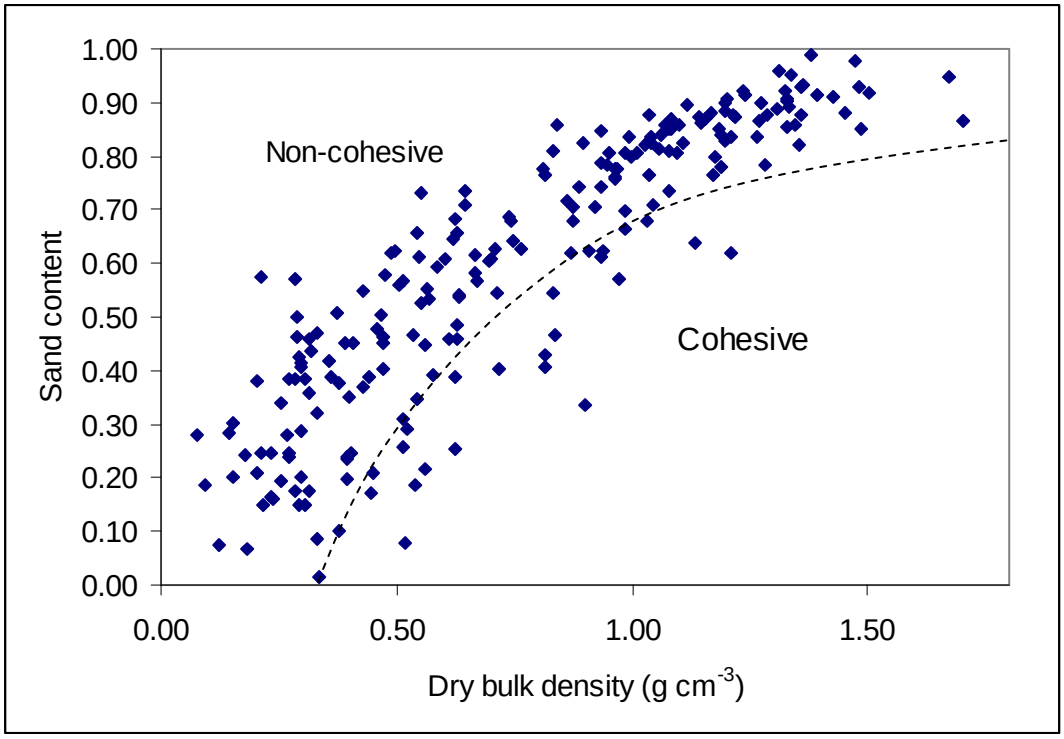

Figure 4.4. A classification of sediment samples as cohesive or non-cohesive based on sand content, bulk density, and the ratio of clay to silt content. The dashed line differentiates cohesive vs. non-cohesive sediment, based on a clay/silt ratio of 0.45, the average for this study, and the empirical plasticity data of van Ledden et al. (2004).

A total of 220 paired sediment cores and CSM erodibility measurements were taken over 6 site visits; January 2009 sampling was aborted for the River Frome due to dangerously high flows. As erosion thresholds are estimated using an optical measure of resuspension, the sediment must contain a minimum mud content (< 63 μm fraction) for the CSM to function properly (for more information, see Sections 3.2.3 & Section 6.3.1). A minimum mud content of 10% was selected based on laboratory trials, excluding 12 samples from analysis. A further 8 samples were removed due to concerns about errors in CSM testing or sediment coring and processing. Out of the remaining data, 15 samples were excluded from analysis because high turbidity levels lowered background transmissometer readings below the manufacturer's recommended threshold. Finally, 31 samples had erosion thresholds lower than the detection limit of the CSM. These null values provide important information on sediment erodibility, so they should not be excluded, but as they do not represent a true zero, the thresholds were corrected to half the value of the lowest detectable erodibility limit (0.15 PSI). In total, 185 samples are included in the following analyses.

4.2 Spatial variations in erodibility

4.2.1 Descriptions of environmental variables and sediment properties

Environmental conditions varied within the study reaches and between the streams, affecting the location of surficial sediment deposits and sediment properties. Fine sediment deposits in the channel centres were found predominantly under stands of the submerged macrophyte *Ranunculus* within both streams (Figs. 4.5 - 4.7). In the Bere Stream, approximately 30% of channel deposits were located within stands of the emergent macrophyte *Rorippa*. In the River Frome, almost all were located within *Ranunculus* stands. Margins were more mixed than the channel centres. In the Bere Stream, *Rorippa* was the dominant species in the margins, followed by *Apium nodiflorum* (Figs. 4.5 & 4.6), whilst in the River Frome, margins were dominated by riparian vegetation, namely *Rubus*, whose stems trailed into the water (Figs. 4.5 & 4.7). Root index was comparable between channel and margins in the Bere Stream, but was substantially lower in the Frome margins (Fig. 4.8). On average water velocities were similar between the streams, but sampling locations within the channel centres had greater water velocities than those in the margins for both streams (Fig. 4.9).

The location of the sediment deposit within the reach had a strong influence on sediment properties. Sediment deposits within the channel centres were coarser-grained and denser than within the margins in both streams (Fig. 4.10). This is due to the greater sand contents found in the channel deposits (Fig. 4.11). On average, sediment in the Bere Stream had greater mud contents (% < 63 μm) than in the River Frome. Normalised cation concentrations were generally greater in the channel centres than in the margins, and in the Bere Stream than in the River Frome (Fig. 4.12a,b,c). Normalised iron content, though, showed a different pattern; it was similar in channel centres and margins, but higher in the Frome than in the Bere Stream (Fig. 4.12d). SAR and normalised M:D ratio were very low (Fig 4.12e,f). SAR was higher in the Bere Stream than River Frome. Normalised M:D is highest in the channel centre of the Bere Stream, but comparable for the other categories. Organic content and colloidal carbohydrate contents were greater in the margins than channel for both streams (Fig. 4.13a,b). Sediment in the Bere Stream had greater organic contents and colloidal carbohydrate contents than the River frome for both the channel centres and margins. Chlorophyll-a content was similar for channel and marginal sediment in Bere Stream, but was substantially lower in the channel in the River Frome (Fig. 4.13c).

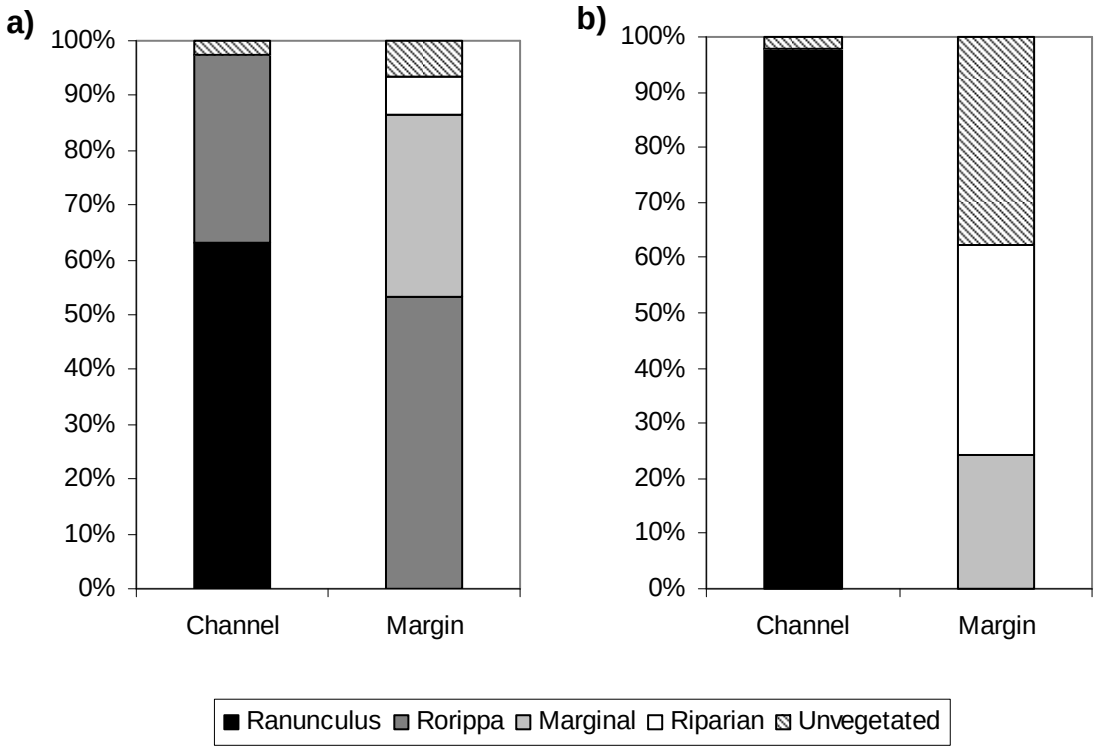

Figure 4.5. Spatial variations in the relative location of fine sediment within the channel according to macrophyte type, by channel centre and margins for the (a) Bere Stream and (b) River Frome. The sampling strategy was stratified random within areas of sediment deposition, therefore, this figure depicts where sediment is found within the stream and not the relative abundance of macrophytes. Ranunculus is a submerged macrophyte; Rorippa is an emergent macrophyte; Marginal is a grouping for all non-Rorippa marginal plant, such as Apium; Riparian is a grouping for terrestrial plants with stems trailing in the water, and Unvegetated is bare sediment without macrophyte cover.

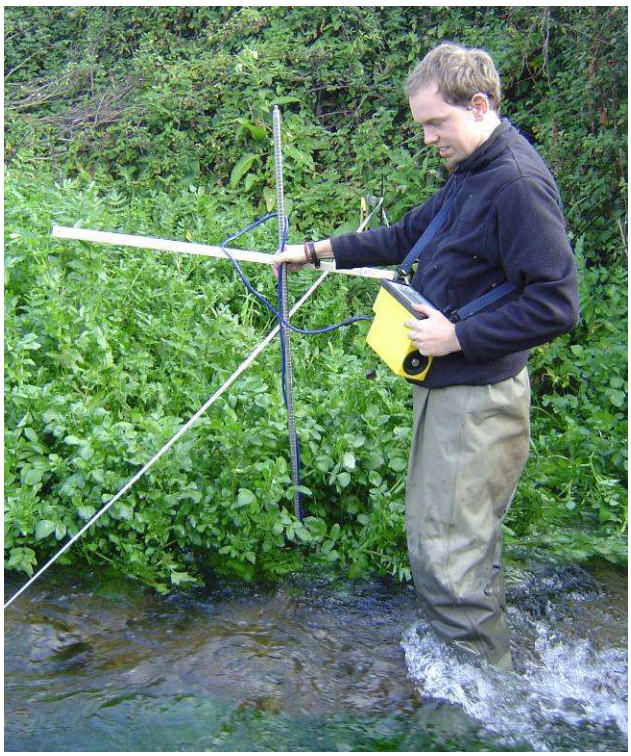

Figure 4.6. The Bere Stream in September 2008. G. Davies is taking water velocity measurements. Behind him, along the margins are the emergent macrophytes, Rorippa and Apium. In the foreground, submerged below the water surface in the channel centre is Ranunculus.

Figure 4.7. The River Frome in September 2008. Ranunculus stands are abundant in the channel centre. In the background, brambles (Rubus) line the left bank with their stems trailing into the water. The channel is 8 m wide.

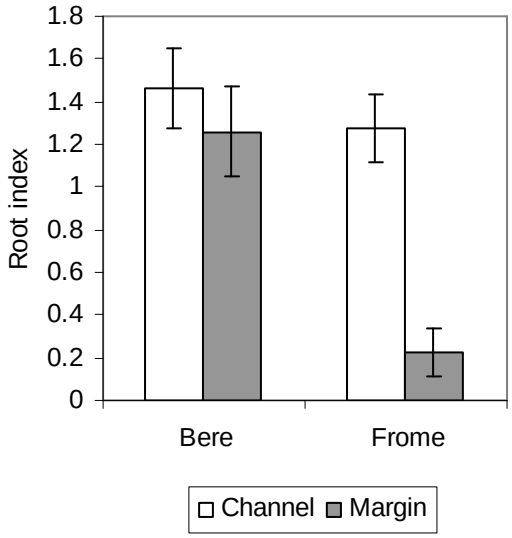

Figure 4.8. Spatial variations in mean root index by stream and channel location. Root index is an ordinal measure of macrophyte root density, ranging from 0 for no roots to 4 for a dense root mass. Error bars are one standard error.

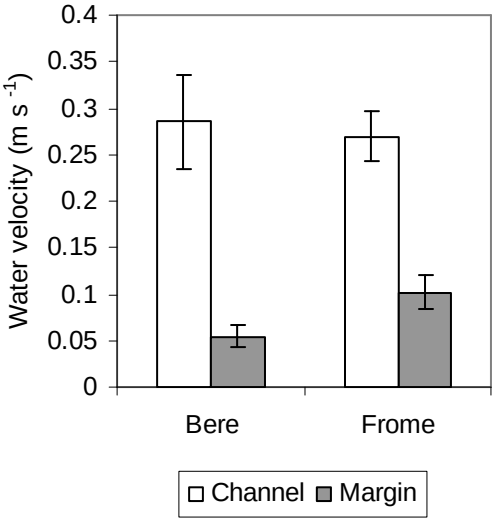

Figure 4.9. Spatial variations in mean water velocity for sampling locations in the channel and margins in the Bere Stream and River Frome. Water velocity measurements were taken at 60% of water depth from the water surface. Error bars are one standard error. For a more detailed representation of cross-stream variations in velocity, see Appendix II.

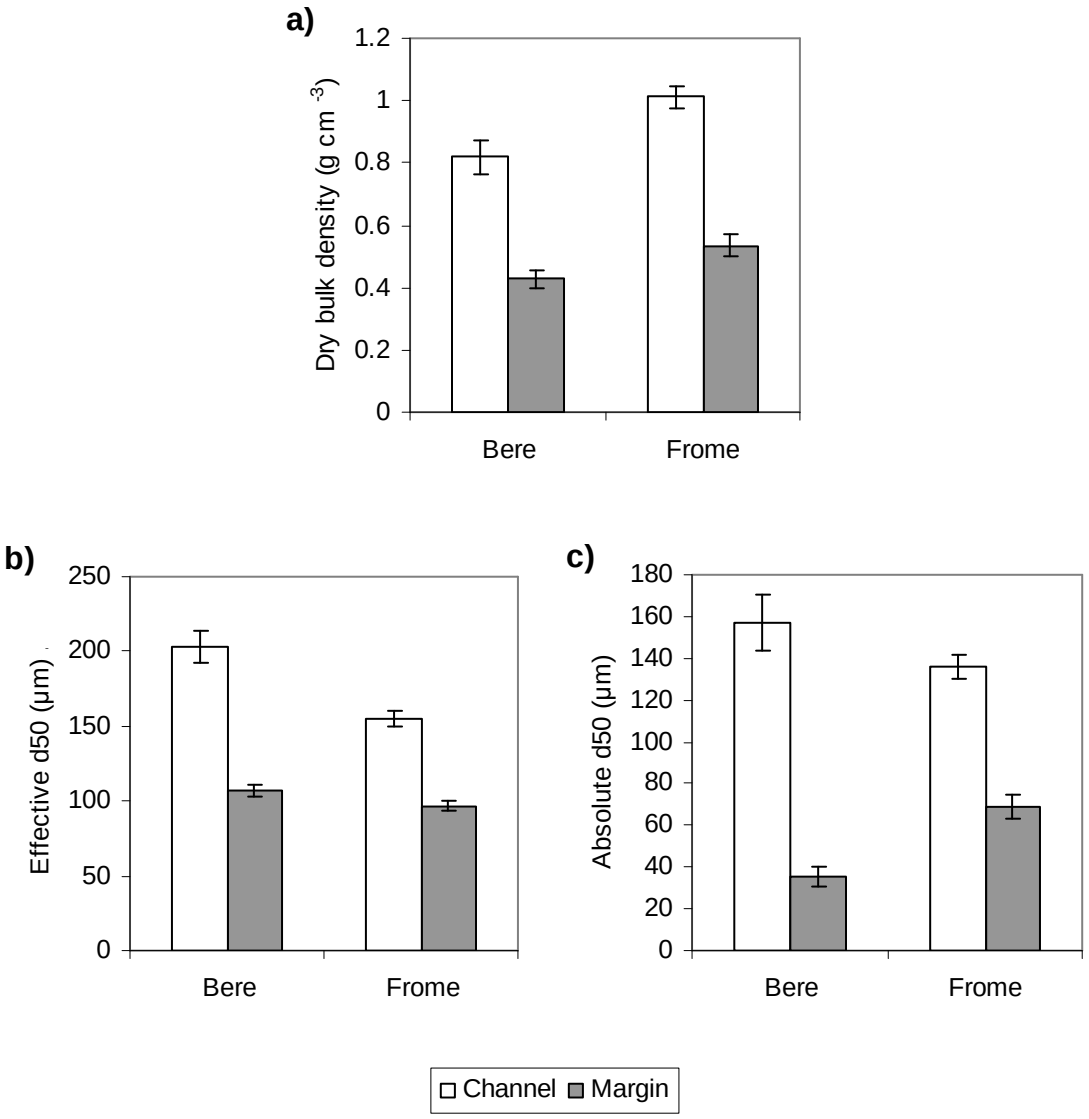

Figure 4.10. Spatial variations in physical sediment properties by stream and location within the channels. (a) Mean dry bulk density, (b) median effective particle size (Effective d50), and (c) median absolute particle size (Absolute d50). Error bars are one standard error.

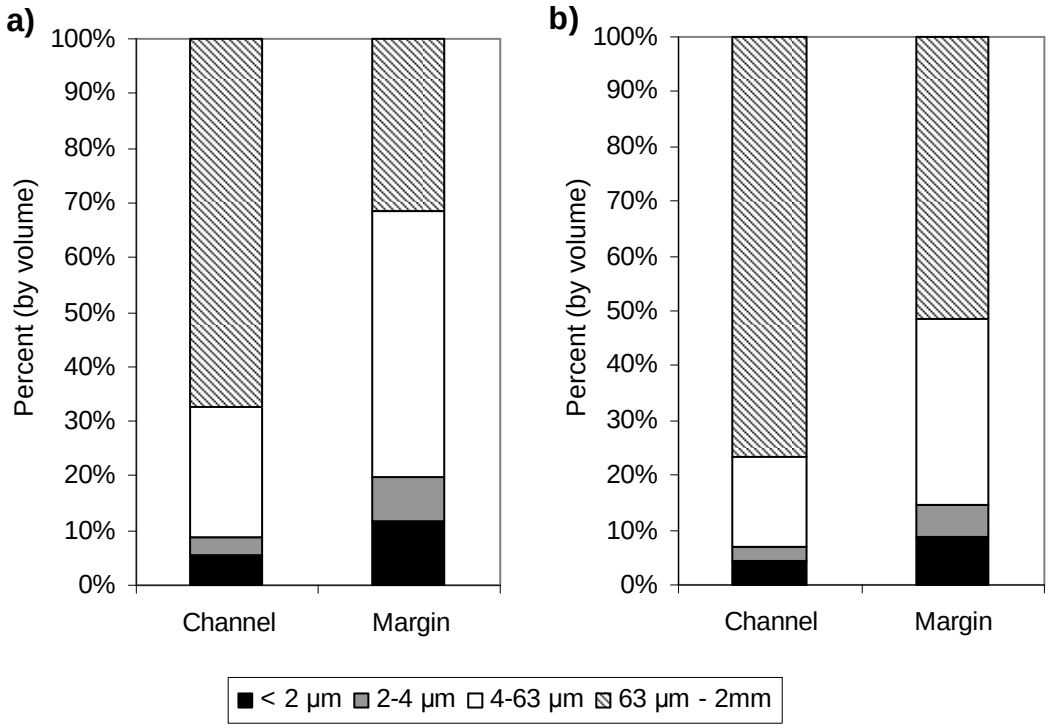

Figure 4.11. Spatial variations in absolute particle size distributions by channel and margin for the (a) Bere Stream and (b) River Frome. Particle size is represented as percent by volume.

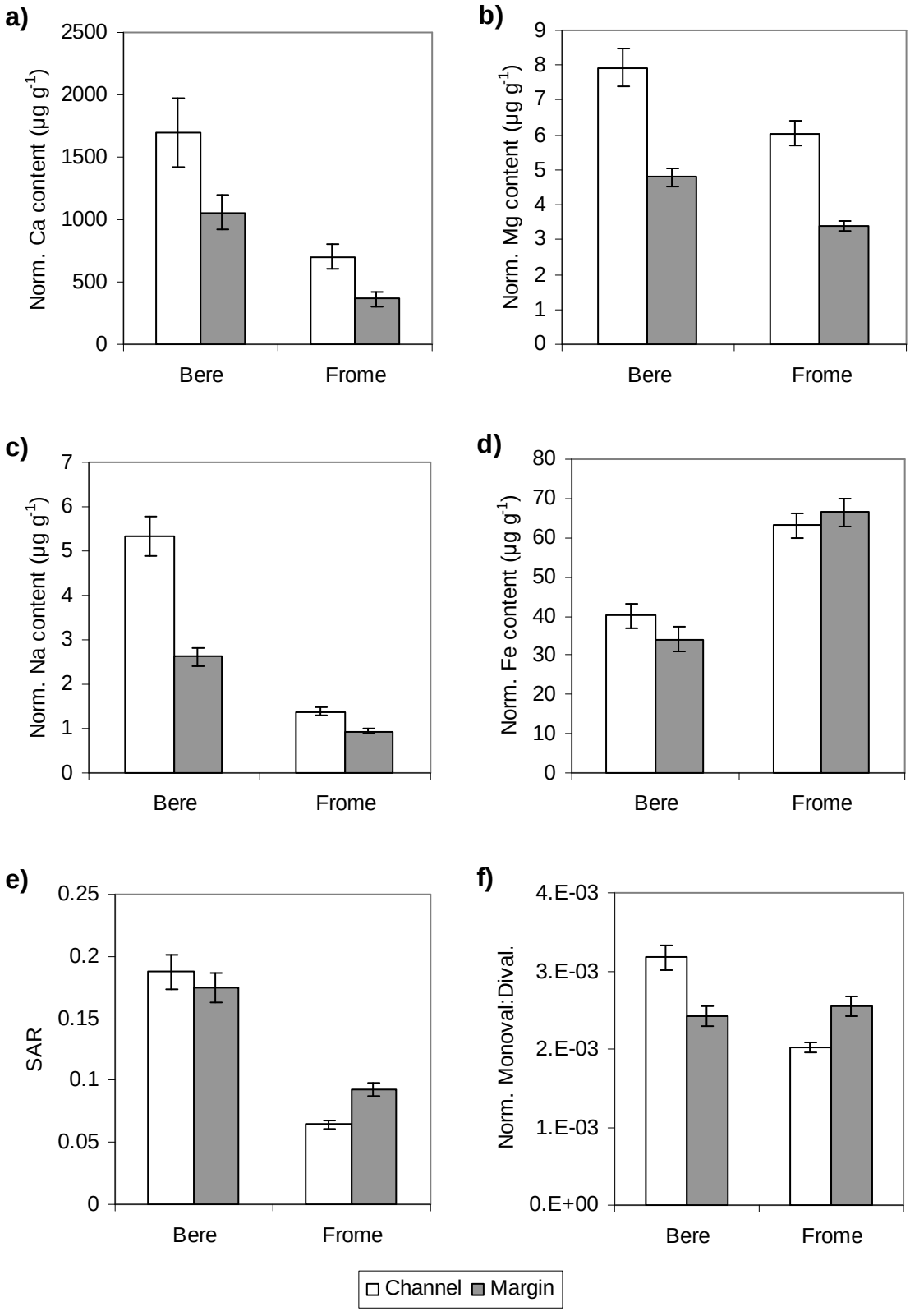

Figure 4.12. Spatial variations in chemical sediment properties by stream and location within the channel. Normalised cation contents for (a) calcium, (b) magnesium, (c) sodium, (d) iron (µg g^{-1} sediment, normalised by absolute mud content), (e) sodium absorption ration (SAR) and (f) the ratio of monovalent to divalent normalised cations by stream and location within the channel. Error bars are one standard error.

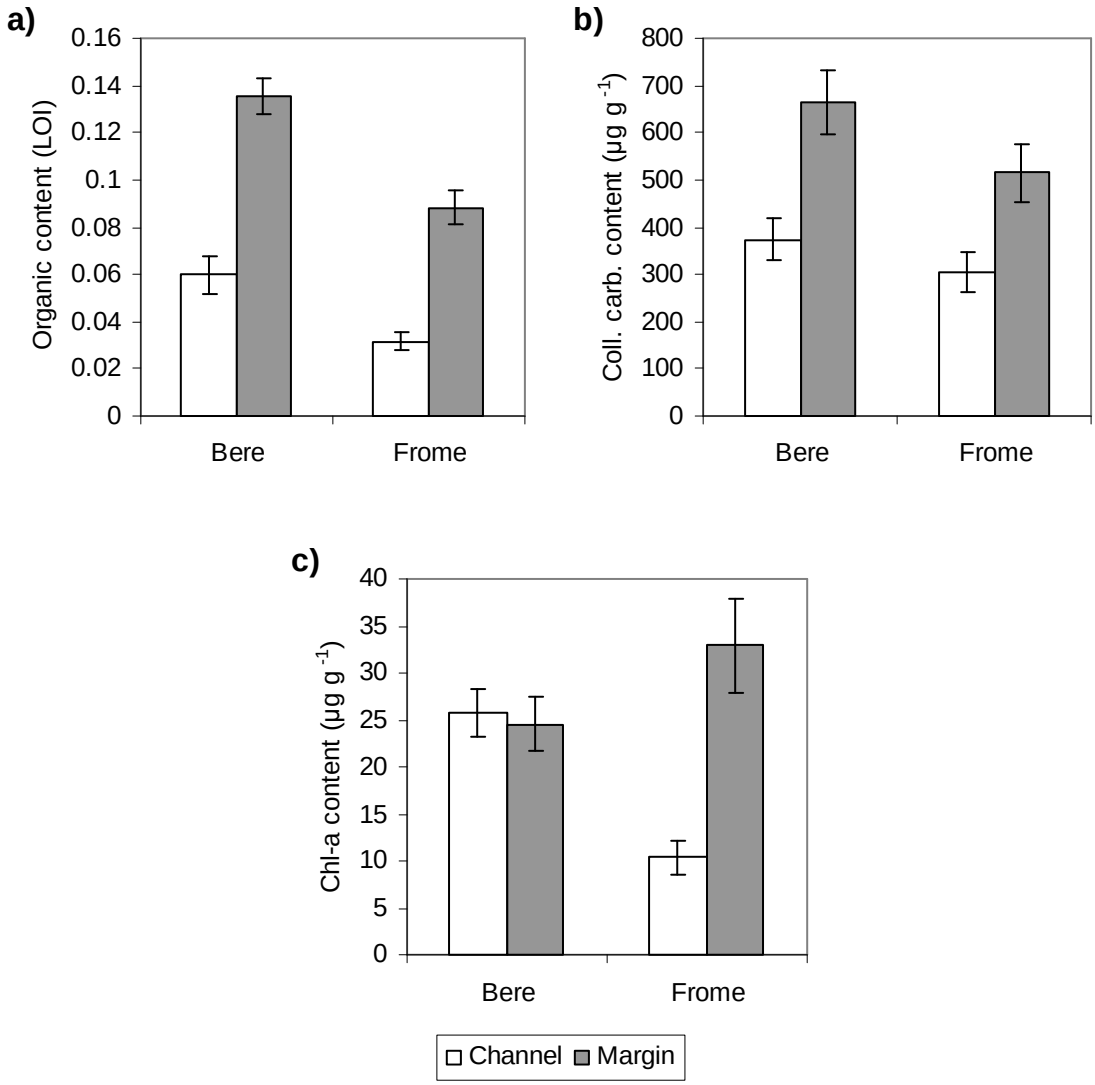

Figure 4.13. Spatial variations in biological sediment properties by stream and location within the channel. (a) Organic content, (b) colloidal carbohydrate content, and (c) chlorophyll-a content. Error bars are one standard error.

Sediment properties also varied depending on the presence and type of macrophyte at the sampling location. *Ranunculus* was found exclusively in the channel centres (Fig. 4.5), and was subjected to the greatest water velocities (Fig. 4.14a). Macrophyte species found in the margins experienced substantially lower water velocities. *Rorippa* was found in both the channel and margins, but water velocity were the same on average in both locations. *Rorippa* preferentially colonises areas of slow moving water (Haslam 2006), and it can annually succeed *Ranunculus* in the channel centres once a substantial sediment deposit formed (pers. obs.). Dry bulk density was greatest in the unvegetated channel centres, followed by *Ranunculus* and *Rorippa* in the channel centres (Fig. 4.14b). It was lowest for macrophytes growing in the margins. The patterns for effective and absolute particle size (Fig. 4.15) were similar to dry bulk density (Fig. 4.14b). Sand content was greatest for unvegetated sediment in the channel centres, followed by *Ranunculus* and *Rorippa* (Fig. 4.16). Sand content was much lower in the margins (Fig. 4.16a), and a declining trend was observed from rooted plants in the margins (*Rorippa* and Marginal) to non-rooted Riparian to bare unvegetated sediment (Fig. 4.16b).

Normalised calcium, magnesium and sodium contents were highest in the channels, and showed a declining trend from root to unrooted marginal groupings (4.17a,b,c). Normalised iron content was highest in *Ranunculus*, lowest in *Rorippa*, and showed an increasing trend from rooted to unrooted marginal groupings (4.18a). SAR and normalised M:D were highest in *Rorippa*, low in *Ranunculus*, with a slight declining trend from rooted to unrooted marginal groupings (Fig. 4.18b,c).

Organic and colloidal carbohydrate contents were greatest under macrophytes in the margins, and a similar declining trend was observed from rooted to unrooted groupings (Fig 4.19a,b). Chlorophyll-a content was lowest in the *Ranunculus* and unvegetated channel centres, highest in the unvegetated margins, and intermediate in the other groupings (Fig. 4.19c). Root index was highest in the Bere Stream in *Ranunculus*, *Rorippa* and Marginal (Fig. 4.20a). It was comparable between streams in *Ranunculus*, but was considerably lower in marginal for the River Frome. Riparian and unvegetated had substantially lower root indices than other groups found in the margins (Fig. 4.20b).

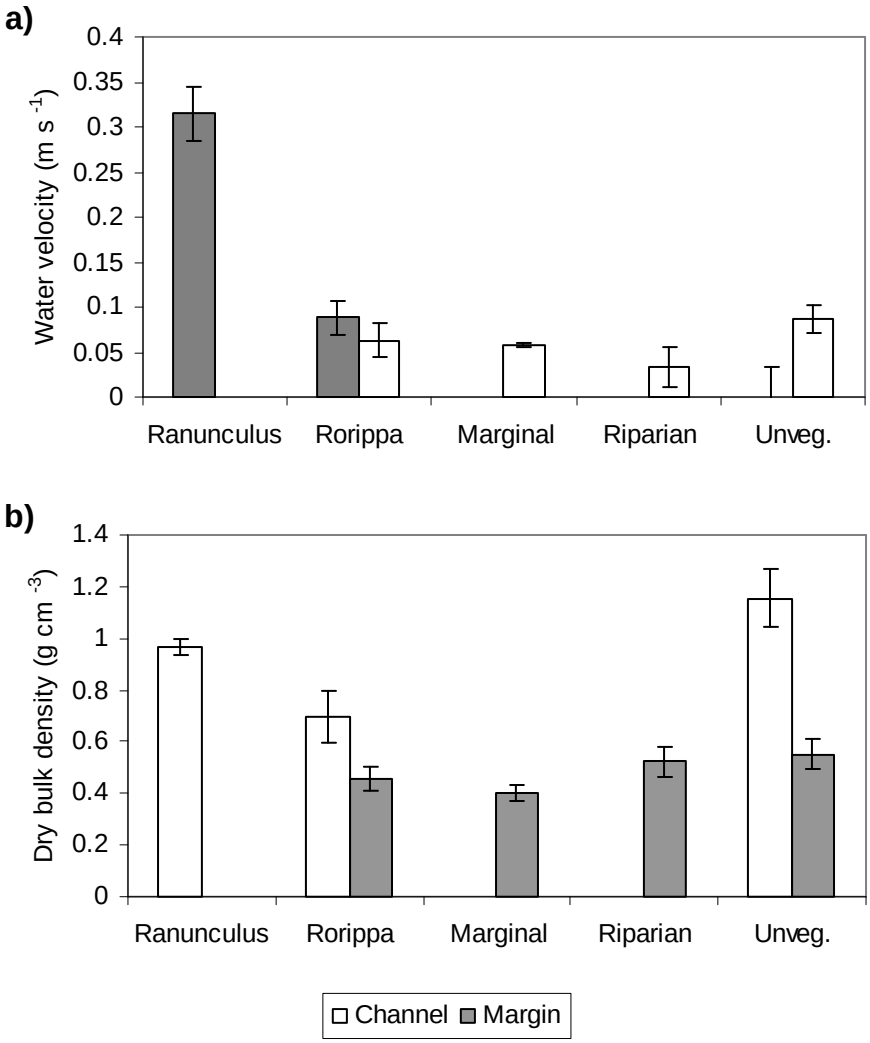

Figure 4.14. Spatial variations in (a) mean water velocity and (b) dry bulk density by macrophyte type and location within the channel, for both streams. Ranunculus is a submerged macrophyte; Rorippa is an emergent macrophyte; Marginal is a grouping for all non-Rorippa marginal plant; Riparian is a grouping for terrestrial plants with stems trailing in the water, and Unveg. is bare sediment without macrophyte cover. Error bars are one standard error.

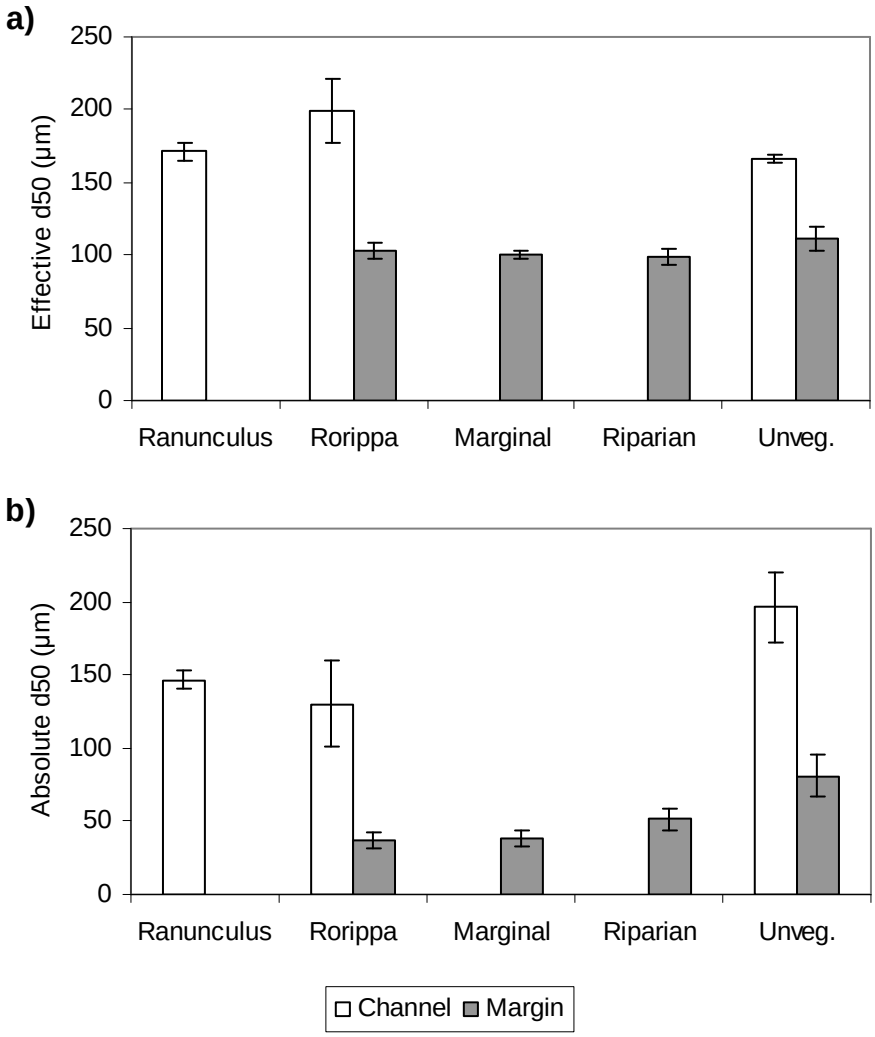

Figure 4.15. Spatial variations in median particle size by macrophyte type and location within the channel, for both streams, (a) effective particle size (Effective d50) and (b) absolute particle size (Absolute d50). Ranunculus is a submerged macrophyte; Rorippa is an emergent macrophyte; Marginal is a grouping for all non-Rorippa marginal plants; Riparian is a grouping for terrestrial plants with stems trailing in the water, and Unveg. is bare sediment without macrophyte cover. Error bars are one standard error.

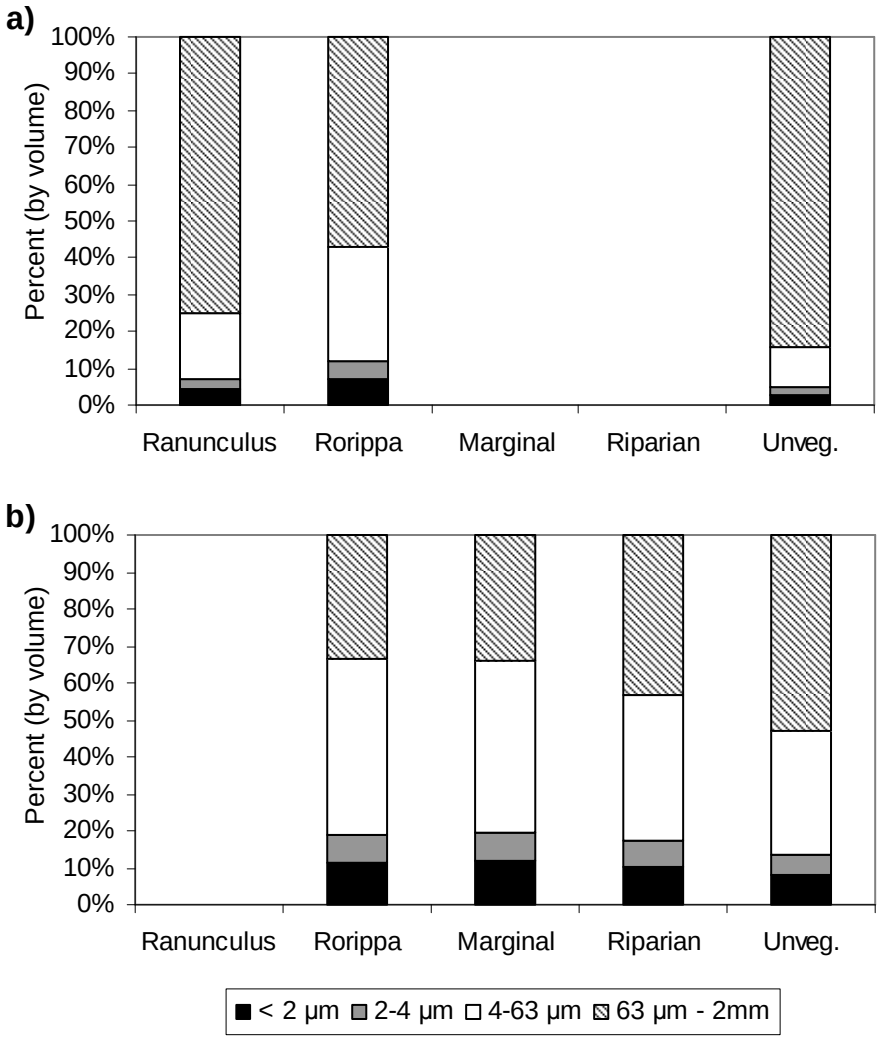

Figure 4.16. Spatial variations in absolute particle size distributions by macrophyte type and location within the channel, for both streams, (a) channel centre and (b) margins. Particle size is represented as percent by volume. Ranunculus is a submerged macrophyte; Rorippa is an emergent macrophyte; Marginal is a grouping for all non-Rorippa marginal plants; Riparian is a grouping for terrestrial plants with stems trailing in the water, and Unveg. is bare sediment without macrophyte cover.

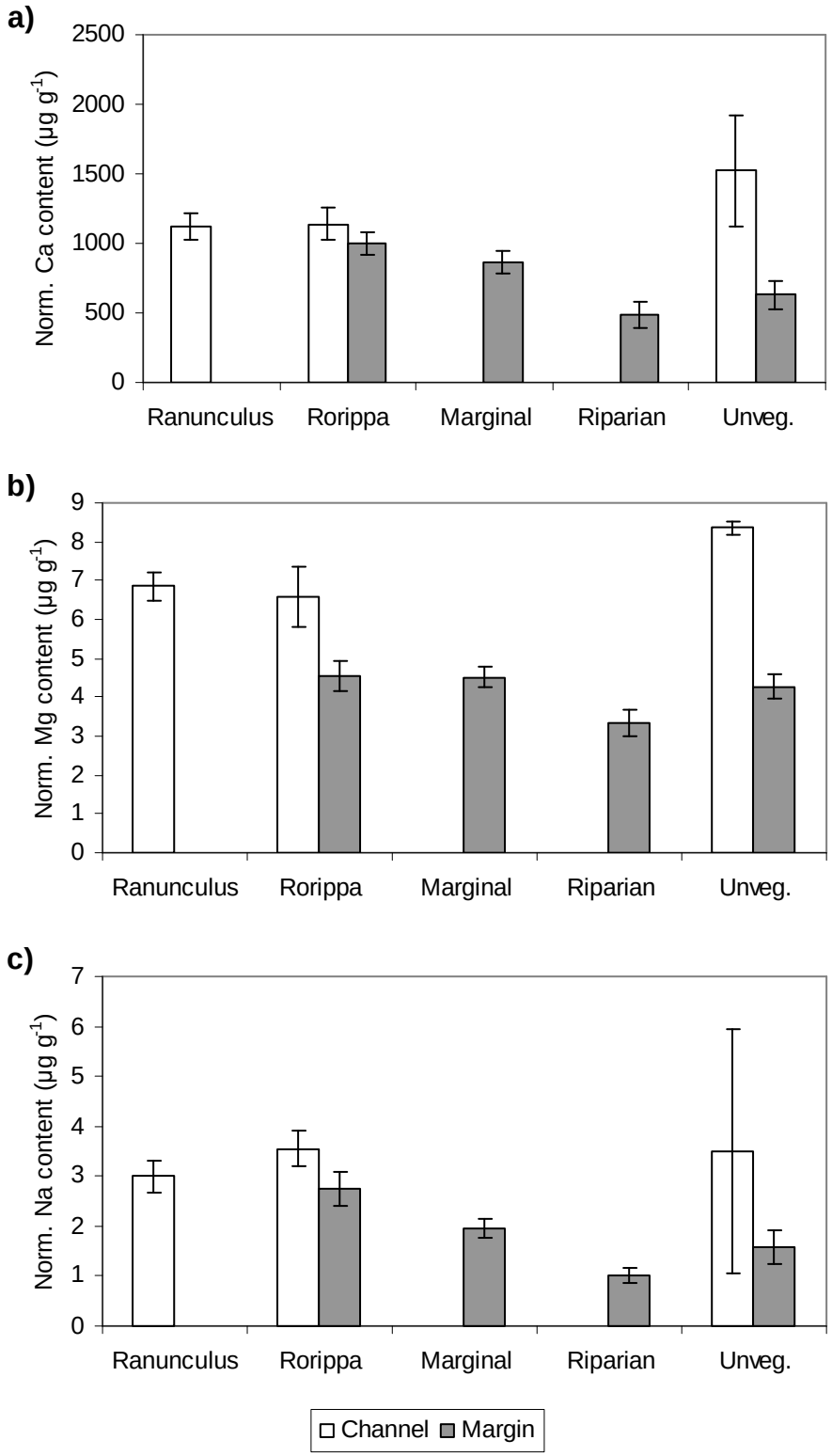

Figure 4.17. Spatial variations in normalised cation contents by macrophyte type and location within the channel, (a) calcium, (b) magnesium, and (c) sodium, (µg g^{-1} sediment). Ranunculus is a submerged macrophyte; Rorippa is an emergent macrophyte; Marginal is a grouping for all non-Rorippa marginal plants; Riparian is a grouping for terrestrial plants with stems trailing in the water, and Unveg. is bare sediment without macrophyte cover. Error bars are one standard error.

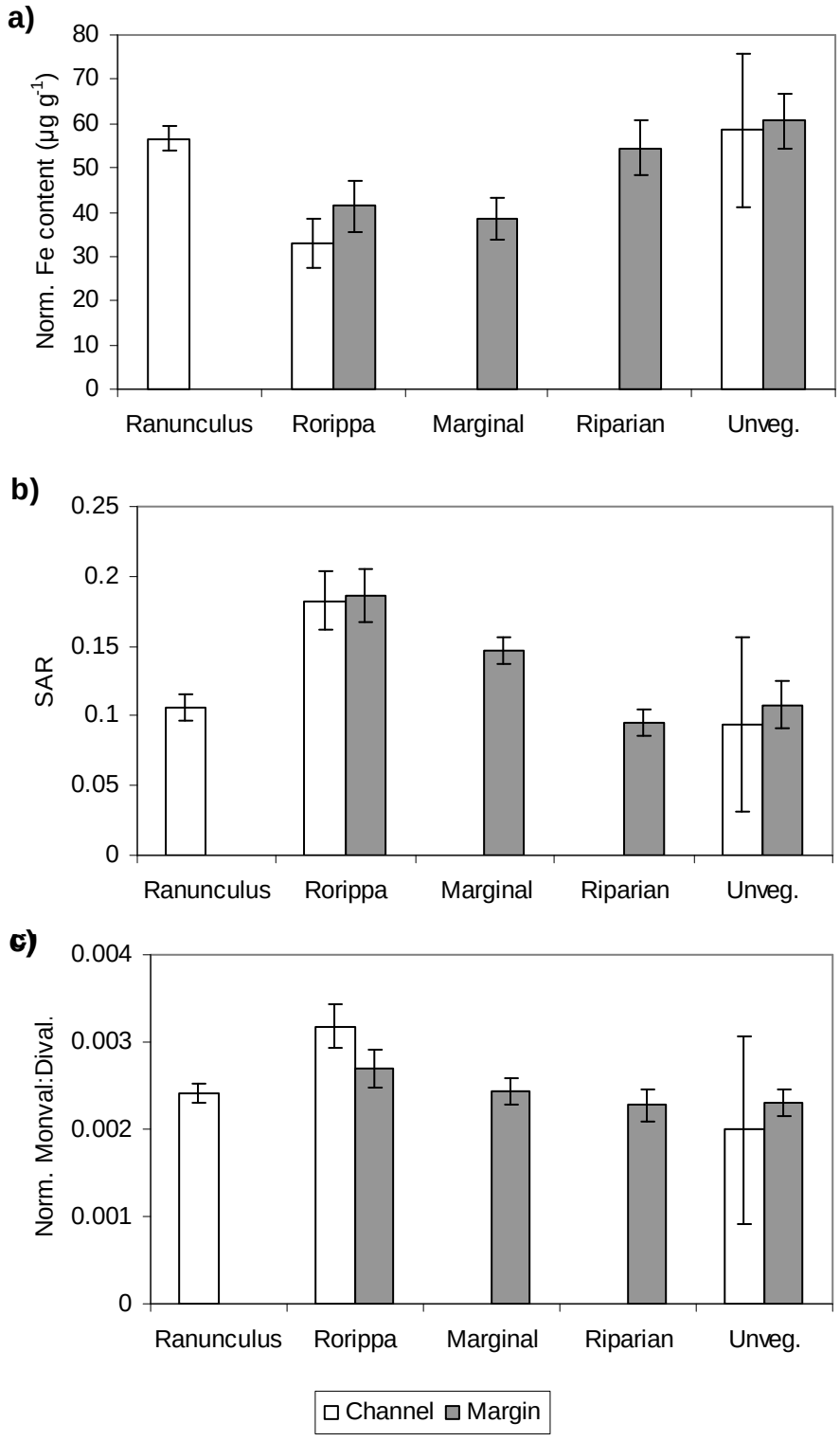

Figure 4.18. Spatial variations in chemical sediment properties by macrophyte type and location within the channel. (a) Normalised Fe content (µg g^{-1} sediment), (b) sodium absorption ratio, and (c) monovalent:divalent cation ratio. Ranunculus is a submerged macrophyte; Rorippa is an emergent macrophyte; Marginal is a grouping for all non-Rorippa marginal plants; Riparian is a grouping for terrestrial plants with stems trailing in the water, and Unveg. is bare sediment without macrophyte cover. Error bars are one standard error.

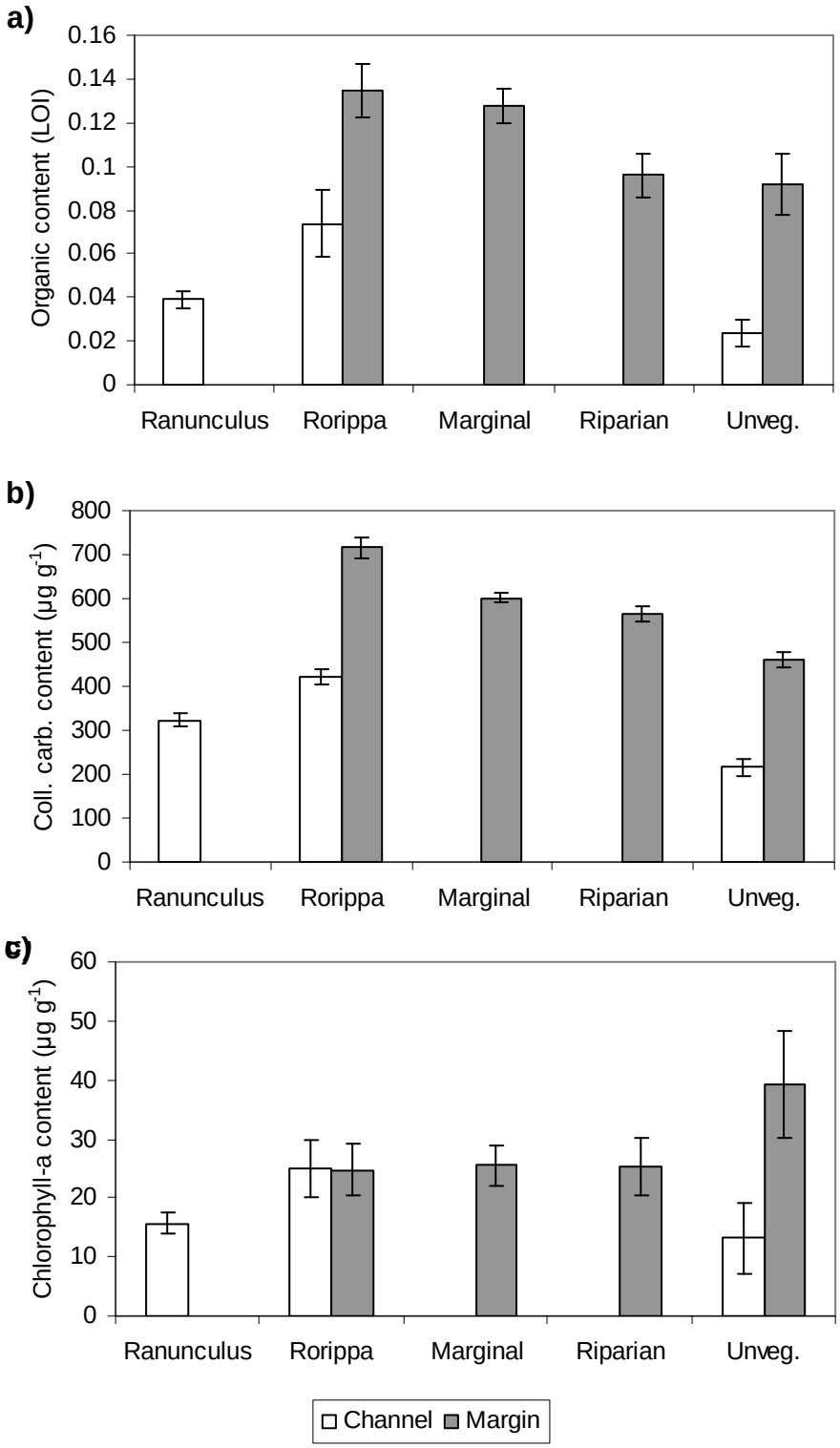

Figure 4.19. Spatial variations in biological sediment properties by macrophyte type and location within the channel. (a) Organic content, (b) colloidal carbohydrate content ($\mu g\ g^{-1}$ sediment) and (c) chlorophyll-a content. Ranunculus is a submerged macrophyte; Rorippa is an emergent macrophyte; Marginal is a grouping for all non-Rorippa marginal plants; Riparian is a grouping for terrestrial plants with stems trailing in the water, and Unveg. is bare sediment without macrophyte cover. Error bars are one standard error.

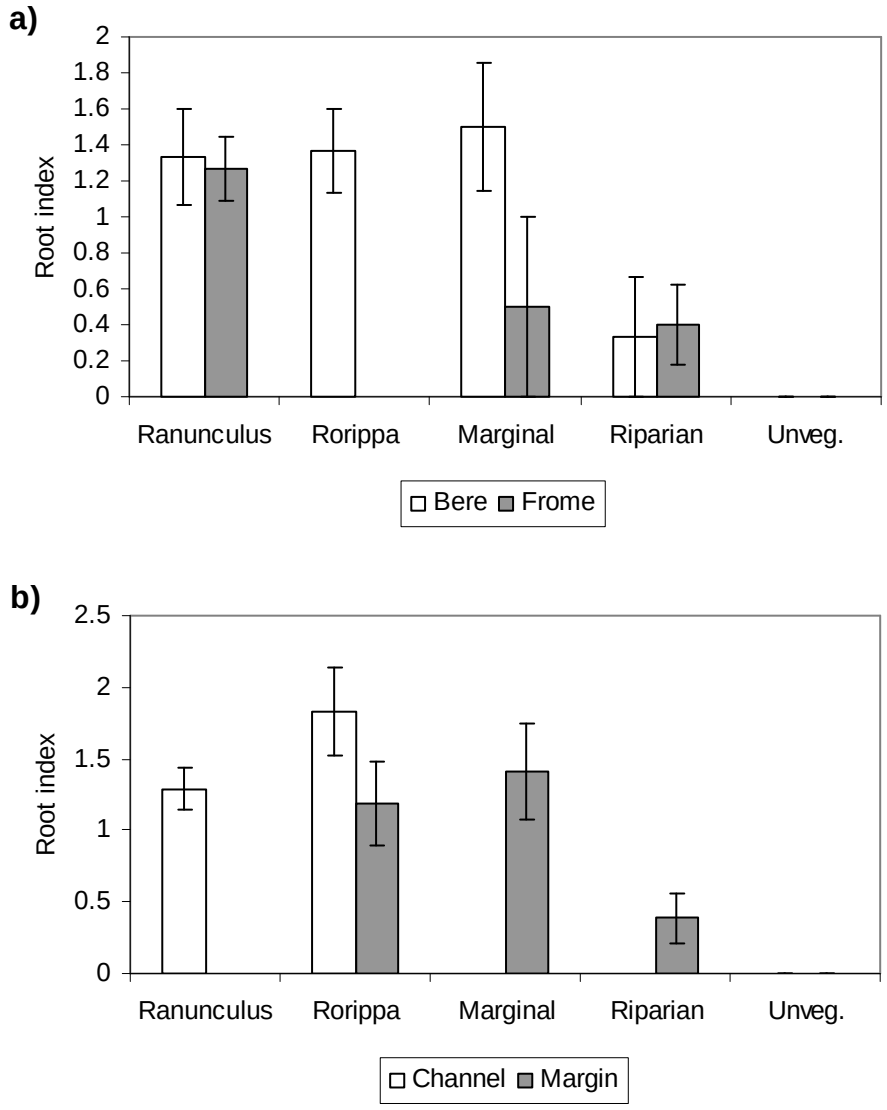

Figure 4.20. Spatial variations in mean root index by macrophyte type by (a) stream and (b) location in channel. Root index is an ordinal measure of macrophyte root density, ranging from 0 for no roots to 4 for a dense root mass. Ranunculus is a submerged macrophyte; Rorippa is an emergent macrophyte; Marginal is a grouping for all non-Rorippa marginal plants; Riparian is a grouping for terrestrial plants with stems trailing in the water, and Unveg. is bare sediment without macrophyte cover. Error bars are one standard error.

4.2.2 CSM-derived erodibility

Over the course of the field survey, CSM-derived erosion thresholds (P_I) ranged from 0.15 to 3.6 PSI, and had a mean of 1.38 with a 95% confidence interval of 0.12 PSI, and a median of 1.5. However, as two different CSM units were used, P_I must be converted to stagnation pressure (P_{stag}), to permit integration of the datasets (Vardy et al. 2007) (Section 3.2.3). P_{stag} ranged from 3.9 to 301.3 Pa, and had a mean of 84.67 with a 95% confidence interval of 9.57, and a median of 72.02 (Fig. 4.21). Normality was tested for P_{stag} using the Kolmorgorov-Smirnov (K-S) test as a precursor to statistical analysis. The K-S test is a goodness of fit test that compares the P_{stag} frequency distribution to a normal distribution (Dytham 2003). The P_{stag} frequency distribution was significantly different from normal (Figs. 4.21a) (K-S, $Z = 1.538$, $p = 0.018$). In addition to statistical tests of normality, quantile-quantile (Q-Q) plots are often used to visually assess the sample distribution against a normal distribution (Fig. 4.21b) (Crawley 2007, Zuur et al. 2007). The ranked samples are compared to ranked samples from a normal distribution. The substantial deviations from linear in the P_{stag} data indicate that the distribution was non-normal (Fig. 4.21). The lack of normality limits the range of statistical tests that can be used, and accordingly non-parametric methods are used in this section.

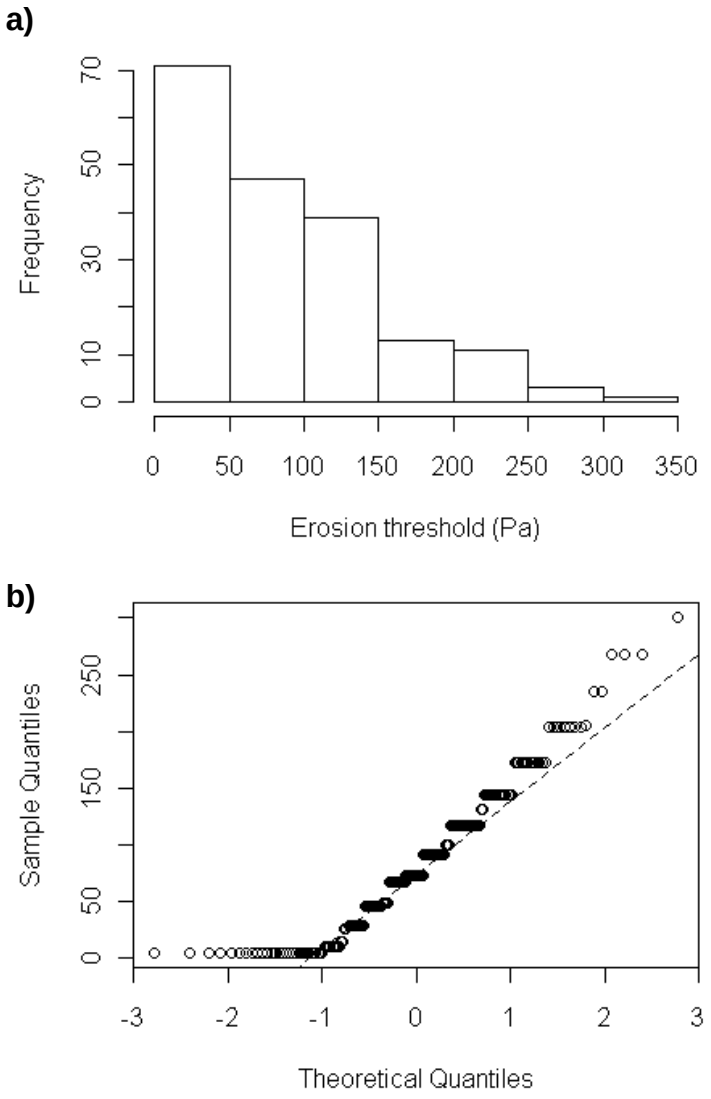

Figure 4.21. (a) Histogram and (b) quantile-quantile (Q-Q) plot to assess normality of erosion threshold data (P_{stag}). The non-linear relationship in the Q-Q plot indicates a departure from normal distribution.

Overall, erosion thresholds were comparable between the study streams. Mean erosion thresholds were not significantly different, 83 and 86 Pa for the Bere Stream and River Frome, respectively (Mann-Whitney, $Z = -0.662$, $p = 0.51$). Erosion thresholds differed significantly between margins and channel centres in the Bere Stream, but were not different for the River Frome (Sheirer-Ray-Hare, $F = 2.14$, d.f. = 1, $P = 0.14$; Mann-Whitney, $p < 0.05$) (Fig. 4.22). These variations could be caused by the coarser sediment particles and greater bulk densities in the channel sediments, and greater mud contents, cation contents, organic contents and chlorophyll-a contents in the Bere Stream channel compared to the River Frome channel (Figs. 4.10-4.13).

The Mann-Whitney U test (M-W) is a non-parametric equivalent of the t-test that tests if two samples come from the same population (Dytham 2003). The test is appropriate for the analysis because P_{stag} is a continuous variable, which is the only assumption of the test. The Scheirer-Ray-Hare (S-R-H) test was used instead of a two-way ANOVA because the dataset violates the assumptions of normality and homoscedasticity (Levene's Test of Equality of Error Variances, $F = 4.004$, df1 = 3, df2 = 181, $p < 0.01$). If a significant difference was detected in the S-R-H test, then M-W tests were applied to pairs of samples (e.g. Bere marginal vs. Bere channel) to test if they were significantly different. M-W tests should not be applied directly without the S-R-H test, because repeated pair-wise testing increases the likelihood of a Type 1 error, which is falsely rejecting the null hypothesis (Dytham 2003). In the same vein, the non-parametric Kruskal-Wallis (K-W) test was used as opposed to a one-way ANOVA in later analyses. As with the S-R-H and M-W tests, the only assumption for the test is that P_{stag} is continuous.

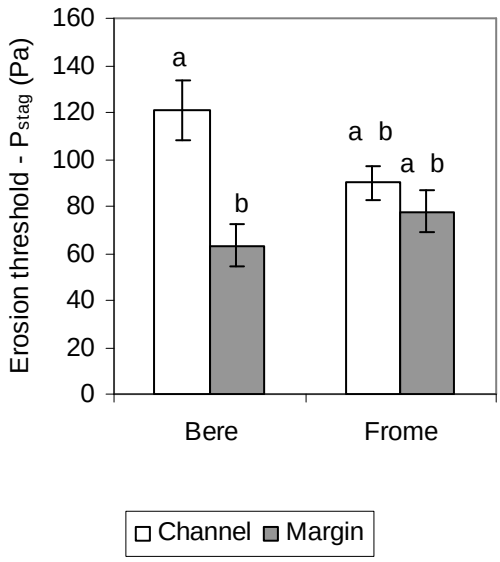

Figure 4.22. Mean CSM-derived erosion thresholds (P_{stag}) by stream and location within the channel. Error bars are one standard error. Locations marked with different letters have significantly different erosion thresholds (Scheirer-Ray-Hare, Mann-Whitney, $p < 0.05$). Means and standard errors were used for presentation only, and were not used in the statistical tests.

Erosion thresholds differed significantly by macrophyte type in the Bere Stream (Fig. 4.23a) (K-W, $\chi^2 = 14.23$, d.f. = 4, $p < 0.01$), but did not in the River Frome (K-W, $p > 0.05$) (Fig. 4.23). In the Bere Stream, erosion thresholds were highest for sediment under *Ranunculus*, and lowest for Marginal (i.e. non-*Rorippa* marginal macrophytes), with *Rorippa* being intermediate. Sediment below trailing, riparian macrophytes and unvegetated sediment did not differ significantly from any of the other groupings (K-W, $p > 0.05$). This pattern in erosion thresholds is mirrored in several of the sediment properties, principally dry bulk density, sand content and chlorophyll-a content (Fig. 4.24). Erosion thresholds for Riparian and Unvegetated sediment were comparable between the River Frome and Bere Stream, but overall there was less variation between macrophyte types in the River Frome (Fig. 4.23).

Sediment found under *Ranunculus* in the Bere Stream had significantly greater erosion thresholds than in the River Frome (M-W, Z = -2.516, n = 73, $p < 0.05$) (Fig 4.23). This was likely caused by the significantly greater median effective particle sizes in the Bere stream samples (M-W, Z = -4.180, p = 0.000), but there may be a biological component as well, as chlorophyll-a contents were also significantly greater (M-Z, Z = -5.190, p =

0.00). Figure 4.23 suggests that erosion thresholds for Marginal differ between the Bere Stream and River Frome. Whilst this was supported statistically (M-W, Z = -2.533, n = 29, $p < 0.05$), it was an artefact of the classification of macrophyte types. When the dominant marginal macrophyte in the Bere Stream (i.e. *Rorippa*) was included in the analysis, there was no statistically significant difference in P_{stag} by stream (M-W, $p > 0.05$).

Spearman's rank correlation analysis reveals significant correlations between environmental variables and erosion thresholds for the Bere Stream, but no correlations for the River Frome (Table 4.1). In the Bere Stream, the strongest correlation was with the location of the sediment across the stream when represented as a continuous, normalised variable (i.e. relative distance across channel) ($r_s = 0.51$, $p < 0.01$). The second strongest was with water velocity ($r_s = 0.42$, $p < 0.01$). The Bere Stream was narrower and had wider marginal areas, due to extensive marginal plant growth, than the River Frome. As a result, there was a steep gradient in mainstream water velocities across the channel (Fig. 4.25a). Therefore, distance across stream correlated well with the average water flows experienced in the reach (i.e. low flow in the margins and high flow in the channel centre) ($r_s = 0.64$, $p < 0.001$). The sediment in the channel centres was composed of coarser grains and had greater erosion thresholds than in the margins (Fig. 4.25c,e). In the River Frome, location across the stream had no correlation to water velocities (Table 4.1; Fig. 4.25b). In the deeper waters of the River Frome, *Ranunculus* stands were often submerged at the upstream end of the stand, but reached the water surface at the downstream end. Water velocity was always measured at 60% depth, but depending on the location of the sample, this point could have been within, or above the macrophyte stand. Median effective particle size increased slightly with distance across stream, but this was not reflected in erosion thresholds (Fig. 4.25d,f). The reason for this is uncertain, but could be related to the stratification of sediment properties over depth observed in many of the channel sediment samples. The sediment below *Ranunculus* stands had high sand contents, but they frequently had thin surficial layers of fine, unconsolidated sediment and organic material (e.g. Fig. 4.2). These surficial layers would have had lower erosion thresholds than the underlying sediment (Thomsen & Gust 2000, Amos et al. 2004, Orvain et al. 2007), but their properties would not have been well-represented in the sediment analysis which integrated over a 3cm depth.

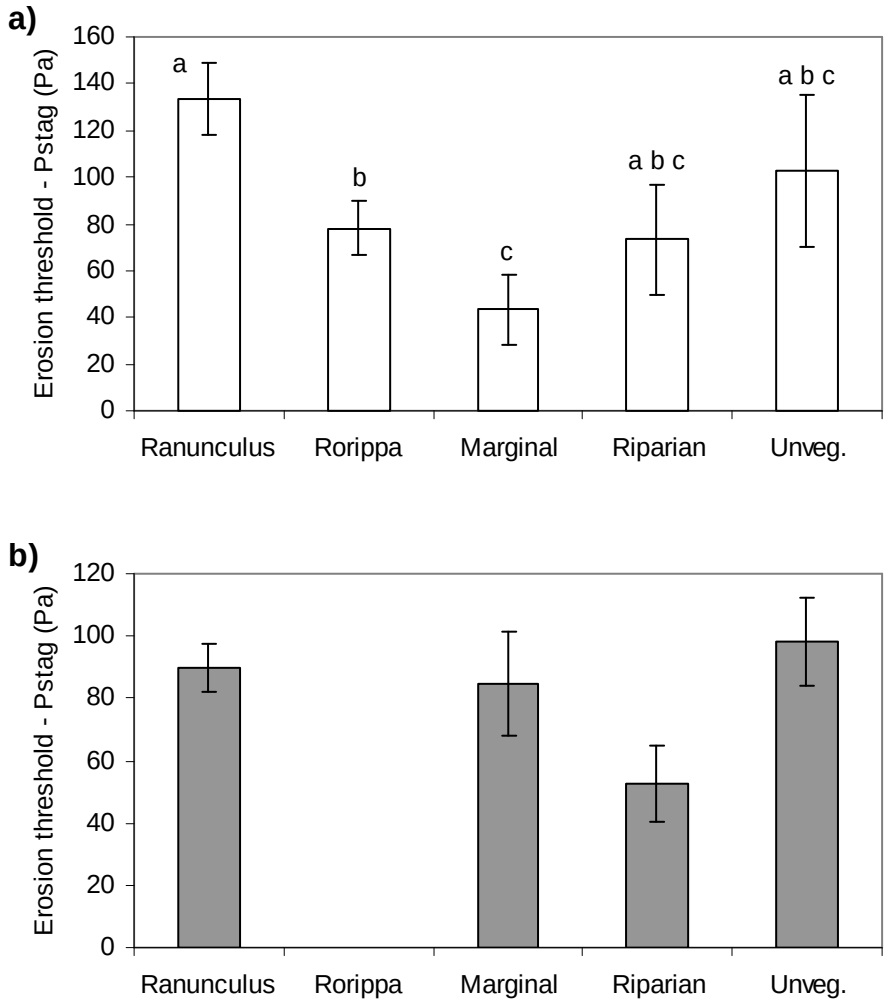

Figure 4.23. Mean CSM-derived erosion thresholds (P_{stag}) by macrophyte type for the (a) Bere Stream and (b) River Frome. Macrophyte types marked with different letters have significantly different erosion thresholds (Kruskal-Wallis, Mann-Whitney, p = 0.05). Erosion thresholds do not differ significantly for the River Frome. Error bars are one standard error. Means and standard errors were used for presentation only, and were not used in the statistical tests. Ranunculus is a submerged macrophyte; Rorippa is an emergent macrophyte; Marginal is a grouping for all non-Rorippa marginal plants; Riparian is a grouping for terrestrial plants with stems trailing in the water, and Unveg. is bare sediment without macrophyte cover.

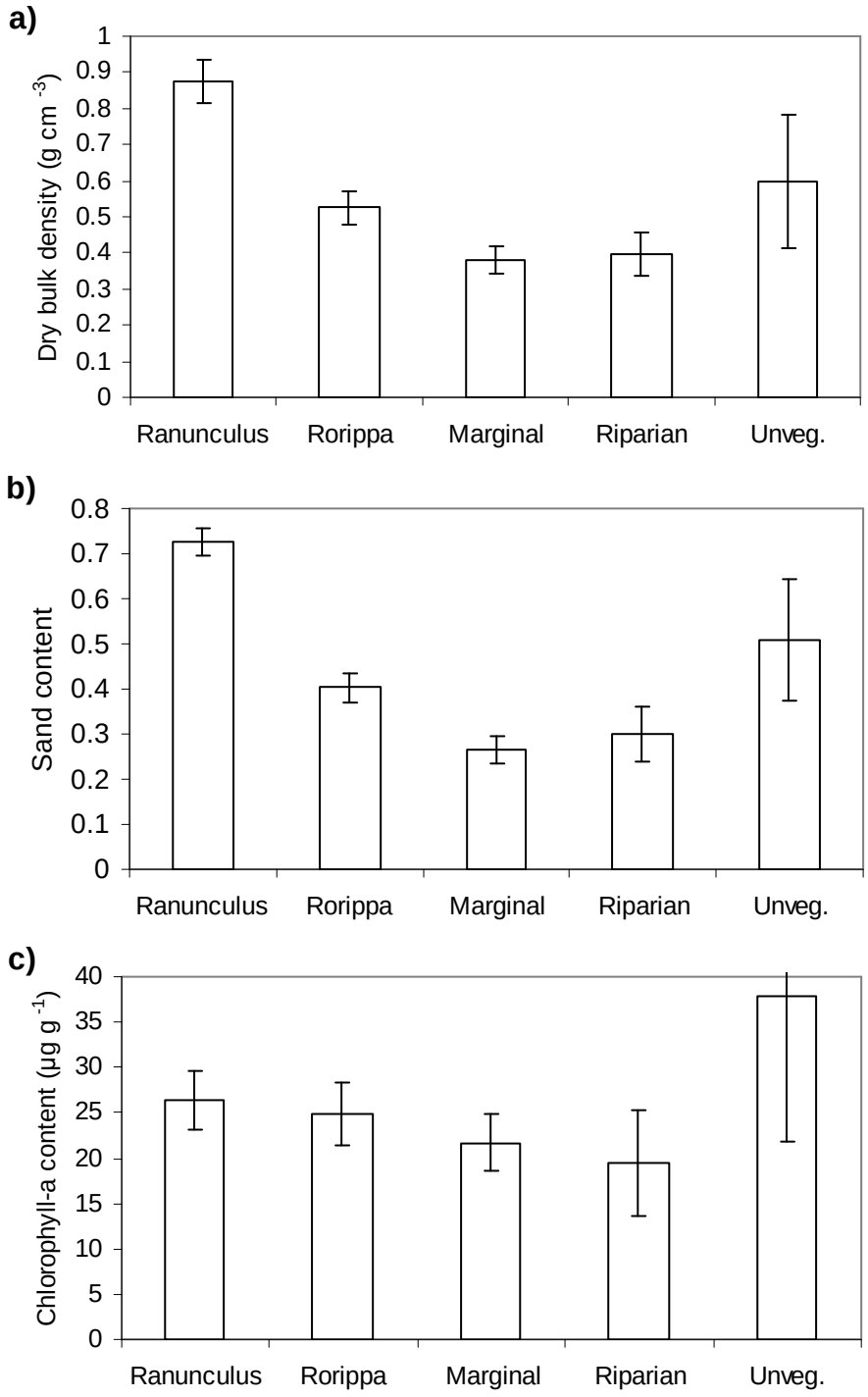

Figure 4.24. Dry bulk density, sand content and chlorophyll-a content (µg g^{-1} sediment) for Bere Stream sediment by macrophyte type. Error bars are one standard error. Ranunculus is a submerged macrophyte; Rorippa is an emergent macrophyte; Marginal is a grouping for all non-Rorippa marginal plants; Riparian is a grouping for terrestrial plants with stems trailing in the water, and Unveg. is bare sediment without macrophyte cover.

*Table 4.1. Spearman's rank correlation for erosion threshold (P_{stag}) and environmental variables. Macrophyte type has 5 categories: unvegetated, Ranunculus, Rorippa, marginal vegetation, and riparian vegetation, and unvegetated. Relative distance across stream ranges from 0 at the bank to 0.5 in the channel centre. Significant at the 0.05 * level and 0.01 ** level (2-tailed).*

	Total	Bere	Frome
Relative distance across channel	0.348 **	0.506 **	0.021
Channel vs. margin	-0.257 **	-0.350 **	-0.097
Water velocity	0.225 *	0.424 **	0.136
Macrophyte type	-0.173 *	-0.285 **	-0.057

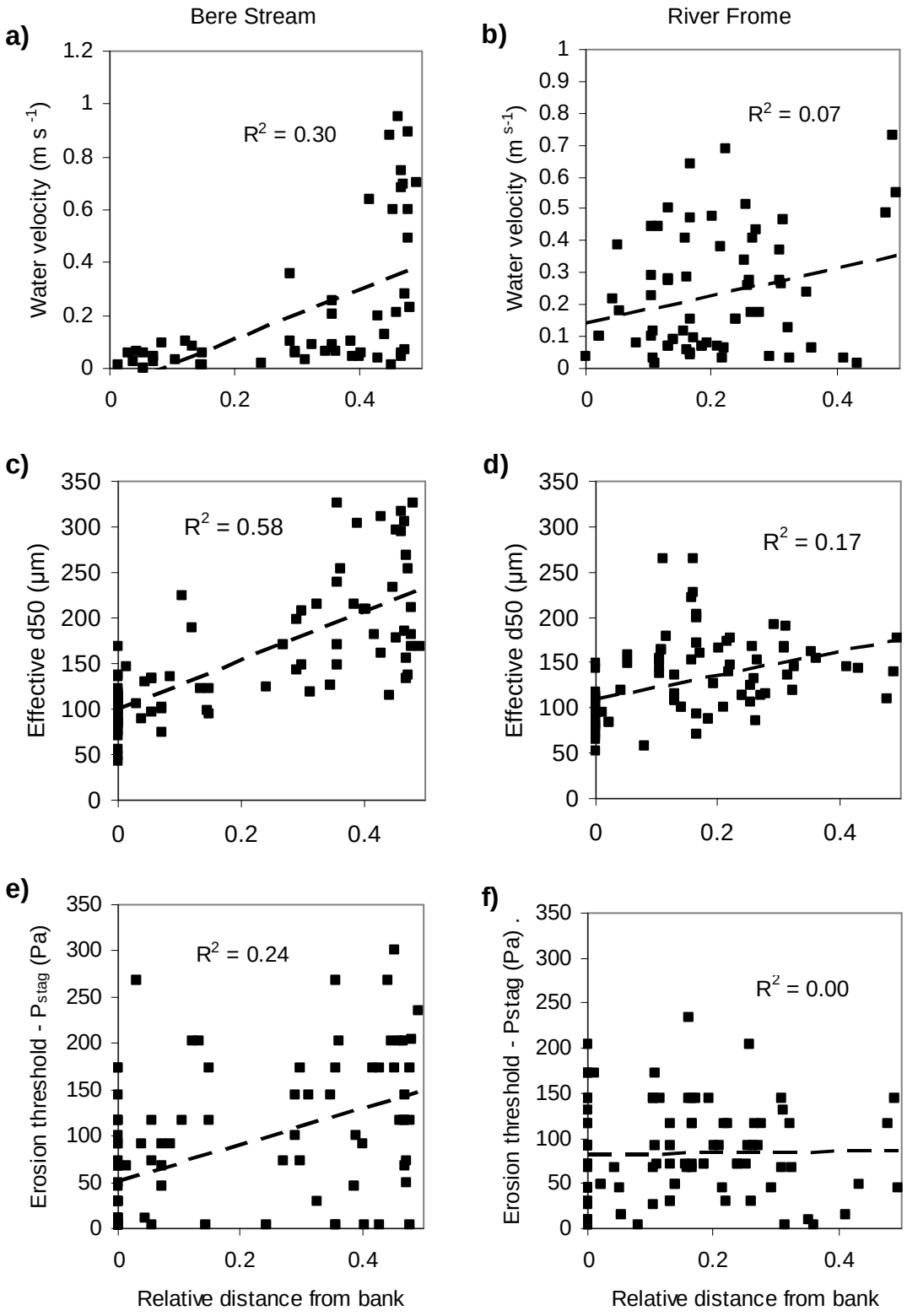

Figure 4.25. Cross-stream patterns in water velocity (a, b), median effective particle size (c, d) and erosion thresholds (e, f) across the channels, from the bank (0) to the channel centre (0.5) for the (a, c, e) Bere Stream and (b, d, f) River Frome.

The spatial patterns in erosion threshold by macrophyte type are best explained by the preferred location of different species within the stream, which influences the composition of the deposited sediment. For both streams, substrate type was significantly correlated to relative distance across the channel (r_s = -0.65, $p < 0.001$). Given the significant correlation between erosion threshold and distance across the channel for the Bere Stream (Table 4.1; Fig 4.25), it is unsurprising that substrates found in the channel centres, like *Ranunculus*, had the highest erosion thresholds. Macrophyte stands in the channel centres will collect coarser material that is transported as bedload, which has higher erosion thresholds (Section 2.2.3) (Sand-Jensen 1998, Horvath 2004). Those macrophytes found in the margins were exposed to lower water velocities, and consequently bedload input would not be a significant source of sediment. Deposits in the margins would have formed predominantly from suspended sediment deposition and retention, and would have a lower erosion threshold if they were unconsolidated. This pattern becomes more obvious if we look at the one macrophyte type found in both the channel centres and margins. *Rorippa* was typically found along the margins, but succeeded *Ranunculus* in the channel centres in early summer. Median effective particle size was higher under *Rorippa* in the channel than in the margins, 200 and 105 μm respectively, consequently mean erosion thresholds were higher as well, 109 and 69 Pa respectively.

The differences in erosion thresholds between streams appears to be caused by differences in particle sizes, particularly the larger median particle sizes found in the Bere Stream channel (Fig 4.25c,d); and chlorophyll-a content, particularly between Bere Stream and River Frome channel sediment (Figs. 4.13c, 4.22, 4.24b) and possibly between vegetated and unvegetated marginal sediment (Figs. 4.19c, 4.23 & 4.24c). The relationships between sediment properties and erosion threshold are rigorously examined in Chapter 5.

4.2.3 Vane-derived shear strength

Shear vane measurements were taken at each sampling location within both streams during the bimonthly surveys from January to July 2009. Measurements were not taken in the River Frome in January due to dangerously high water. A total of 128 triplicate measurements were recorded over that time span. Overall, sediment shear strength ranged from 0 to 7.76 kPa, and had a mean of 2.61 with a 95% confidence interval of 0.30, and a median of 2.5. The frequency distribution of shear strengths was not significantly different from normal (K-S, z = 0.755, n = 129, p = 0.620) (Fig. 4.26). The Q-Q plot shows that the frequency distribution largely adhered to a normal distribution, but was truncated at zero (Fig. 4.26b).

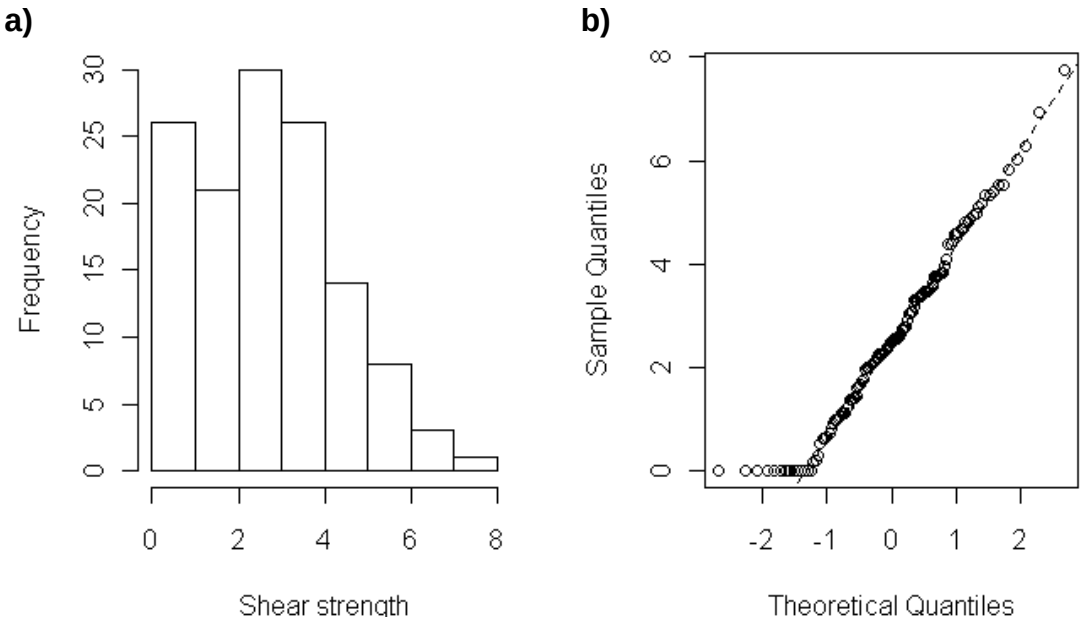

Figure 4.26. (a) Histogram and (b) quantile-quantile plot for shear strength as measured by the Pilcon hand shear vane tester. The distribution is not significantly different from normal (Kolmogorov-Smirnov, p > 0.05)

Overall, shear strength did not differ significantly by stream or location within channel (S-R-H, $p > 0.05$) (Fig. 4.27). Parametric tests, such as T-test and ANOVA, were not used for this analysis, because, despite adhering to the assumption of normality, the dataset violated the assumptions of homogeneous variance (Levene's, $p > 0.05$) (Dytham 2003). This lack of significant difference by location is surprising considering bulk density was substantially greater in channel than marginal sediments (Fig. 4.10), and root index was considerably lower in the Frome margins (Fig. 4.8).

Shear strength varied significantly by macrophyte type (Fig. 4.28), but in a different way than CSM-derived erodibility (Fig. 4.22) (Levene's, $F = 2.43$, $df1 = 4$, $df2 = 124$, $p = 0.051$; ANOVA, $F = 5.621$, $p = 0.00$). Shear strength was highest for sediment under *Ranunculus*, Marginal and Riparian. *Rorippa* and unvegetated sediment had significantly lower shear strengths (Fig. 4.28) (ANOVA, LSD Posthoc, $p < 0.05$). The results for Marginal and Riparian groupings are counterintuitive, particularly for Riparian. The sediment under riparian plants had very low root indices (Fig. 4.20) and similarly low bulk densities as unvegetated margins (Fig 4.14b), so shear strength should be similar between the groups. Marginal and Riparian groupings, though, differed in one important way from unvegetated margins; the vast majority of those samples were located at the wetted perimeter, whereas unvegetated margins were located on average 10cm away from the bank. Consequently, shear strength readings taken at the wetted perimeter may in fact be estimates of bank sediment stability and not surficial sediment in the channel. When the results of Marginal and Riparian samples were excluded, shear strength decreased from *Ranunculus* to *Rorippa* to unvegetated, and under *Rorippa* was lower in marginal than channel sediment (Fig. 4.29). This suggests that macrophyte roots and sediment properties such as bulk density or median particle size may be responsible for variations in shear strength, but that there was a possible bias in measurements near the bank.

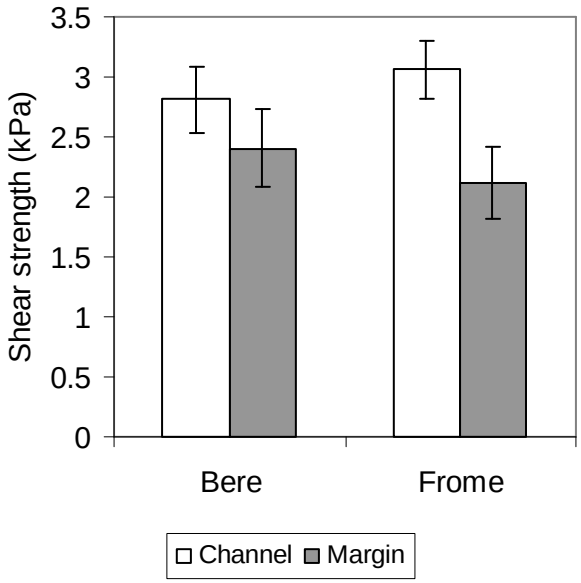

Figure 4.27. Shear strength by stream and location within the channel. Error bars are one standard error. Shear strength does not differ significantly between groups (Scheirer-Ray-Hare, $p > 0.05$)

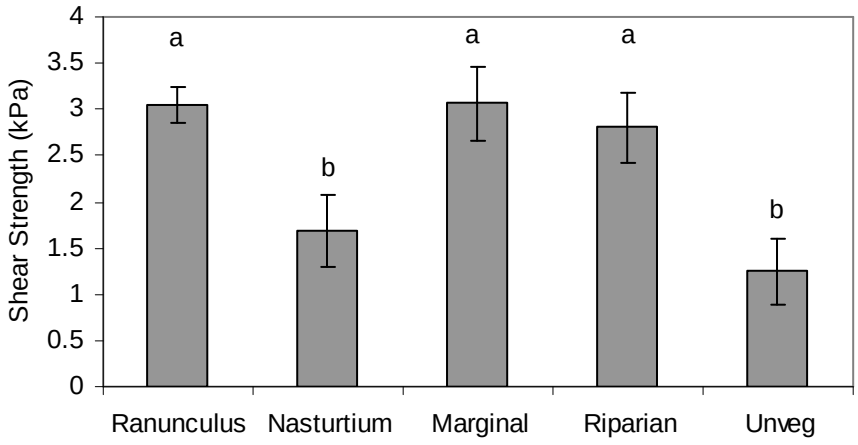

Figure 4.28. Mean shear strength for both streams by macrophyte type. Error bars are one standard error. Macrophyte types marked with different letters have shear strengths that are significantly different (ANOVA, LSD posthoc, $p < 0.05$).

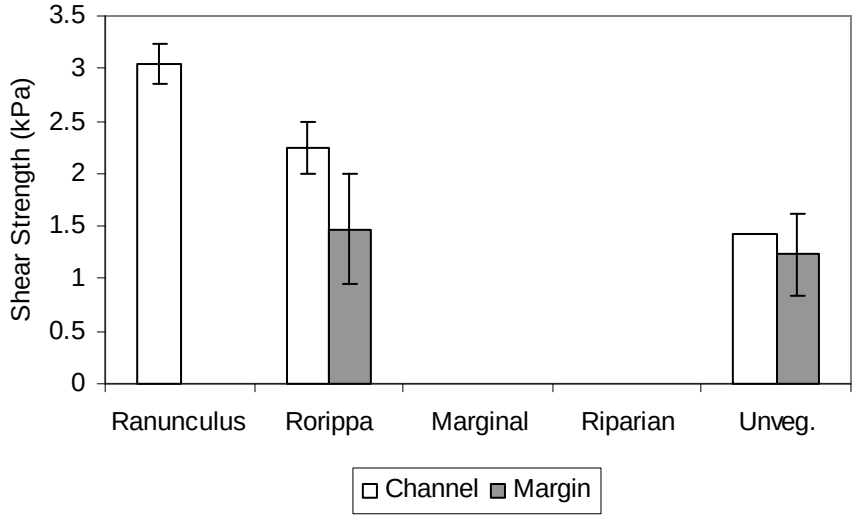

Figure 4.29. Mean shear strength for both streams by macrophyte type and location within channel, with Marginal and Riparian excluded. Error bars are one standard error.

A Spearman's rank correlation analysis identified significant correlations between shear strength and environmental variables (Tables 4.2 & 4.3). When the entire dataset was analysed, though, none of the environmental variables were significantly correlated to shear strength for both streams individually (Table 4.2). The removal of Marginal and Riparian samples from the dataset increased the strength of correlations, and resulted in significant correlations to substrate type and location in the channel (channel centre vs. margin) (Table 4.3).

*Table 4.2. Spearman's rank correlations between shear strength and environmental variables. Significant at the 0.05 * level and 0.01 ** level (2-tailed).*

	Total	Bere	Frome
Substrate type	-0.231 **	-0.083	-0.373 **
Relative distance across channel	0.099	0.028	-0.311 *
Channel vs. margin	-0.245 **	-0.178	-0.320 *
Water velocity	0.318 **	0.292	0.441 **
CSM erosion threshold (P_{stag})	0.001	-0.051	0.050

*Table 4.3. Spearman's rank correlations between shear strength and environmental variables, with Marginal and Riparian categories excluded. Significant at the 0.05 * level and 0.01 ** level (2-tailed).*

	Total	Bere	Frome
Substrate type	-0.471 **	-0.465 **	-0.464 **
Relative distance across channel	0.249 *	0.367 *	-0.031
Channel vs. margin	-0.447 **	-0.416 **	-0.464 **
Water velocity	0.268 *	0.164	0.469 **
CSM erosion threshold (P_{stag})	0.090	0.015	0.156

4.3 Temporal variations in erodibility

4.3.1 Descriptions of environment and sediment

Environmental conditions varied over the course of the study period. Discharge fluctuated significantly over the yearlong study in line with expectations for a groundwater dominated river in England (Figs. 4.30 & 4.31). Flows were greatest in the winter when heavy rainfalls had recharged the aquifer, and lowest in the late summer after several months of low rainfall. The River Frome was flashier than the Bere Stream, and experienced more high water events (Fig 4.31). Average water velocities at the sampling points displayed a similar annual pattern, particularly for the samples in the channel centre (Fig. 4.32). Flows in marginal locations were consistently low in the Bere Stream, but showed some seasonal variation in the River Frome.

The location of fine sediment accumulation in the streams varied over time. In the Bere Stream, patterns in fine sediment accumulation were tied to the dynamics of *Rorippa* (Figs. 4.33 & 4.34). Fine sediment was found predominately within *Rorippa* from September 2008 to January 2009. High flows in late 2008, though, washed out the majority of the *Rorippa* (Fig 4.31 & 4.34). In March 2009, most of the sediment was found beneath other non-*Rorippa* marginal macrophytes (Marginal). Once *Rorippa* began to recolonise the reach, fine sediment began to accumulate beneath the stands (Figs. 4.33 & 4.34). *Ranunculus* represented on average 20-30% of the sampling locations throughout the survey period until it dropped in July 09 when little *Ranunculus* was found growing in the stream. In the River Frome, *Ranunculus* was the dominant vegetation type in the channel, and stands showed little temporal variation in size or abundance (pers. obs.). Variations in the relative location of fine sediment accumulation appear to be tied to the seasonal dynamics of macrophytes in the margins (Fig 4.33). As marginal macrophytes began to dieback in autumn 2008, the relative proportion of sampling locations in *Ranunculus* increased. As macrophytes began to regrow in the margins in the spring, the relative proportion in *Ranunculus* decreased again. (For more information on temporal variations in water velocity, sediment accumulation, and plant distributions, see Appendix II).

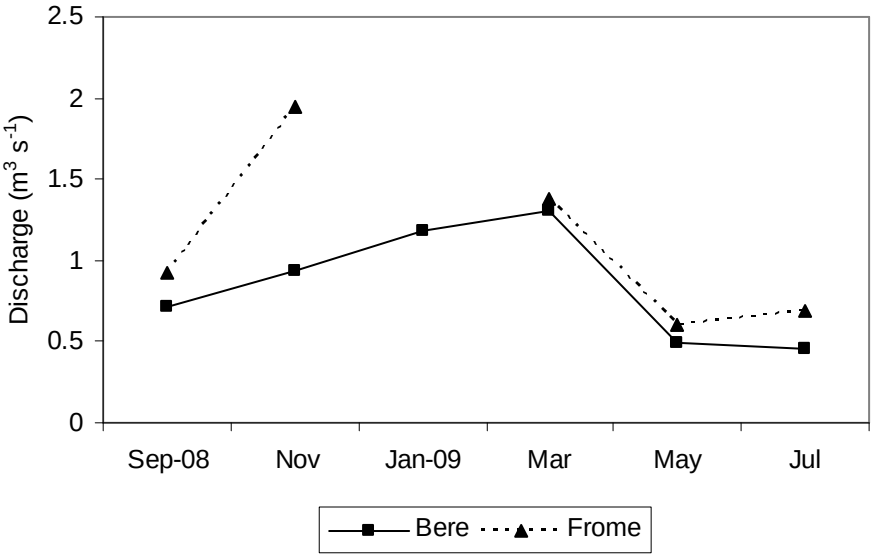

Figure 4.30. Stream discharge for the Bere Stream and River Frome, calculated based on velocity transects and channel cross-sectional area (3 transects per month), during the site visits.

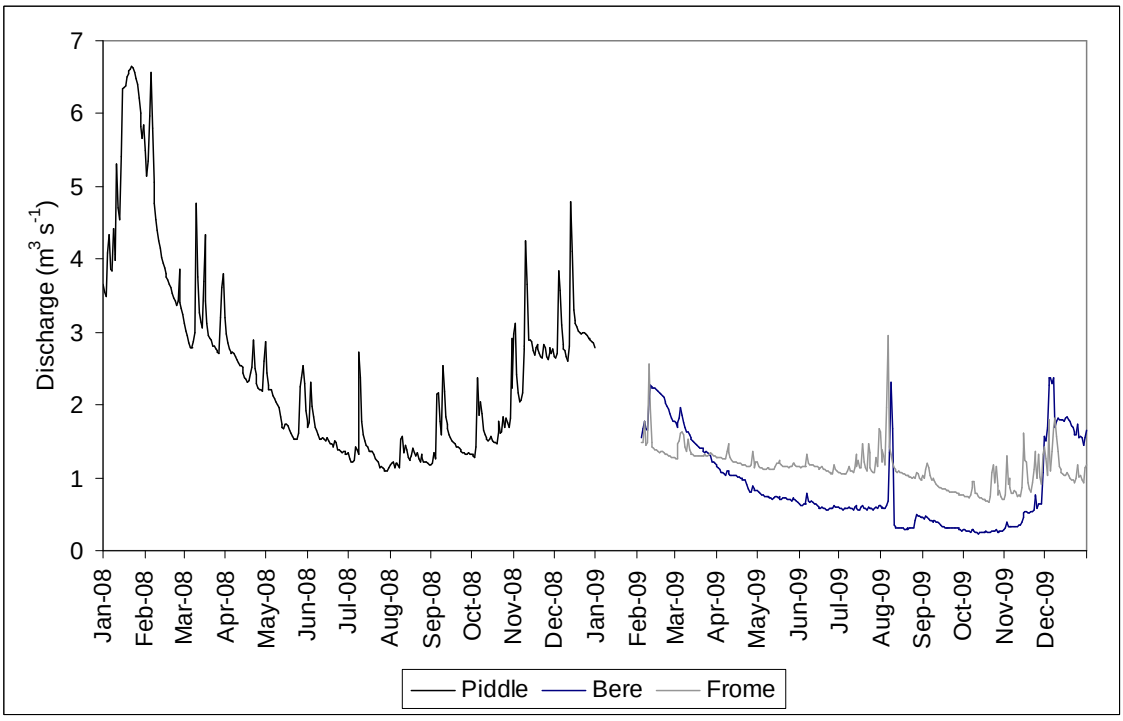

Figure 4.31. Discharge for the River Piddle, based on the Environment Agency gauging station downstream at Bagg's Mill, and the two stream reaches, based on stage and discharge measurements by G. Davies. The Bere Stream is a tributary of the River Piddle.

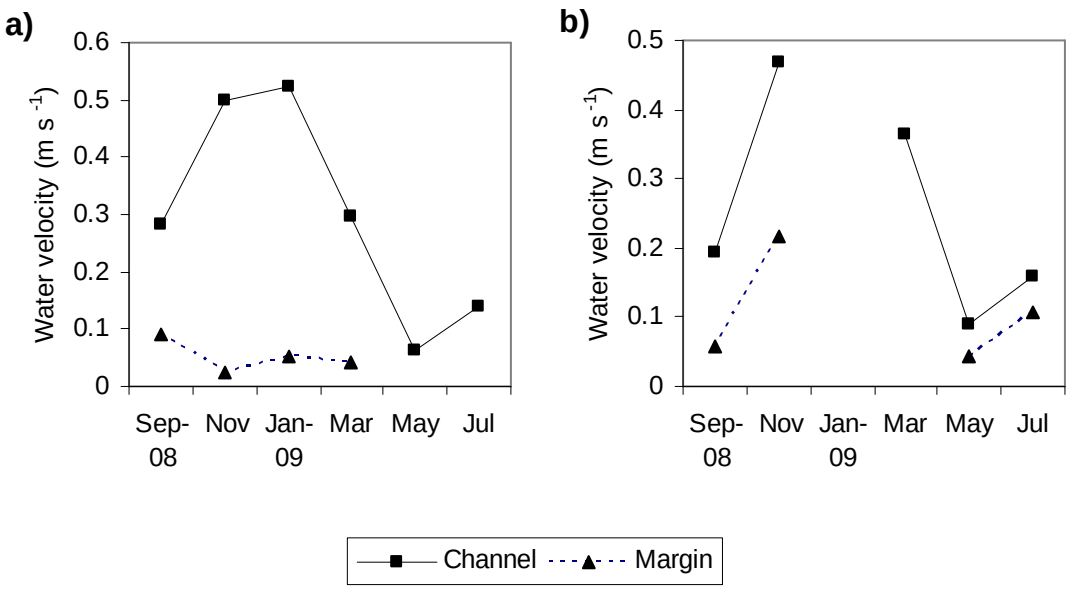

Figure 4.32. Temporal variations in mean water velocity at sampling locations, for the (a) Bere Stream and (b) River Frome. Measurements were taken at 60% water depth.

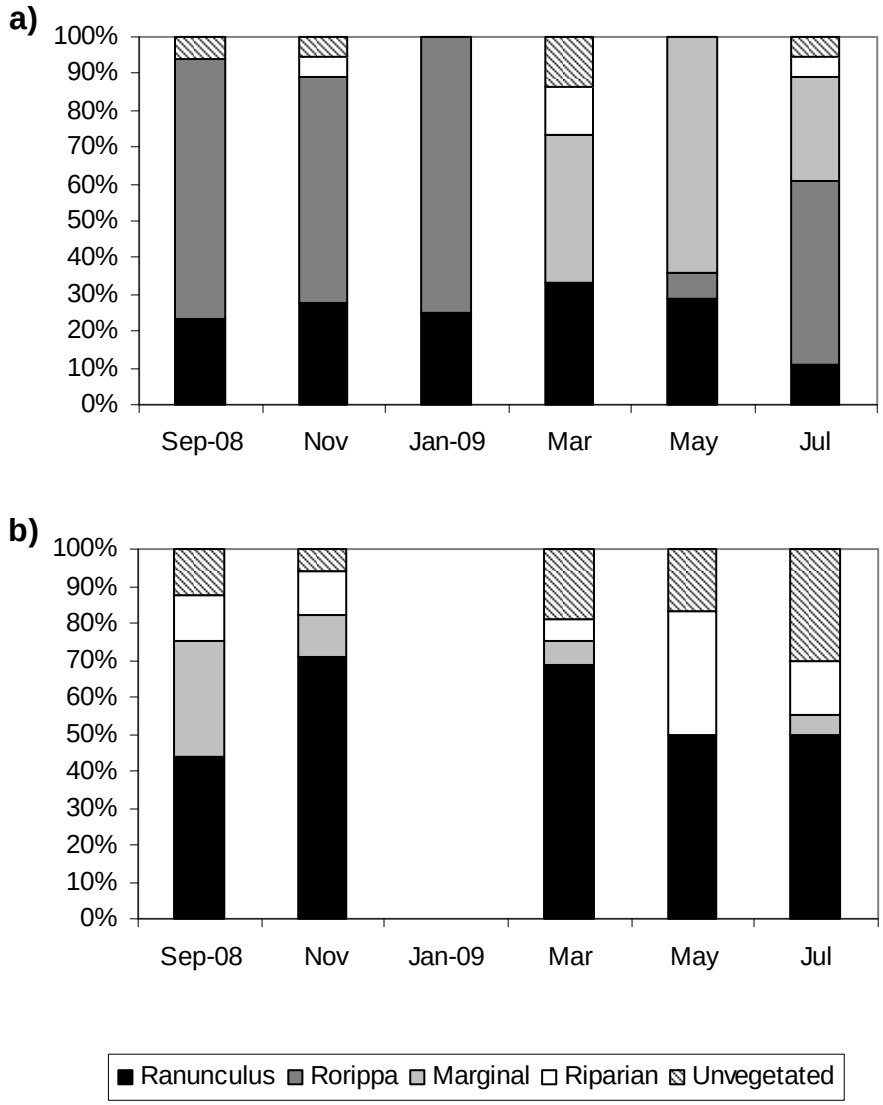

Figure 4.33. Temporal variations in the relative location of fine sediment within the channel, according to macrophyte type, for the (a) Bere Stream and (b) River Frome. The sampling strategy was stratified random within areas of sediment deposition, therefore, this figure depicts where sediment is found within the stream and not the relative abundance of macrophytes. Ranunculus is a submerged macrophyte; Rorippa is an emergent macrophyte; Marginal is a grouping for all non-Rorippa marginal plants; Riparian is a grouping for terrestrial plants with stems trailing in the water, and Unveg. is bare sediment without macrophyte cover. Error bars are one standard error.

Figure 4.34. Seasonal changes in the abundance and species composition of the aquatic macrophyte community in the Bere Stream. Note: Rorippa colonised Ranunculus stands from April to July 2008. They subsequently spread to cover most of the reach, leaving a narrow channel with fast flowing water. Much of the Rorippa was then removed by high flows in the autumn. Ranunculus re-established in the new channel in September 2008, and grew over the winter and spring.

Sediment properties showed considerable seasonal variation, particularly ones related to water chemistry and biological activity. Dry bulk density increased over most of the study period for channel sediment in the Bere Stream, but decreased in the River Frome (Fig. 4.35a,b). In the margins, dry bulk density was highest in January 2009 for the Bere Stream and in March 2009 for the River Frome (Fig. 4.35a,b). Effective particle size was largely unchanged over the course of the survey; channel sediment, including inorganic and organic material, was characterised as fine sand-sized, whilst margin sediment was very fine sand-sized (Fig. 4.35c,d). Though, sediment in the channel centres of the Bere stream did show a slight increase in size over the study period (Fig. 4.35c). The temporal patterns in absolute particle size mirror those for dry bulk density, particularly for channel sediment (Figs 4.35a,b,e,f & 4.36a,b).

Normalised calcium, magnesium and sodium contents were greater and more variable in the Bere Stream than in the River Frome (Fig. 4.37). They were higher in the channel than margins, and for the Bere Stream, peaked from November 2008 to January 2009 and then declined to July 2009 (Fig. 4.37a,c,e). They decreased slightly for the River Frome over time. Normalised iron content was higher in the River Frome than Bere Stream (Fig. 4.38a,b), but showed more variability in the Bere Stream, with peak contents in January 2009. SAR and normalised M:D showed strong declining trends in the Bere Stream, reaching a minimum in March 2009 (Fig.4.38 c,e). The pattern was similar for the River Frome, except that the magnitude of change in SAR was considerably smaller (Fig. 4.38d,f).

Organic content decreased over the study period in the Bere Stream for channel and marginal sediment (Fig. 4.39a). In the River Frome it decreased initially, but increased in the spring and summer (Fig. 4.39b). Colloidal carbohydrate and chlorophyll-a content also decreased over time for the Bere Stream (Fig. 4.39c,e). Colloidal carbohydrate contents peaked in March 2009 for the channel centre and May 2009 for the margins, whilst chlorophyll-a increased in July and May 2009, respectively. For the River Frome, colloidal carbohydrate and chlorophyll-a contents fluctuated over time (Fig 4.39d,f). Colloidal carbohydrate content peaked for channel sediment in May 2009, but marginal peaked in November 2008 and again in May 2009 (Fig. 4.39d). Chlorophyll-a content peaked for marginal sediment in November 2008 and July 2009, and in May 2009 for sediment in the channel centres (Fig. 4.39f). Root index displayed different temporal trends by stream (Fig. 4.40). In the Bere Stream, root index fluctuated over time, and

was highest in March 2009 in the channel and May 2009 in the margins (Fig. 4.40a). In the River Frome, root index decreased to a minimum in July 2009 for the channel, but increased slightly, whilst remaining low, in the margins (Fig. 4.40b)

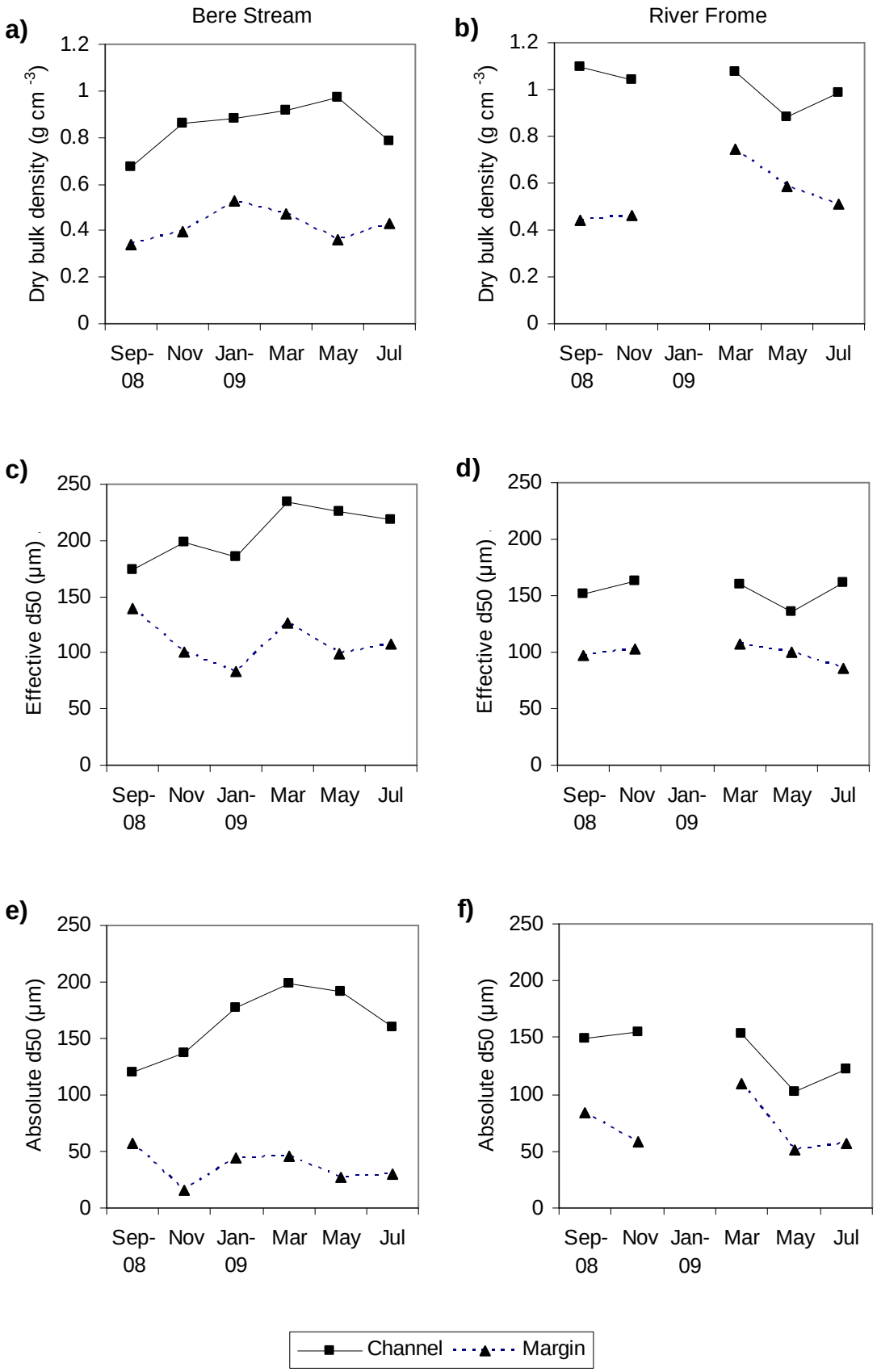

Figure 4.35. Temporal variations in physical sediment properties. (a,b) Dry bulk density, (c,d) median effective particle size), and (e,f) absolute particle size for channel and marginal sediment in the (a,c,e) Bere Stream and (b,d,f) River Frome.

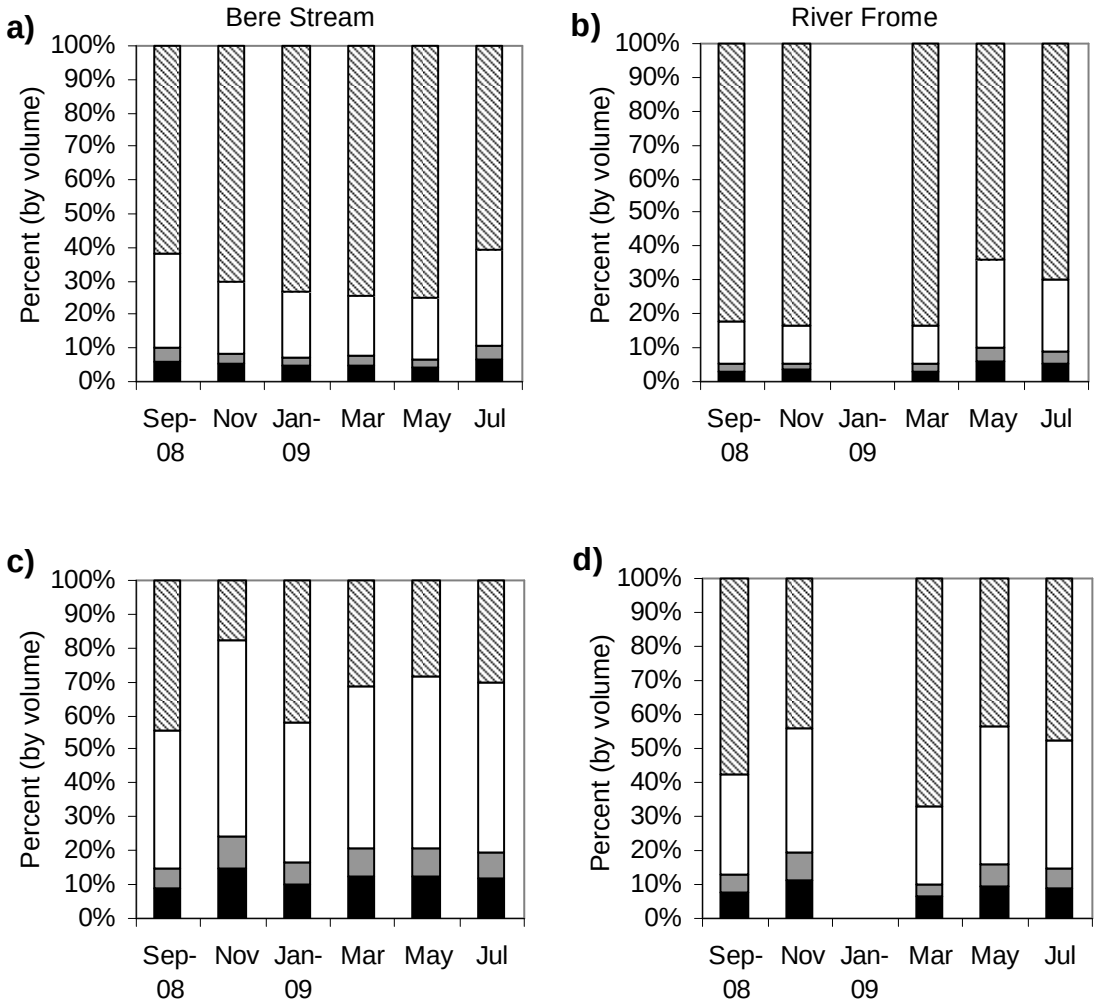

Figure 4.36. Temporal variations in absolute particle size distribution for (a,b) channel and (c,d) marginal sediment in the (a,c) Bere Stream and (b,d) River Frome. Particle size is represented as percent by volume.

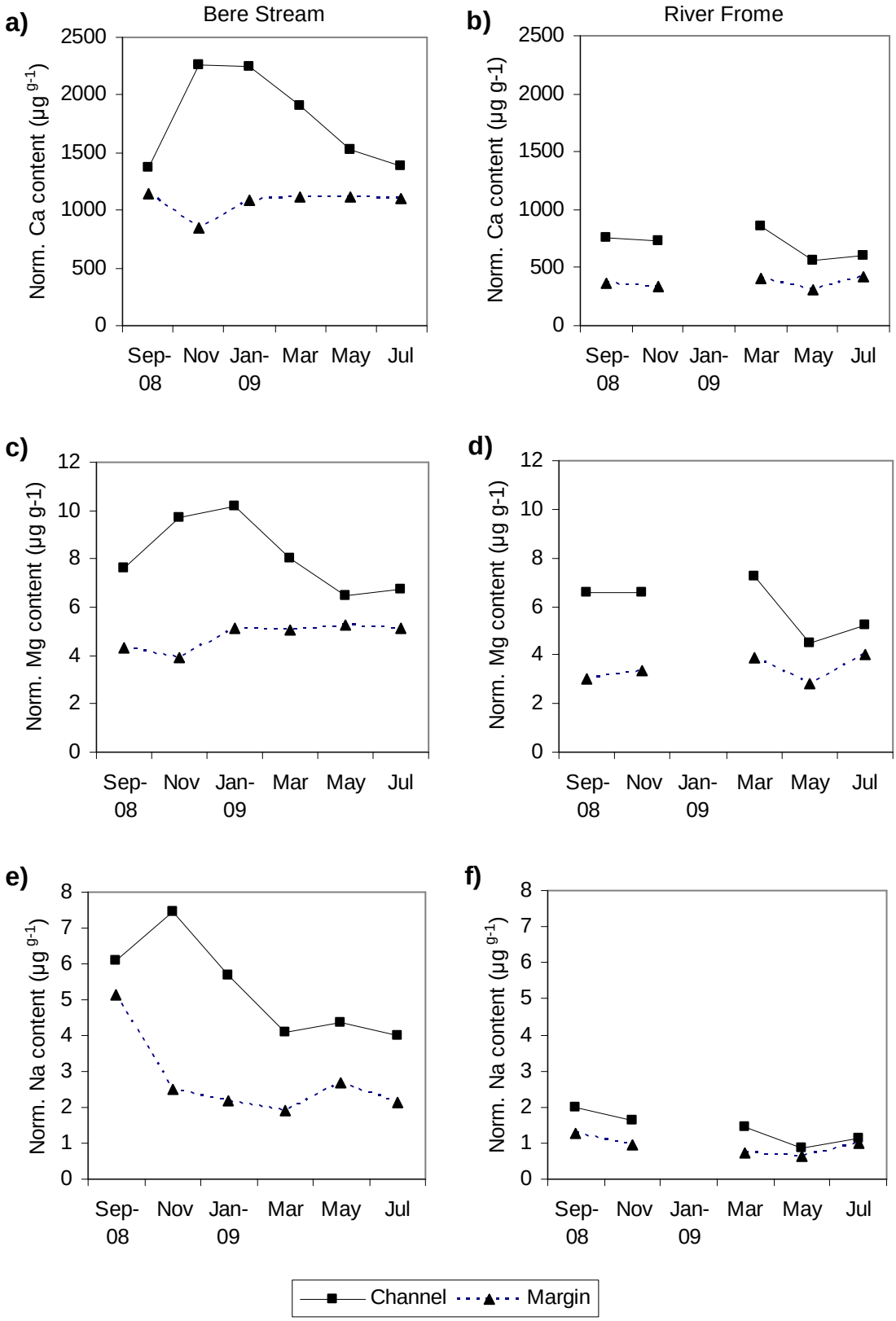

Figure 4.37. Temporal variations in normalised cation contents by stream and location within the channel, (a, b) calcium, (c, d) magnesium, and (e, f) sodium (µg g^{-1} sediment, normalised by absolute mud content) for channel and marginal sediment in the (a,c,e) Bere Stream and (b,d,f) River Frome.

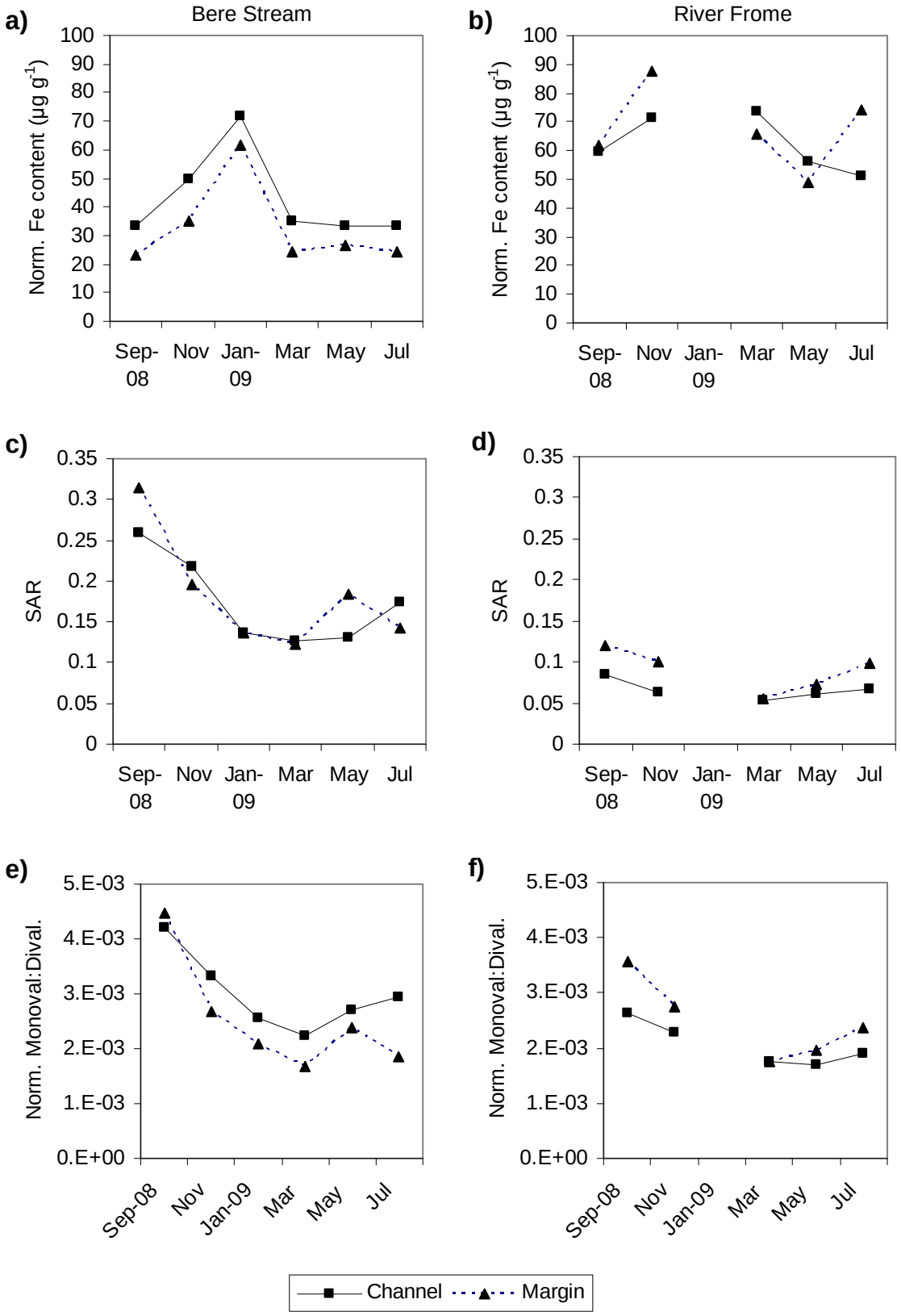

Figure 4.38. Temporal variations in chemical sediment properties (cont.) (a,b) Normalised Fe content (µg g^{-1} sediment), (c,d) sodium absorption ratio (SAR), and (e,f) the ration of normalised monovalent to divalent cations for channel and marginal sediment in the (a,c,e) Bere Stream and (b,d,f) River Frome.

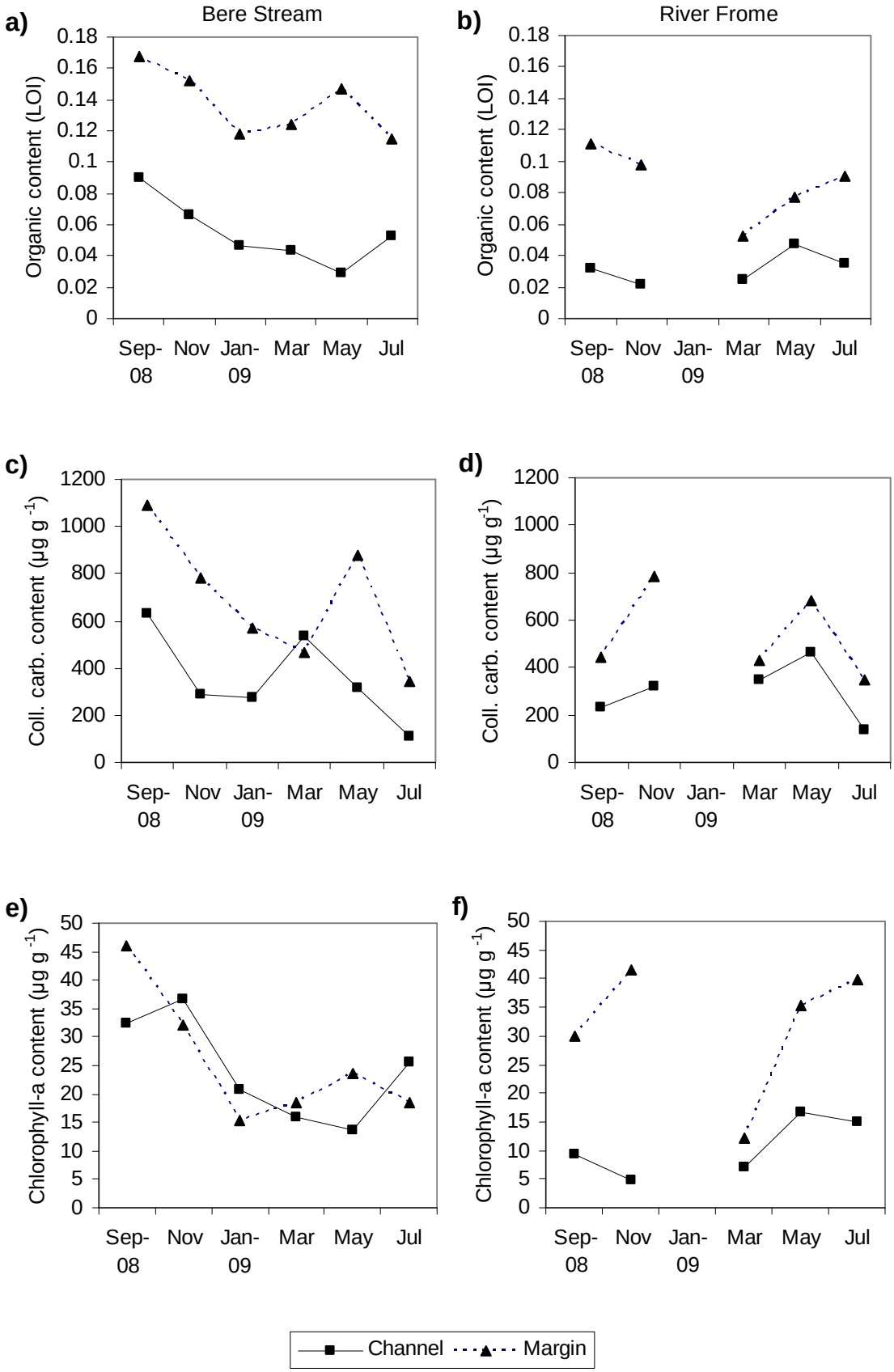

Figure 4.39. Temporal variations in biological sediment properties. (a,b) Organic content, (c,d) colloidal carbohydrate content (µg g^{-1} sediment), and (e,f) chlorophyll-a content (µg g^{-1} sediment) for channel and marginal sediment in the (a,c,e) Bere Stream and (b,d,f) River Frome.

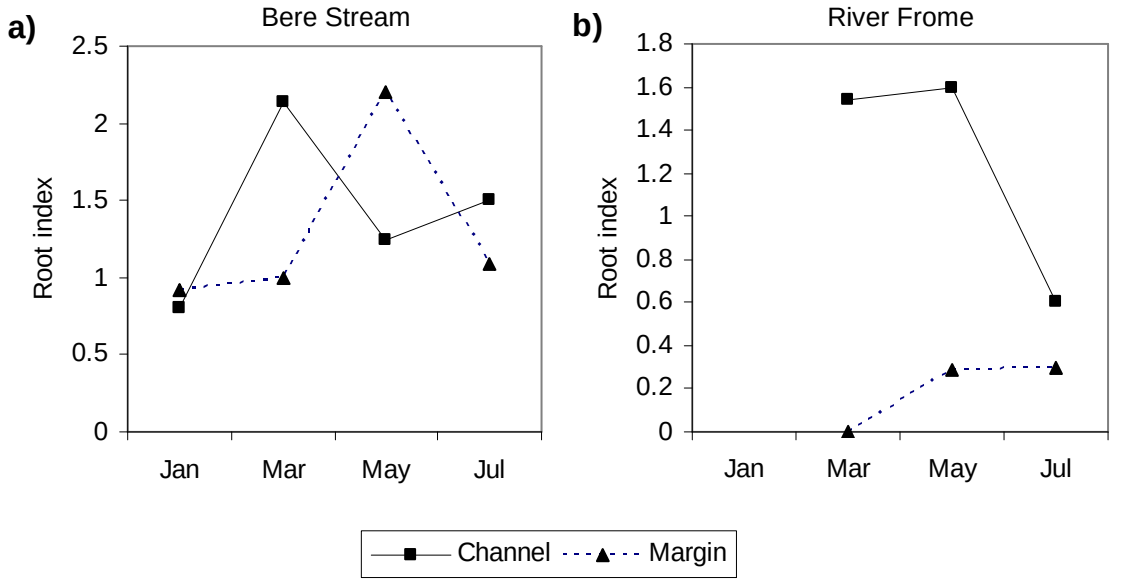

Figure 4.40. Temporal variations in root index at sampling locations for the (a) Bere Stream and (b) River Frome. Root index is an ordinal measure of macrophyte root density, ranging from 0 for no roots to 4 for a dense root mass.

4.3.2 CSM-derived erodibility

Mean CSM-derived erosion thresholds (P_{stag}) for both streams varied significantly over the study period (Fig. 4.41). P_{stag} was highest in September 2008, and lowest in May 2009, with a small peak in March 2009. Mean erosion thresholds declined significantly over this period, by over 50% (r_s = -0.269, $p < 0.01$). As in the earlier section on spatial patterns, temporal trends in erosion threshold were analysed using non-parametric tests because the data violates the assumptions of normality and homogeneous variances (i.e. homoscedasticity) (Levene's Test of Equality, F = 6.2, d.f.1 = 5, d.f.2 = 183, p = 0.00) (Dytham 2003). A significant difference was detected by sampling date (K-W, $\chi 2$ = 18.9, d.f. = 5, $p < 0.05$), and M-W tests were used to detect significant differences between sampling date pairs. These tests are appropriate for the investigation of temporal variations in erodibility because: (1) erosion threshold is a continuous variable, (2) measurements were not repeated for specific locations, in other words, random sampling ensured measurements were independent, and (3) the temporal resolution is sufficiently coarse to consider time as independent variable, which would likely not be the case for daily or weekly measurements, which would have a significant autocorrelation component (Dytham 2003, Gotelli & Ellison 2004).

Erosion thresholds were comparable between the two study streams. There were no statistically significant differences between average erosion thresholds by sampling date (S-R-H, F = 0.66, d.f. = 4, p = 0.95) (Fig. 4.42). Erosion threshold was significantly correlated with sampling date for both the Bere Stream (r_s = -0.272, p < 0.01) and the River Frome (r_s = -0.282, p < 0.01). The Bere Stream was substantially more variable than the River Frome, with mean erosion thresholds per sampling period ranging from 37 to 148 Pa compared to 60 to 101 Pa, respectively (Fig. 4.42).

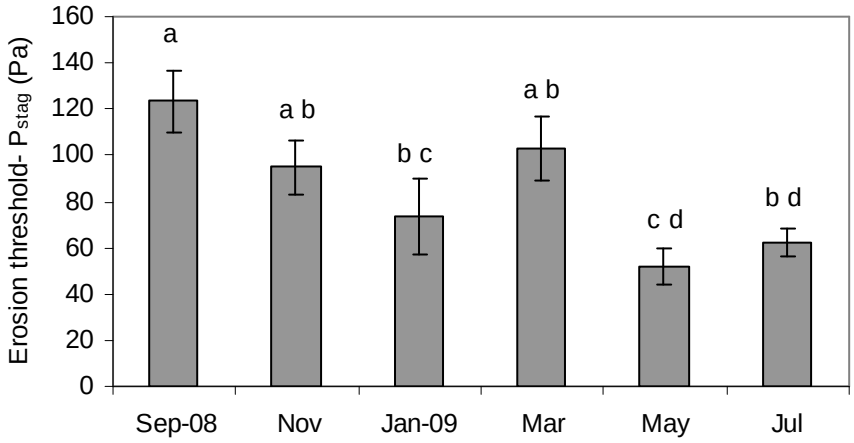

Figure 4.41. Mean CSM-derived erosion threshold (P_{stag}) by sampling date for both the Bere Stream and River Frome. Error bars are one standard error. Months marked with the same letter have erosion thresholds that are not significantly different (Kruskal-Wallis, Mann-Whitney, p < 0.05). Means and standard errors were used for presentation only, and were not used in the statistical tests.

Fine sediment from the channel had slightly higher erosion thresholds than marginal sediment for both streams at each sampling date (Fig. 4.43). Notable exceptions are the substantially greater erosion threshold for sediment in the channel centre for November 2008 in the Bere Stream (Fig 4.43a), and the greater erosion threshold for sediment in the margins in March 2009 for the River Frome (Fig. 4.43b).

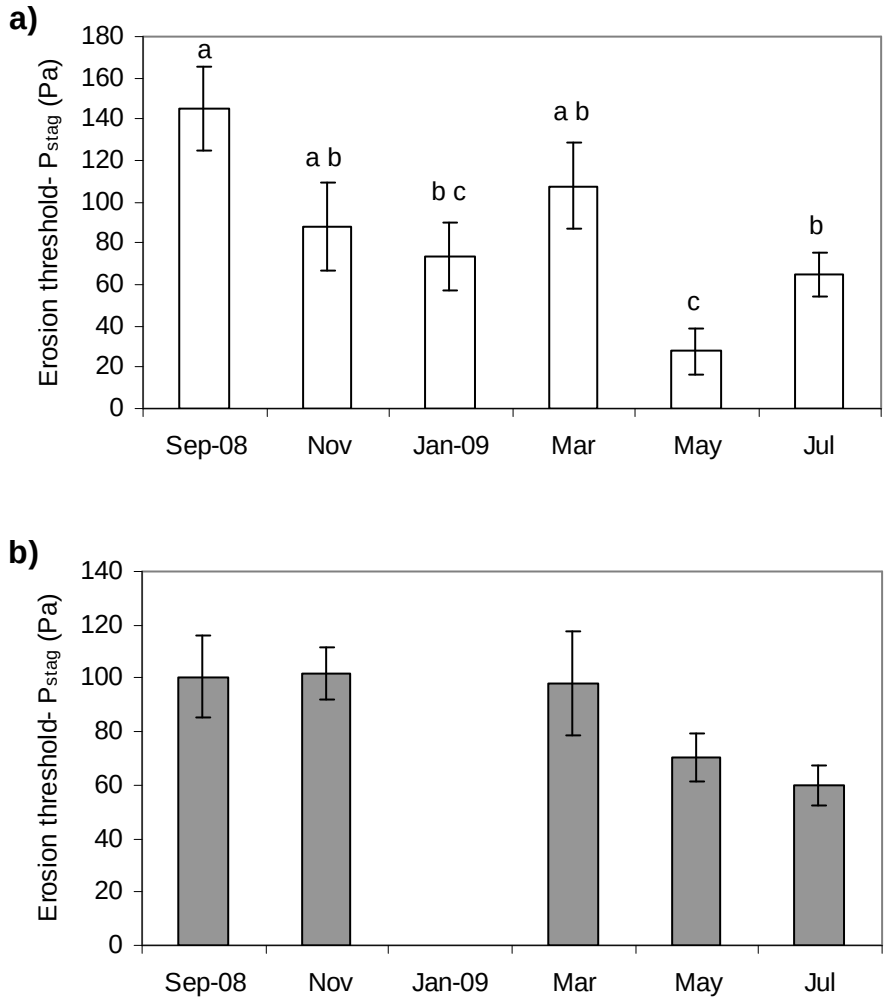

Figure 4.42. Mean CSM-derived erosion threshold (P_{stag}) by sampling date for the (a) Bere Stream and (b) River Frome. Error bars are one standard error. Months marked with the same letter have erosion thresholds that are not significantly different (Kruskal-Wallis, Mann-Whitney, $p < 0.05$). Note: Erosion threshold did not differ significantly for the River Frome by sampling date. Means and standard errors were used for presentation only, and were not used in the statistical tests.

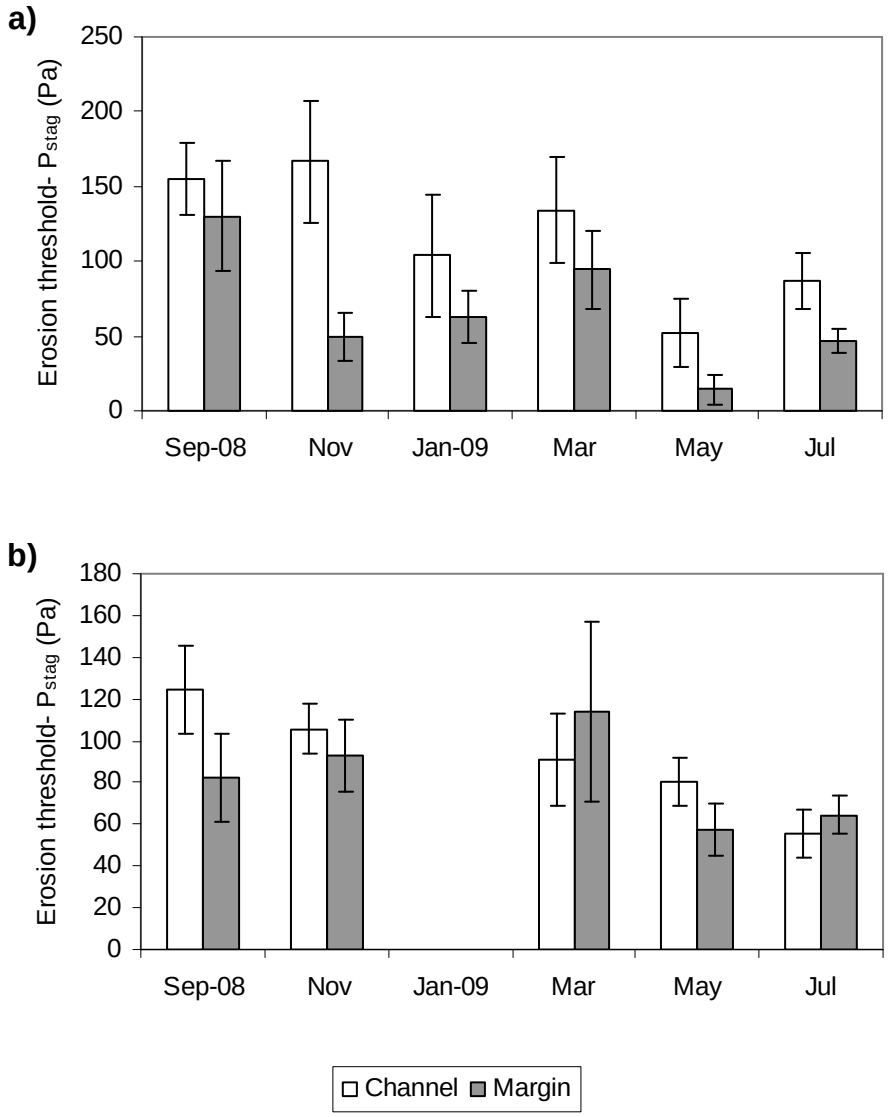

Figure 4.43. Mean erosion threshold (P_{stag}) by sampling date and location within the channel for the (a) Bere Stream and (b) River Frome. Error bars are one standard error.

The temporal trends in mean erodibility could be caused by macrophyte community dynamics, such as changes in species composition, percent cover or stand location within the channel, particularly in the Bere Stream. On average, sediment under *Ranunculus* had significantly higher erosion thresholds than marginal sediment (*Rorippa* and Marginal) (Fig 4.23a). Therefore changes in the relative abundance of *Ranunculus* vs. marginal macrophytes could have caused variations in average erodibility for the stream (Fig. 4.33). This did not seem to be a significant cause of variation, though, when temporal trends in erosion threshold by macrophyte types were investigated (Fig. 4.44). For example, months with low average erosion thresholds, such as May 2009, have low erosion thresholds for all major macrophyte types (Fig. 4.44a). The greater relative proportion of weak marginal sediment in May 2009 did push the monthly average lower, but erosion thresholds for *Ranunculus* were also at their lowest (Figs. 4.33 & 4.44a). In the River Frome, a declining trend in erosion thresholds was evident for all macrophyte types, and a large peak in erosion thresholds was observed in March 2009 for unvegetated marginal sediment (Fig. 4.44b).

Could changes in sediment properties be responsible for the temporal trends? Water velocity and effective particle size were implicated in the spatial patterns of erodibility. The greater discharge and faster flows in winter (Figs. 4.30-4.32) appear to correspond with an increase in particle size, particularly absolute particle size in the Bere Stream channel (Fig. 4.35e), but sediment erodibility in the Bere Stream channel was largely unchanged from September 2008 to March 2009 (Fig 4.43a). The chemical and biological sediment properties, though, displayed temporal trends that were similar to erodibility, particularly in the Bere Stream (Figs. 4.37 & 4.39). Calcium, magnesium and sodium contents declined over time (Fig. 4.37), mirroring the trend for discharge (Fig. 4.31). The trends in organic content and microbial abundance agree with general seasonal patterns in biological activity and the accumulation of organic matter. The steep decline in autumn and winter can be explained by decreases in biological production, and the removal of fine organic material during high water events. An increase in organic matter would be expected over the summer, however an earlier spring peak could occur due to benthic diatom blooms (Berrie 1992, Flynn et al. 2002). The timing of the erosion threshold peak for unvegetated marginal sediment in the Frome suggests seasonal stabilisation by benthic diatom activity (Fig. 4.44b), but this is not supported by temporal trends in colloidal carbohydrate and chlorophyll-a content (4.39d,f). The relationship between sediment properties and erodibility is difficult to

assess visually, so statistical techniques will be used to examine them in more detail in Chapter 5.

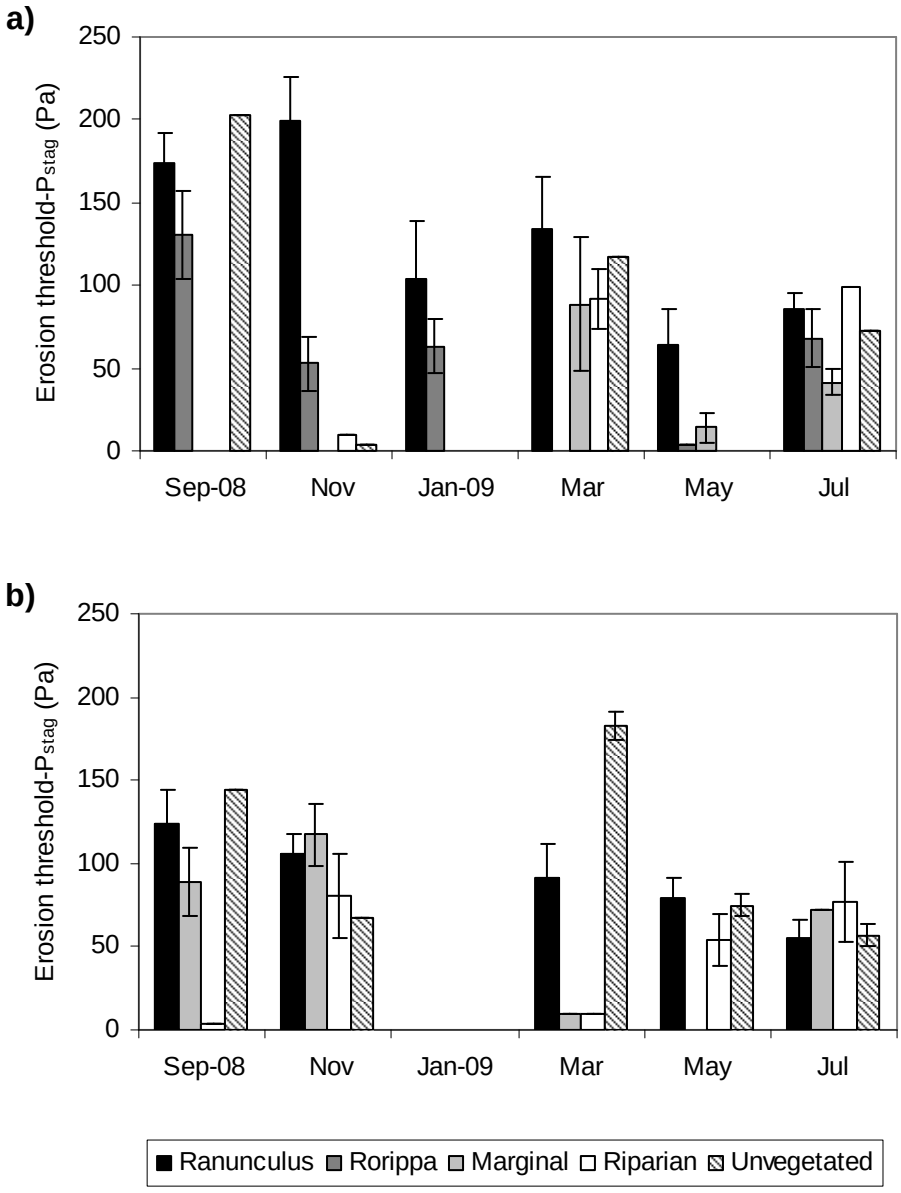

Figure 4.44. Erosion threshold by macrophyte type and sampling date for the (a) Bere Stream and (b) River Frome.

4.3.3 Vane-derived shear strength

Shear strength varied significantly between sampling dates for both streams, Bere Stream (K-W, $\chi^2 = 9.01$, d.f. = 3, p = 0.00) and the River Frome (K-W, $\chi^2 = 22.712$, d.f. = 2, p = 0.00) (Fig. 4.45). A one-way ANOVA was not applied, because the dataset, whilst satisfying the assumption of normality, violated the assumption of homogeneity in variance (Levene's, p > 0.05). In the Bere Stream, mean shear strength increased from January to May 2009, then decreased in July (Fig. 4.45a). In the River Frome, mean shear strength declined by over half from March to July (Fig. 4.45b). Shear strength did not differ between streams by sampling date (S-R-H, F = 2.69, d.f. = 2, p = 0.26).

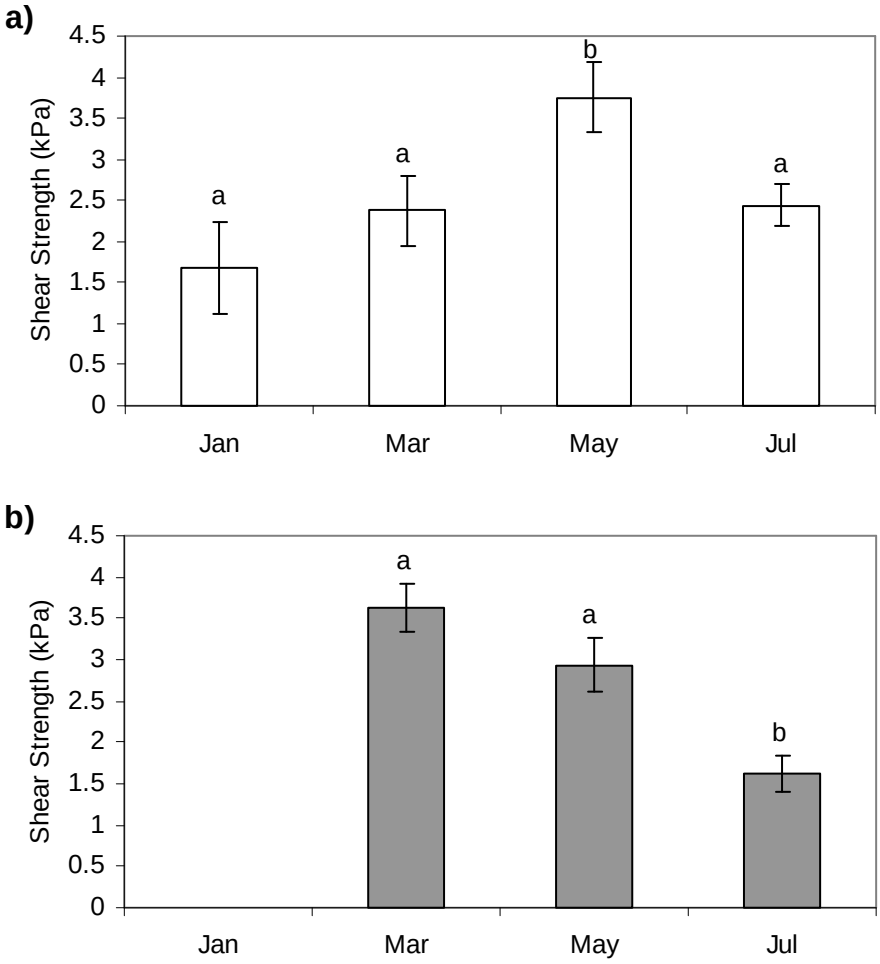

Figure 4.45. Shear strength of the sediment for each sampling date in 2009 for (a) the Bere Stream, and (b) the River Frome. Months marked with the same letter have shear strengths that are not significantly different (Kruskal-Wallis, Mann-Whitney, p = 0.05). Error bars are one standard error. Means and standard errors were used for presentation only, and were not used in the statistical tests.

The temporal variations in shear strength are similar to trends in dry bulk density (Fig. 4.35a,b), absolute particle size (Fig. 4.35e,f), and root index (Fig. 4.40). Shear strength was significantly, positively correlated to root index (r_s = 0.441, p <0.01) and was significantly different by root index category (Fig 4.46).

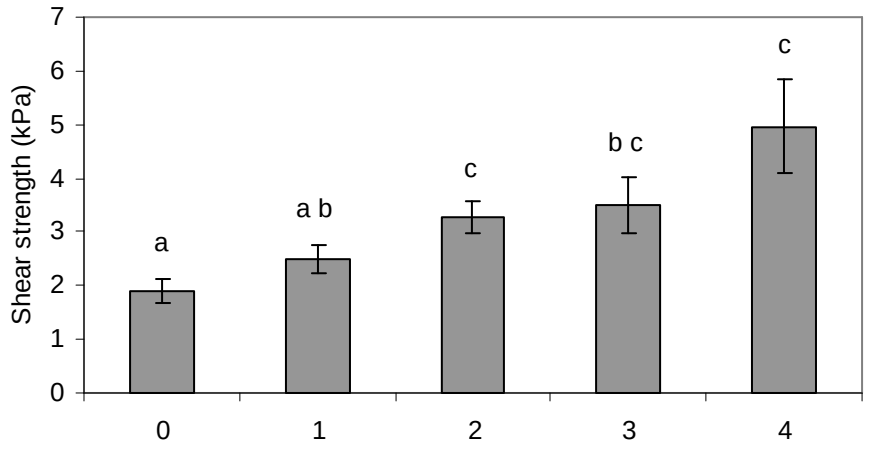

Figure 4.46. Shear strength by root index category. Error bars are one standard error. Categories marked with the same letter have shear strengths that are not statistically different (Kruskal Wallis, Mann-Whitney, p < 0.05). Means and standard errors were used for presentation only, and were not used in the statistical tests.

The temporal variations in shear strength appear to be caused by changes in root index in each macrophyte type, and changes in the relative proportion of substrate types each sampling period. For example, the peak in shear strength in May 2009 in the Bere stream (4.45a) was caused by high rooting indices for the two dominant macrophyte types, *Ranunculus* and Marginal (Fig. 4.47). For the River Frome, the high shear strength estimates in March and low estimates in July 2009 correspond to high and low rooting index values for dominant macrophyte types (Fig. 4.48). These observations strongly suggest that macrophyte roots are responsible for variations in shear strength, and the earlier conclusions drawn about potentially inaccurate measurements for Marginal and Riparian are rescinded (Section 4.2.3).

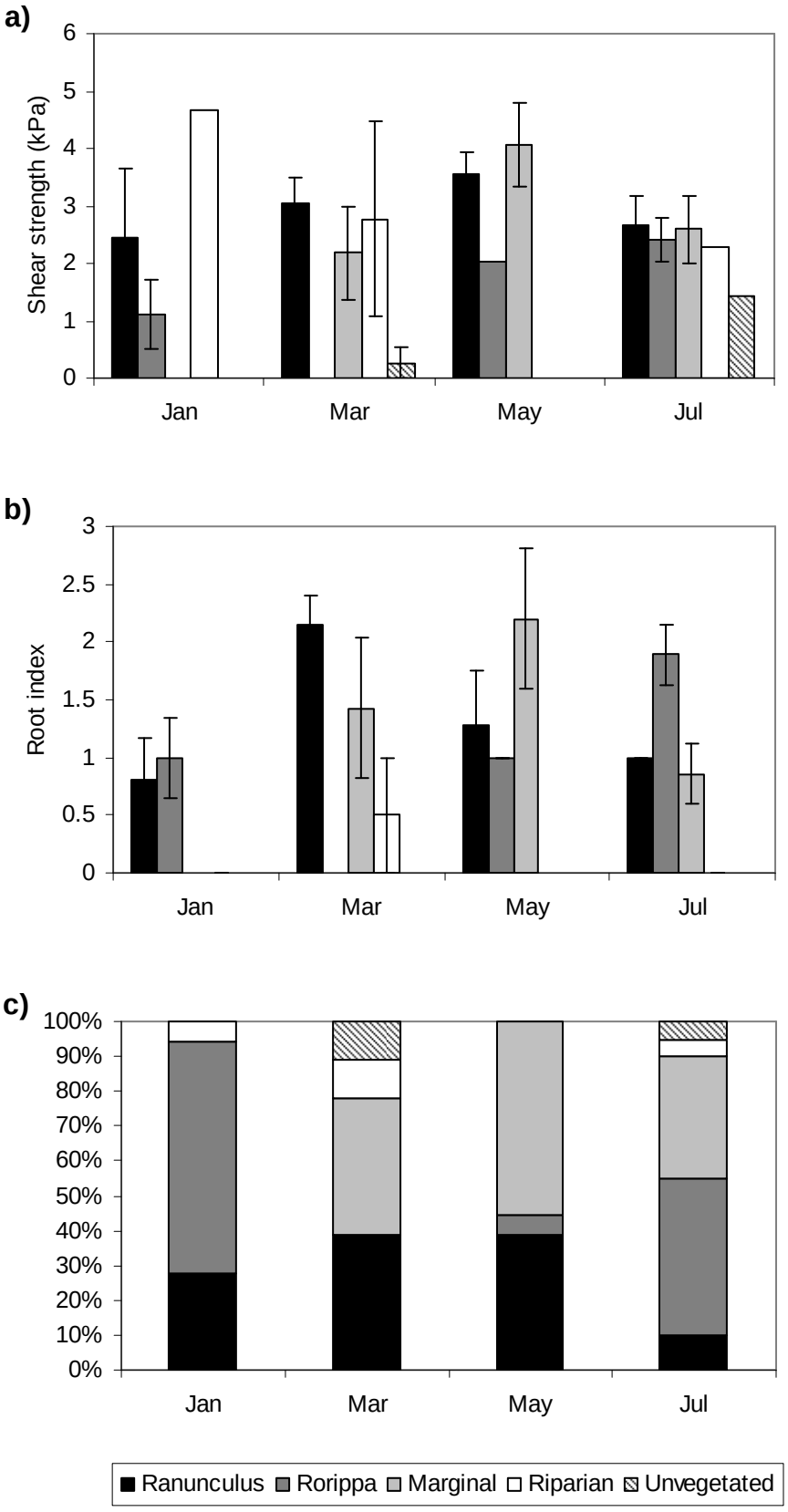

Figure 4.47. (a) Shear strength, (b) root index, and (c) frequency of macrophyte types by sampling date for the Bere Stream. Error bars are one standard error.

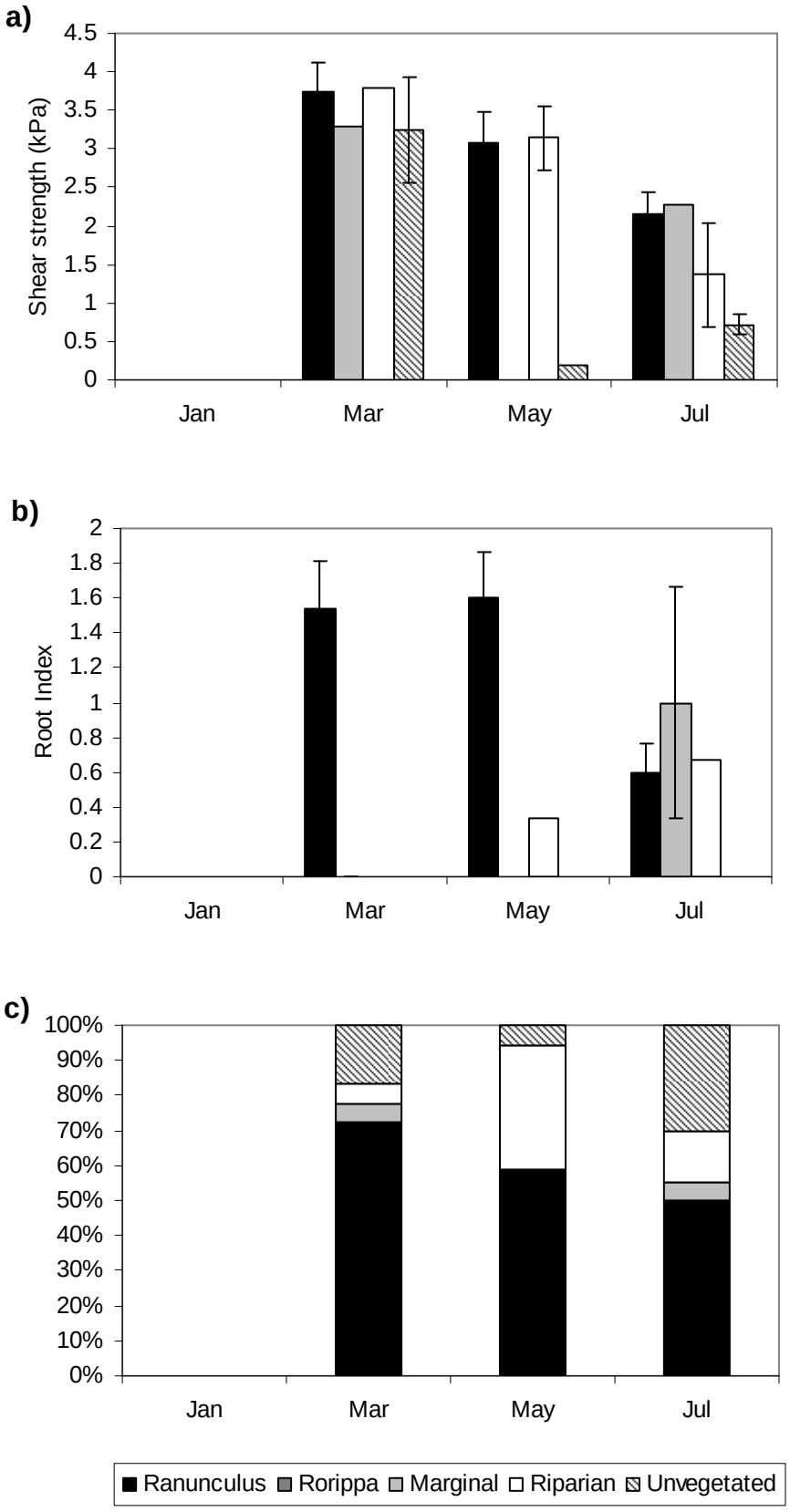

Figure 4.48. (a) Shear strength, (b) root index, (c) and frequency of macrophyte types by sampling dates for the River Frome. Error bars are one standard error.

4.4 Regression tree analysis

The previous sections described the spatial and temporal patterns in erosion thresholds and shear strength from the field survey. Statistical analysis techniques can be used to examine these patterns more closely.

Several analytical techniques are available to investigate relationships in ecological data. Principal components analysis (PCA) is probably the most widely-used approach for analysing multivariate datasets. It is often used in univariate analyses as a preliminary step to examine colinearity between variables, but does not directly examine relationships between explanatory variables (Crawley 2007). Other techniques, such as cluster analysis and discriminant analysis, can be used to determine groups in datasets based on similarities in their characteristics, and, in the case of discriminate analysis, examine how explanatory variables relate to the groups (Zuur et al. 2007). Whilst these techniques could be applied to the field survey dataset, the dataset is essentially univariate, as the objective was to examine how environmental factors and sediment properties factors influence erodibility. Consequently, techniques that directly test causal relationships between explanatory and response variables are most appropriate.

Regression trees are an ideal approach for the investigation of causal relationships for univariate datasets with multiple explanatory variables (Zuur et al. 2007). The aim of regression tree analysis is to divide the dataset into groups based on the explanatory variables in a way that minimise variances within groups. A regression tree is basically an inverted tree with a single root at the top, nodes are the locations of branching, and the branches terminate at leaves (Crawley 2007). The value given below a leaf is the mean value of the response variable. The regression tree model is fitted using binary recursive partitioning so that each split creates the maximum difference in data between the left and right branches (Zuur et al. 2007). The explanatory variable used for the split is identified above the node along with an argument, with the argument being true for the left branch. In the following sections, regression trees were used to examine which environmental variables were responsible for the variations in erosion threshold and shear strength.

4.4.1 CSM-derived erosion thresholds

The regression tree model identified relative distance across the channel as the most important environmental variable, with a split at a relative distance of 0.08 (Fig. 4.49). Further splits occurred by distance downstream (upstream or downstream of transect 9) and between measurements taken from September to March and May to July. Root mean square error (RMSE) is a measure of the prediction error of the model, and is simply the mean squared difference between predicted and actual erosion threshold. For this model RMSE was +/- 38 Pa. Before the tree is interpreted, though, it is necessary to simplify the model (i.e. prune the tree). As with linear regression, increasing the number of variables may improve model fit but it may make it more difficult to interpret, and risks overfitting the model to the data, in other words responding to random features of the data (Crawley 2007, Zuur et al. 2007). For example, a model with 185 variables would perfectly fit the field survey data, but would have no explanatory power. A cost-complexity measure (cp) can be used to balance model fit and explanatory power. For regression trees, cross-validation is used to estimate error in the prediction of erosion thresholds based on different sizes of trees. General guidance is to prune the trees down to the minimum size that has a relative error within 1 standard deviation of the minimum error. For this dataset, a tree size of 3 or 5 was appropriate (Fig. 4.50). A regression tree model, with a tree size of 5, identified relative distance across the channel, month, stream and water velocity as significant variables (RMSE = 55) (Fig. 4.51).

What this means is that sediment has the lowest erosion thresholds closest to the bank, < 8% of the relative channel width. For sediment located further out into the channel centre, there was a time component, and sediment tested in May and July 2009 had the next lowest erosion thresholds. For sediment collected earlier in the study, erosion thresholds were lower in the River Frome than in the Bere Stream, in which water velocity was an important determinant of erosion thresholds. This agrees with the earlier observations on the importance of relative distance and water velocity and the existence of variations between streams and over time. Whilst the temporal component is interesting, the resulting model would be more informative if it was based solely on environmental descriptors. The model was rerun without time, and the resulting model identified relative distance across channel and water velocity as significant variables. (RMSE = 60) (Fig. 4.52). The prediction error was slightly higher, but both models produce coarse estimates of erosion threshold.

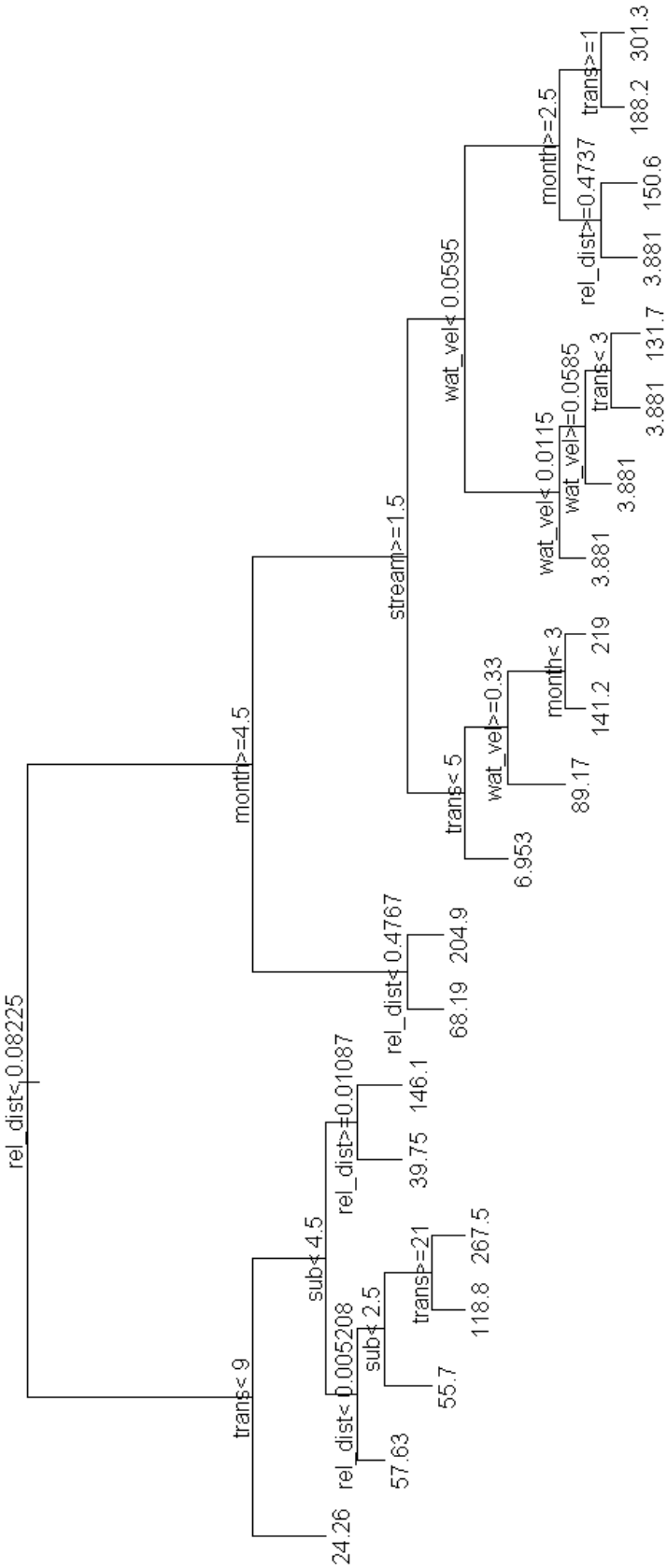

Figure 4.49 Regression tree model for CSM-derived erosion thresholds (P_{stag}). RMSE = 38.27. Rel_dist = relative distance across channel; month is an ordinal variable (1-6); trans = transect #; sub = macrophyte type, a = Ranunculus, b = Rorippa, c= Marginal, d = Riparian, e = Unvegetated; stream, 1 = Bere, 2 = Frome; wat_vel = water velocity.

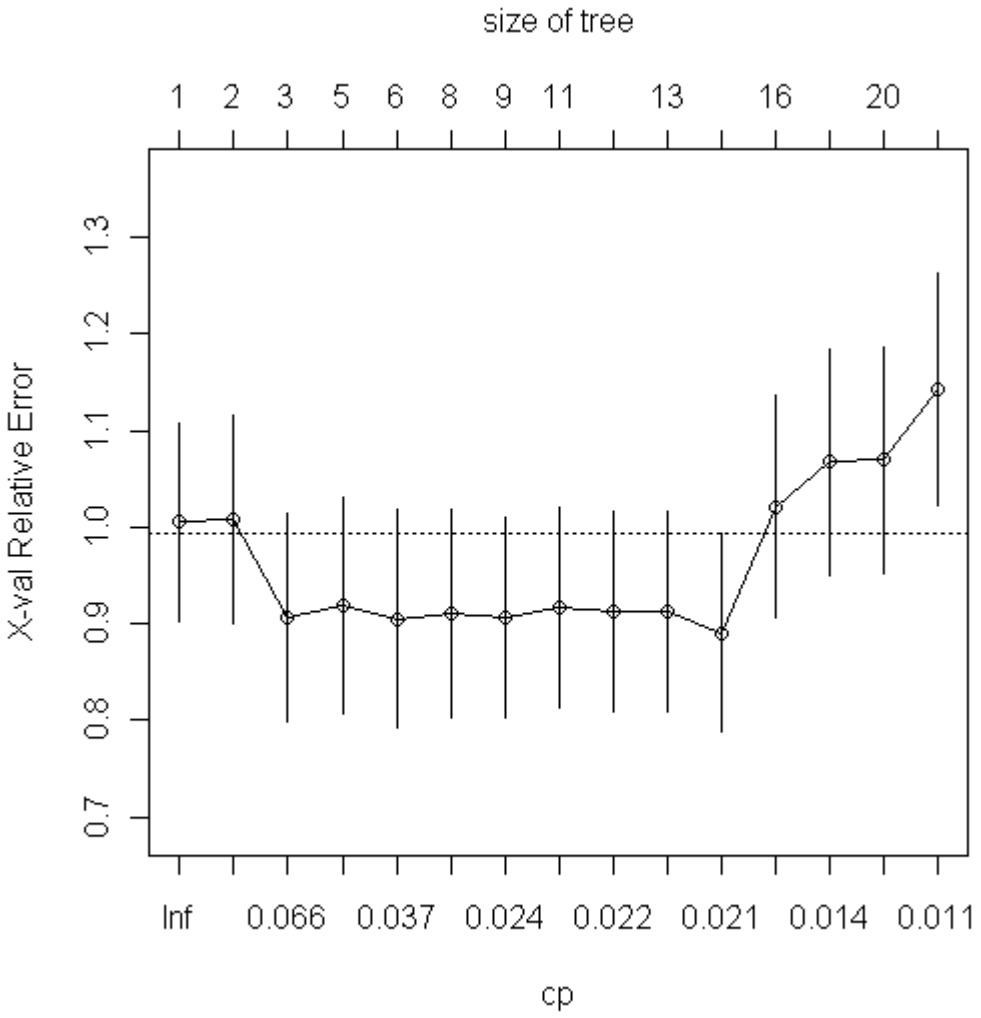

Figure 4.50. A plot of relative error, tree size and the cost-complexity parameter (cp) used to prune the regression tree model for CSM-derived erosion thresholds (P_{stag}). This plot indicates a tree size of 3 or 5 is appropriate.

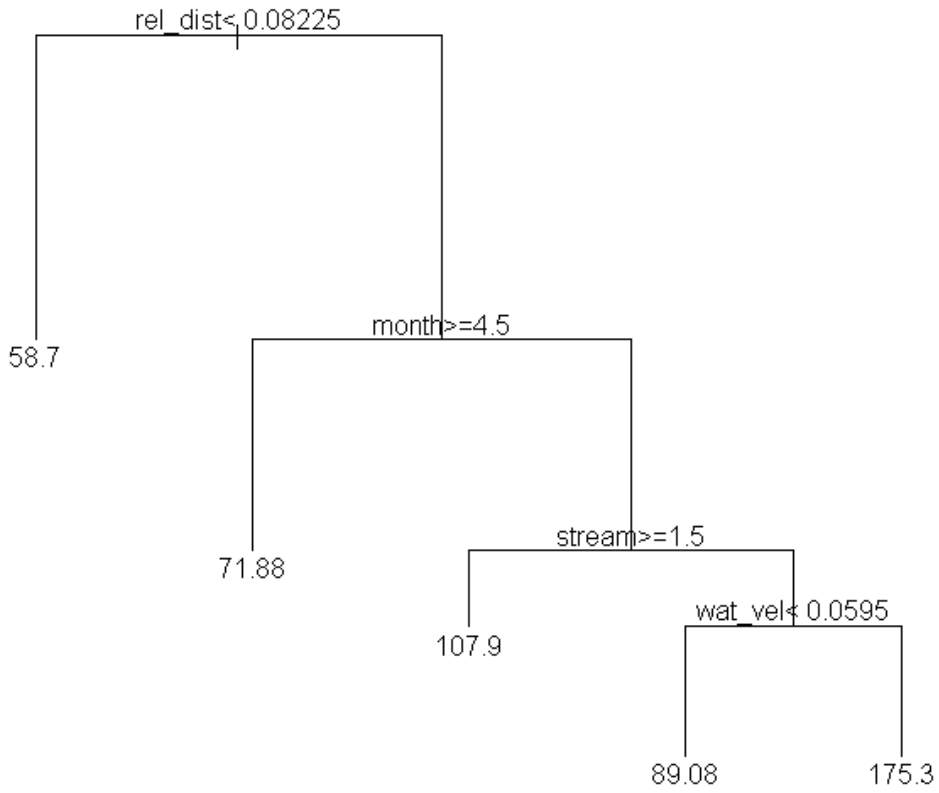

Figure 4.51. The pruned regression tree model for CSM-derived erosion thresholds (P_{stag}). RMSE = 55.16. rel_dist = relative distance across channel; month is an ordinal variable (1-6); stream, 1 = Bere Stream, 2 = River Frome; wat_vel = mainstream water velocity at each sampling location.

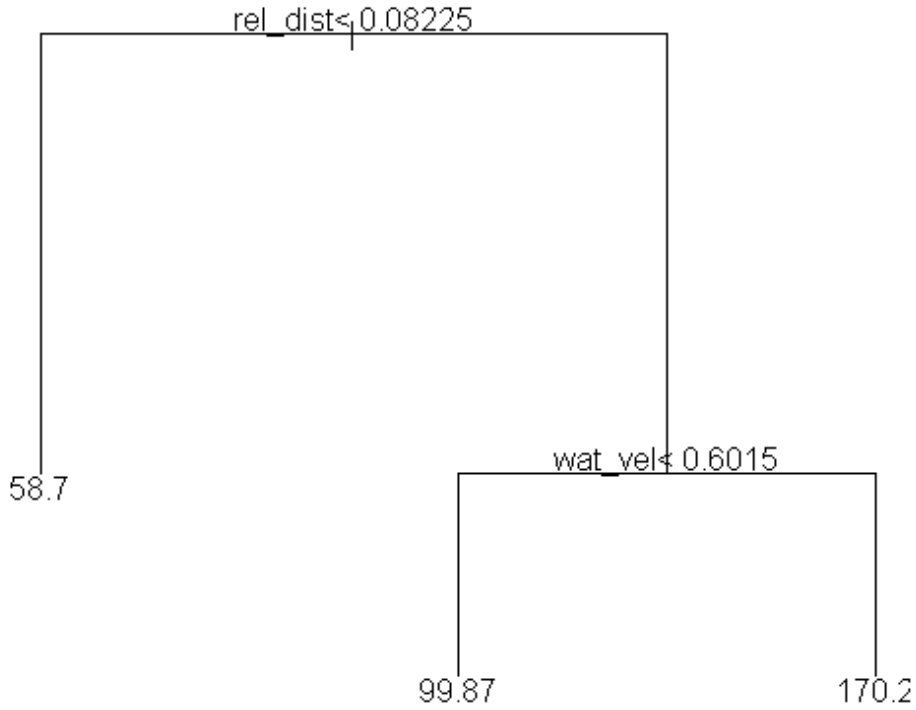

Figure 4.52. The final pruned model for CSM-derived erosion thresholds (P_{stag}), with time excluded as an explanatory variable. RMSE = 60.07. rel_dist = relative distance across channel; wat_vel = mainstream water velocity at each sampling location.

4.4.2 Vane-derived shear strength

A regression tree was attempted for the shear vane dataset, but the creation of a valid model based on environmental variables was not possible. Inspection of the cost-complexity plot (cp) shows that adding variables to the model did not decrease model error (Fig. 4.53). In other words, the environmental variables did not account for any of the variation in the dataset. The analysis was repeated using the reduced dataset described in the discussion of spatial patterns, with Margin and Riparian samples excluded (Section 4.2.3), but this did not improve the model fit. In summary, shear strength was not correlated with location within the channel, water velocity, or macrophyte type. Shear strength does appear to be correlated with sediment properties, such as root index (Fig. 4.46), and these relationships are explored in following chapter (Chapter 5).

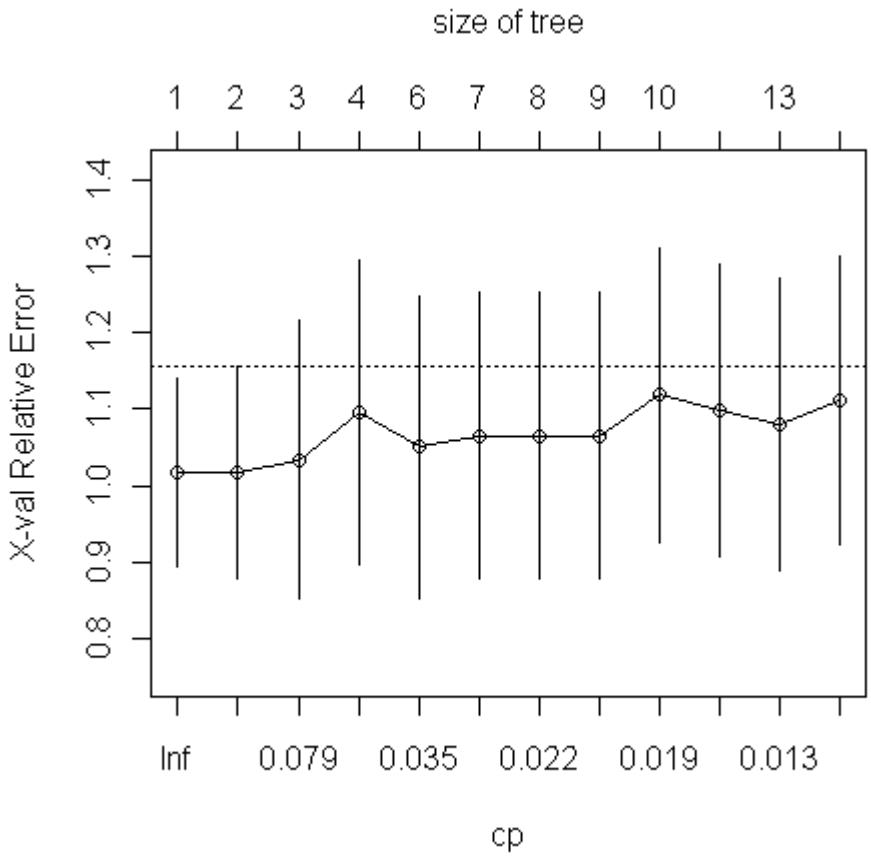

Figure 4.53. A plot of tree size and the cost-complexity parameter (cp) for the regression tree model of vane-derived shear strength.

4.5 Discussion

The field study investigated the spatial and temporal variability in the erodibility of fine sediment deposits in lowland chalk streams. Previous studies in these streams have established the crucial role macrophytes play in altering the hydrodynamics and sediment dynamics in these systems (Cotton et al. 2006, Gurnell et al. 2006, Wharton et al. 2006). They have demonstrated that the lower velocity, reduced turbulence patches created by the macrophytes encourage the deposition and retention of fine sediment within the stands. These sediment deposits constitute significant stores of fine material, up to 10 kg m^{-2} for the Snatford Bridge site on the Bere Stream and 10-70 kg m^{-2} for a site on the River Frome just upstream of the Frome Vauchurch site (Heppell et al. 2009). Whilst some sediment is stored in the gravel bed itself, due to colmation, the majority of the fine sediment is found within the macrophyte stands. Temporal variations in the amount of sediment stored in the reaches are correlated to the percent cover of the aquatic vegetation, which exhibits strong seasonality (Heppell et al. 2009). This field survey builds upon this foundation of research by demonstrating that the erodibility of surficial fine sediment deposits in lowland chalk streams vary significantly within reaches and over time.

4.5.1 Spatial variations in CSM-derived erodibility

CSM-derived erosion thresholds varied significantly over space within stream reaches (Figs. 4.22 & 4.23; Table 4.1). These variations are principally explained by the location of the sediment across the channel and water velocity at the location (Fig. 4.52). These two variables are closely linked to one another. Surficial fine sediment deposits form in areas of reduced flow, in which hydrodynamic conditions are conducive to sediment deposition and erosion is less likely. Water velocity decreases from the centre of a channel towards the channel bank due to the effects of friction (Fig. 4.25a) (Knighton 1998). The decrease in water velocities from channel towards margins produces a gradient in the size of sediment particles/aggregates deposited at the bed (Fig. 4.25c). In this study, surficial sediment grades from gravel and coarse sand in high flow regions, such as the thalweg, to fine sand-sized particles in channel *Ranunculus* deposits to very fine sand- and coarse silt-sized particles/aggregates towards the bank. The lower velocities near the bank mean that the water has less energy to erode and transport sediment, allowing for the development of large surficial fine sediment deposits. These fine sediments have lower erosion thresholds than sand-sized particles,

particularly when coupled with low bulk densities (e.g. Postma diagram, Dade et al. 1992). Cohesion is not a significant resistive force in these unconsolidated sediments, which likely erode in a non-cohesive manner (El Ganaoui et al. 2007). These results support Hypothesis 1a, which predicted high erosion thresholds in the channel centre than in the margins (Section 2.4).

Water velocity is indicative of the hydrodynamic conditions and sediment characteristics in a stream in general, but it becomes less so for a vegetated stream. Dense patches of vegetation significantly reduce water velocity and turbulence within the patches, creating microenvironments favourable to sediment deposition, even within the centre of a stream channel (Sand-Jensen 1998, Gacia et al. 1999, Horvath 2004, James et al. 2004, Cotton et al. 2006). Dense stands of emergent macrophytes baffle hydrodynamic forces over the entire vertical profile. However, submerged macrophyte stands will reduce water velocities over less of the vertical profile, and may actually increase flow immediately above them due to the convergence of flow lines. Therefore, water velocity measurements at a set depth may not accurately reflect the hydrodynamic forces acting upon the sediment in that location. An estimate of discharge may better represent the overall hydrodynamic forces operating on the reach, whilst measurements of boundary layer shear stress may better represent the specific conditions at each sampling location.

The patterns in erosion threshold by macrophyte type for the Bere Stream appear to be a result of a covariation between macrophyte and location within the stream. Different aquatic macrophyte species display a preference for channel centres or margins (Fig. 4.5), and the differences in particle sizes in these locations may be the principal cause for differences in erosion thresholds (Fig. 4.10 & 4.11). This is clearest when comparing erosion thresholds and particle sizes between *Ranunculus* and Marginal in the Bere Stream (Figs. 4.15 & 4.23). It was also evident for *Rorippa*, which was found in both the channel centres and margins of Bere Stream. The sediment was coarser in the channel centres (Figs. 4.15 & 4.16) and had erosion thresholds almost twice as high as in the margins (Section 4.2.2). Variations in erosion thresholds may also be caused by macrophyte type or morphology. *Rorippa* succeeded *Ranunculus* in some of the stands in the channel of Bere stream. This change in macrophyte type corresponded to a decrease in mean erosion thresholds from 132 to 102 Pa. This decrease, although not significant, suggests that plant morphology may influence sediment erodibility. The

emergent stands of *Rorippa* could alter hydrodynamic conditions differently than the emergent macrophyte *Ranunculus*, or have different biological communities, causing a change in the properties of the sediment. Unfortunately, the dataset is not well-suited to this analysis due to low sample sizes and significant temporal covariations with sediment properties.

4.5.2 Temporal variations in CSM-derived erodibility

CSM-derived erosion thresholds decreased significantly over the study period from September 2008 to July 2009 (Fig. 4.41). The decline was observed in both study reaches, but was more pronounced in the Bere Stream, which saw mean thresholds drop by over 50% (Fig 4.42).

Erosion thresholds were substantially more variable over time in the Bere Stream than in the River Frome (Fig. 4.42). It was originally hypothesised that temporal fluctuations in macrophyte abundance would influence erosion thresholds (Hypothesis 1b-2; Section 2.4). Since distance across the channel is significant correlated to erosion thresholds (Figs. 4.25 & 4.43), a logical step is to hypothesise that changes in the relative abundance of macrophytes in the channel or margins would affect temporal averages. However, this is not supported by the data. Erosion thresholds varied within each macrophyte type over time (Fig. 4.44), and the relative proportion of macrophyte types, or location in the margins vs. channel centre had little influence on the temporal means (Figs. 4.44 & 4.33). Therefore the temporal patterns must be caused by changes in the sediment properties over time.

The temporal patterns in CSM-derived erosion thresholds are similar to trends in chemical and biological properties. SAR and M:D displayed remarkably similar temporal patterns to erosion thresholds for both stream reaches (Figs. 4.38c-f & 4.42). However it is unlikely that a decrease in the relative concentration of monovalent to divalent cations is responsible for the decrease in erodibility. The decrease in SAR is two-fold, but remains well below the limit at which SAR affects erodibility of soils (13-15). Changes in the cation content could have affected erodibility, though. Normalised calcium, magnesium and sodium decreased over the study period (Figs. 4.37). Total salinity has been shown to be positively correlated with erosion thresholds (Aberle et al. 2004, Debnath et al. 2007, Spears et al. 2008), because it increases the cohesion of

colloids (inorganic and organic) and the stability of EPS (Section 2.3.2) (Decho 2000, Korstgens et al. 2001, Winterwerp & Van Kesteren 2004, Ravisangar et al. 2005, de Kerchove & Elimelech 2006, Partheniades 2007).

The temporal patterns in biological properties also mirror CSM-derived erosion thresholds, particularly for the Bere Stream (Figs. 4.39 & 4.42). There was a general decrease in organic content, colloidal carbohydrate content and chlorophyll-a content over time (Fig. 4.39). These results tentatively support Hypothesis 1b-1, which predicted a cyclical pattern in erosion thresholds due to seasonal biological activity.

Further examination of the temporal patterns in erosion threshold for the individual streams reveals more complex patterns. In the Bere Stream, mean erosion threshold displayed a periodic pattern over time that suggests a greater influence of biological properties, particularly for sediment in the margins (Fig. 4.43). Erosion thresholds were highest in the margins in September 2008, dropped in November, then increased to March 2009. The peak in March 2009 is clearly represented in all marginal macrophyte types (Fig. 4.44). The subsequent drop to May 2009 coincided with the appearance of a substantial unconsolidated surficial layer (pers. obs.; Fig. 4.39a). For the River Frome, whilst there is a steady decline in erosion thresholds for sediment under *Ranunculus*, the erosion thresholds for sediment in the margins showed more variability (Figs. 4.43 & 4.44). Of particular interest are the temporal patterns for bare, unvegetated sediment. The study reach in the River Frome had a large area of marginal sediment located immediately downstream of large woody debris, and shaded by riparian trees. This area of the reach consistently had fine sediment accumulation, however erodibility varied substantially over time (Fig. 4.44). In March 2009, the sediment had markedly high erosion thresholds, higher than most of the other measurements taken in the River Frome over the entire study. The sediment had a visible, green biofilm on the surface. Whilst sample sizes are low, it is evidence for the biostabilisation of fine riverine sediment by the benthic microbial community. However it should be noted that the presence of a visible biofilm was not expressed as higher chlorophyll-a or colloidal carbohydrate content.

4.5.3 Shear vane-derived erodibility

Sediment strength as measured by the shear vane also differed significantly over space and time (Figs 4.28 & 4.45). However, regression tree analysis found no significant correlation between environmental variables and shear strength (Section 4.4.2). Sediment properties, particularly root index, appear to be driving variations in shear strength (Fig. 4.46), and these relationships will be investigated in more detail in Chapter 5.

Shear vane-derived shear strengths and CSM-derived erosion thresholds were not correlated in this study (Table 4.2). As discussed earlier, the CSM measures an aspect of surface erodibility, whilst the shear-vane quantifies the sediment's resistance to mass erosion (Section 2.2.5 & 3.2.3). It was hypothesised that the tools could be used in tandem to generate a comprehensive picture of the erodibility of fine sediment in the stream reaches. However, one study has demonstrated a significant positive correlation between CSM-derived erosion thresholds and an estimate of geotechnical strength (Watts et al. 2003). The study found that on an estuarine mudflat, drop cone penetration tests and the CSM produced comparable results. The drop cone penetration test is not directly comparable to a shear vane test, though. It measures the sediment's resistance to penetration at the sediment surface, so in fact both the CSM and drop cone test surficial sediment.

4.5.4 Conclusion

In conclusion, the yearlong field survey provides evidence of significant spatial and temporal variations in fine sediment erodibility. CSM-derived erosion thresholds were positively correlated with distance across the channel, which is due to the greater water velocities and larger particle sizes found in the channel centres (Table 4.1; Figs. 4.22, 4.25a,c,e & 4.52). Erosion thresholds were at their highest at the start of the study in September 2008 and decreased over the study period to a low in 2009 (Fig. 4.43). In the Bere Stream, there was a three-fold decrease in erosion thresholds for sediment in the channel centres from September 2008 to May 2009 (Fig. 4.43). In the River Frome, there was a two-fold decrease from September 2008 to July 2009 (Fig. 4.43). The temporal trends do not appear to be caused by macrophyte community dynamics, but rather general changes in sediment properties, particularly chemical and biological ones. The implications of the results for sediment stability, inclusive of hydrodynamic effects,

are discussed in the Synthesis section (Chapter 7). The following chapter, Chapter 5, presents statistical analyses of the dataset, which identify the key sediment properties responsible for the variations in erodibility in the field survey.

Chapter 5: Sediment properties affecting erodibility

This chapter presents an analysis of the sediment properties that influence the erodibility of fine sediment within chalk streams. The previous chapter demonstrated that erodibility varied significantly within stream reaches and over the course of the field survey, and found significant correlations between environmental variables and erodibility. Erodibility, though, is dependent on sediment properties (Winterwerp & Van Kesteren 2004). Therefore, the objective of the following analyses was to identify the key sediment properties that influence erodibility, and then generate an empirical model of erodibility based on those properties.

The chapter employs a range of multivariate statistical techniques to identify the major sediment properties that influence erodibility, starting with data exploration (Section 5.1), then progressing to linear regression analysis (Section 5.2), and finishing with mixed effects modelling (Section 5.3). (Note: Generalised linear modelling and generalised additive modelling approaches were also attempted, but did not significantly improve model fit (Appendix III)). Then, the analysis procedure is repeated for vane-derived shear strength (Section 5.4). Finally, the results of the analyses are discussed and recommendations are given for future studies (Section 5.5).

5.1 Descriptive statistics and data processing

The first step in analysing complex environmental datasets is to visually explore the response and predictor variables to uncover information on the distribution of the data and inform the selection of statistical analytical technique. As discussed in the previous chapter (Section 4.2.2), the frequency distribution of erosion threshold P_{stag} differs

significantly from normal (K-S, Z = 1.538, p = 0.018). The histogram and Q-Q plot are recreated here for convenience (Fig. 5.1).

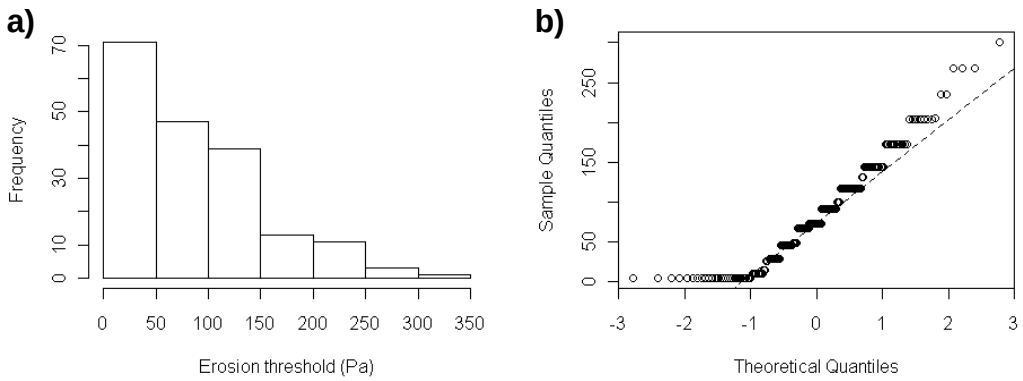

Figure 5.1. (a) Histogram and (b) quantile-quantile (Q-Q) plots to assess normality of erosion threshold data (P_{stag}). The non-linear relationship in the Q-Q plot indicates a departure from normal distribution.

All statistical techniques require some level of assumptions to be made about the dataset, and normality is an important one, particularly for parametric techniques. The lack of normality in the erosion threshold frequency distribution will need to be rectified using transformations if linear regression analysis is to be used. Alternatively, a generalised linear modelling approach (GLM) could be employed, and another frequency distribution would be used in the analysis. Normality and the other key assumptions for different statistical analytical techniques will be discussed in the following sections in relation to the field survey data.

5.1.1 Correlations, scatter plots and coplots

CSM-derived erosion threshold (P_{stag}) was significantly correlated to a wide range of sediment properties (Table 5.1, Fig. 5.2). Physical properties, particularly those based on effective size, had the highest correlation coefficients. Median effective particle size demonstrated the clearest positive correlation with erosion threshold (r_s = 0.34) (Table 5.1). Properties based on absolute particle size also had significant correlations, as did dry bulk density, organic content, normalised magnesium and sodium contents, and normalised monovalent:divalent ratio. There were substantial covariations between sediment properties, with virtually all properties showing strong correlations with bulk density and particle size (Fig. 5.2). Consequently, caution must be exercised during

statistical analysis to avoid superfluous variables, such as assess collinear variables using variance inflation factors (VIFs) in linear regression analysis (Fox 2002).

*Table 5.1. Spearman rank correlation for CSM-derived erosion threshold (P_{stag}) and sediment properties. Significant at the 0.05 * level and 0.01 ** level (2-tailed).*

	Total	Bere	Frome
Dry bulk density	0.22 **	0.27 *	0.11
Median effective particle size	0.34 **	0.40 **	0.23*
Effective % < 63 μm	-0.32 **	-0.39**	-0.22*
Median absolute particle size	0.33 **	0.38 **	0.22*
Absolute % < 2 μm	-0.30 **	-0.38 **	-0.16
Absolute % Sand	0.29 **	0.35 **	0.18
Organic content	-0.22 **	-0.24 *	-0.14
Colloidal carbohydrate content	-0.11	-0.17	-0.01
Chlorophyll a content	-0.02	0.13	-0.14
Sodium absorption ratio	0.01	0.10	0.09
Ca (Normalised)	0.11	0.26*	0.15
Fe (Normalised)	0.09	0.15	0.04
Mg (Normalised)	0.20 **	0.28**	0.14
Na (Normalised)	0.17*	0.31**	0.22*
M:D (Normalised)	0.20**	0.25*	0.18

Interestingly, there were differences in the number and significance of correlations for the Bere Stream and River Frome (Table 5.1). Erosion threshold was more strongly correlated to sediment properties in the Bere Stream. All of the properties significant for the full dataset were significant for the Bere Stream, with the addition of normalised calcium content (Table 5.1, Fig. 5.3). In the River Frome, erosion threshold was only significantly correlated to median particle size (effective and absolute), effective mud content, and normalised sodium content (Table 5.1; Fig. 5.4). This observation suggests that there are differences between streams that are not represented by the sediment property data, and which may need to be incorporated into the statistical analysis. This may be done directly, using stream as a predictor variable in linear regression, or indirectly, as a random effect in mixed effect modelling. In recognition of the high levels of covariance between the explanatory variables, partial correlation analysis was also run, controlling for dry bulk density and effective particle size (Dytham 2003). Correlation coefficients were comparable to the Spearman rank correlations for all variables with one exception; when dry bulk density was controlled for, chlorophyll-a content had a significant correlation to P_{stag} ($r = 0.18$, $p < 0.05$).

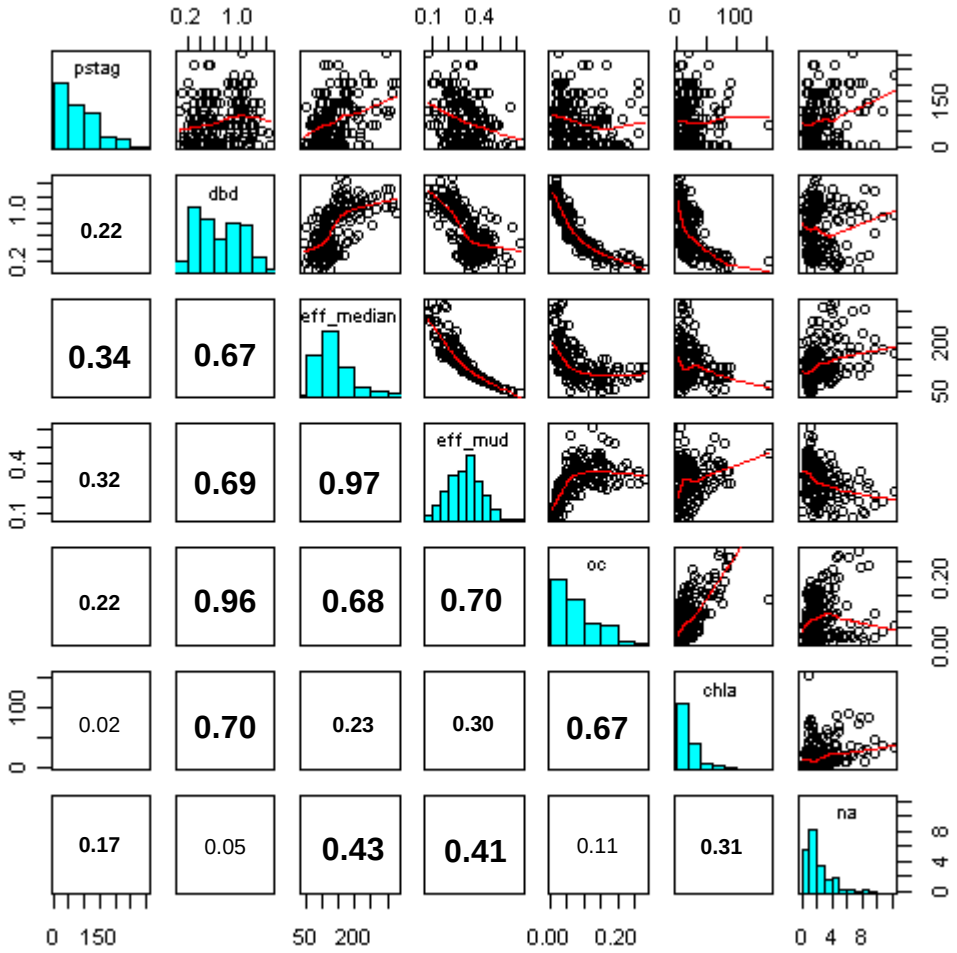

Figure 5.2. Scatterplot of CSM-derived erosion threshold (pstag) and selected sediment properties for both streams with histograms along the diagonal and Spearman rank correlation coefficients in the lower panels. Bold font indicates the correlation is significant at the 0.05 level. dbd = dry bulk density; eff_median = median effective particle size; eff)mud = mud content based on effective size; oc = organic content (LOI), chla = chlorophyll-a content; na = normalised sodium content.

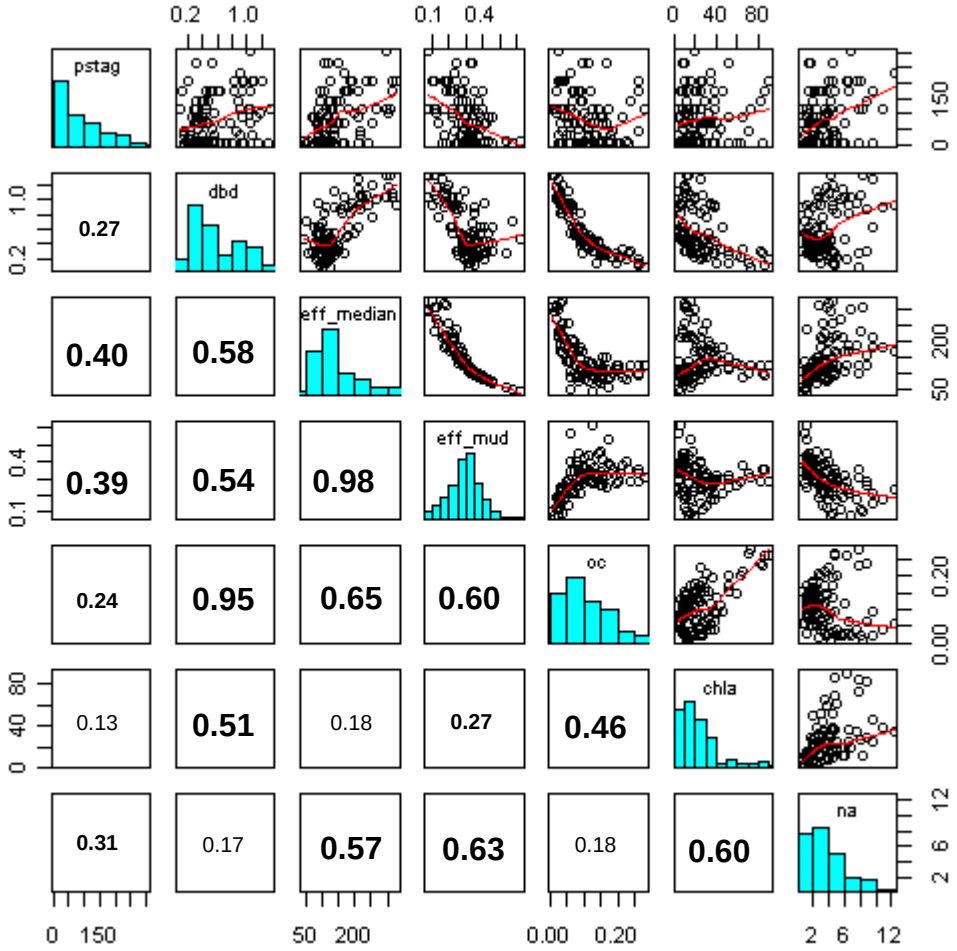

Figure 5.3. Scatterplot of CSM-derived erosion threshold (pstag) and sediment properties for the Bere Stream, with histograms along the diagonal and Spearman rank correlation coefficients in the lower panels. Bold font indicates the correlation is significant at the 0.05 level. dbd = dry bulk density; eff_median = median effective particle size; eff_mud = mud content based on effective size; oc = organic content (LOI), chla = chlorophyll-a content; na = normalised sodium content.

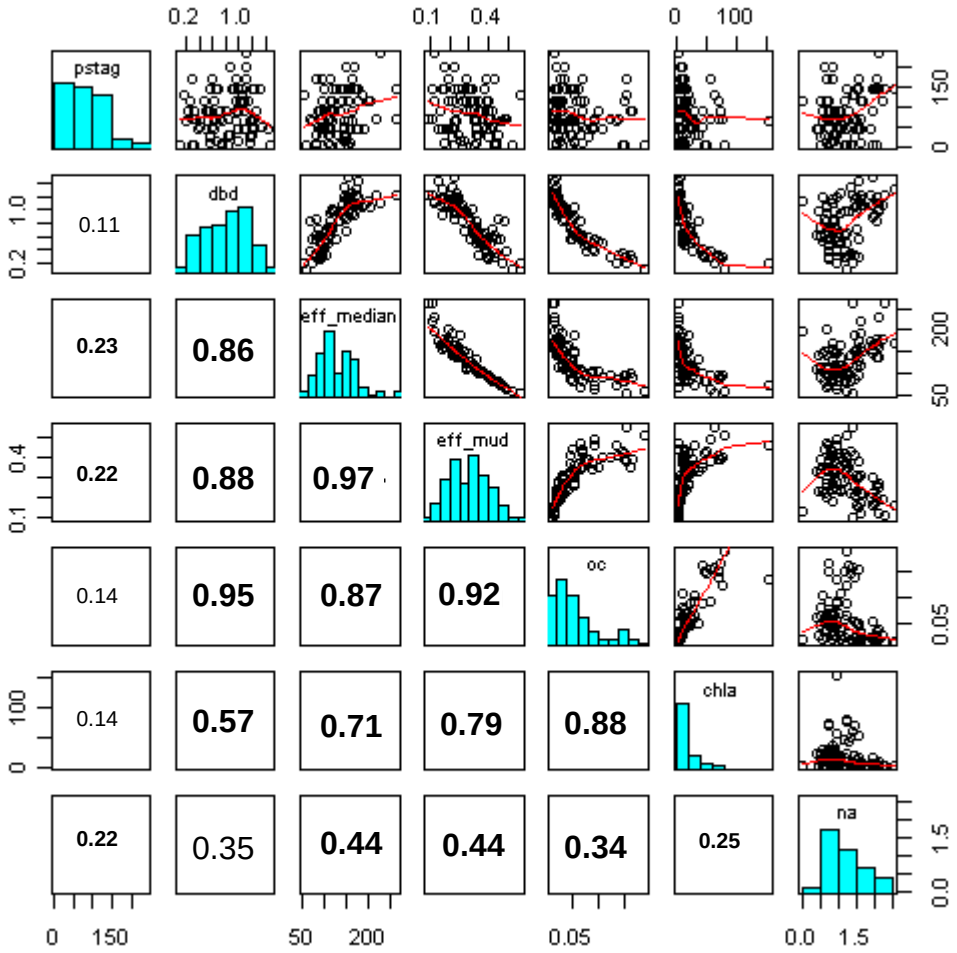

Figure 5.4. Scatterplot of CSM-derived erosion threshold (pstag) and sediment properties for the River Frome, with histograms along the diagonal and Spearman rank correlation coefficients in the lower panels. dbd = dry bulk density; eff_median = median effective particle size; eff_mud = mud content based on effective size; oc = organic content (LOI), chla = chlorophyll-a content; na = normalised sodium content.

Conditional scatterplots (i.e. coplots) can be used to visualise the relationship between a response and explanatory variable based on additional explanatory variables. So, they are good tools to identify possible interaction effects between the sediment properties and erosion thresholds. For example, median effective particle size had the strongest correlation with erosion threshold ($r_s = 0.337$, $p < 0.01$), however its effects appear to be partially dependent on bulk density (Fig. 5.5). At the lowest dry bulk densities (< 0.4 g cm^{-3}), no apparent relationship exists between particle size and erosion threshold.

Coplots can also be used to examine how the relationships between sediment properties and erosion thresholds vary over time and between streams. Substantial variations are noted for median effective particle size, dry bulk density and organic content. The magnitude and slope of the linear relationship between erosion threshold and median effective particle size decreases over time, and is lower in the River Frome than in the Bere Stream (Fig. 5.6). In other words, sediment with a similar effective particle size was more resistant to erosion in autumn 2008 (1 & 2) than spring/summer 2009 (5 & 6), and in the Bere Stream (b) than River Frome (f). The magnitude and slope of the correlation between dry bulk density and erosion threshold change in a similar manner over time for the Bere Stream (Fig 5.7). So, sediment with the same bulk densities was more resistant to erosion in autumn 2008 than in spring/summer 2009. However, there was no correlation for the River Frome. Finally, erosion threshold displayed a negative unimodal response to organic content in autumn 2008 for the Bere Stream, but this relationship transitions to negative linear with time (Fig. 5.8). When considered together, these coplots indicate a significant effect of time on erosion threshold that is unexplained by the measured variables. As with a stream variable, time will likely need to be included in models, either as a variable in linear modelling, or as a random effect in mixed effect modelling.

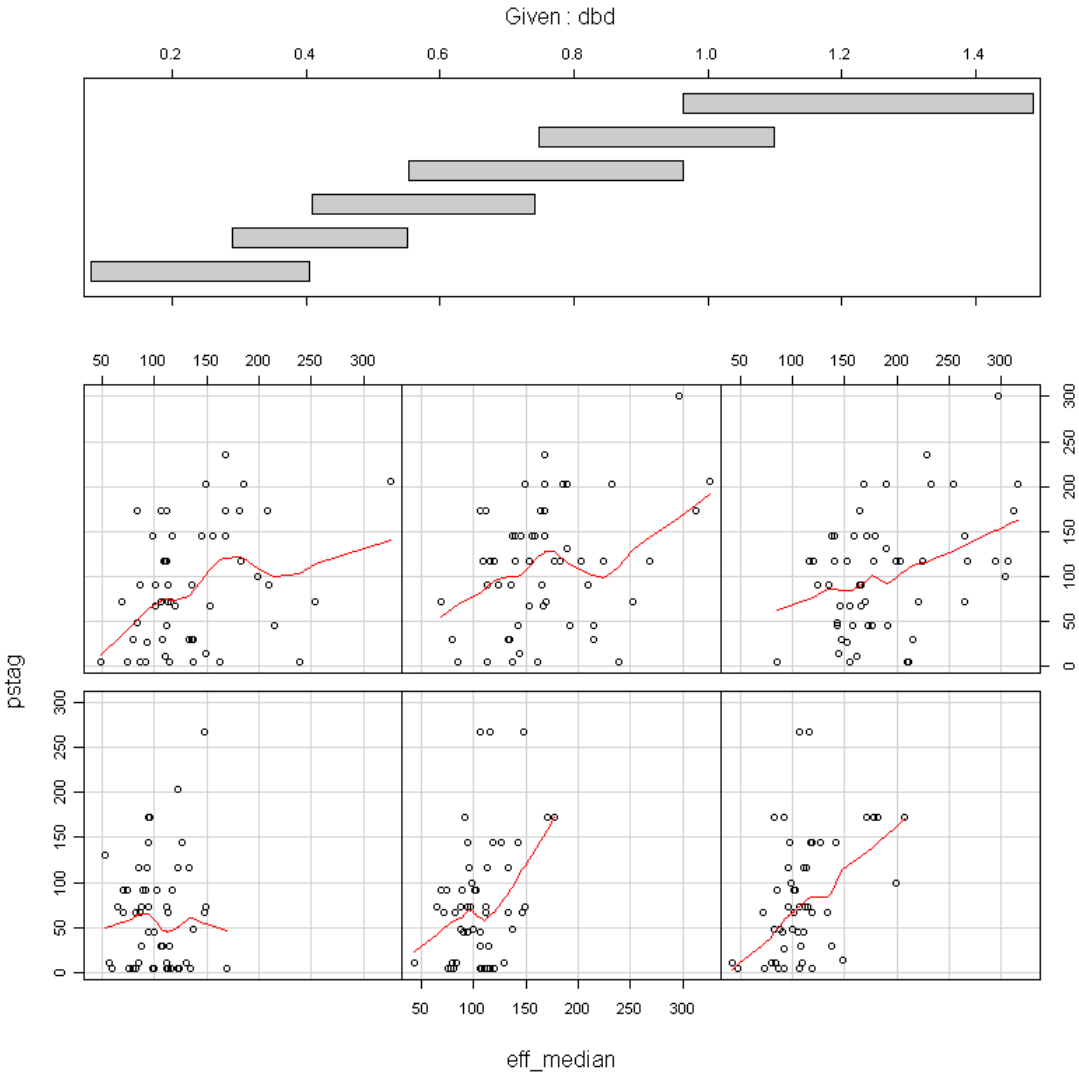

Figure 5.5. Conditional scatterplot of median effective particle size (eff_med) and erosion threshold (P_{stag}) with dry bulk density (dbd) as a third conditional variable. Best fit lines are generated by a LOWESS regression (R Core Development Team 2009). The lowest bulk density category (0 – 0.4 g cm^{-3}) is located in the bottom left-hand corner of the plot, and increases to the right.

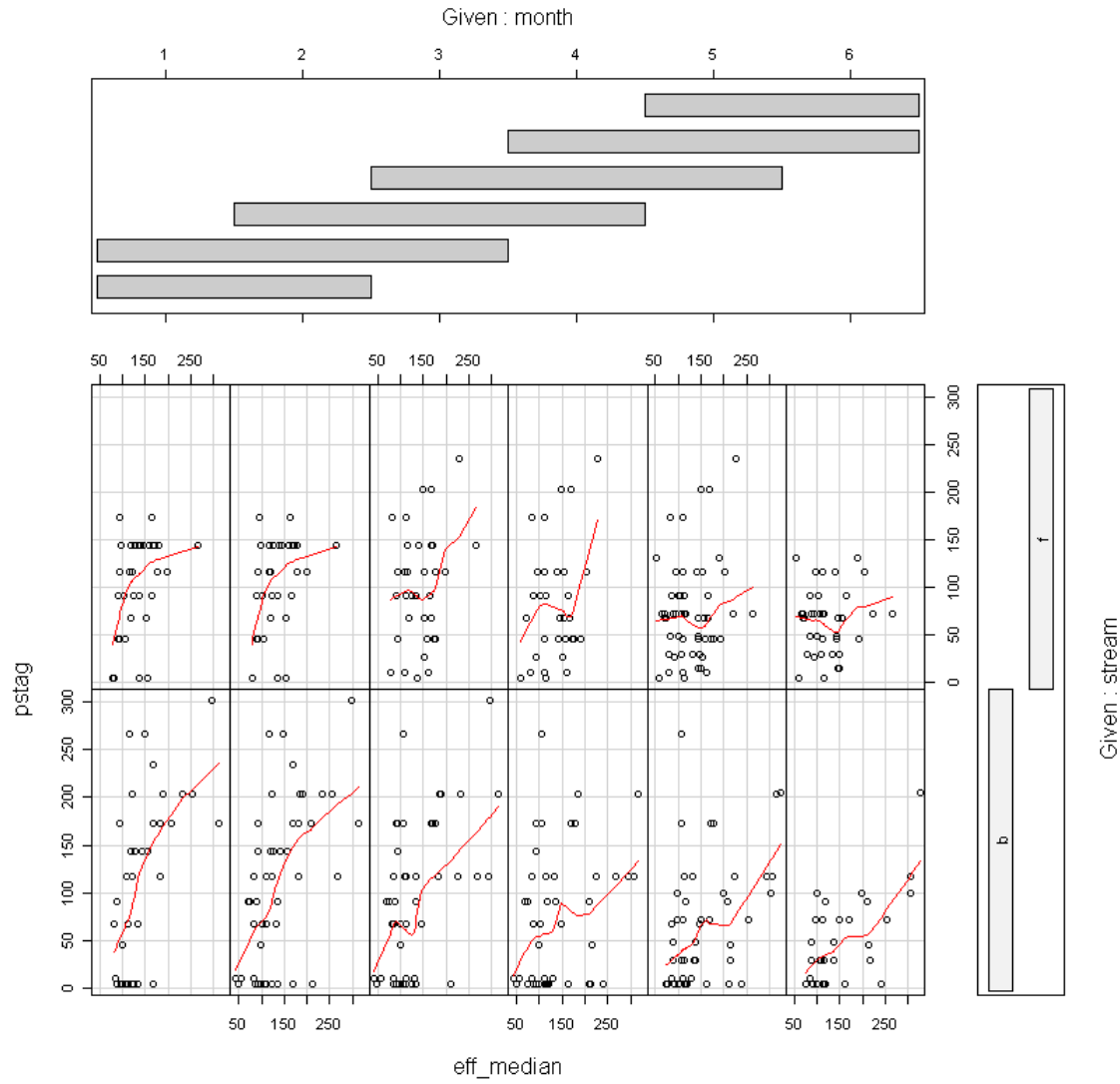

Figure 5.6. Conditional scatterplot of median effective particle size (eff_med) and erosion threshold (P_{stag}) over time (month, ordered 1-6 for bimonthly visits from Sep 08 to Jul 09) and by stream (b = Bere Stream, f = River Frome). Best fit lines are generated by a LOWESS regression (R Core Development Team 2009).

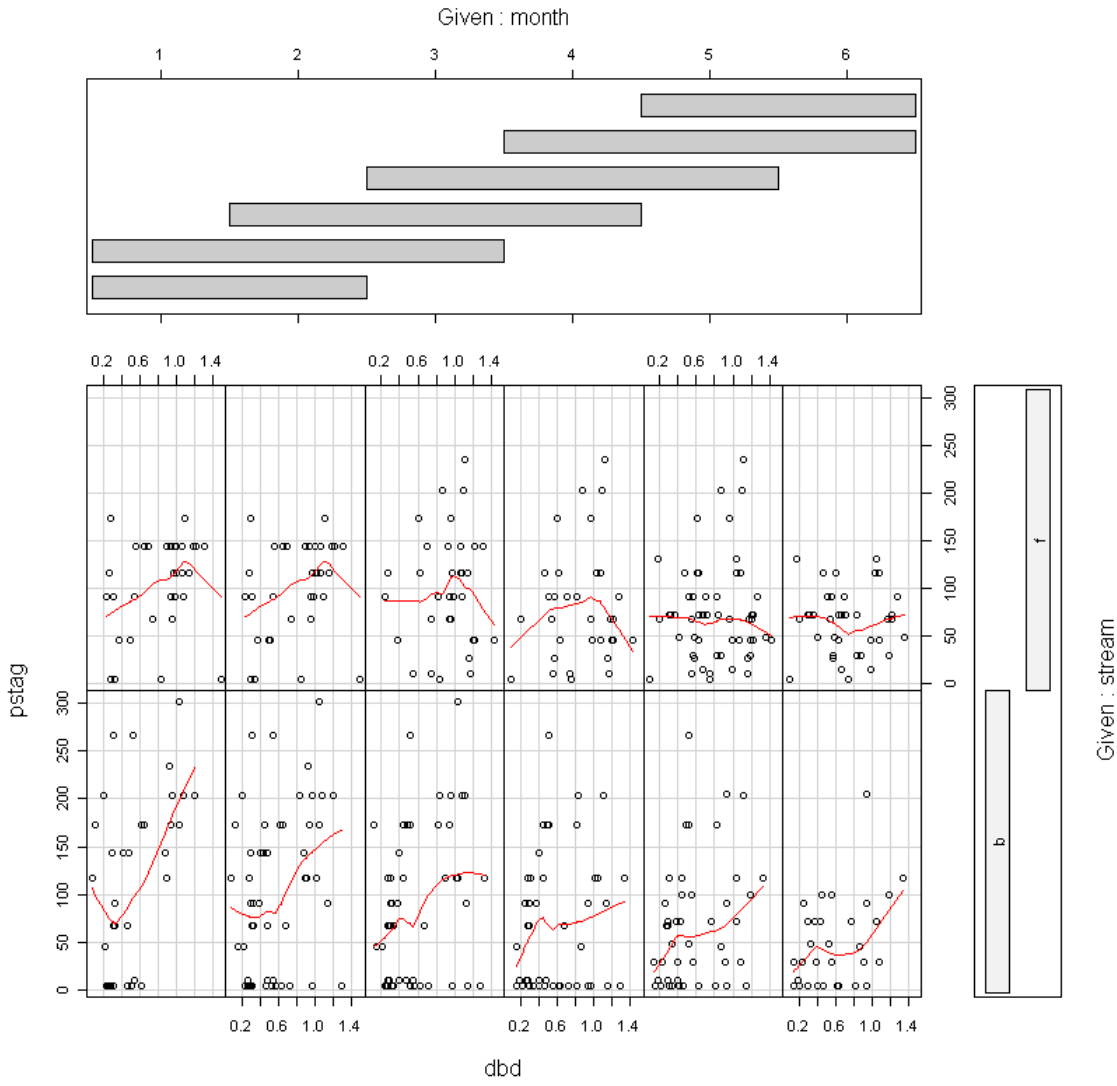

Figure 5.7. Conditional scatterplot of dry bulk density (dbd) and erosion threshold (P_{stag}) over time (month, ordered 1-6 for bimonthly visits from Sep 08 to Jul 09) and by stream (b = Bere Stream, f = River Frome). Best fit lines are generated by a LOWESS regression (R Core Development Team 2009).

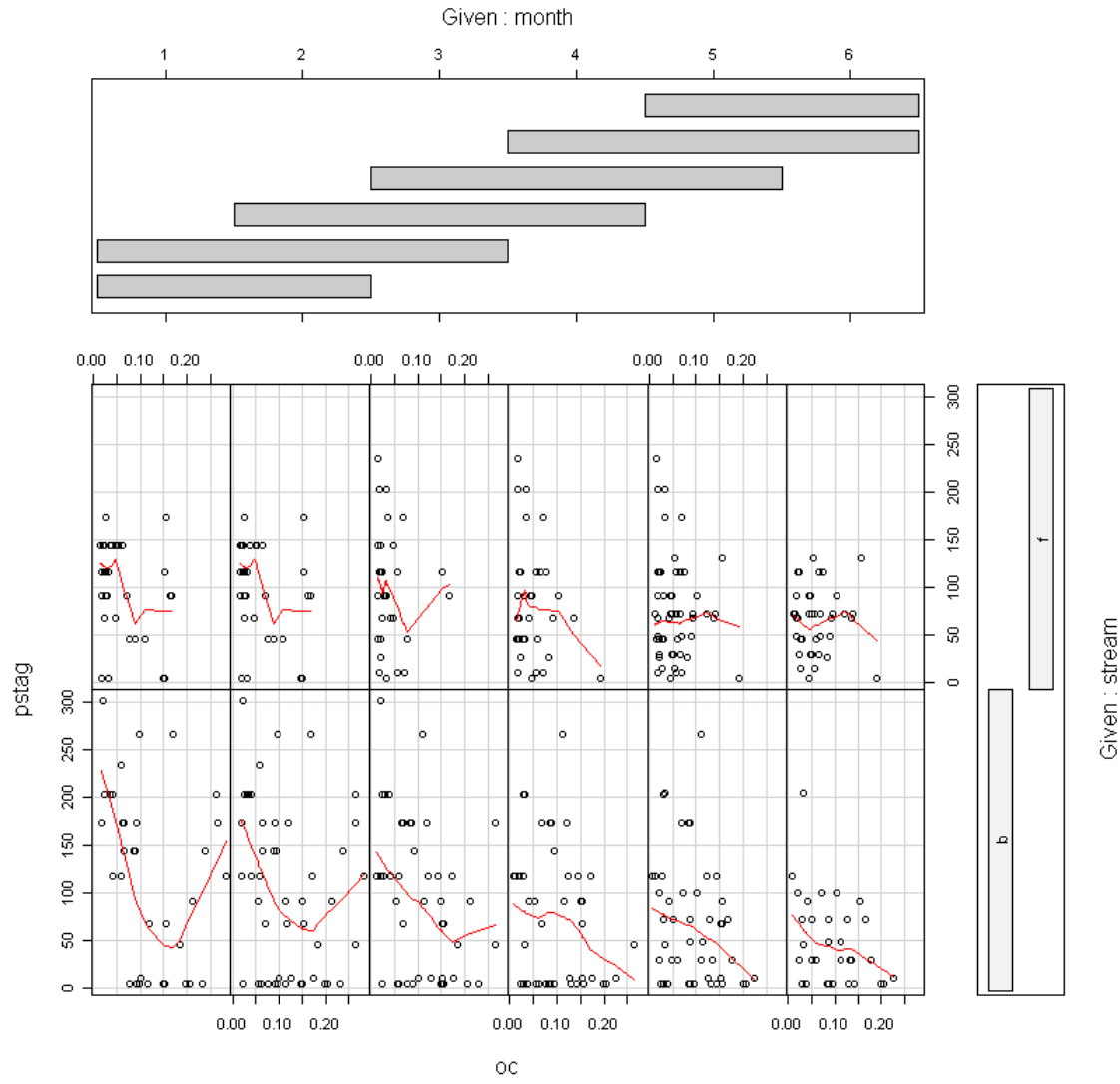

Figure 5.8. Conditional scatterplot of organic content (oc) and erosion threshold (P_{stag}) over time (month, ordered 1-6 for bimonthly visits from Sep 08 to Jul 09) and by stream (b = Bere Stream, f = River Frome). Best fit lines are generated by a LOWESS regression (R Core Development Team 2009).

5.1.2 Regression Trees

Regression tree models were used in the previous section to investigate the relationship between erodibility and the environmental variables. In this section, they are used to investigate the relationship between erodibility and the sediment properties. Regression trees are an excellent tool for data exploration, helping to identify significant explanatory variables and interactions, and are better able to deal with non-linearities and interactions than other statistical techniques, such as regression, GLM and GAM (Crawley 2007, Zuur et al. 2007). For more information, see the earlier description of regression trees (Section 4.4)

A regression tree model was created using the sediment property dataset and pruned based on the cost-complexity parameter (cp) (Section 4.4). The final model contained one explanatory variable, median effective particle size with a node at 164 μm (Fig. 5.9). In other words, the sediment was classified as having either a low erosion threshold, with a mean of 71 Pa, or a high erosion threshold, with a mean of 125, depending if median particle size was less than or greater than 164. The prediction error for this model was comparable to the earlier regression models based on environmental variables (RMSE = 63 Pa), but was high when compared to the average P_{stag} for, and difference between, the two groups.

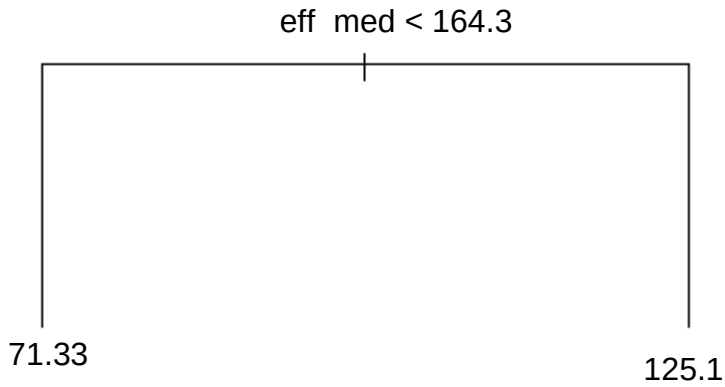

Figure 5.9. The pruned regression tree for CSM-derived erosion thresholds only has one explanatory variable, median effective particle size with a node at 164 μm (RMSE = 62.79)

The correlation analysis and coplots indicated that there were differences in the magnitude and significance of correlations between sediment properties and erosion thresholds between the two streams and over time (Section 5.1.1). These observations, combined with the significant spatial and temporal variations in erodibility identified in the earlier chapter (Section 4.5), suggest that time and stream should be incorporated into the regression tree model. Therefore, a revised model was created with these variables. The cost-complexity parameter plot suggested that the minimally adequate model has a single split, which would produce a pruned model identical to Fig. 5.9 (Fig. 5.10). As regression tree analysis was being used as a data exploration tool, a pruned model was created with a larger number of splits to identify possible interactions. With a tree size of 4, the pruned regression tree was still composed of a single sediment property, but has two interactions with time (Fig. 5.11). It suggested that sediment finer than 164 μm had higher erosion thresholds in September 2008 than in the rest of the study period, and that sediment coarser than 164 μm had higher erosion thresholds in the September and November 2008 than in the rest of the study period. This aligns with the earlier analysis of temporal patterns in erodibility (Section 4.3.2).

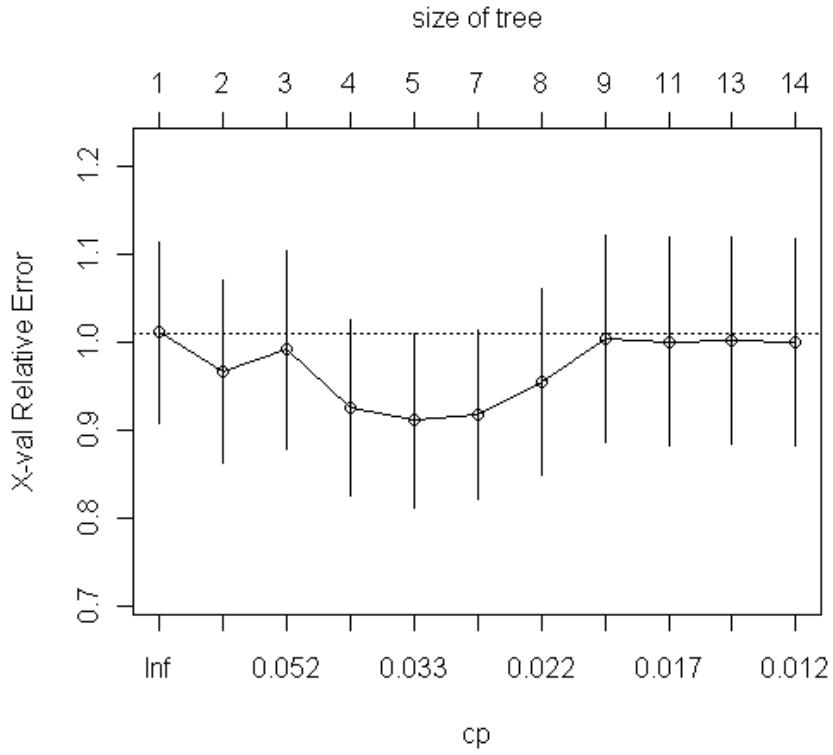

Figure 5.10. Relative error as a function of tree size for the regression tree model of CSM-derived erosion thresholds and sediment properties, with time and stream effects incorporated.

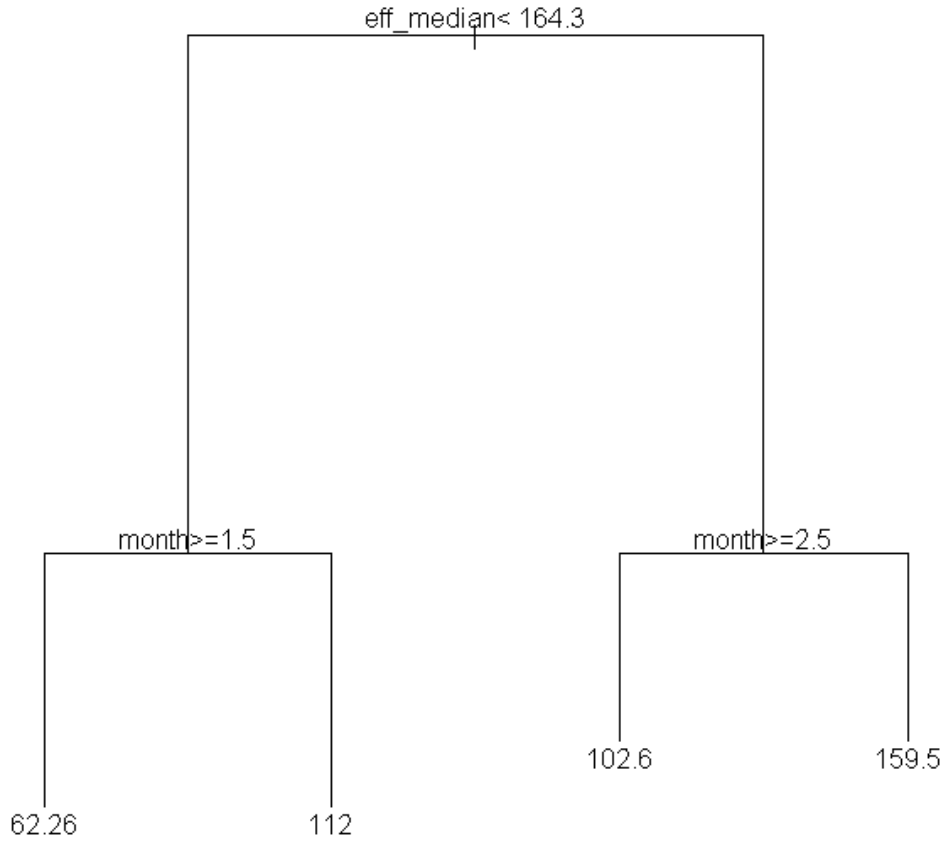

Figure 5.11. Pruned regression tree model of CSM-derived erosion thresholds based on sediment properties, and incorporating variations between streams and over time. month is an ordinal variable (1-6)

Regression tree analysis suggests that median effective particle size was the most important explanatory variable for the erosion threshold data, but that there may be a substantial temporal component not accounted for in the sediment property data. This provides us with a good starting point to use linear regression analysis.

5.2 Linear regression

Multiple linear regression (LR) analysis is a commonly used modelling approach that is relatively simple to implement. However, the assumptions associated with LR are restrictive, and many environmental datasets should not be analysed with the technique (Zuur et al. 2009). The following LR protocol was used to ensure that the LR analysis was conducted properly: (1) examination of the normality of the response variable; (2) application of a transformation if necessary; (3) selection of an optimal model based on statistical criteria, such as AIC, BIC and adjusted R^2; (4) inspection of residuals for evidence of normality, homogeneity and independence.

The three major assumptions are normality, homogeneity, and independence in the response variable. The frequency distribution of erosion threshold is significantly different from normal (K-S, Z = 1.538, p = 0.018) (Fig. 5.1). A common approach to deal with a lack of normality is to apply a transformation to the response variable (Zuur et al. 2007). Logarithmic, squared, and square root transformations are the most frequently used. The application of a square root transformation ($P_{stag}^{0.5}$) caused the distribution of erosion threshold values to more closely resemble normal (Fig. 5.12c,d), making it more appropriate for linear regression analysis. In the analysis of spatial and temporal patterns, a departure from heterogeneity was noted for erosion threshold by month and macrophyte type. This would suggest that linear regression would not be an appropriate technique for the dataset, however it is advisable to apply a linear model first and then investigate heterogeneity with the residuals (Zuur et al. 2009). The final assumption, independence, is also best assessed by investigating patterns in residuals when plotted against explanatory variables.

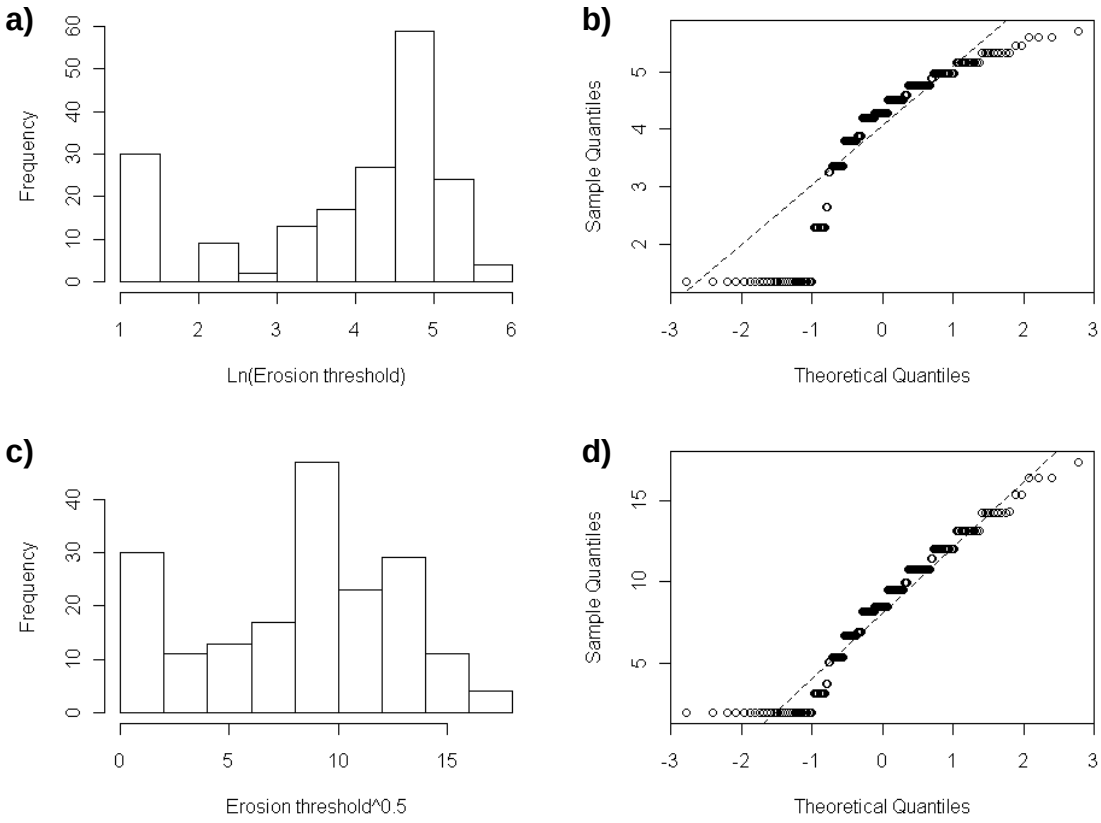

Figure 5.12. (a,c) Histogram and (b,d) quantile-quantile (Q-Q) plots to assess normality of transformed CSM-derived erosion thresholds (P_{stag}), using (a,b) a natural log transformation and (c,d) a square root transformation.

A base linear regression model was created with $P_{stag}^{0.5}$ and all of the sediment properties included as explanatory variables, along with several potentially important interaction terms such as bulk density*chlorophyll a. The optimal model was selected using three different approaches: (1) hypothesis testing; (2) forward/backward selection using the Akaike information criterion (AIC); and (3) best subsets regression using the Bayesian information criterion (BIC) (Gotelli & Ellison 2004, Zuur et al. 2009). First, in the hypothesis testing approach, non-significant variables were dropped from the base model one at a time, based on *t*-statistics and *p*-values. In the second and third approaches, an information criterion statistic was used to compare different models. The criterion combines a measure of the model's goodness of fit with a penalty associated with the number of variables in the model. The Akaike Information Criterion (AIC) is a conservative statistic that penalises superfluous parameters, and is used in many statistical software packages as a basis for model selection. In backward selection, a linear regression is run on all combinations of the base model with one variable

removed. The new model that has the lowest AIC is selected, and the process continues until the removal of a variable causes no additional decrease in AIC. Model selection was conducted in both backward and forward directions for the erosion threshold dataset. Finally, best subsets regression determines, as the name suggests, the best models for any given number of variables, and uses BIC as the information criterion. BIC penalises extra model parameters more than AIC, so is even more conservative. As with AIC, BIC should be minimised in the optimal model.

The three approaches to model selection produced similar optimal models with comparable R^2 (Table 5.2). The hypothesis testing and the best subsets regression approaches selected only one sediment property as an explanatory variable, median effective particle size, along with month and stream. Models 1 and 3b were identical, and whilst the removal of stream as a factor reduced BIC (Model 3a) (Table 5.2, Fig. 5.13), it caused a significant decrease in model fit (ANOVA<, $F = 4.35$, $p < 0.05$). Selection using AIC identified dry bulk density, organic content, and an interaction between them as important explanatory variables (Table 5.2). However, only the interaction term was significantly different from zero ($t = 2.090$, $p < 0.05$), and there was a high level of correlation between dry bulk density, organic content and median effective particle size. This was evident in the variance inflation factors from Model 2 (Table 5.3). One weakness of the automatic selection process is that highly correlated variables may be selected together, so caution must be exercised to ensure that they are excluded from the analysis (Zuur et al. 2007).

Table 5.2. Summary of optimal LR models of CSM-derived erosion thresholds: eff_median = median effective particle size, dbd = dry bulk density, oc = organic content.

	Approach	Optimal Model	R^2	R^2_{adj}	p
1	Hypothesis testing	$P_{stag}^{0.5}$ = eff_median + month + stream	0.20	0.19	< 0.001
2	Selection (AIC)	$P_{stag}^{0.5}$ = eff_median + dbd + oc + dbd:oc + month + stream AIC = 1011	0.23	0.20	< 0.001
3a	Best subsets (BIC)	$P_{stag}^{0.5}$ = eff_median + month BIC = -21	0.18	0.17	< 0.001
3b		$P_{stag}^{0.5}$ = eff_median + month + stream BIC = -20	0.20	0.19	< 0.001
3c		$P_{stag}^{0.5}$ = eff + month + stream + dbd:oc BIC = -19	0.21	0.19	< 0.001

Table 5.3. Variance inflation factors for the LR model selected by backward selection with AIC (Model 2). eff_median = median effective particle size, dbd = dry bulk density, oc = organic content.

eff_median	dbd	oc	dbd:oc	month	stream
2.84	5.73	5.07	2.02	1.08	1.93

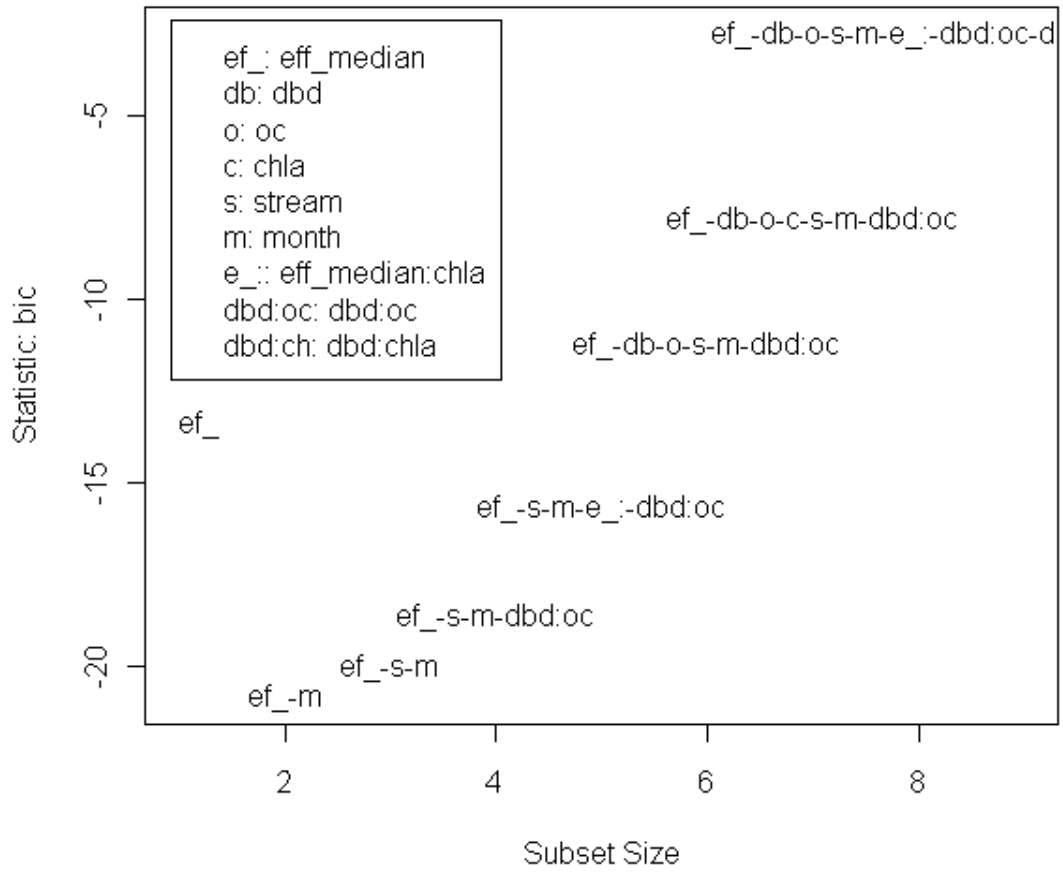

Figure 5.13. The optimal LR model has the lowest BIC with best subsets regressions, i.e. a two variable model with median effective particle size and month. eff_median = median effective particle size, dbd = dry bulk density, oc = organic content, chla = chlorophyll-a content, stream = Bere or Frome, month is an ordinal variable (1-6). A colon (:) between two variables indicates an interaction term, e.g. dbd:oc is an interaction between dry bulk density and organic content.

The optimal model to describe CSM-derived erosion thresholds was Model 1/3b, as all of the explanatory variables were significant and it had a low BIC (Table 5.4; Fig. 5.13). The linear regression is significant ($p = 0.05$), though it only explained approximately 20% of the variance in the data. The original goal was to generate a model using only sediment properties as explanatory variables. As suggested in the previous sections, though, there was a significant temporal component as well as differences between the streams that were not captured by the sediment property data alone. Validation plots confirmed that the model conformed to the assumptions of normality; the Q-Q plot of residuals was similar to a normal distribution (Fig. 5.14b). Residuals are predominantly homogeneously distributed, although there is a slight increase in variance with an increase in fitted value (Fig. 5.14a,c). Residuals plotted against explanatory factors showed no significant patterns either, suggesting that the model also conformed to the third assumption of linear regression, independence in residuals from the explanatory variables (Fig. 5.15a,b,c).

Table 5.4. Summary statistics for the optimal LR model of CSM-derived erosion threshold (Model 1/3b), where eff_median is the median effective particle size (μm), month is an ordinal variable (1-6) (e.g. Sep 08 = 1 and Nov 08 = 2) and stream is a nominal variable defined as 1 (Bere) or 2 (Frome).

	Estimate	Std. Error	t value	Pr(>|t|)
(Intercept)	5.07	1.22	4.14	5.31e-05
eff_median	0.026	0.004	5.43	1.78e-07
month	-0.56	0.15	-3.78	2.1e-4
stream	1.14	0.54	2.09	0.038

Residual standard error: 3.669 on 181 degrees of freedom

Multiple R-squared: 0.1983, Adjusted R-squared: 0.185

F-statistic: 14.93 on 3 and 181 DF, p-value: 1.006e-08

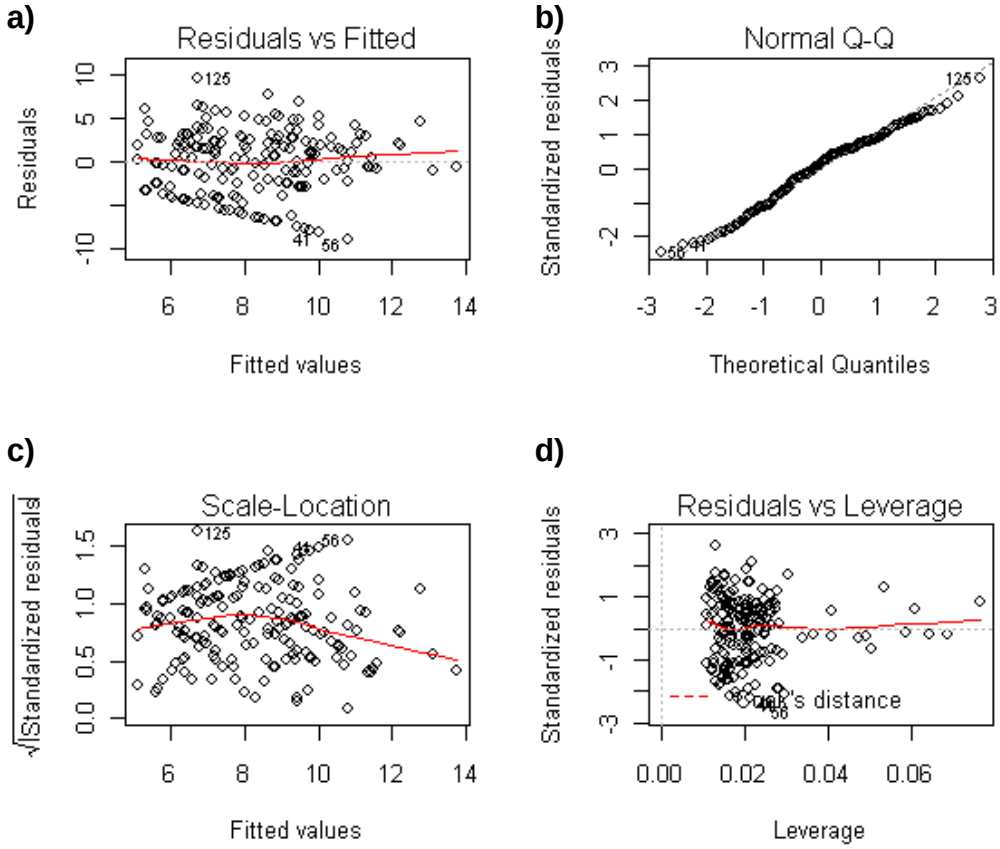

Figure 5.14. Validation of the optimal linear regression model (Model 1/3b). (a) Model residuals plotted against fitted values, (b) Q-Q plot of standardised residuals, (c) standardised residuals plotted against fitted values, and (d) standardised residuals plotted against Cook's leverage, a measure of the disproportionate impact of a data point on the model regression.

Whilst the validation plots broadly supported the assumption of homogeneity, a pattern did exist that was worth investigating further (Fig. 5.14a). The lowest negative residuals decreased with an increase in fitted values. Most of these residuals corresponded to the tests in which the sediment was too weak for measurement with the CSM. These tests were given a value of half the minimum erosion threshold measured by the CSM (0.15 PSI), because they provided important information on the spatial and temporal patterns in average erodibility (Section 4.1). However, these erosion thresholds do not represent a true erodibility value, and given their strong pattern in residuals, it is worthwhile running the LR analysis without the values.

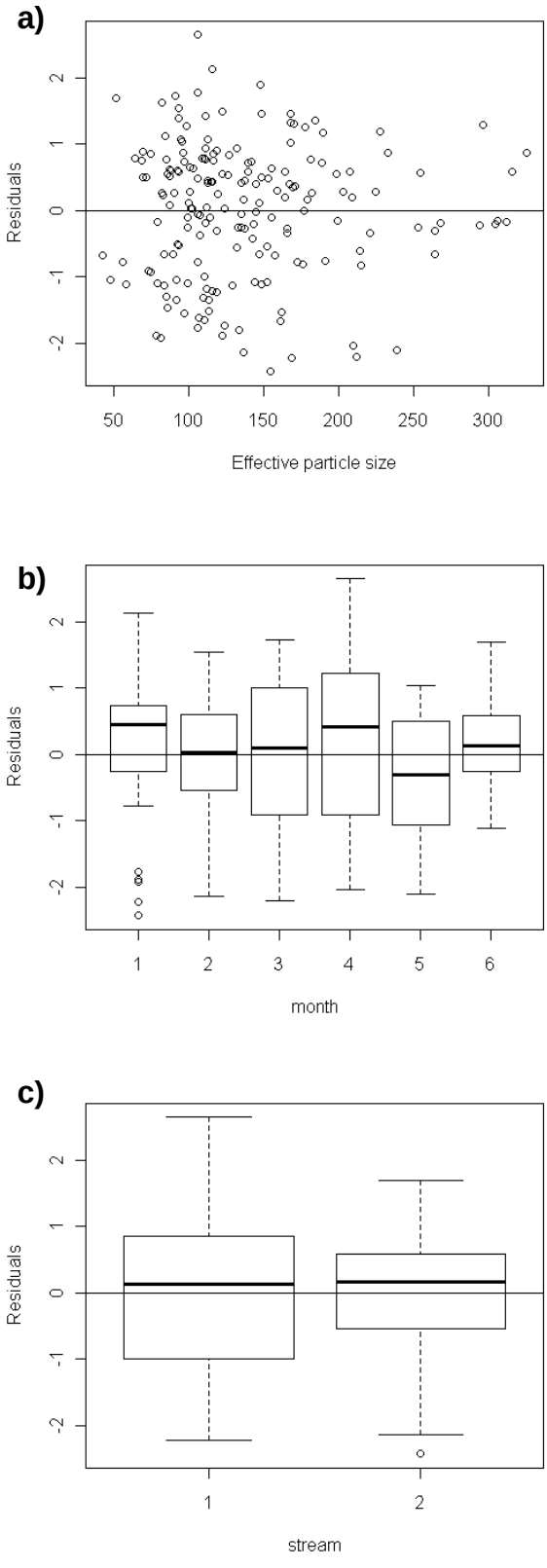

Figure 5.15. Model validation plots displaying model residuals for the explanatory variables used in the optimal LR model, (a) median effective particle size, (b) month, an ordinal variable from 1-6 (e.g. Sep 08 = 1 and Nov 08 = 2) and (c) stream, Bere = 1 and Frome = 2.

The three approaches to model optimisation generated slightly different models for the datset without 0.15 PSI values (Table 5.5). Stream was no longer identified as an important explanatory variable, and the models explained substantially more of the variation in the dataset than in the previous analysis (35% vs. 20%) (Tables 5.4 & 5.5). All the models contained effective median particle size and month, but some also contained chlorophyll-a content, organic content and dry bulk density (Table 5.5). The optimal model was identified as Model 1, because all of the variables were significantly different from zero ($p < 0.05$) (Table 5.6) and the removal of chlorophyll-a content, the least significant variable, resulted in a significant decrease in model fit (ANOVA, $F = 5.58$, $p = 0.034$). Dry bulk density and organic contents were not statistically significant explanatory variables, and had high covariances with effective particle size (VIF = 5.72 and 5.42, respectively). The interaction between dry bulk density and chlorophyll-a content (dbd:chla) was statistically significant but did not yield a better model fit than chlorophyll-a content (Model 3b vs. Model 1) (Table 5.5). Model validation plots showed no major deviations from normality (Fig. 5.16b), homogeneity (Figs. 5.16a,c & 5.17), and independence (Fig. 5.17). However, Cook's leverage did identify one data point that had a significant impact on the estimation of model parameters (Point 54, Fig. 5.16d)

Table 5.5. Summary of optimal LR models of CSM-derived erosion threshold with 0.15 PSI erosion threshold values excluded: eff_median = median effective particle size, dbd = dry bulk density, oc = organic content, chla = chlorophyll a content.

	Approach	Optimal Model	R^2	R^2_{adj}	p
1	Hypothesis testing	$P_{stag}^{0.5}$ = eff_median + chla + month	0.35	0.34	< 0.001
2	Selection (AIC)	$P_{stag}^{0.5}$ = eff_median + dbd + chla + oc + dbd:oc + month AIC = 745	0.37	0.35	< 0.001
3a	Best subsets (BIC)	$P_{stag}^{0.5}$ = eff_median + month BIC = -47	0.33	0.32	< 0.001
3b		$P_{stag}^{0.5}$ = eff_median + month + dbd:chla BIC = -47	0.35	0.34	< 0.001
3c		$P_{stag}^{0.5}$ = eff_median + month + oc + dbd:chla BIC = -44	0.36	0.34	< 0.001

Table 5.6. Summary statistics for the optimal LR model with 0.15 PSI values excluded, where eff_median is the median effective particle size (μm), chla is the chlorophyll-a content (μg g^{-1} sediment), and month is an ordinal variable (1-6) (e.g. Sep 08 = 1 and Nov 08 = 2).

	Estimate	Std. Error	t value	Pr(>|t|)
(Intercept)	8.92	0.80	11.13	< 2e-16
eff_median	0.021	0.004	5.64	8.28e-08
chla	0.021	0.01	2.14	0.034
month	-0.78	0.12	-6.78	2.59e-10

Residual standard error: 2.625 on 151 degrees of freedom

Multiple R-squared: 0.3518, Adjusted R-squared: 0.3389

F-statistic: 27.31 on 3 and 151 DF, p-value: 3.617e-14

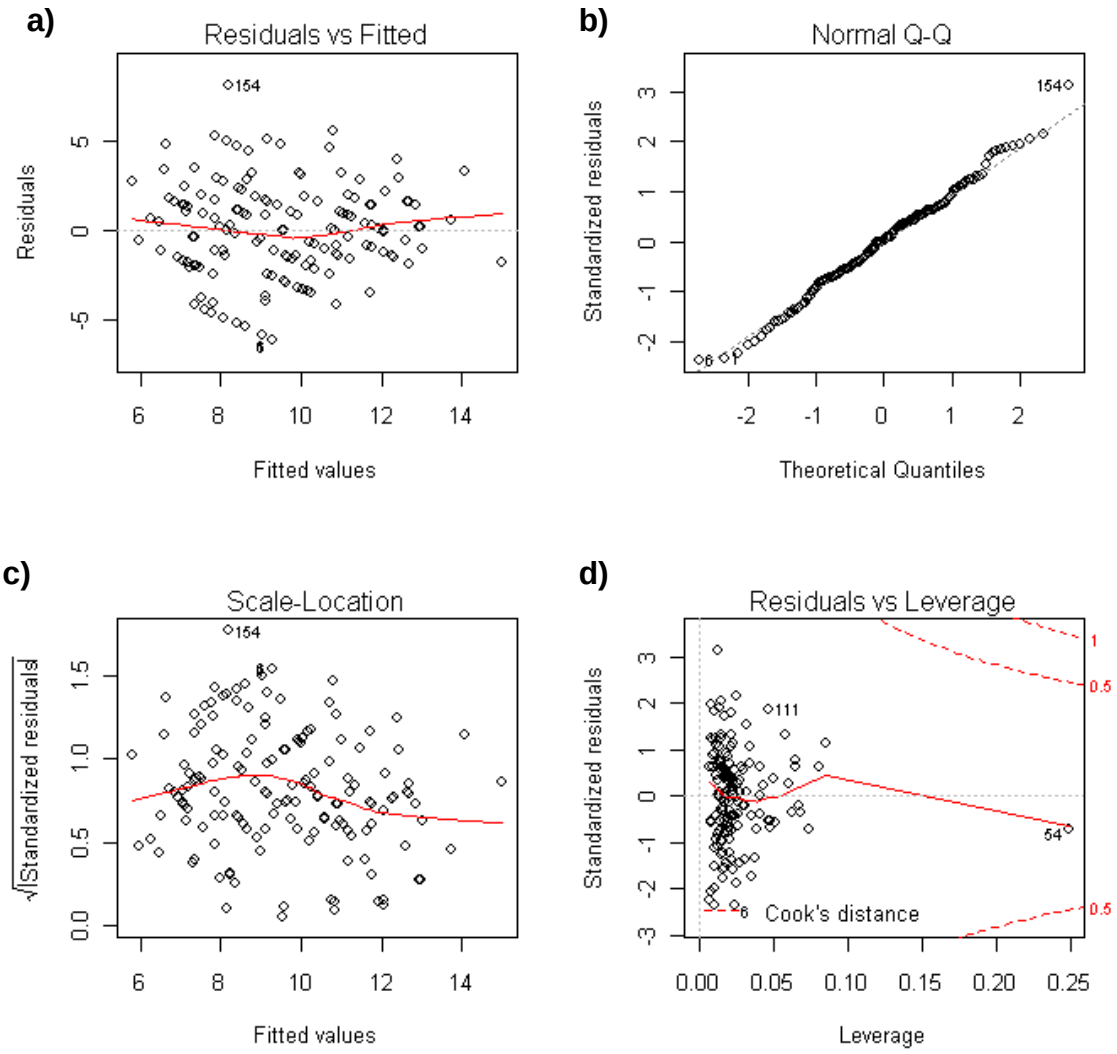

Figure 5.16. Validation plots of the optimal LR model with 0.15 PSI values excluded, showing that the residuals conform to the assumptions of normality and homogeneity, but identifying one data point with a strong influence on the model (# 54), (a) model residuals plotted against fitted values, (b) Q-Q plot of standardised residuals, (c) standardised residuals plotted against fitted values, and (d) standardised residuals plotted against Cook's leverage, a measure of the disproportionate impact of a data point on the model regression.

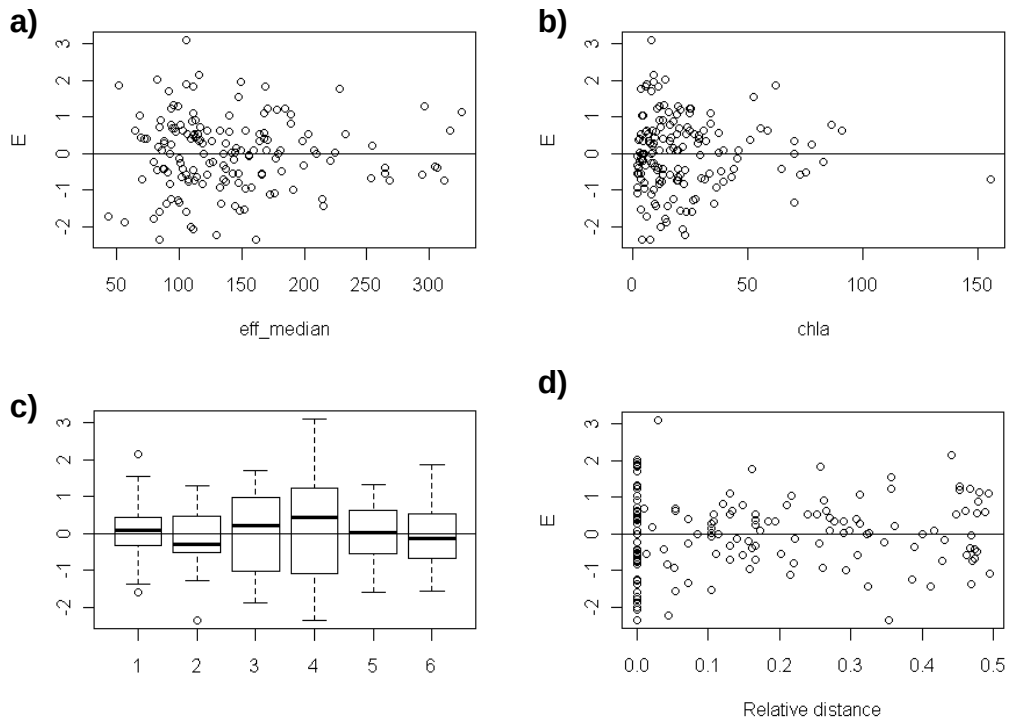

Figure 5.17. Model validation plots showing residuals vs. explanatory variables for the optimal LR model with 0.15 PSI values excluded. The lack of pattern in the plots supports the assumption of independence, (a) median effective particle size, (b) chlorophyll-a content, and (c) month, an ordinal variable from 1-6, e.g. Sep 08 = 1, Nov 08 =2. (d) Relative distance is included as it was identified as a significant environmental variable in Section 4.3.2.

The standard linear regression protocol recommends running the linear regression again with the high leverage point removed. The point corresponded to the highest chlorophyll-a content recorded during the study (Fig. 6.17b), from a poorly consolidated (dry bulk density = 0.2), unvegetated sediment sample, River Frome (May 2009). This point showed up as a potential outlier in the earlier scatterplots, particularly in the relationship between organic content and chlorophyll-a content (Figs. 5.2 & 5.4). When LR was run without this data point, the estimate for chlorophyll-a content increased and there were slight changes in the estimates for intercept and month (Table 5.7). The model explains the same amount of variation in the data (R^2 = 0.35), but the significance for chlorophyll-a content increases slightly. In this situation, both models could be reported as valid (Zuur et al. 2009). However, given that the sediment sample was extreme in both chlorophyll-a content and dry bulk density (4^{th} percentile), this revised model may more accurately reflect the relationships between the explanatory variables and erosion threshold for the dataset (Fig. 5.18). The visualisation of the final

optimal model demonstrates the large effect median particle size had on erosion threshold. Chlorophyll-a had a slightly greater slope estimate than effective median particle size (Table 5.7), but it had less of an impact on erosion threshold because its observed range was smaller (Fig. 5.18). The temporal effect that remained accounted for a *ca.* 50 Pa difference at a given median effective particle size and chlorophyll-a content (Fig. 5.18). Validation plots remain largely the same, and continue to suggest normality, homogeneity and independence (e.g. Fig. 5.19).

Table 5.7. Summary statistics for the optimal LR model, excluding 0.15 PSI values and the highest chlorophyll-a data point, where eff_median is the median effective particle size (μm), chla is the chlorophyll-a content (μg g^{-1} sediment), month is an ordinal variable (1-6) (e.g. Sep 08 = 1 and Nov 08 = 2).

	Estimate	Std. Error	t value	Pr(>|t|)
(Intercept)	8.81	0.82	10.74	< 2e-16
eff_median	0.021	0.004	5.650	7.82e-08
chla	0.025	0.011	2.21	0.029
month	-0.77	0.12	-6.66	4.87e-10

Residual standard error: 2.63 on 150 degrees of freedom

Multiple R-squared: 0.3532, Adjusted R-squared: 0.3402

F-statistic: 27.3 on 3 and 150 DF, p-value: 3.802e-14

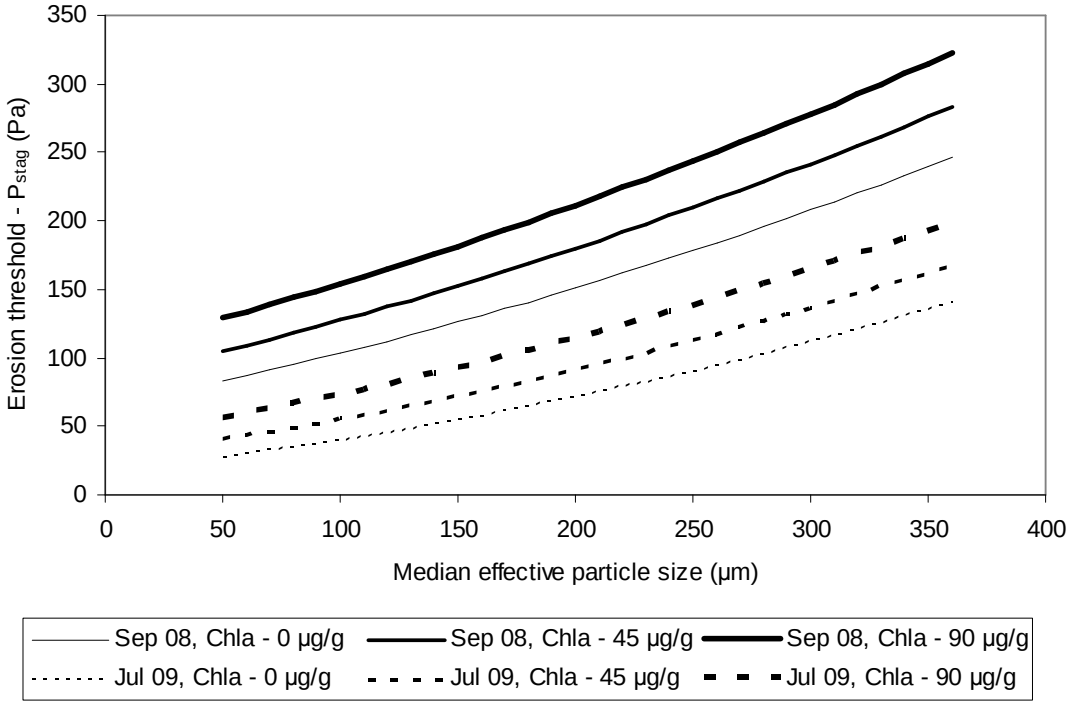

Figure 5.18. Visualisation of the optimal LR model for CSM-derived erosion threshold, excluding 0.15 PSI values and the highest chlorophyll-a data point, based on median effective particle size, chlorophyll-a content (Chla) (µg g^{-1} sediment) and month an ordinal variable (1-6) (e.g. Sep 08 = 1 and Nov 08 = 2).

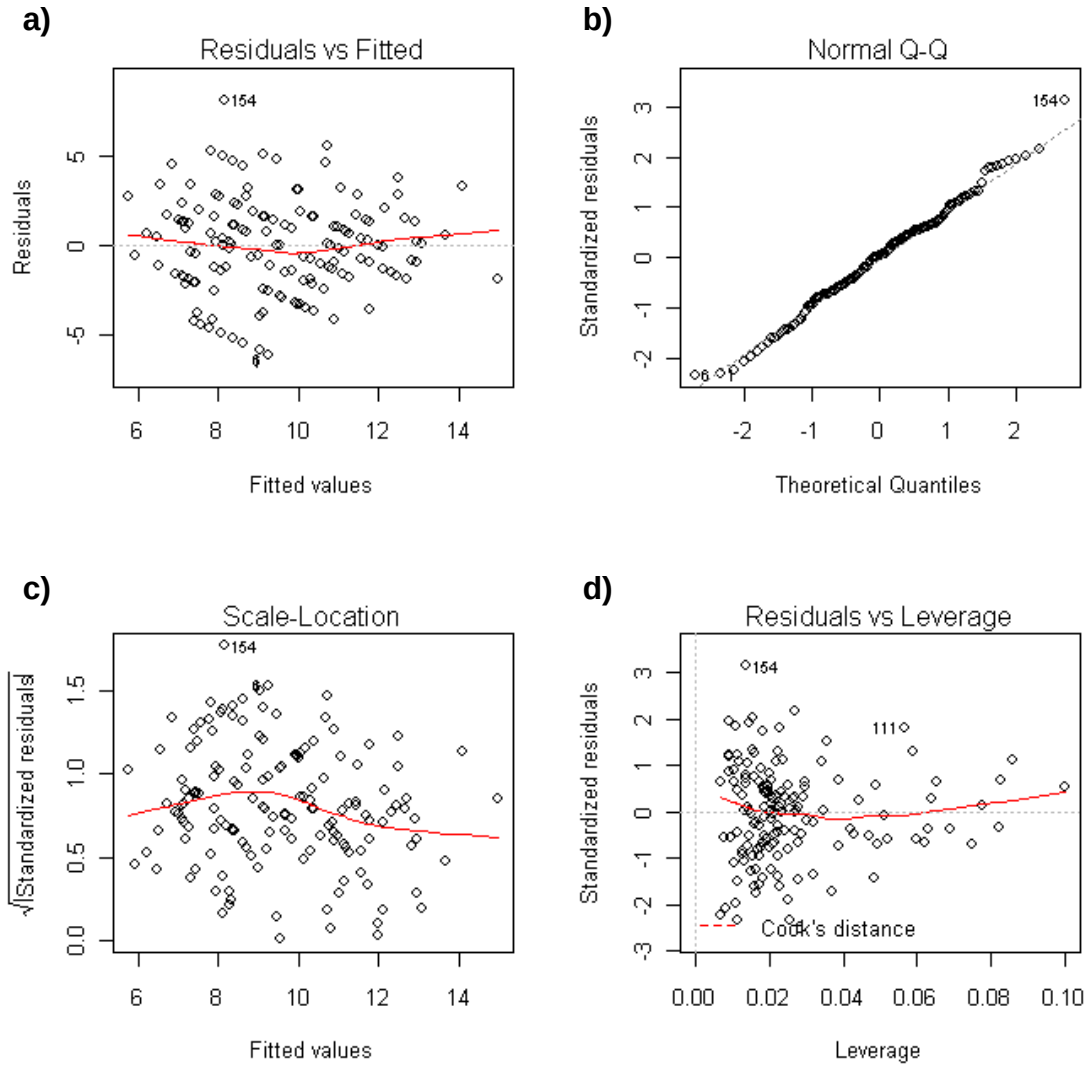

Figure 5.19. Residuals vs. explanatory variables for the optimal LR model, excluding 0.15 PSI values and the highest chlorophyll-a data point, (a) model residuals plotted against fitted values, (b) Q-Q plot of standardised residuals, (c) standardised residuals plotted against fitted values, and (d) standardised residuals plotted against Cook's leverage, a measure of the disproportionate impact of a data point on the model regression.

5.3 Mixed effects modelling

In the previous section, LR analysis identified two sediment properties as significant explanatory variables, median effective particle size and chlorophyll-a content. However, time was also significant. Erosion thresholds decreased over time, but this was not captured entirely by changes in the sediment properties. An optimal model containing a time variable may be considered appropriate; time points were spaced sufficiently far apart so that temporal autocorrelation is minimised, and sampling locations were randomly selected each month so there are no repeat measures. Yet, an optimal model containing time does not fulfil the objectives of a model with only sediment properties as explanatory variables. This conflict leads us into the territory of mixed effects modelling (MEM).

Explanatory variables can be divided into two groups: fixed effects and random effects (Crawley 2007). Fixed effects are the explanatory variables that are responsible for the changes in the response variable. They are the unknown parameters estimated during regression. Random effects are the factors that affect the variance-covariance structure of the response variable. Of primary concern are instances of spatial or temporal autocorrelation, in which samples that are located in close proximity (over space or time) are more similar to one another. In these situations, within group variances are lower than total variances, and may differ between groups. Common examples of autocorrelation include studies relying on repeated measures over time, nested experiment designs, and hierarchical observations. MEM incorporates random effects into a model containing the fixed effects, to ensure that the model does not violate the assumption of independence of errors.

As the objective of the statistical modelling was to develop an optimal model of erosion threshold based on sediment properties, MME can be used to estimate a model using sediment properties as the fixed effects, and environmental factors, such as month or stream, as random effects to account for spatial or temporal autocorrelation (Zuur et al. 2009). The correct procedure for MME is as follows: (1) create a *beyond optimal* model that contains as many explanatory variables as possible as fixed effects; (2) find the optimal structure of the random component, using restricted maximum likelihood estimation (REML), (3) find the optimal fixed effects component, using maximum likelihood estimation (ML) if fixed effects are nested, (4) create the final model and validate based on REML (Zuur et al. 2009).

The model optimisation process is similar to that described for LR, with a few added steps. First, the beyond optimal model was created with all of the sediment properties and potential interactions, such as dry bulk density and chlorophyll-a content (dbd:chla). Second, several different random structures were tested using REML: random effects, random intercept and random slope and intercept. A random effects model has no explanatory variables, and all variation in the dataset is accounted for by the random effects (Zuur et al. 2009). A random intercept structure allows the y-intercept of the fixed effects model to change based on the random factors. A random slope and intercept structure allows both the slope and the intercept of the regression to change. These structures were tested using different environmental factors, and the structure with the lowest AIC was selected. Despite evidence for a random slope structure (Figs. 5.6 - 5.8), the random intercept model with time as a random effect had the lowest AIC. Third, the optimal model was selected using backward selection based on AIC and hypothesis testing. The optimal MEM model had $P_{stag}^{0.5}$ as the response variable, time as a random effect, and median effective particle size and chlorophyll-a content as fixed effects. Finally, the model was rerun using REML estimates (Table 5.8). The ML estimator is biased because both its slope and intercept must be estimated. REML replaces the slope and intercept with a matrix that is orthogonal to the matrix of data, and is applied directly to the response variable matrix **Y**, generating an unbiased estimation of σ^2 (Zuur et al. 2009). The standardised within group residuals are normally distributed, show no substantial deviations from homogeneity, though higher variance in March is noted, and are independent from the explanatory variables (Table 5.8; Figs. 5.20 & 5.21).

Table 5.8. Summary statistics for the optimal model created using MEM, excluding 0.15 PSI values, where median effective particle size and chlorophyll-a content (Chla) (μg g^{-1} sediment) are the fixed effects, and time is the random effect (random intercept model).

Random effects:				AIC = 777	BIC = 792
Formula: ~1 | month	(Intercept)	Residual			
StdDev:	1.41	2.65			
Fixed effects: pstag.0.5 ~ eff_median + chla					
	Value	Std.Error	DF	t-value	p-value
(Intercept)	6.15	0.88	147	6.97	0.000
eff_median	0.021	0.004	147	5.51	0.000
chla	0.023	0.010	147	2.23	0.028
Standardised within group Residuals	Min	Q1	Med	Q3	Max
	-2.46	-0.66	0.05	0.60	2.94

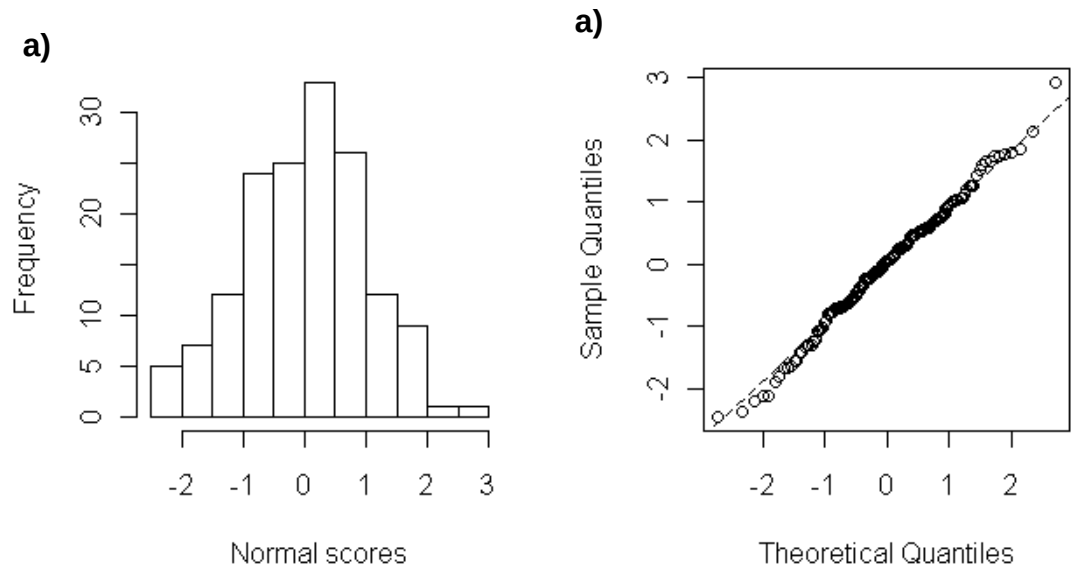

Figure 5.20. (a) Histogram and (b) Q-Q plot of residuals of the optimal mixed effects model of CSM-derived erodibility, excluding 0.15 PSI values, to test the assumption of normality.

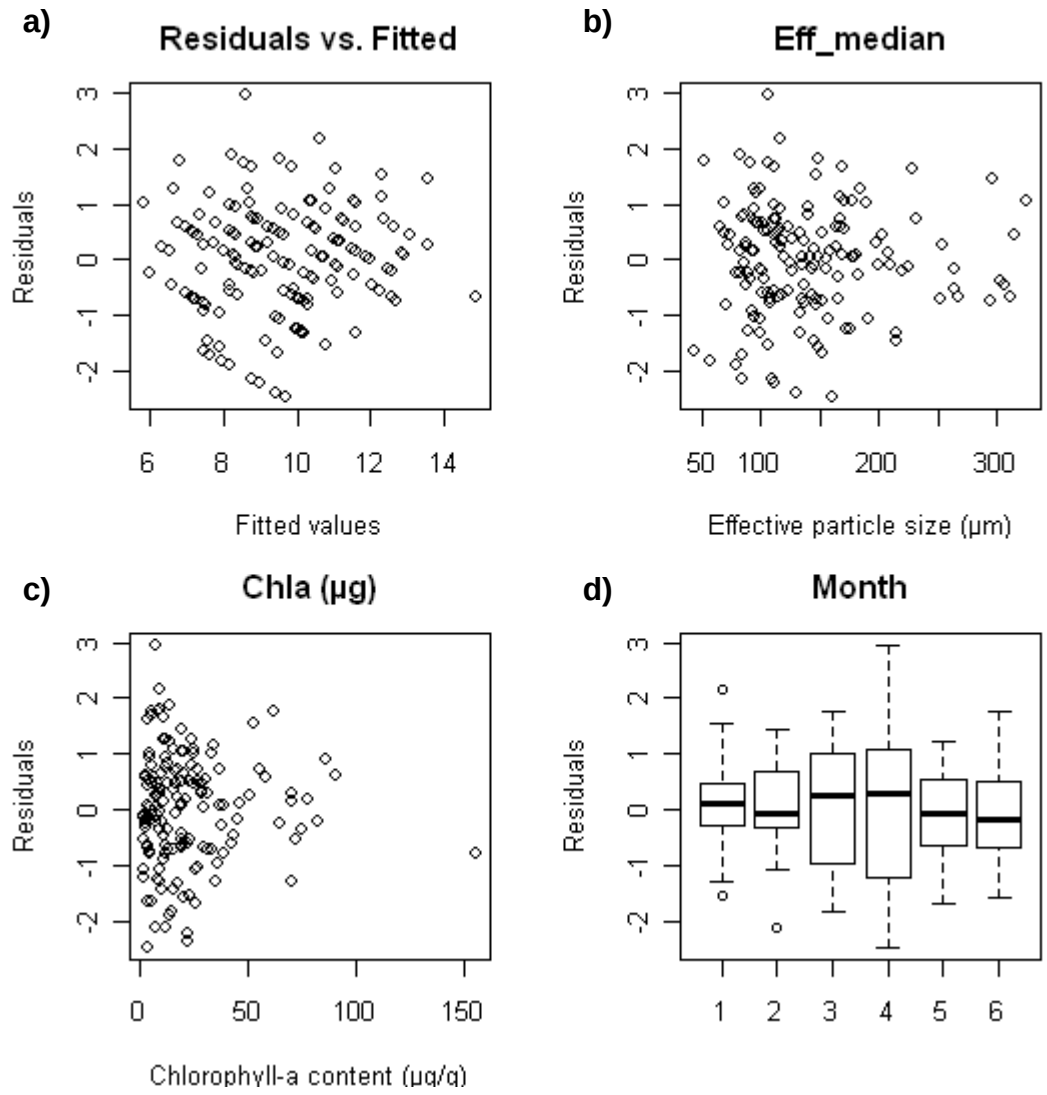

Figure 5.21. Validation plots of residuals vs. fitted values and explanatory variables to test the assumptions of homogeneity and independence for the MEM model of CSM-derived erodibility, excluding 0.15 PSI values. Model residuals plotted against (a) fitted values, (b) effective particle size, (c) chlorophyll-a content (µg g^{-1} sediment), and (d) month, an ordinal variable (1-6, bimonthly).

The validation plot of residuals vs. chlorophyll-a content highlighted one sample as a potential outlier (Fig. 5.21c). This is the data point that was identified as having high leverage on the model fit in the LR analysis (Section 5.2). Therefore, the analysis was rerun with the potential outlier excluded. The resulting model has a slightly lower intercept and higher slope for chlorophyll-a content, as well as lower information criteria (Table 5.9). Again, the model residuals conformed to the assumptions of normality, heterogeneity and independence (Figs. 5.22 & 5.23). As in the previous LR analysis, both MEM models are valid, but considering that the excluded sample is extreme in both chlorophyll-a content and bulk density, the revised model better represent the dataset (Table 5.9).

Table 5.9. Summary statistics for the optimal model created with MEM, excluding 0.15 PSI values and the high chlorophyll-a content data point, where median effective particle size and chlorophyll-a content (Chla) (μg g^{-1} sediment) are the fixed effects, and time is the random effect (random intercept model).

Random effects:				AIC = 771	BIC = 787
Formula: ~1 | month	(Intercept)	Residual			
StdDev:	1.39	2.65			
Fixed effects: pstag.0.5 ~ eff_median + chla					
	Value	Std.Error	DF	t-value	p-value
(Intercept)	6.03	0.89	146	6.81	0.000
eff_median	0.021	0.004	146	5.55	0.000
chla	0.028	0.012	146	2.39	0.018
Standardised within group Residuals	Min	Q1	Med	Q3	Max
	-2.44	-0.64	0.06	0.63	2.95

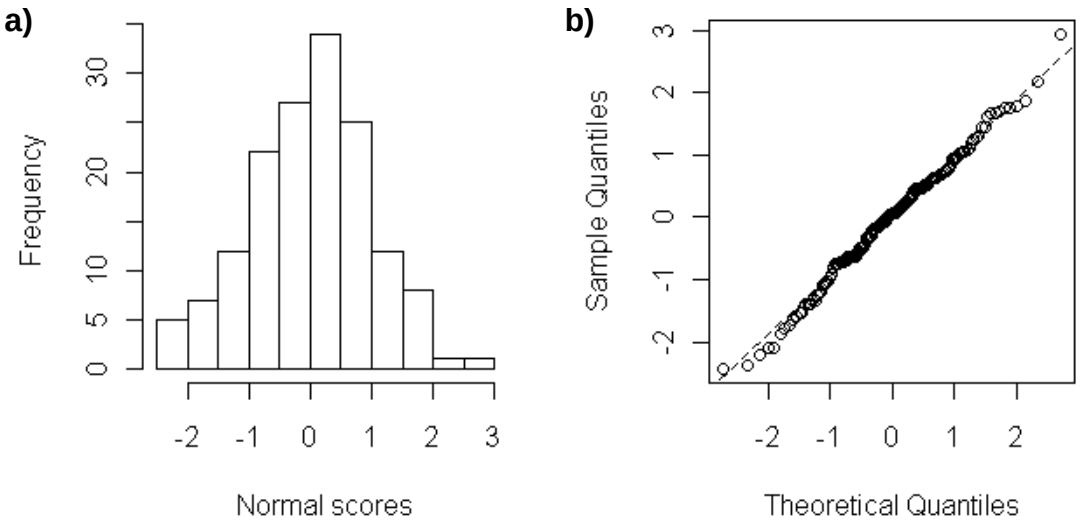

Figure 5.22. (a) Histogram and (b) Q-Q plot of model residuals to test assumption of normality for the MEM model of CSM-derived erodibility, excluding 0.15 PSI values and the high chlorophyll-a content data point.

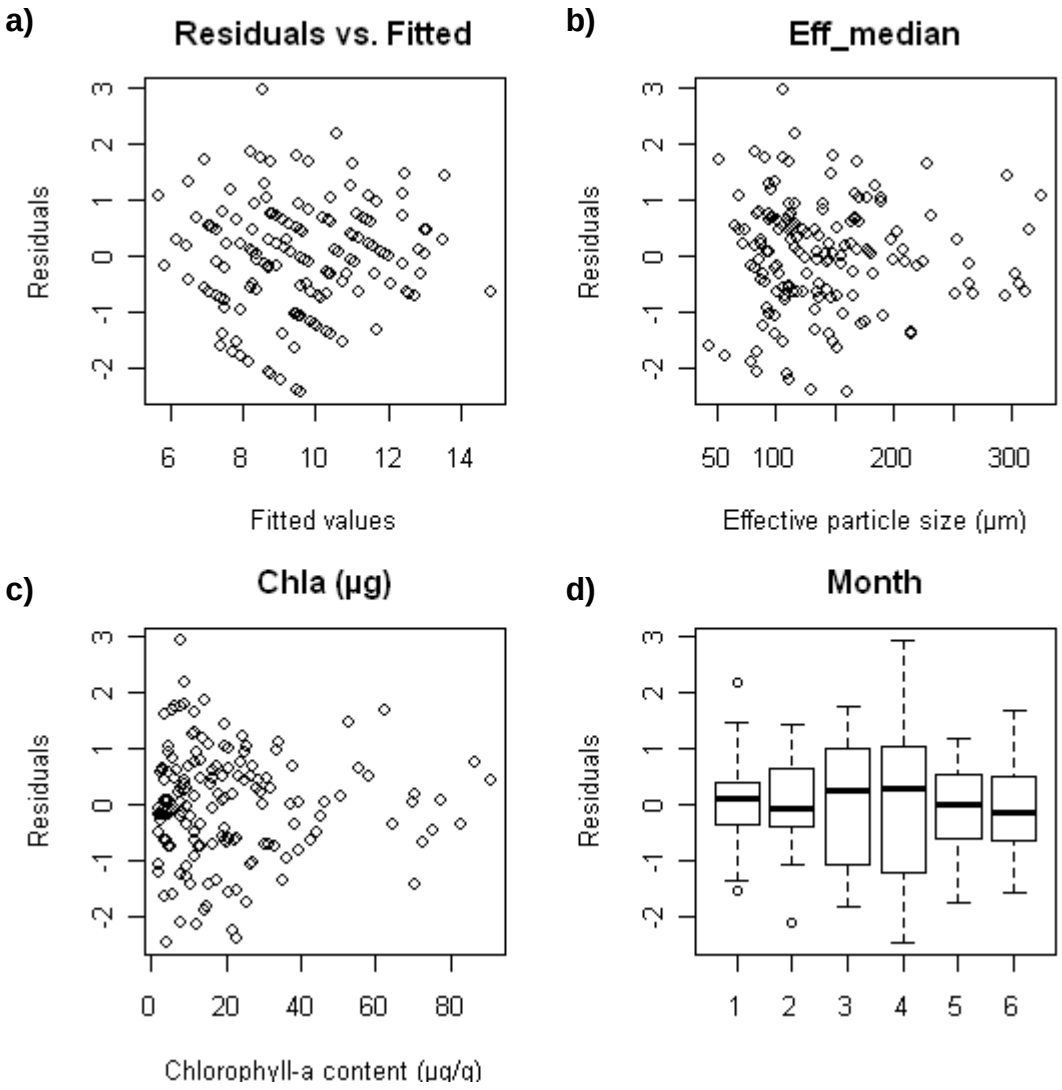

Figure 5.23. Validation plots of residuals vs. fitted values and explanatory variables to test the assumptions of homogeneity and independence for the MEM model of CSM-derived erodibility, excluding 0.15 PSI values and the high chlorophyll-a content data point. Model residuals plotted against (a) fitted values, (b) effective particle size, (c) chlorophyll-a content (µg g^{-1} sediment), and (d) month, an ordinal variable (1-6, bimonthly).

5.4 Sediment properties affecting shear strength

The same procedure for statistical analysis, as presented above, was used to investigate the factors responsible for variations in shear strength. As presented in Section 4.2.3, the frequency distribution for shear strength was not significantly different from normal (K-S, $Z = 0.755$, $p = 0.620$), though the lower end is truncated at zero (Fig 5.24). Since the dataset adheres to the assumption of normality, parametric tests were considered for the analyses, but often rejected in favour of non-parametric tests because of a violation in the assumption of homogeneity in variance.

Shear strength was significantly correlated to several sediment properties. Root index had the highest correlation ($r = 0.43$, $p < 0.001$), followed by organic content and effective mud content (Table 5.10). Covariation amongst the properties was high, particularly between organic content, sand content, and effective mud content (i.e. effective % < 63 μm) ($r = 0.62 – 0.88$) (Fig. 5.25), so care was exercised during model selection to avoid superfluous variables. Root index was the only variable correlated significantly to shear strength for both streams ($r = 0.45$ for both streams). It was the only variable significant for the Bere Stream. In the River Frome, SAR and chlorophyll-a also had negative correlations with shear strength. Whilst we would expect a negative correlation with SAR (Section 2.3.2), the fact that both cholorphyll-a and SAR are negatively correlated to shear strength suggests that it is in fact bulk density driving the relationship. Bulk density is negatively correlated to both chlorophyll-a ($r = -0.81$) and SAR ($r = -0.82$). Pearson correlation analysis was used because shear strength is a continuous variable and normally-distributed (Dytham 2003). Regression tree analysis identified root index as the only significant explanatory variable, with a node at 1.5, which split the dataset into a low shear strength (2.14 kPa) and high strength (3.45 kPa) group (Fig 5.26)

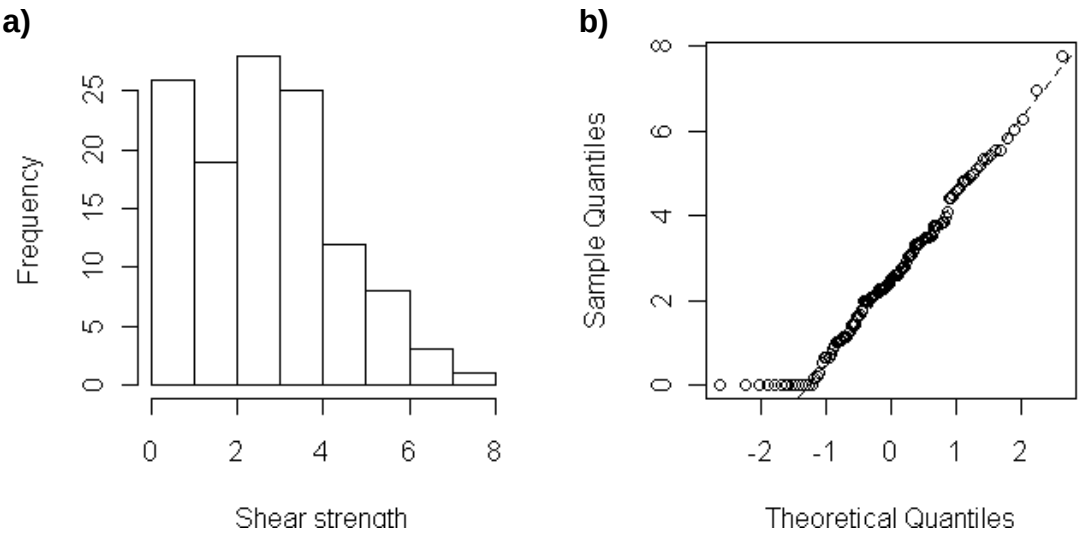

Figure 5.24. (a) Histogram and (b) Q-Q plot of shear strength indicate that the frequency distribution is similar to a normal distribution.

*Table 5.10. Pearson correlation coefficients for shear vane-derived shear strength and sediment properties. Significant at the 0.05 * level and 0.01 ** level (2-tailed).*

	Total	Bere	Frome
Dry bulk density	0.15	0.12	0.18
Effective median particle size	0.06	0.17	-0.11
Effective % < 63 μm	-0.19 *	-0.19	-0.20
Absolute median particle size	0.12	0.14	0.04
Absolute % < 2 μm	-0.18 *	-0.18	-0.18
Absolute % Sand	0.18 *	0.16	0.22
Organic content	-0.20 *	-0.03	-0.23
Chlorophyll-a content	-0.16	-0.06	-0.30*
SAR	0.00	0.14	-0.29*
Root Index	0.43 **	0.45**	0.45 **

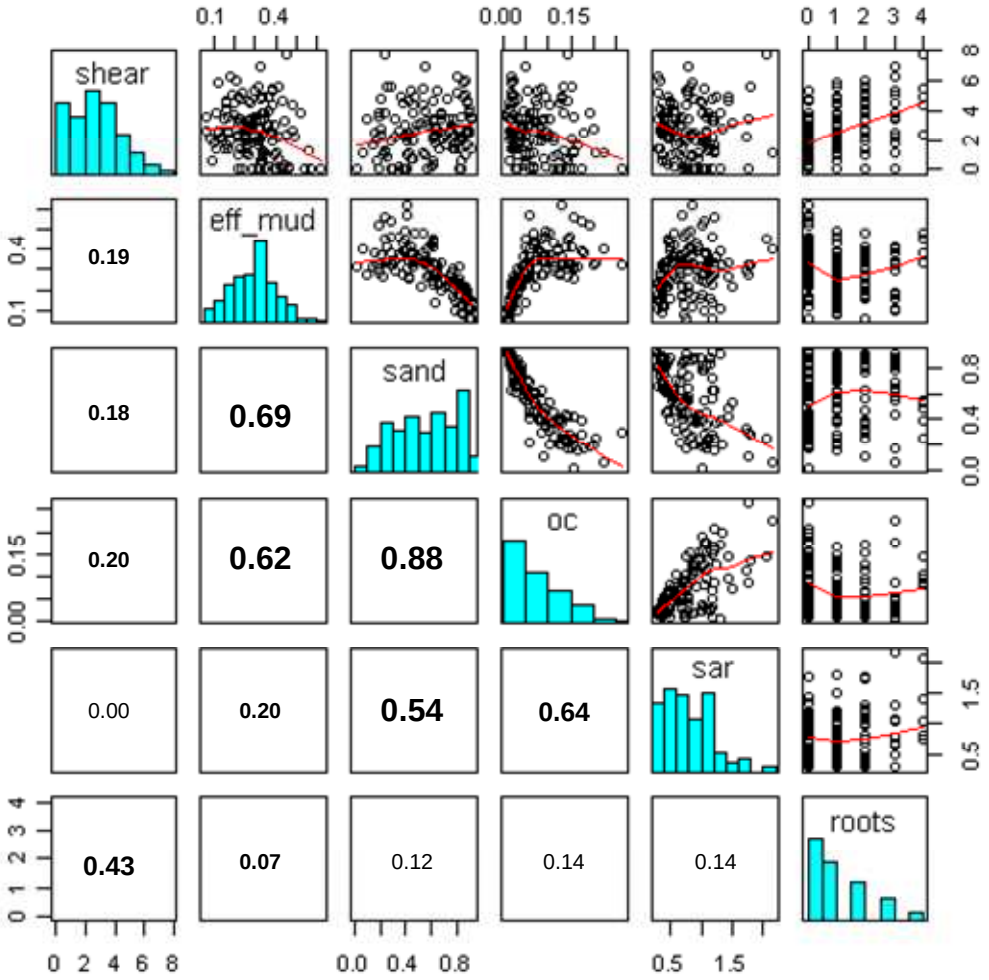

Figure 5.25. Scatterplot for shear strength and sediment properties for both streams with histograms along the diagonal and Pearson correlation coefficients in the lower panels. Bold font indicates the correlation is significant at the 0.05 level. shear = vane-derived shear strength; eff_mud = mud content based on effective size; sand = sand content based on absolute site, oc = organic content (LOI); sar = sodium absorption ratio; roots = ordinal measure of root density (0-4).

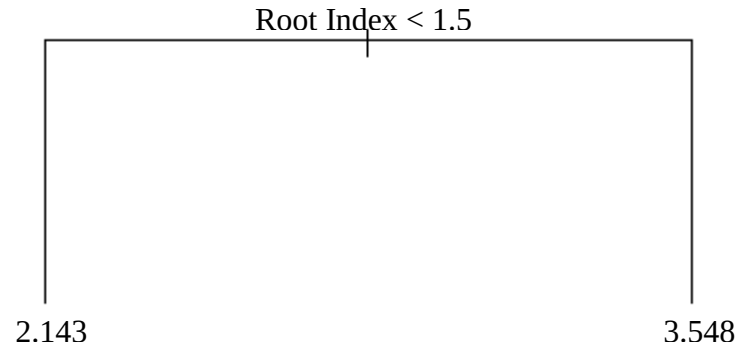

Figure 5.26. The pruned regression tree for vane-derived shear strength has only one significant explanatory variable, root index with a node at 1.5.

The optimal model for linear regression analysis was selected from a beyond optimal model using a combination of hypothesis testing and information criteria. A LR model containing root index and effective mud content was selected as the optimal model (Table 5.11). Shear strength was negatively related to mud content and positively related to root index (R^2_{adj} = 0.19) (Fig. 5.27). Model validation plots confirmed that residuals follow a normal distribution (Fig. 5.28). Residuals were broadly homogeneous, though there was a small increase in residual variance with fitted values (Fig. 5.29). Residuals were independent of the explanatory variables, but showed a significant trend for time. Consequently, a mixed effect model may be a more appropriate technique for the dataset.

Table 5.11. Summary statistics for the optimal linear regression model for shear strength. roots = root index, an ordinal measure of root density; eff_mud = mud content based on effective size.

	Estimate	Std. Error	t value	Pr(>|t|)
(Intercept)	2.71	0.46	5.92	3.14e-08
roots	0.63	0.12	515	1.04e-6
eff_mud	-2.68	1.32	-2.032	0.04

Residual standard error: 1.57 on 119 degrees of freedom

Multiple R-squared: 0.21, Adjusted R-squared: 0.1991

F-statistic: 16.04 on 2 and 119 DF, p-value: 6.784e-07

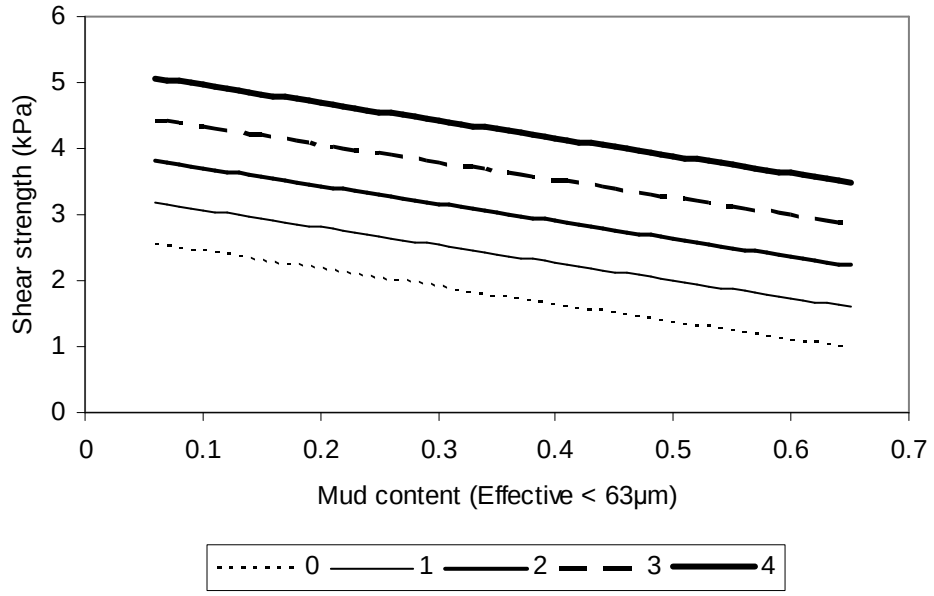

Figure 5.27. Optimal linear regression model of shear strength with mud content (Effective < 63 um) and root index (0-4) as explanatory variables (R^2 = 0.19).

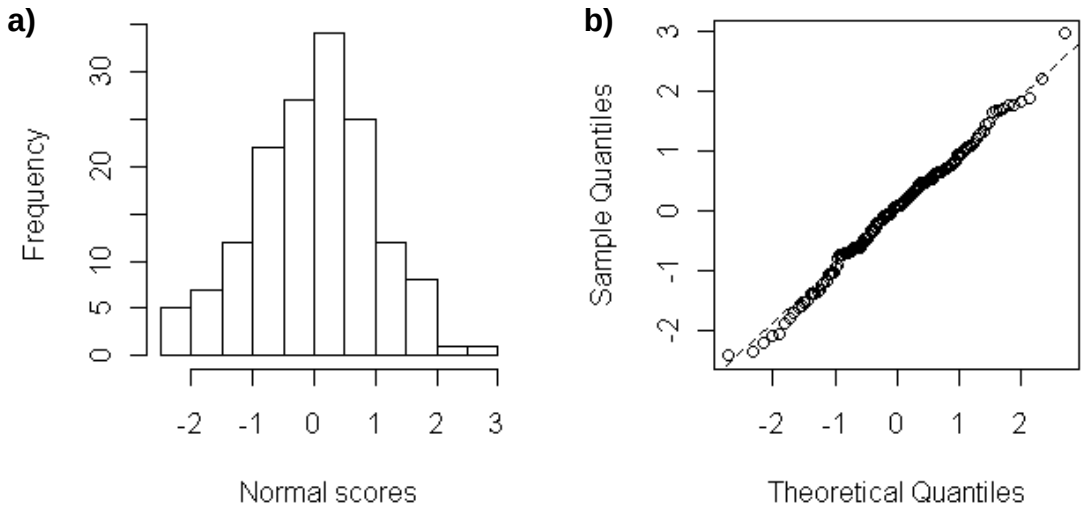

Figure 5.28. (a) Histogram and (b) Q-Q plot to test assumption of normality of residuals for the optimal LR model of shear strength.

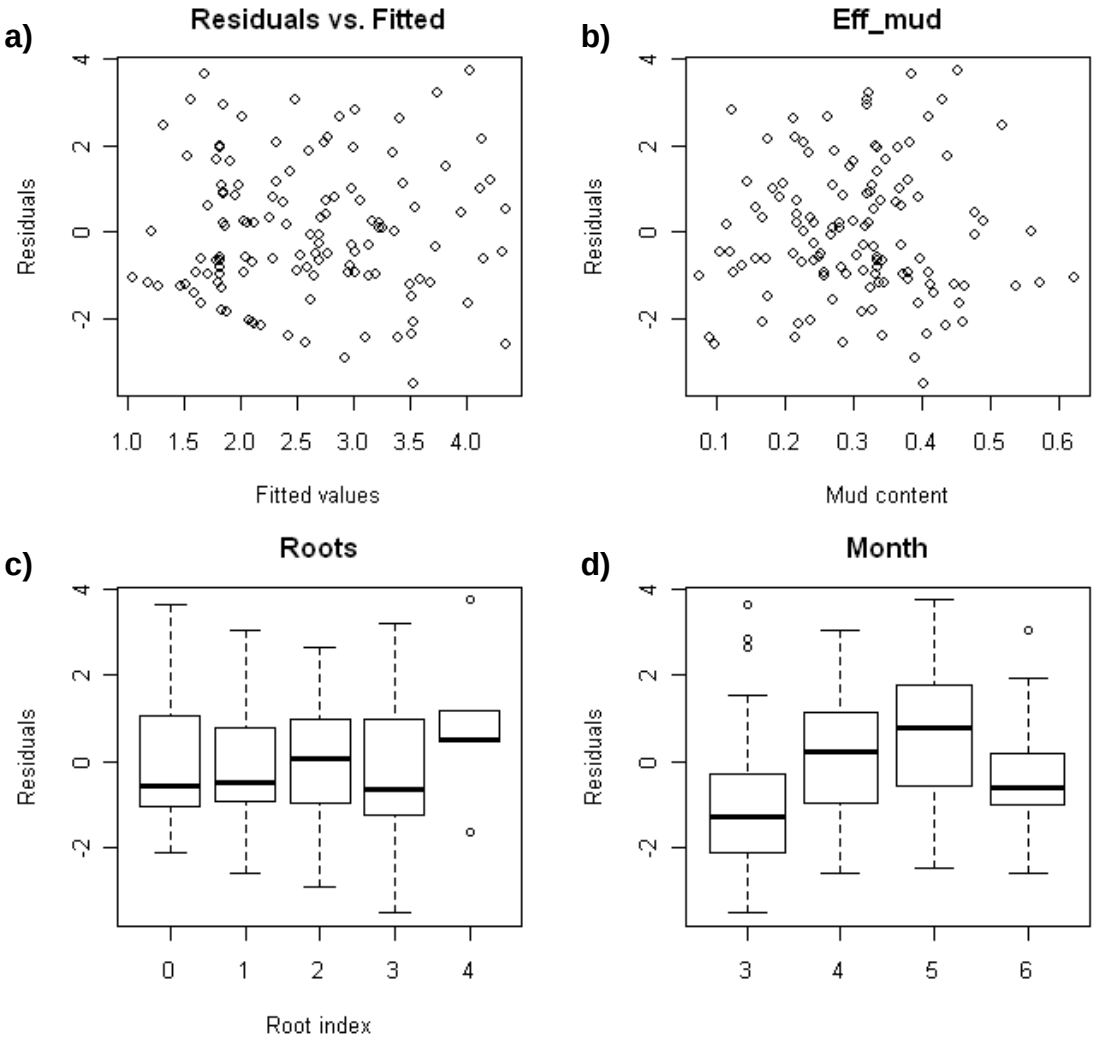

Figure 5.29. Validation plots to test the assumptions of homogeneity and independence for the LR model of shear strength. Model residuals are plotted against (a) fitted values; (b) mud content based on effective size, (c) root index, and (d) month, an ordinal variable (3-6)

The optimal mixed effects model for shear strength was a random intercept model based on month and fixed effects with a single explanatory variable, root index (Table 5.12). The model was selected anew from the beyond optimal model. The second-best MEM model had effective mud content and root index as fixed effects. Although the AIC was marginally lower, a single point lower, there was no statistically significant difference between the models (ANOVA, L. Ratio = 2.97, p = 0.085), so the more parsimonious model was selected. Model validation plots show that residuals were normally distributed (Fig. 5.30), homogeneous, and independent of explanatory variables (Fig. 5.31a-c). A temporal signal was still present, but residuals were reduced (Fig. 5.31d). However, residuals varied more between rooting indices than in the LR model (Fig. 5.31b).

In summary, root index is the single most important explanatory variable for predicting shear strength. A negative correlation with effective mud content was identified in LR, but was not significant in MEM.

Table 5.12. Summary statistics for the optimal mixed effects model for shear strength, fit by REML, roots = root index, an ordinal measure of root density (0-4).

Random effects:				AIC = 463	BIC = 474
Formula: ~1 | month	(Intercept)	Residual			
StdDev:	0.64	1.51			
Fixed effects: shear ~ roots					
	Value	Std.Error	DF	t-value	p-value
(Intercept)	1.91	0.37	117	5.13	0.000
roots	0.56	0.12	117	4.65	0.000
Standardised within group Residuals	Min	Q1	Med	Q3	Max
	-2.00	-0.71	-0.07	0.64	2.69
Number of Observations: 122					
Number of Groups: 4					

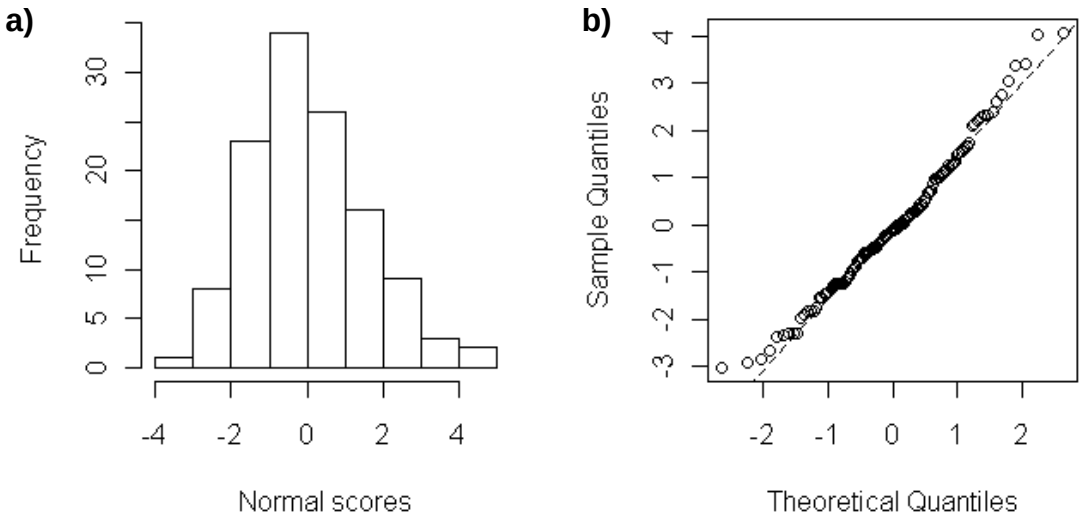

Figure 5.30. (a) Histogram and (b) Q-Q plot to test assumption of normality of residuals for the optimal mixed effects model of shear strength.

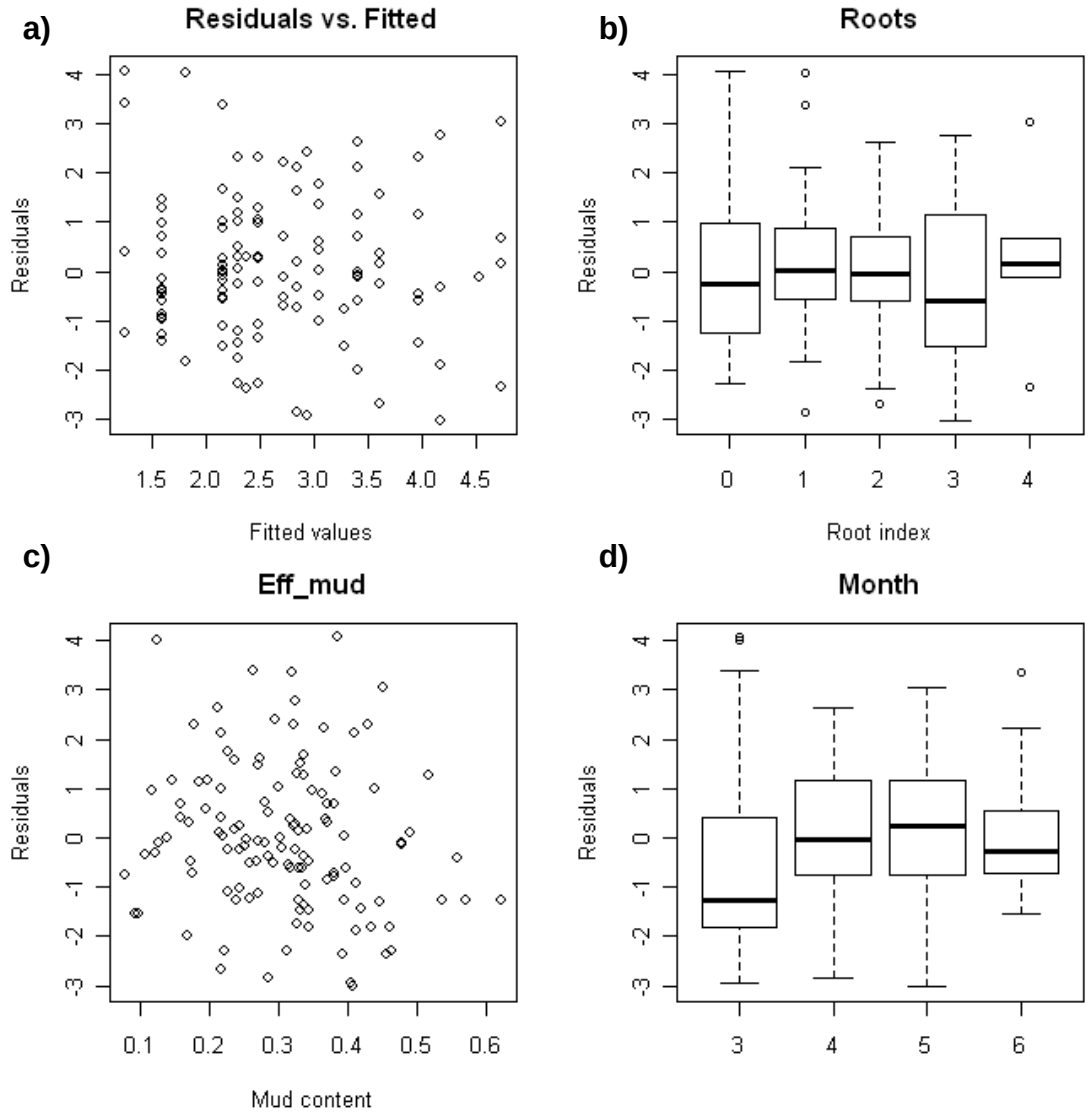

Figure 5.31. Validation plots to test the assumptions of homogeneity and independence of the mixed effects model of shear strength. Model residuals are plotted against (a) fitted values; (b) root index, (c) mud content based on effective size, and (d) month, an ordinal variable (3-6)

5.5 Discussion

The statistical analyses indentified three key physical and biological sediment properties that were primarily responsible for the variations in erodibility observed in the field study. For CSM-derived erosion thresholds, effective median particle size and chlorophyll-a were the most important variables, whilst for vane-derived shear strength, it was root index.

5.5.1 CSM-derived erosion thresholds

For the CSM-derived erosion thresholds, optimal models were created using LR and MEM. How do we compare the models, in order to select a single one to describe the dataset? It is not possible to calculate an R^2 for an MEM, but information criteria can be used to identify the model that meets the objective of the analysis. If we want the model with the best fit to the dataset, then the standard LR analysis that includes month produces the model with the lowest AIC (AIC = 745, generalised least squares). However, a model based solely on sediment properties is the goal. Therefore, a better comparison would be a mixed effects model and a linear regression with only median effective particle size and chlorophyll-a content as explanatory variables. The mixed effects model had a lower AIC than the linear regression (AIC, 760 vs. 784), making it the preferred model. Incorporating time as a random effect significantly improved the model fit (ANOVA, L. Ratio = 25.4, $p < 0.001$). So the variations in fine sediment erodibility are best explained by two sediment properties, median effective particle size and chlorophyll-a content, but a significant temporal component must be accounted for in the model.

These results support Hypothesis 2b which listed median effective particle size and chlorophyll-a content as potential explanatory variables for erodibility (Section 2.4). Particle size is arguably the most widely-used indicator of cohesiveness and erodibility for sediments, because it summarizes the magnitude of the major resistive forces in the sediment, gravity and electrochemical cohesion (Section 2.3.2). The positive correlation between effective particle size and erosion threshold supports early theories on particle entrainment (for a review, see Dade et al. 1992). Average effective particle sizes were in the silt and sand-sized fractions, which combined with the low bulk density of the finer-grained sediments, led to a linear increase in erosion threshold with particle size. This is because gravity is the major resistive force operating in the sediment, and smaller

particles weigh less. At lower water contents (i.e. higher bulk densities), forces of cohesion and adhesion within the sediment become more dominant, and erosion thresholds for fine sediment increase, producing the familiar negative unimodal entrainment curves of Hjulström and Postma (Dade et al. 1992).

The conclusion that effective particle size explains more of the variation in erosion thresholds than absolute size is noteworthy. Absolute particle size is the size of the mineral grains, whereas effective particle size is the size of the natural aggregates. Virtually all fine sediment is aggregated due to the effects of cohesion between clay minerals and adhesion to organic material (Droppo et al. 1997, Droppo 2001). Furthermore, the properties and behaviour of an aggregate differ from a mineral grain of the same size. Aggregates typically have lower densities and lower settling velocities than mineral grains of the same diameter. Accordingly, recent research on fine sediment transport in rivers has emphasised the need to measure effective particle sizes (Walling & Amos 1999, Droppo 2001, Cotton et al. 2006, Heppell et al. 2009). The results of the field study strengthen this claim, by providing the first empirical evidence of the importance of effective particle size on the erodibility of fine sediment deposits in rivers.

The optimal mixed effects model identifies chlorophyll-a content as having an equally important influence on erosion thresholds as particle size. Chlorophyll-a content is a proxy for photoautotrophic microbial biomass, which includes cyanobacteria and unicellular and filamentous algae. The photoautotrophic community can affect the erodibility sediment through surficial armouring and the production of EPS. Laboratory and field studies have noted that EPS increase erosion thresholds and decrease erosion rates for fine cohesive and non-cohesive sediment, by physically binding sediment grains (i.e. adhesion), creating a pliant structural matrix, and reducing boundary layer roughness (Paterson 1989, Dade et al. 1990, Yallop et al. 1994, Black et al. 2002, Droppo et al. 2007b, Lundkvist et al. 2007). Difficulties in extracting and characterising EPS, though, have led many researchers to use chlorophyll-a content as a proxy for EPS content. Several studies have demonstrated a significant correlation between chlorophyll-a content and erosion threshold (Austen et al. 1999, Paterson & Black 2000, Tolhurst et al. 2003, Gerbersdorf et al. 2008a).

Only a few studies, though, have investigated the role of EPS in the erosion of fine riverine sediment (Gerbersdorf et al. 2005, Gerbersdorf et al. 2008a, Spears et al. 2008), most of this research has been done in estuarine environments. The research for riverine sediment is in its infancy, and remains inconclusive. Gerbersdorf et al (2008) found signification correlation between chlorophyll-a content and erosion thresholds for riverine sediment. However, Spears et al. (2008) found higher chlorophyll-a contents but lower bulk densities and erosion thresholds in riverine than estuarine sediment, which points to interactions with salinity and bulk density. If salinity does influence the stabilising potential of EPS, perhaps the high dissolved calcium concentrations in chalk streams were an important factor underlying the significant role of benthic autotrophic community identified in this study (Section 2.3.2) (Decho 2000, Ravisangar et al. 2005). This field survey on chalk streams adds to this small and growing body of literature, but more research is needed to clarify the relationships between sediment properties and erodibility for fine riverine sediment.

Several recommendations are suggested for future studies. Whilst the presence of a significant temporal component in the optimal model is acceptable for a descriptive model, it is not ideal for predictive purposes, even when represented as a random effect in a mixed effects model. A predictive model should be based solely on sediment properties, which are the factors ultimately responsible for erodibility. The temporal component represents changes to sediment properties that were not captured by the laboratory analyses used in this study. This could be due to aspects of sediment sampling or analysis, or the choice of laboratory methodology, e.g. colloidal vs. cation exchange resin for extraction of EPS.

Two alterations to the field survey may help to improve the quality of data and model development: (1) a tighter match between the sediment analysed and the sediment tested by the device; and (2) modifications to the laboratory methods. First, laboratory analyses were conducted on the top 3 cm of the sediment core, but the CSM only acts on the very surface of the sediment. The depth was selected as a compromise between the surface erodibility measurements estimated by the CSM and the depth-integrated shear strength estimates from the shear vane. Sediment properties often varied substantially within the first 3cm, visually apparent as a surficial lens of fine particles on a sandy substrate, or changes in bulk density. Consequently, the sediment tested with the CSM may not have been well represented by the laboratory analysis. Second, the

laboratory techniques used to estimate effective particle size and characterise EPS could be improved upon. The pump speeds for the particle size analyser had to be set to maximum to fully resuspend the sediment within the test chamber. These high speeds, though, could have disrupted natural aggregates. Perhaps a visual technique based on microscopy, as commonly used for suspended sediment, would more accurately estimate aggregate size distributions.

Next, no standard approach exists to characterise EPS. Colloidal carbohydrate is the most common measure of EPS content, but some colloids may not be large enough to be called EPS (de Brouwer et al. 2002, Perkins et al. 2004). Other methods that attempt to extract and quantify the more recalcitrant fractions of the sediment are either too destructive, causing cells to lyse and spill their contents; are significantly more laborious, limiting the number of samples that can be processed; or have not yielded significant correlations to erosion thresholds (de Brouwer et al. 2000, Yallop et al. 2000). Cation exchange resins hold promise (Frølund et al. 1996, Gerbersdorf et al. 2005), but more work is needed to ascertain the levels of cell lysis and contamination by intracellular polymers. The standardisation of methods for the quantification and characterisation of EPS, for a broad range of fractions, is essential to investigating how biological organisms influence fine sediment erodibility. With these improvements to future methodologies, future studies are more likely to uncover the significant sediment properties and interaction effects that dictate erodibility, and hopefully lead to the development of a predictive model of erodibility.

5.5.2 Vane-derived shear strength

Root index was identified as the most significant explanatory variable for vane-derived shear strength. This supports Hypothesis 2a, which predicted a stabilisation effect by roots, however the short time span of the measurements prevents discussion of a temporal pattern (Section 2.4). However, the interpretation of these results in terms of sediment shear strength is debatable. Is the shear vane measuring sediment's resistance to erosion, or the density and strength of plant roots, or both? Bulk density is often cited as the most important factor affecting shear strength (Lick & McNeil 2001, Amos et al. 2004, Bale et al. 2007), but was not significant in this study (Table 5.11). Mud content was identified as a significant explanatory variable in the LR model. It was highly correlated to bulk density (r_s = -0.69, p = 0.000), though, which suggests a possible bulk

density effect, but is more likely linked to median particle size (r_s = -0.97, p = 0.00). Coarser-grained sediments had lower mud contents, high bulk densities and, therefore, higher shear strengths than siltier ones (Figs. 4.4 & 5.25). However, it is important to remember that residuals in the LR model were not independent of time, and the optimal mixed effects model does not contain mud content. Therefore, we are left with a model containing solely root index.

Roots have been shown to significantly increase the shear strength of soil (Gyssels et al. 2005). However the fine sediment in the chalk streams ranged from dense sandy material to fine light consolidated muds, and the ability of roots and rhizomes to stabilise this wide range of sediment types is unclear. Despite research that demonstrates the stabilising effects of plant roots on streambanks (Simon et al. 2006, Wynn & Mostaghimi 2006) and a classification of the rooting strengths of aquatic plants (Haslam 2006), no studies have explicitly measured the effects of plant roots on fine sediment erodibility. However, it is feasible that the impact of roots is dependent on the bulk density of the sediment.

Roots may be able to reinforce the denser sandy channel sediment, but may be largely ineffectual for the marginal sediment. For example, shear strength was greater for channel sediment with macrophyte cover than for unvegetated (Fig. 4.29). Furthermore, it was greater within *Ranunculus* than *Rorippa*. These findings suggest that the roots and rhizomes of these macrophytes increase the shear strength of the channel sediment, and that the stabilising effect is dependent on the macrophyte species. However, it is difficult to imagine that roots influence the erosion thresholds of silts with water contents that exceed 200-300%. Sediment and roots may not operate as one functional structure when exposed to flowing water; poorly consolidated fine sediment and roots could conceivably erode independently. This is supported by observations of bare *Rorippa* roots in the months following high water events, particularly November 2008 and January 2009. Therefore, we cannot be certain if the shear strength results should be interpreted as a measure of the sediment's resistance to shear, from which we can infer resistance to bulk erosion, or simply the density and strength of root fibres.

5.5.3 Conclusions

The statistical analyses identified three key sediment properties responsible for the variations in erodibility observed in the field study. Effective particle size and chlorophyll-a content were primarily responsible for the variations in surface erodibility, as measured by the CSM, which agrees with published field and laboratory studies. The resistance to bulk erosion, as measured by the shear vane, was principally impacted by macrophyte roots and rhizomes. The fact that other key sediment properties, such as bulk density, were not included in the final MEM model suggests that the shear vane may be measuring simply rooting strength and not the sediment's resistance to bulk erosion, particularly in low density marginal sediment. Overall, the empirical models explain a small amount of the variance in the dataset (e.g. 34 and 19% for the LR models of CSM and shear vane-derived erodibility), and consequently are best used for descriptive purposes only. A MEM approach was selected over LR because of significant temporal variations in erodibility that were unexplained by the sediment properties. Recommendations were given on revisions to field methods and laboratory analyses to improve future studies, such as better methods for quantifying effective particle size and EPS.

Chapter 6: CSM calibration

This chapter presents a methodology to estimate critical shear stress from cohesive strength meter (CSM)-derived erosion thresholds. It outlines the rationale for the development of the methodology, presents the results of two laboratory studies, and discusses the importance and use of the resulting calibration. This chapter formed the basis of a manuscript, which has been accepted for publication in *Limnology and Oceanography – Methods* (Grabowski et al. *In Press*)

6.1 Introduction

Models of cohesive sediment transport rely on accurate estimates of erodibility to predict sediment fluxes. At present, cohesive sediment erodibility cannot be predicted, and must be measured for the sediment in question (Black et al. 2002, Winterwerp & Van Kesteren 2004). Historically, this has been accomplished by measuring erosion thresholds and rates for sediment cores in laboratory flumes. Erodibility, though, varies significantly over space and time in aquatic environments (e.g. Hanson & Simon 2001, Bale et al. 2006, Tolhurst et al. 2006, Spears et al. 2008) and is affected by sediment handling and storage (Maa 2008). Consequently, techniques that permit quick, *in situ* measurements of erodibility have been advanced in recent years.

Several *in situ* erosion devices have been used to quantify erosion thresholds for natural muds. These are broadly divided into two categories: straight and annular field-deployable flumes (e.g. Sea Carousel or Gust erosion chambers), and small-held erosion devices (e.g. EROMES and the cohesive strength meter (CSM)) (Amos et al. 2003, Widdows et al. 2007). The field-deployable flumes generate horizontal water flows across the sediment surface, and can be flow-through or recirculating, and straight or

annular in form. The Gust erosion chamber is, in essence, a small annular flume (20 cm diam.), in which horizontal flows are generated by a rotating lid (e.g. Tolhurst et al. 2000a). EROMES is a compact erosion chamber that directs vertical water flow towards the sediment using a rotating propeller (e.g. Widdows et al. 2007). Whilst several of these devices are capable of measuring stability over small spatial (cm) and temporal scales (min), the CSM is the only one that is commercially available, making it more readily accessible to researchers. However, the device is best suited to relative measurements of erosion thresholds for cohesive sediment, because of difficulties in correlating the erosive forces generated by the vertical jet to horizontal shear stress (Vardy et al. 2007, Widdows et al. 2007).

A theoretical calibration of the eroding force of the CSM jet was developed based on the suspension of pure sand (Tolhurst et al. 1999). In that study, the CSM was used to resuspend uniform sand beds of varying grain sizes (> 200 μm). The relationship between grain size and critical CSM pressure was then compared to the equivalent horizontal bed shear stress calculated based on the Shields' criterion. Whilst this theoretical approach produces a calibration for the average forces generated by the CSM, it does not take into consideration how cohesive sediment will behave under the eroding jet. As such, caution should be exercised when applying the calibration to sediments with mean particle sizes less than the tested minimum of 200 μm.

Several studies have attempted to calibrate the CSM by comparing erosion rates and thresholds for natural muds between erosion devices (Tolhurst et al. 2000a, Tolhurst et al. 2000c, Widdows et al. 2007). The conclusion from these studies, though, is that only devices that generate similar forces (i.e. horizontal or vertical) are comparable. Laboratory and field flumes generate predominately horizontal water flows across the sediment surface, and their critical shear stress estimates are strongly correlated (Widdows et al. 2007, Bohling 2009). Similarly, devices that use a vertical flow of water to erode the sediment, such as EROMES and the CSM, generate comparable erosion thresholds (Tolhurst et al. 2000c). However, no correlation has been found between erosion thresholds derived from CSM and flumes for natural muds (Tolhurst et al. 2000a, Widdows et al. 2007). These studies suggest that the lack of correlation is primarily due to differences in the nature of the eroding forces, operational procedures (e.g. sediment loading, filling the device with water, shear step increments and timing, and consolidation/submergence time), definitions of erosion parameters (e.g. threshold

suspended sediment concentrations, standardization and calibration), and significant differences in device footprints coupled with a high spatial variability in the erodibility of natural sediment.

The lack of correlation between CSM- and flume-derived erosion thresholds is problematic. Flumes produce controlled and well-understood hydrodynamic conditions, making them ideal for measuring erosion thresholds. However, they are not as well-suited to investigate spatial and temporal variations in erodibility as the CSM, and are difficult to use when vegetation is present. Recently, a calibration has been developed that permits comparisons of erosion thresholds between different models of the CSM, but without a calibration to horizontal shear stress, CSM-derived erosion thresholds for cohesive sediment remain a relative measure and cannot be incorporated into sediment transport models (Vardy et al. 2007).

The objective of this chapter was to develop a methodology to estimate critical shear stress values from CSM-derived erosion thresholds to permit future integration into models of sediment dynamics in chalk streams. Here, a novel methodology is presented based on predictable changes in erosion thresholds with changes in sediment properties, and a calibration based on an inter-comparison of erosion thresholds from the CSM and a laboratory annular flume.

6.2 Methodology

The methodology is based on previously-published studies that demonstrate a positive linear correlation between clay/mud content and critical shear stress for cohesive sediment mixtures (Mitchener & Torfs 1996, Panagiotopoulos et al. 1997) (Fig. 2.4). A preliminary study was conducted to determine if CSM-derived erosion thresholds exhibited a similar positive relationship to clay content. In the final experiments, sediment mixtures with varying clay contents were tested with both the CSM and a laboratory flume, and the erosion thresholds were compared to develop the calibration.

6.2.1 Preliminary experiments

Sediment mixtures were created using fine quartz sand (d_{50} = 224 μm, Sibelco) and kaolin (china clay, Potclays). Clay contents varied between 0 – 30% by dry weight. The

dry minerals were measured out into a large container and homogenized using an electric mixing drill with mortar mixing paddle. Water content was kept low (25% w/w) to ensure a homogeneous sediment mixture; above 30% water content, a layer of kaolin would form on the sediment surface. Tap water was added to the dry minerals, and the mixture left to hydrate for 15 minutes. The sediment was mixed with a mortar mixing drill and split between 3 sample containers (15 l plastic buckets). The sediment surface in each container was leveled with a trowel. An insulated, floating plastic sheet (i.e. bubble wrap) was placed on top of the sediment surface to minimize clay resuspension during filling, and 7cm of water was added on top of the sediment. The sediment was left to consolidate overnight.

The following morning, CSM (MK4, Partrac) measurements (n = 5) were taken within each bucket. The Sand 1 routine for the CSM was used, which has the lowest initial jet pressure (0.3 PSI), a short jet pulse duration (0.3 s), small pressure increments (0.3 PSI), and a high maximum jet pressure (12 PSI). The CSM monitors erosion based on resuspension. A transmissometer sensor is located at 1 cm above the sediment surface within the CSM test chamber. Erosion thresholds are defined by the manufacturer as the pressure at which average transmission within the test chamber drops below 90% of the maximum. Average transmission is calculated for the 2^{nd} to 12^{th} data logged, which corresponds to 1 s for the Sand 1 routine. The CSM records the internal pressure (P_I) for each step in PSI, but stagnation pressure (P_{stag}) is dependent on the specifics of the CSM model, the sampling routine, the length and diameter of tubing, and the height of the jet orifice above the sediment surface (Vardy et al. 2007). P_{stag} was calculated based on P_I for the specific CSM unit following the methods of Vardy et al. (2007) (n=3). P_{stag} is reported in SI units for pressure (Pa) and for the MK4 CSM model is calculated according to the following equation,

$$P_{stag} = 3.47\ (6.89\ P_I)^{1.40} \qquad (R^2_{adj} = 0.94,\ p < 0.001) \qquad (6.1)$$

for P_I up to 4.8 PSI. The calculation of P_{stag} allows erosion thresholds to be compared between CSM models and individual units. Erosion thresholds were modelled as a function of clay content using locally weighted (LOWESS) analysis (R Core Development Team 2009)

6.2.2 Calibration experiments

The CSM calibration experiments were conducted at the Hydraulics Laboratory, Environment Canada, Burlington, ON, Canada. Artificial sediment mixtures were created in the same manner as for the preliminary experiments. Fine quartz sand (d_{50} = 175 μm, Wedron Silica, #505) and kaolin (Georgia Kaolin Co.) (5 – 35% w/w) were mixed with degassed tap water (20 – 25% w/w) using a mortar mixing paddle (Fig. 6.1a). Water content was allowed to increase slightly with clay content to compensate for the greater water absorption capacity of clay, producing sediments with similar consistencies, assessed visually. The sediment mixtures were split and laid into an annular flume (Fig. 6.1b,c) and a sampling container (15 L bucket), overlaid with degassed tap water, and left to consolidate overnight (Fig. 6.1d).

Figure 6.1. Preparation of the sediment mixtures for use in the annular flume calibration experiments. (a) Sediment mixing using a mortar mixing drill, (b) transferring the sediment to the flume, (c) spreading and levelling the sediment in the flumel, and (d) filling the flume.

Erosion thresholds were estimated for the CSM following the protocol as described above. P_{stag} was calculated anew for these experiments, following routine maintenance to the CSM, and is represented as:

$$P_{stag} = 2.80\ (6.89\ P_I)^{1.47} \qquad (R^2_{adj} = 0.93,\ p < 0.001) \qquad (6.2)$$

for P_I up to 4.8 PSI.

The annular flume had a 2 m external diameter, a 20 cm channel width, and a maximum channel depth of 12 cm (Fig. 6.2). Water flow was generated by a rotating glass lid that was lowered onto the water surface. Average bed shear stress is calculated as:

$$\tau = 0.1\ (0.164\ RPM)^2 \qquad (6.3)$$

where τ is bed shear stress (Pa) and RPM is the flume lid speed (rotations per minute) (Lau & Droppo 2000). Lid speeds were increased to produce 0.1 Pa steps in average bed shear stress, and held constant for 10 minutes. The critical shear stress for erosion (τ_c) was identified based on the same criteria as for the CSM; the shear stress at which CSM transmissometer readings drop below 90% of background levels. As it was impossible to place the CSM directly into the flume to monitor suspended sediment levels during a run, CSM transmissometer readings were correlated to optical backscatter readings (OBS) that were continuously measured in the flume. OBS was measured at mid water column and averaged per minute. Suspended sediment samples (100 ml) were taken from mid water column at 1, 5, and 9 minutes after a step increase to calibrate OBS values based on suspended sediment concentration. The samples were filtered through preweighed/predried 0.2 μm cellulose acetate filters and dried at 105 C for 1hr. CSM transmissometer readings strongly correlate to OBS ($R^2_{adj} = 0.97$, $p < 0.001$) and suspended sediment ($R^2_{adj} = 0.98$, $p < 0.001$). The 90% transmission threshold corresponds to an OBS of 100 and a suspended sediment concentration of 35 mg l^{-1}. Mean erosion thresholds for each clay content treatment from the CSM and flume were compared to develop a calibration between the devices.

Figure 6.2. The annular flume at the National Water Research Institute, Environment Canada. The flume measures 2 m in external diameter and has a channel width of 20 cm. Water flow is generated by a rotating lid that is lowered onto the sediment surface.

6.2.3 Routine selection

The CSM has over 40 predefined routines, which differ in jet pressure steps, jet duration and transmissometer logging times. Few studies have investigated how routine selection influences critical shear stress estimation. Four routines (Mud 1, Sand 1, Sand 4 and Sand 7) were selected to investigate the effects of jet duration and transmissometer logging time on critical shear stress (Table 6.1). Sediment mixtures were split between 4 sampling containers. Routines were selected randomly, and CSM tests (n = 5) were conducted within each container. Erosion thresholds are reported as P_I and P_{stag}, which is calibrated using the method above for each routine. Data were analyzed statistically using an ANOVA and post-hoc Tukey test as the data conformed to the assumptions of equal variance.

Table 6.1. Manufacturer-defined settings for four of the CSM routines (MK IV).

	Mud 1	Sand 1	Sand 4	Sand 7
Jet duration (s)	0.3	0.3	0.5	1.0
Data logged for (s)	30	3	3	3
Data logged every (s)	1	0.1	0.1	0.1

6.3 Results

6.3.1 Preliminary Experiments

CSM erosion thresholds show a negative unimodal response to clay content for the artificial kaolin:sand sediments, with a minimum at 5% clay content (Fig. 6.1). For clay contents greater than 5%, erosion threshold and clay content are positively correlated, exhibiting a similar pattern to flume-derived critical shear stress values (Mitchener & Torfs 1996, Panagiotopoulos et al. 1997) (Fig. 2.4). Below 5% clay, though, the CSM thresholds are markedly greater than flume-derived estimates. Previous flume studies report that pure sand has the lowest erosion threshold, forming a baseline in erodibility (Mitchener & Torfs 1996, Panagiotopoulos et al. 1997) (Fig. 2.4). Increasing clay contents cause an increase in erosion thresholds due to hydrodynamic smoothing, clay-sand adhesion, and clay cohesion (Mitchener & Torfs 1996, Lick et al. 2004, van Ledden et al. 2004).

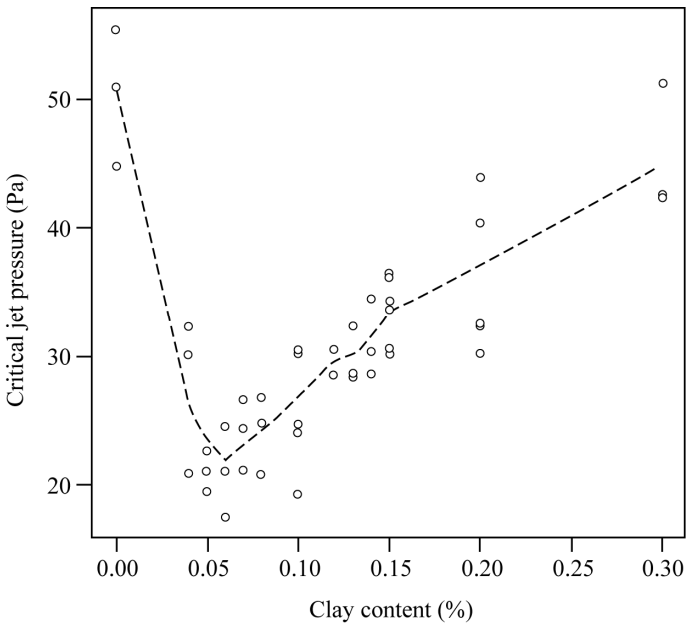

Figure 6.3. Erosion thresholds generated by the CSM for artificial kaolin/sand sediments (LOWESS regression, span = 0.3). Each data point is an average of 5 erosion tests, with a minimum of 3 replicates per clay content. Some data points are offset vertically to aid visualization.

The difference in CSM- and flume-derived erosive thresholds for sediment with less than 5% clay content likely has two causes, one sedimentological and the other methodological. First, previous research on the erosion of sand/clay mixtures reports that a minimum clay content is needed to produce a cohesive sediment. Estimates for this critical clay content range from 4 – 10% clay (Mitchener & Torfs 1996, van Ledden et al. 2004). Below this value, the clay particles are not abundant enough to form a structural matrix. As a result, the sediment erodes in a granular fashion with clay and sand particles eroding independently (van Ledden et al. 2004, Winterwerp & Van Kesteren 2004). Second, the CSM and flume experiments use different criteria and techniques to identify the moment when sediment begins to erode. For example, Panagiotopoulos et al. (1997) used visual criteria based on bursts of sediment motion per second, whilst Mitchener and Torfs (1996) cite experiments by Torfs that used the mass of eroded material, suspended and bedload. However, the CSM estimates erosion thresholds are based on an optical measure of sediment resuspension. The device has a transmissometer sensor located 1 cm above the sediment surface in the test chamber. Pure sand, though, would be entrained and transported as bedload at much lower forces than what is necessary for resuspension up to 1 cm off the sediment surface (Leeder 1999). Consequently, erosion thresholds for pure sand would be substantially greater

when measured by the CSM as compared to laboratory flume (Fig. 6.3). The decrease in erosion thresholds from 0 – 5% clay content suggests that clay particles are eroding independently from the sediment, and resuspending at lower erosive forces than sand grains. Therefore, the CSM produces erosion estimates comparable to critical shear stress derived from laboratory flumes for cohesive sediment mixtures above a critical clay content, which for this experiment is 5% kaolin.

6.3.2 Calibration experiment

Erosion thresholds for cohesive sediment mixtures were measured using the CSM and a laboratory annular flume over a range of clay contents to develop a calibration between the devices. Despite their differences in design, the CSM and flume produced erosion thresholds exhibiting similar positive correlations with clay content (Fig. 6.4). Both devices show a two-fold increase in erosion thresholds as clay content increases from 5% to 35%.

The calibration was developed by comparing the mean erosion thresholds derived by the CSM and flume for each clay content treatment (Fig. 6.5). Critical shear stress (τ_c) is estimated as:

$$\tau_c = 0.0013P_{stag} + 0.047 \qquad (R^2_{adj} = 0.87,\ p < 0.01) \qquad (6.4)$$

Mean erosion thresholds were used in the calibration because both devices suffer from high variability at the higher clay contents. This was particularly noticeable for clay contents greater than 20% (Fig. 6.4). For both the CSM and flume, the variations at high clay contents are likely related to the optical measure of erosion threshold. The 10% reduction in transmission that signals erosion has occurred correlates with 35 mg l^{-1} of suspended sediment. As a result, only extremely small quantities of sediment need to be eroded for erosion to be recorded. For example, in a flume experiment that uses 30 kg of sediment and over 100 l of water, erosion “occurs” when just 4 g of sediment is suspended. For the CSM, the variation is exacerbated by the compact nature of the CSM jet and slight differences in the surface characteristics of the sediment. Homogeneous artificial sediments were used in the experiment to minimize spatial variability in sediment properties, however subtle differences in surface properties were visually apparent within the containers. A thin, patchy clay layer formed on the sediment surface

by minor resuspension of clay when the containers were filled with water. As the CSM jet erodes a tiny area of sediment (ca. 1 cm^2) and has a small chamber volume (ca. $4x10^{-5}$ m^3), a small difference in surficial clay accumulation could influence transmissometer readings. This is a natural outcome for a portable device with an extremely narrow footprint that can be used at high spatial resolutions.

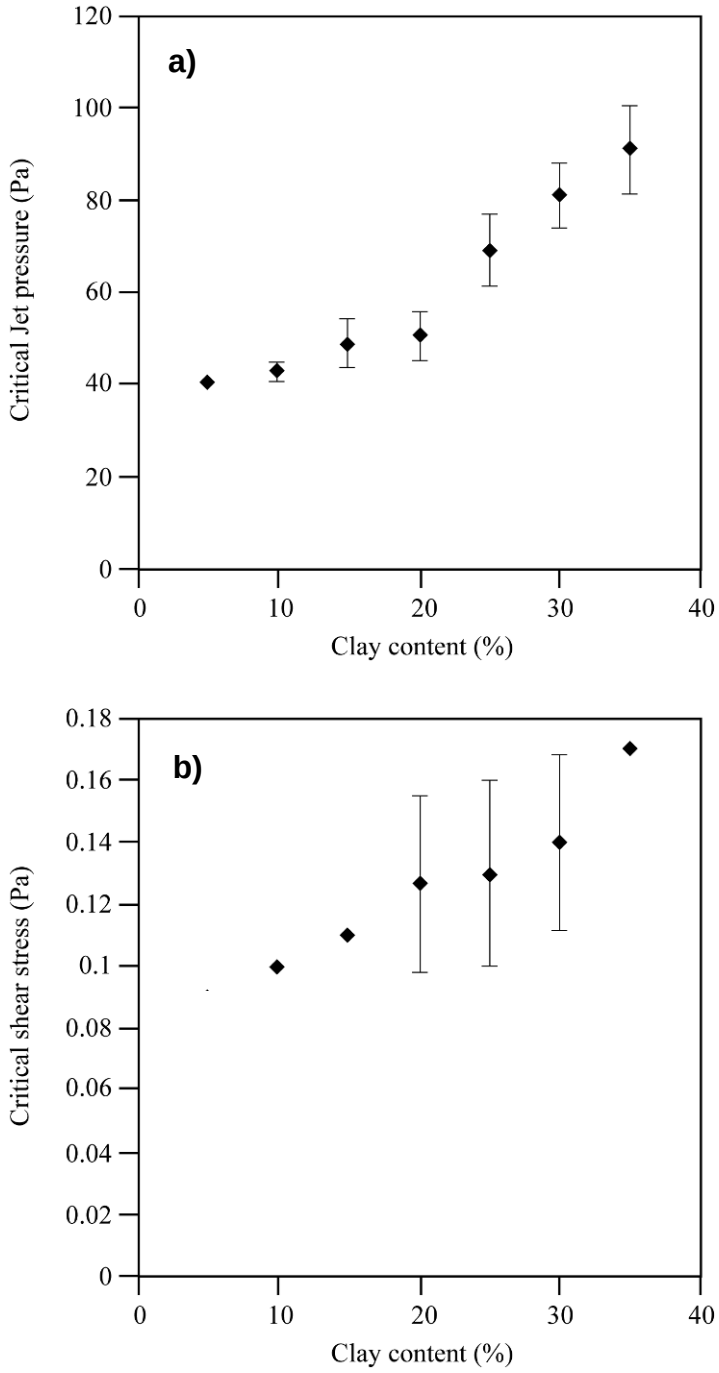

Figure 6.4. Mean erosion thresholds for sand/kaolin sediment mixtures estimated using (a) the CSM and (b) a laboratory annular flume. The number of replicates varies from 1-3 for each data point. For the CSM, each replicate is composed of 5 individual tests. Error bars are one standard error.

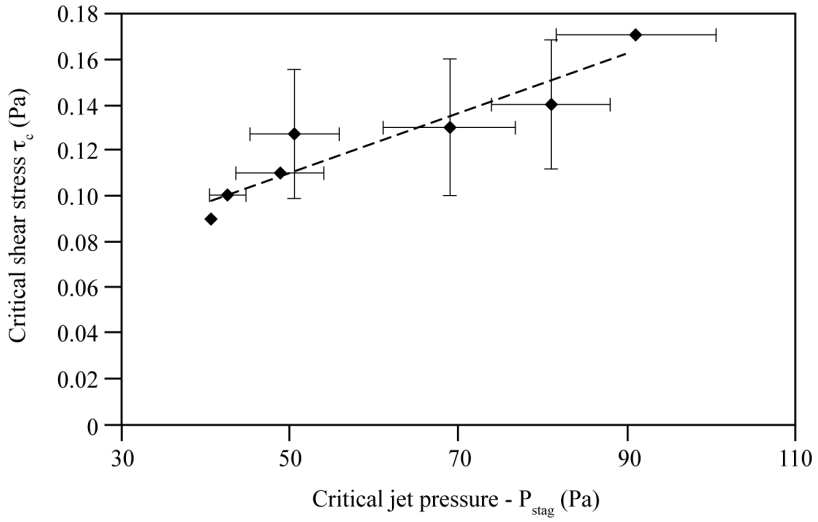

Figure 6.5. Correlation between mean critical shear stress and mean CSM erosion thresholds by clay content (R^2_{adj} = 0.87, P<0.01). Error bars are standard error.

6.3.3 Routine selection

The CSM has two major categories of routines, Sand and Mud, which differ by transmissometer logging time (3 s vs. 30s). Within each category, the routines differ by jet pressure steps and jet duration. In this experiment, pressure steps were kept equal to investigate the effects of jet duration and transmissometer logging time.

The choice of routine has a significant impact on the estimation of erosion thresholds. Three Sand routines (1, 4 and 7) were selected to examine the effects of jet duration on erosion thresholds. At each clay content, erosion thresholds decrease with an increase in jet duration (Fig. 6.6). For example, the sediment eroded at a significantly lower internal pressures (P_I) for the Sand 7 routine compared to Sand 1 (ANOVA, P<0.001) (Fig. 6.6a). The pattern largely holds when thresholds are represented as critical stagnation pressure (P_{stag}) (Fig. 6.6b), because the calculated jet pressure at the sediment surface was similar between the Sand routines

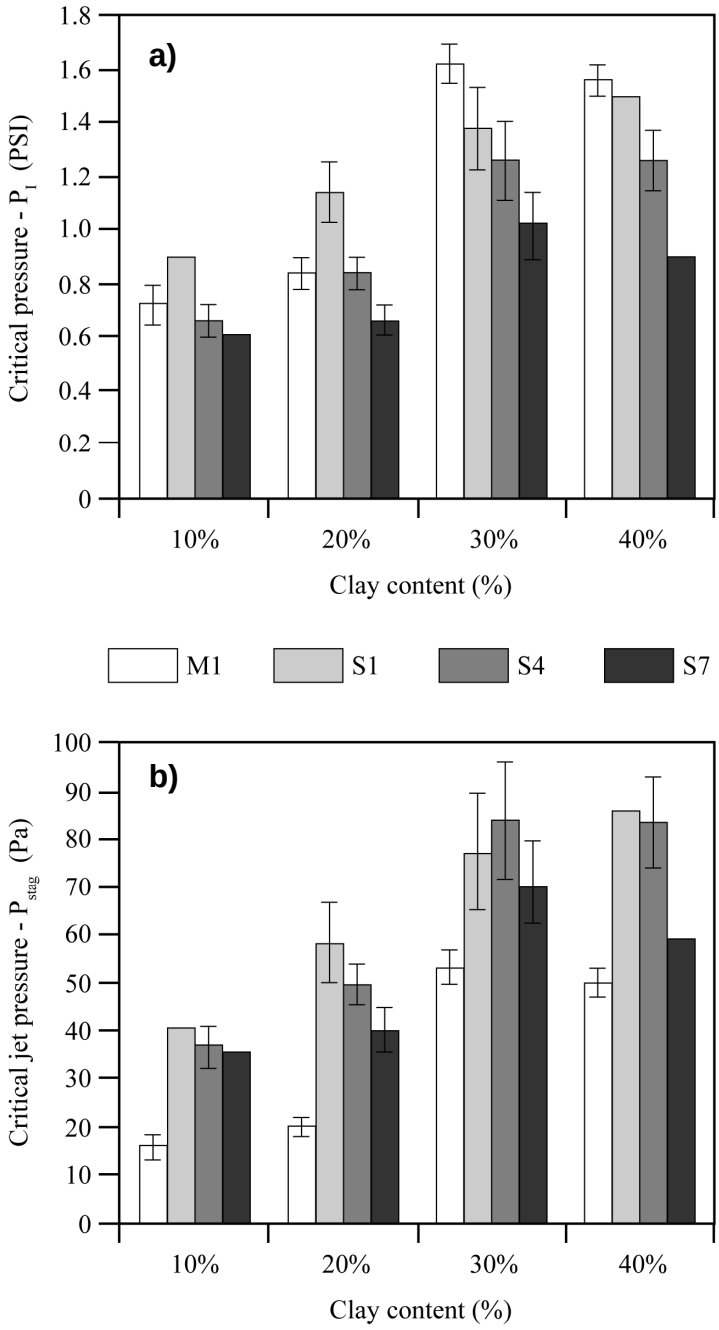

Figure 6.6. Mean erosion thresholds for cohesive sediment mixtures of varying clay content, and using different CSM routines. (a) Erosion thresholds represented as the internal pressure (P_I) as recorded by the CSM. (b) Erosion thresholds converted to stagnation pressure (P_{stag}) (Vardy et al. 2007). M1 = Mud 1, S1 = Sand1, S4 = Sand 4, and S7 = Sand 7. Error bars are standard error.

The effect of transmission logging time was examined by comparing erosion threshold from Mud 1 and Sand 1 routines. It was hypothesized that the 10-fold difference in logging times between the routines would result in greater erosion thresholds for Mud 1 (Table 6.1). This is because the longer transmission logging time for the Mud 1 routine means that transmission values are averaged over 10 s, compared to only 1 s for Sand 1. Following particle resuspension by the jet burst, particles would settle out of suspension, and transmission values would increase with time. Therefore, longer logging periods would result in higher average transmission values per jet step, so greater jet pressures would be needed to drop transmission below 90%.

Patterns in erosion thresholds between Mud and Sand 1 were ambiguous when represented as P_I, but, when corrected to P_{stag}, Mud 1 clearly generated significantly lower erosion thresholds than Sand 1 for all clay contents (ANOVA, $p < 0.001$) (Fig. 6.4). It was originally thought that this was caused by a software problem that altered the amount or pressure of water ejected from the jet. The P_{stag} calibration data showed that the Mud 1 routine ejects on average 25% less water than Sand 1 at each pressure step. However, this observation would not explain the disparity in thresholds. If less water was ejected from the jet, erosion should be less likely to occur at each step, and erosion thresholds would be higher for Mud 1 than Sand 1. Other explanations were considered, the most plausible being a discrepancy in transmissometer data. Based on the raw transmissometer data from the Mud 1 test, it appears that transmission continued to decrease for 5-6 seconds after a jet burst. The Sand 1 routine logs transmission readings for 3 s, but average transmission values are calculated from 0.2 to 1.2 s. So, Sand 1 transmission readings may not capture the minimum in transmission values, and would be skewed higher than Mud 1. This discrepancy makes it difficult to compare erosion thresholds between Mud and Sand routines, but should not cause a problem if the same routine is used for an entire study. It should be noted that a previous study found little difference between erosion thresholds using Sand routines 3, 7 and 9 when using natural muds, suggesting that some of the differences observed in this study may be due to the kaolinite in the sediment (Tolhurst et al. 2000b).

6.4 Discussion

This study demonstrates that the CSM produces erosion thresholds comparable to critical shear stress derived from laboratory flumes. It has yielded the first CSM calibration based on cohesive sediment. The successful inter-comparison is attributable to three important considerations. First, the methodology used cohesive sediment mixtures composed of pure sand and clay, which minimized variations in sediment erosion thresholds. Second, the inter-comparison was based on a previously identified relationship between erosion threshold and clay content for sand/clay mixtures. Finally, erosion thresholds were identified using the same criteria for both the CSM and flume, an optical measure of sediment resuspension. By minimizing confounding factors and controlling for methodological differences, mean erosion thresholds show a strong correlation between the erosion devices. As a result, a simple formula can be proposed to convert CSM-derived erosion thresholds to critical shear stress, so that they can be incorporated in sediment transport models (Eq. 6.4).

As with all empirical calibrations, the calibration equation is only valid within the tested range using the same settings. So the calibration formula (Eq. 6.4) should only be used to interpolate between approximately 40 – 90 Pa stagnation pressure (P_{stag}) when using the Sand 1 routine, which is equivalent to 9 – 17 Pa shear stress. The range of the calibration is narrow in comparison to the forces that the CSM is capable of delivering. However, this range is similar to recently reported mean erosion thresholds for the Eden Estuary (P_{stag}: riverine, ~40 Pa; estuarine mudflat, ~100) (Spears et al. 2008). Whilst the original objective was to apply the calibration to the field survey data, this cannot be done universally because many of the CSM-derived erosion thresholds fell outside of the empirical calibration. As a demonstration of the use of the calibration, Table 6.2 presents critical shear stress values converted from critical stagnation pressure for July 2009.

*Table 6.2. CSM-derived erosion thresholds by macrophyte type and stream for July 2009, converted from stagnation pressure to critical shear stress. *The stagnation pressure for Bere Stream Ranunculus sediment fell outside the range of the empirical calibration, so was not converted to critical shear stress.*

	Stagnation pressure P_{stag} (Pa)		Critical shear stress τ_{crit} (Pa)	
	Bere	Frome	Bere	Frome
Ranunculus	134	90	*	0.16
Rorippa	78		0.15	
Marginal	42	85	0.10	0.16
Riparian	73	53	0.14	0.12
Unvegetated	77	98	0.15	0.17
Mean	65	60	0.13	0.12

6.4.1 Future research

There are two main areas for development of a CSM calibration. First, the calibration experiments could be repeated for other routines. The Mud routines are commonly used, and would be good candidates for a future calibration. Second, the range of the empirical calibration could be expanded. This could be done using the same methodology but by altering clay mineralogy and water chemistry. For example, montmorillonite could be used instead of kaolin, and when paired with water with high calcium concentrations this should yield sediment with higher erosion thresholds than in this study (Section 2.3.2). If montmorillonite clays were paired with low total salinities, but high SARs, this should yield lower erosion thresholds. Alternatively, the calibration could be extended downwards by using pure clays and increased water contents to generate a fluid mud, and then altering consolidation times.

Chapter 7: Implications and future directions

Fine sediment is an important component of aquatic environments. The results of this thesis are pertinent to discussions of the stability of fine sediment in chalk streams and its effects on stream health, as well as a wider-reaching discussion on the need to quantify and model erodibility.

7.1 Stability of fine sediment deposits in chalk streams

The results of the field survey provide several important insights into the fine sediment dynamics of chalk streams. The first is an observation. Fine sediment deposits do not automatically wash away during winter high water events. Whilst this was noted by Heppell et al. (2009), the observation is worth revisiting because of its significance to sediment transport.

In this study, surficial fine sediment deposits remained stable in parts of the reach for more than a year, having survived numerous high water events capable of mobilising the gravel bed. For example, several large sediment deposits found underneath *Ranunculus* stands in the channel centre of Bere stream were documented as early as August 2007. These were well-developed stands with considerable fine sediment accumulation (> 40 cm) that were not washed away until the high water events of October/November 08 (Figs 4.31 & 4.34). In the flashier River Frome, most of the *Ranunculus* stands remained stable in size and location over the course of the study, and many had consistently deep fine sediment deposits (> 20cm deep). Sediment in the margins, though, was more prone to erosion than in the channel centres. For example, the amount of fine sediment accumulated in the margins fluctuated markedly over the year in the Bere Stream. Following the high water events in winter, bare gravel and fine

sand were visible in the margins, where previously fine silts and organic matter had accumulated. This fine material reappeared in spring with the growth of marginal macrophytes.

Why is the channel sediment more stable than the margins? Recall that sediment stability is dependent on the erodibility of the sediment and the hydrodynamic conditions. In this study, channel sediment had higher CSM-derived erosion thresholds than the margins (i.e. lower erodibility). This difference was attributed primarily to the greater effective particle sizes found in the channel sediment. Median effective particle size for the channel sediment was 205 and 155 μm for the Bere Stream and River Frome, respectively, compared to 110 and 100 μm for the margins (Figure 4.10b). The difference in erosion thresholds alone does not explain the stability of the channel deposits, as entrainment velocities for particles of these sizes (~ 0.2 m s^{-1}) are well below the velocities observed in the river channels (0.3 – >1 m s^{-1}) (Knighton 1998). In fact, sand grains could be observed moving as bedload in the stream during most visits. Therefore, the stability of the deposits is also dependent on a reduction of the erosive hydrodynamic forces, namely water velocity and turbulence.

Surficial fine sediment deposits in the channel centres of chalk streams are associated with obstructions to water flow, such as aquatic macrophyte stands, large woody debris, and uneven bed topography (Wood & Armitage 1999). In the study reaches, aquatic macrophyte stands were the principal location for fine sediment accumulation, and *Ranunculus* was the most abundant macrophyte in the channel centres. *Ranunculus* is a submerged macrophyte that forms dense stands of trailing shoots, which have been shown to significantly reduce local water velocities and turbulence (Green 2005, Cotton et al. 2006, Wharton et al. 2006). At low water velocities the plant shoots float towards the water surface, but in high flows the flexible stems are forced downward forming a flexible carpet over the sediment. The plants have shallow roots that are difficult to erode, and erosion resistance shows little seasonal variation (Haslam 2006). *Ranunculus* shoots are very tolerant of turbulence, but only moderately resistant to drag; high flows during a storm event will break the stems of the plant, but leave the roots intact. The margins are dominated by *Rorippa* in the Bere Stream, and by trailing riparian vegetation in the River Frome. *Rorippa* is a rigid-stemmed emergent macrophyte that grows preferentially in low flow environments. Stands of *Rorippa* would certainly alter water flow patterns, however they did not appear to have as significant dampening

effect on velocity as *Ranunculus* in this study (however the hydrodynamic data in this study does not allow for a formal comparison). Water was observed flowing through the more open framework of stems, except when the stands retained vegetative debris at the upstream end. The fine sediment that accumulated within these stands was easily washed out, and during the winter visits bare root networks were left uncovered by fine sediment. This suggests that *Rorippa* is less efficient at dampening flows and stabilising fine marginal sediment. Furthermore, according to Haslam (2006), *Rorippa* has shallow roots that are very easily eroded, particularly when the plant is growing in fine sediment. The plant stems are very resistant to breakage, so high water events cause whole plants to be uprooted (Haslam 2006). So, *Rorippa* does not reduce the erosive hydrodynamic forces as well as *Ranunculus*, and sediment stored within their roots is more easily washed out during high flows.

In the River Frome, whilst fine sediment accumulation in the margins fluctuated over the year, marginal locations consistently represented at least 30% of the sampling locations within the reach (Fig. 4.33). As the percent cover of *Ranunculus* did not change appreciably over the study period in this reach, the decrease in number of sampling locations in marginal locations over the autumn and winter can be interpreted as a decrease in the spatial coverage of fine sediment in the margins (Fig. 4.33). Therefore, there was a net erosion of sediment from the margins from September to November 2008, likely caused by high flow events (Fig 4.31). The removal of sediment, though, was not uniform within the margins.

Fine sediment was found in three types of marginal locations: (1) within marginal aquatic macrophytes (Marginal), (2) underneath the trailing woody stems of brambles, *Rubus* (Riparian); and (3) found in a small “backwater” cut into the left bank and protected upstream by large woody debris (Unvegetated). From September to November 2008, there was a large reduction in Marginal locations, a small reduction in Unvegetated ones, and no change in the number of Riparian ones. This means that sediment under Marginal plants was more prone to erosion than Riparian or Unvegetated locations. Two mechanisms could explain the differences in stability: (1) woody debris and riparian stems reduce hydrodynamic forces better than the herbaceous stems of aquatic macrophytes, thereby increasing sediment stability; and/or (2) hydrodynamic forces remain lower along the bank, where Riparian and Unvegetated sediments were located, than further out into the channel, where marginal sediments

were found (*ca*. 0.1 relative distance across channel; Section 4.2.3), even during high water events. More research would need to be conducted during high water events to determine how the macrophyte types impact water velocities and sediment erosion over a range of discharges. This approach would be similar to previous research on hydraulic conditions in riffle-pool sequences at low, medium and high discharges (Emery et al. 2003).

7.2 Implications for chalk stream health

Lowland chalk streams in the UK have been experiencing an increase in fine sediment deposition over recent decades. This is attributable to decreased basewater flows due to groundwater abstraction and increased allochthonous fine sediment inputs due to changes in land use practices (Walling & Amos 1999, Wood & Armitage 1999, Collins & Walling 2007b). Chalk stream ecosystems are dependent on low turbidity levels and clean gravel beds. Their low gradients, low stream powers and stable hydrographs make these systems less able to flush the sediment out, leading to significant storage in the river channels (Wharton et al. 2006, Heppell et al. 2009). Colmation of gravel beds has been shown to reduce the permeability and porosity of riverbeds, choking salmonid spawning grounds (Acornley & Sear 1999), obstructing surface-ground water exchange (Boulton et al. 1998, Packman & Salehin 2003), altering interstitial communities and affecting nutrient processing in the hyporheic (Hancock 2002, Pretty et al. 2006). The formation of surficial fine sediment has the potential to impact aquatic ecosystems (Wood & Armitage 1997), as well as contribute to the storage of contaminants, such as nutrients, pesticides, heavy metals, and pathogenic bacteria (Jarvie et al. 2005a, Luoma & Rainbow 2008, Droppo et al. 2009).

Phosphorus levels in surfaces waters have been enriched due to urbanisation and industrialised agriculture, leading to problems of eutrophication (Withers & Jarvie 2008). Whilst phosphorus loading is principally from terrestrial sources, river bed sediment can be a significant source of phosphorus to the water column, particularly when external sources have been controlled (Jarvie et al. 2005a). Dissolved phosphorus binds to fine sediment particles and associated organic matter, and deposits along with them to create stores of phosphorus that can be remobilised when the sediment is resuspended.

An increase in fine sediment deposition in gravel-bed rivers, though, does not result necessarily in an increased uptake of phosphorus from the water column. There is a balance between abiotic uptake by clays and silts, and biological uptake by hyporheic organisms in the hyporheic zone. With greater quantities of fine particles, there is a greater surface area for sorption of dissolved phosphorus (Lottig & Stanley 2007, Ryan et al. 2007). Thus, phosphorus concentrations in the water should decrease due to abiotic uptake. However, colmation of the gravel bed decreases biologically-mediated uptake because of reduced flow, altered biogeochemical conditions, and changes to hyporheic communities. So phosphorus retention in the sediment may decrease with increasing fine sediment loads.

Aquatic macrophytes play a major role in determining phosphorus dynamics within streams (Kleeberg et al. 2010). Phosphorus will accumulate within the fine sediment that collects within macrophyte stands. Some of the phosphorus will be taken up by the macrophyte roots, some will be used by microbes, and the rest stored within the fine sediment. However, the phosphorus is stored only as long as the macrophytes are physically stable in the reach. Leaf decay, breakage of the macrophytes, or erosion of the sediment will result in an export of phosphorus from the reach. If plant growth and decay is annual, then the plant stands would not decrease phosphorus loads downstream, but would simply change the dynamics of its transport. With *Ranunculus* stands showing stability for greater than a year, it is possible that they serve as a longer-term store of phosphorus.

A similar conclusion can be drawn for the importance of macrophyte stand dynamics on the storage of pesticides and heavy metals. Heppell et al. (2009) found that the fine sediment in the Bere Stream and River Frome has a high propensity to sorb organic pesticides, but there were significant intra- and inter-stream differences. Pesticide sorption was higher in the Bere Stream than the River Frome, and higher in the margins than channel in the Bere Stream, even after a correction for organic content. The results indicate that sediment in the margins of the Bere Stream would bind significantly more pesticides, 3x more, than in the margins of the River Frome. The pesticides were moderately polar, and the authors suggest that the differences in sorption coefficient were due to differences in the organic matter content or composition. Whilst the authors did not investigate pesticide concentrations in the sediment itself, it strongly suggests that the commonly-used pesticides tested in their study could be stored within fine

sediment deposits in the streams. Many studies have highlighted the importance of sediment for heavy metal storage and transport (Johnson et al. 2005, Segura et al. 2006, Luoma & Rainbow 2008, Rothwell et al. 2008), but none to my knowledge have looked at sediment within aquatic macrophyte stands. The study sites in the Frome/Piddle catchment have low levels of urbanisation and no significant industrial legacy, so heavy metals contamination is not expected. Heavy metal contents (Ca, Cu, Ni, Pb and Zn) were quantified for the thesis, but were well below the benchmarks set by US government agencies, such as the threshold effects level (TEL) (Luoma & Rainbow 2008). (Note: the UK does not have sediment quality standards). The storage of heavy metals in macrophyte stands is more likely to be a problem in urbanised rivers (Old et al. 2004, Scoles et al. 2008) or those with a history of industrial contamination (Luoma & Rainbow 2008).

7.3 Predicting erodibility

A diverse toolbox of sediment transport models has been created by government agencies and consultancies to predict the deposition and erosion of fine sediment in aquatic systems, including SEDZL/ECOMSED, EFDC, TELEMAC/SISYPHE, HSCTM (Imhoff et al. 2003). These advanced models create 3D sediment beds, often with sediment properties varying with depth, and then merge hydrodynamic and sediment transport equations to predict fine sediment transport dynamics. Many of these models have a long history of successful application, particularly SEDZL. However, all of these models share a similar limitation. They rely on at least one empirical measure of sediment erodibility to be specified by the user (Imhoff et al. 2003).

The transport models predict erosion for cohesive sediment based on one of several variants of the Ariathurai-Partheniades stress-flux equation (Eq 2.1), which is repeated here for convenience:

$$E = \alpha\left(\frac{\tau_b - \tau_c(z)}{\tau_c}\right)^{\beta} \qquad (7.1)$$

where E is the erosion rate (kg m^{-2} d^{1}), α is an empirical rate constant (kg m^{-2} d^{1} Pa^{-1}), τ_b is the shear stress applied to the sediment bed by the flowing water, $\tau_c(z)$ is a depth-

dependent critical shear stress, and β is an empirical constant (Sanford & Maa 2001, Tolhurst et al. 2009). The model can be simplified to:

$$E = M\left(\tau_b(t) - \tau_c(z)\right) \tag{7.2}$$

where α is replaced by M, β equals 1, and $\tau_{b(t)}$ is the time dependent shear stress (Winterwerp & Van Kesteren 2004, Sanford 2008).

In the thesis, erodibility was represented exclusively as $\tau_c(0)$. The CSM estimated a threshold for erosion for the surface sediment. Erosion rates were not quantified, and there was no attempt to parameterise constants in the stress-flux equations. When erosion is modelled according to equations 7.1 and 7.2, though, there are several measures of erodibility. In Eq. 7.1, sediment erodibility is represented by three parameters, α, β, and $\tau_c(z)$, whilst in Eq. 7.2, it is reduced to two parameters, M and $\tau_c(z)$. These parameters specify the critical shear stress for erosion (τ_c), which can vary over depth (z), and the relationship between excess shear stress ($\tau_b - \tau_c$) and erosion rates. They are all measures of the sediment's resistance to erosion, and are dependent on the specific sediment properties at that location (Ziegler & Nisbet 1995, Mehta & Parchure 2000, Sanford & Maa 2001, Winterwerp & Van Kesteren 2004, Sanford 2008).

Critical shear stress cannot be predicted yet for cohesive sediment, so it is either measured directly for the sediment or is assigned a representative value, for example 0.05 or 0.1 Pa (Sanford & Maa 2001). The rate constants, M or α and β, can be derived from flume erosion experiments for the specific sediment (e.g. Ziegler & Nisbet 1995), or estimated based on sediment properties (Winterwerp & Van Kesteren 2004, Sanford 2008). The use of empirical data for the model undoubtedly improves its accuracy for a specific site, but consequently the erosion predictions within the sediment transport models are specific to the tested sediment, and cannot be easily transferred to other sediments with different properties, even though they may be within the same riverine or estuarine system.

This study has demonstrated that the erodibility of fine sediment in chalk streams varies significantly within a reach over space and time. Many other studies have also noted significant variations in erodibility for riverine (e.g. Hanson & Simon 2001, McNeil &

Lick 2004) and estuarine environments (e.g. Widdows et al. 2000, Bale et al. 2006, Spears et al. 2008, Dickhudt et al. 2009). However, erodibility is typically represented as a single τ_c and/or M for a model even in large-scale sediment transport models because of the difficulty in obtaining accurate erodibility estimates (e.g. Kuhrts et al. 2004, Borsje et al. 2008). Given the high spatial and temporal variability observed in many systems, an approach is needed to predict erodibility from more easily-measured sediment properties.

In my opinion, our current inability to predict cohesive sediment erodibility is due primarily to a paucity of comparable field data over a sufficient breadth of environments, which is exacerbated by a lack of consensus on the definition and measurement of erodibility. Much of the fundamental research on cohesive sediment transport is based primarily on laboratory flume experiments (c.f. Partheniades 1971, Dade et al. 1990, Mehta & Parchure 2000). Whilst these studies have significantly advanced our understanding of cohesion and the process of erosion, the results are not directly transferable to the field. When natural sediment is used in flume experiments, the resulting erodibility measurements are often dramatically different from those measured *in situ*, even when using the same erosion device, because of changes to sediment properties during coring, transport, storage, and handling (e.g. Maa 2008). Moreover, field studies have been limited in number and scope. Most previous studies focused on individual sites, such as a single mudflat or a few point locations in a river. If we want to understand the underlying relationships between sediment properties and erodibility, we need to expand our investigations. We need a large-scale field survey of fine sediment erodibility.

7.3.1 An empirically-based approach to modelling erodibility

An empirically-based model of fine sediment erodibility could be developed using a large-scale survey of sediment and erosion characteristics from a range of aquatic environments. It would correlate critical shear stress and/or erosion rate parameters with physical, chemical and biological properties of the sediment. To be successful, the survey would need to: (1) incorporate a diversity of depositional locations (e.g. freshwater/marine, lentic/lotic, exposed/sheltered sites); (2) capture the temporal and spatial variations implicit in these locations; (3) measure the key physical, chemical and biological properties of the sediment; and (4) adhere to consistent definitions and

techniques for erosion parameter estimation and sediment property quantification. This approach is comparable to the development of the soil erodibility factor, k, for the Universal Soil Loss Equation (USLE) that predicts soil erosion based on a suite of environmental factors (e.g. rainfall intensity, land cover, topography, soil particle sizes) (Brady and Weil 2001).

The advantages of an empirically-based model are: (1) it can be developed without a clear understanding of the physics underlying the process; (2) a large dataset would be generated on natural variations in sediment properties and erodibility; and (3) the relationships between properties and erodibility would be constrained by the natural ranges in the variables and would incorporate significant covariations. With an appropriate dataset, a model could be developed easily using modern multivariate statistical techniques. These techniques can cope with covariations between explanatory and response variables and address issues of temporal or spatial dependence, particularly techniques such as regression trees, canononical correspondence analysis, and mixed effects modelling (Zuur et al. 2007, Zuur et al. 2009).

The approach has two significant limitations, however: (1) the model is only valid for the tested sediment, and (2) it does not directly incorporate a mechanistic understanding of the processes underlying erodibility. The first limitation can be easily overcome if the scale of the study is relatively limited (e.g. national-scale), in which the benefits of the model are clearly definable to funding agencies, such as contaminated sediment assessment and management. However, it should be noted that the development of the USLE spanned several decades and involved countless researchers obtaining data from over 10,000 experimental plots distributed across 49 of the 50 states in the US. Despite that effort and its wide application inside and outside of the US, the USLE is still criticized for being applicable only to temperate environments, and for its lack of inclusion of physics-based mechanisms.

An empirical model is clearly not the end goal for an erodibility model. However, it would be a promising first step. The extensive fieldwork associated with developing an empirical model will greatly advance our knowledge of sediment properties and their relationship to erodibility, which is essential in the development of a physics-based model of fine sediment erodibility. Recently, several studies have reported promising models of erodibility based on theoretical derivations of the resistive forces within the

sediment. Lick et al. (2004) developed a model of critical shear stress for silt and sand-sized particles that incorporates adhesion between surface coatings of organic colloids. Ternat et al. (2008) present a model of critical shear stress based on sediment properties that incorporate bulk density, represented as porosity, as well as the entire particle size distribution. Winterwerp and van Kesteren (2004) present a model of erosion rate M, based on bulk sediment properties. The authors of these studies report impressive fits between measured and predicted erodibility values, but the models have only been validated on very limited empirical data, typically a single set of experiments or a few sediment cores. These models are excellent advances in the field, but more empirical data are needed to be able to incorporate further key sediment properties into a physics-based model, such as water chemistry, mineralogy and EPS.

7.3.2 Gaps in knowledge

Considerable progress has been made in elucidating the sediment properties that underlie the spatial and temporal variations in erodibility observed in nature. Significant questions and gaps in knowledge remain, though, and include:

1) What are the key sediment properties affecting erodibility? Are there sediment properties that have a universal effect across all depositional locations? How do they interact in natural systems to influence erodibility?

2) How should we measure erodibility? The same sediment sample measured by different erosion devices generates different measures of erodibility (Tolhurst et al. 2000a, Widdows et al. 2007). Even when using the same device, slight differences in procedures can dramatically change interpretations. For example, Sanford and Maa (2001) argue that erosion types I (depth-limited) and II (uniform) are largely an artefact of the time steps in erosion experiments. If the change in shear stress is slow in comparison to the erosion rate, then erosion appears to be depth limited (i.e. τ_c or M increases with depth). If the change in shear stress is fast in comparison to erosion rates, then it appears to be uniform with depth (i.e. a constant τ_c or M with depth). Consequently, a consensus must be reached on procedures and interpretation for erodibility measurement if research is to be comparable.

3) How many parameters do we need to characterise erodibility? Currently, at least two erodibility parameters are used to predict erosion rates (eqs 7.1 & 7.2). However, these formulae arose as a way to describe the results of flume experiments, and may not be best suited to describe erodibility in natural sediments (Sanford & Maa 2001).

4) If we want to create an empirical model of erodibility, how do we balance accuracy with usability? For example, if the model required a dozen measurements of sediment properties, for which some require specialist laboratory equipment, then the model would not be beneficial. Users could more easily measure erodibility. Could we combine environmental descriptors with easily-measurable sediment properties?

5) Finally, if future physics-based models are to predict the erodibility of cohesive sediment caused by physical and chemical properties, how do we incorporate biology? Organisms can impact the sediment at scales greater than the particle-based theoretical models, but this can vary over space and time (e.g. Widdows et al. 2000, Le Hir et al. 2007). Perhaps these biologically-mediated aspects of sediment erodibility prediction may need to be site specific and empirically-based (Defew et al. 2002).

In conclusion, to accurately predict fine sediment transport in aquatic systems, we need to know more about erodibility. In particular, how it varies over space and time, and what sediment properties are responsible for those variations. A large-scale survey of fine sediment properties and erodibility will enable use to address those key questions and develop a preliminary empirical model of erodibility. The survey would also generate important information on sediment properties and transport dynamics relevant to researchers and managers dealing with sediment transport, contaminant transport, and aquatic ecosystem health.

Chapter 8: Conclusions

This research has produced three outcomes that will advance knowledge in the fields of sedimentology and fluvial geomorphology.

First, the field survey uncovered significant spatial and temporal variations in surface erodibility. CSM-derived erosion thresholds varied significantly by location within the channels and with macrophyte type, particularly in the Bere Stream. Sediment was more resistant to erosion in the channel centres than in the margins, and more resistant to erosion within *Ranunculus* stands than within other macrophyte types (Section 4.2.2). These spatial patterns are best explained by the preferred location of the macrophytes (e.g. channel centre vs. margin), and the greater water velocities and particle sizes found in the channel centres. As for temporal variations, mean CSM-derived erosion thresholds dropped by half over the yearlong survey from autumn 2008 until summer 2009 (Section 4.3.2). The temporal trend did not appear to be caused by macrophyte community dynamics, such as species composition, which would change the relative proportion of sediment within channel centres and margins, and was instead linked to general changes in sediment properties over the year.

Secondly, the findings highlight the importance of physical and biological sediment properties on surface erodibility. The statistical analyses identified two sediment properties, median effective particle size and chlorophyll-a content, as having significant impacts on CSM-derived erosion thresholds (Section 5.6.1). Both explanatory variables show a positive relationship with erosion threshold, which is consistent with the literature. There remained a significant temporal component, though, so a mixed effects model was used with time as a random effect to develop a model based solely on sediment properties. Given the small number of studies on riverine

sediment erodibility, these results will be a significant addition to the literature when published.

Thirdly, an empirical calibration was derived for the cohesive strength meter (CSM) (Chapter 6). The CSM is a portable device for estimating *in situ* erosion thresholds for fine sediment, however its use has been restricted to relative measurements due to a difficulty in correlating the vertical forces generated by the device to horizontal bed shear stress. The development of a calibration for the CSM benefits a wide audience, because it makes it possible to convert CSM-derived erosion thresholds to critical bed shear stress, allowing them to be incorporated into models of sediment transport. The range of erosion thresholds covered by the calibration could be widened in further laboratory studies using the described methodology, so that it can be more widely applied to CSM data.

Fine sediment deposition in chalk streams is linked to serious environmental impacts, including benthic habitat degradation and the storage of sediment-associated contaminants. By identifying the significant spatial and temporal variations in erodibility, and uncovering the significant factors underlying those variations, this study provides essential information on the stability of fine sediment deposits in chalk streams, which is a crucial step in assessing their impacts on humans and the environment.

References

Aberle J, Nikora V, Walters R (2004) Effects of bed material properties on cohesive sediment erosion. *Marine Geology* 207: 83-93.

Aberle J, Nikora V, Walters R (2006) Data interpretation for in situ measurements of cohesive sediment erosion. *Journal of Hydraulic Engineering-ASCE* 132: 581-588.

Acornley RM, Sear DA (1999) Sediment transport and siltation of brown trout (*Salmo trutta L.*) spawning gravels in chalk streams. *Hydrological Processes* 13: 447-458.

Alldredge AL, Passow U, Logan BE (1993) The abundance and significance of a class of large, transparent organic particles from the ocean. *Deep-Sea Research Pt I* 40: 1131-1140.

Amaryan LS (1993) *Soft soil properties and testing methods*, A.A. Balkema. Rotterdam, 128 pp.

Amos CL, Droppo IG, Gomez EA, Murphy TP (2003) The stability of a remediated bed in Hamilton Harbour, Lake Ontario, Canada. *Sedimentology* 50: 149-168.

Amos CL, Bergamasco A, Umgiesser G, Cappucci S, Cloutier D, DeNat L, Flindt M, Bonardi M, Cristante S (2004) The stability of tidal flats in Venice Lagoon - The results of in-situ measurements using two benthic, annular flumes. *Journal of Marine Systems* 51: 211-241.

Andersen TJ, Lund-Hansen LC, Pejrup M, Jensen KT, Mouritsen KN (2005) Biologically induced differences in erodibility and aggregation of subtidal and intertidal sediments: a possible cause for seasonal changes in sediment deposition. *Journal of Marine Systems* 55: 123-138.

Austen I, Andersen TJ, Edelvang K (1999) The influence of benthic diatoms and invertebrates on the erodibility of an intertidal a mudflat, the Danish Wadden Sea. *Estuarine Coastal and Shelf Science* 49: 99-111.

Avnimelech Y, Ritvo G, Meijer LE, Kochba M (2001) Water content, organic carbon and dry bulk density in flooded sediments. *Aquacultural Engineering* 25: 25-33.

Bale AJ, Widdows J, Harris CB, Stephens JA (2006) Measurements of the critical erosion threshold of surface sediments along the Tamar Estuary using a mini-annular flume. *Continental Shelf Research* 26: 1206-1216.

Bale AJ, Stephens JA, Harris CB (2007) Critical erosion profiles in macro-tidal estuary sediments: Implications for the stability of intertidal mud and the slope of mud banks. *Continental Shelf Research* 27: 2303-2312.

Berrie AD (1992) The chalk-stream environment. *Hydrobiologia* 248: 3-9.

Bickerton M, Petts G, Armitage P, Castella E (1993) Assessing the ecological effects of groundwater abstraction on chalk streams - 3 examples from eastern England. *Regulated Rivers-Research & Management* 8: 121-134.

Black KS, Tolhurst TJ, Paterson DM, Hagerthey SE (2002) Working with natural cohesive sediments. *Journal of Hydraulic Engineering-ASCE* 128: 2-8.

Blott SJ, Pye K (2001) GRADISTAT: A grain size distribution and statistics package for the analysis of unconsolidated sediments. *Earth Surface Processes and Landforms* 26: 1237-1248.

Bohling B (2009) Measurements of threshold values for incipient motion of sediment particles with two different erosion devices. *Journal of Marine Systems* 75: 330-335.

Borsje BW, de Vries MB, Hulscher SJMH, de Boer GJ (2008) Modeling large-scale cohesive sediment transport affected by small-scale biological activity. Estuarine Coastal and Shelf Science 78: 468-480

Boulton AJ, Findlay S, Marmonier P, Stanley EH, Valett HM (1998) The functional significance of the hyporheic zone in streams and rivers. *Annual Review of Ecology and Systematics* 29: 59-81.

Bouma TJ, De Vries MB, Low E, Peralta G, Tanczos C, Van de Koppel J, Herman PMJ (2005) Trade-offs related to ecosystem engineering: A case study on stiffness of emerging macrophytes. *Ecology* 86: 2187-2199.

Bouma TJ, van Duren LA, Temmerman S, Claverie T, Blanco-Garcia A, Ysebaert T, Herman PMJ (2007) Spatial flow and sedimentation patterns within patches of

epibenthic structures: Combining field, flume and modelling experiments. *Continental Shelf Research* 27: 1020-1045.

Bowes MJ, Leach DV, House WA (2005) Seasonal nutrient dynamics in a chalk stream: the River Frome, Dorset, UK. *Science of the Total Environment* 336: 225-241.

Brady NC, Weil RR (2001) *The nature and properties of soils*, Prentice Hall, Upper Saddle River, N.J. 960 pp.

Casey H, Newton PVR (1973) The chemical composition and flow of the River Frome and its main tributaries. *Freshwater Biology* 3: 317-333.

Chiovitti A, Molino P, Crawford SA, Teng RW, Spurck T, Wetherbee R (2004) The glucans extracted with warm water from diatoms are mainly derived from intracellular chrysolaminaran and not extracellular polysaccharides. European *Journal of Phycology* 39: 117-128.

Clarke SJ (2002) Vegetation growth in rivers: influences upon sediment and nutrient dynamics. *Progress in Physical Geography* 26: 159-172.

Clarke SJ, Wharton G, Cotton JA (2006) Spatial and temporal variations in the sediment habitat of *Ranunculus spp.* in lowland chalk streams - implications for ecological status? *Water, Air and Soil Pollution: Focus* 6: 393-401.

Collins AL, Walling DE (2007a) Fine-grained bed sediment storage within the main channel systems of the Frome and Piddle catchments, Dorset, UK. *Hydrological Processes* 21: 1448-1459.

Collins AL, Walling DE (2007b) The storage and provenance of fine sediment on the channel bed of two contrasting lowland permeable catchments, UK. *River Research and Applications* 23: 429-450.

Cotton JA, Wharton G, Bass JAB, Heppell CM, Wotton RS (2006) The effects of seasonal changes to in-stream vegetation cover on patterns of flow and accumulation of sediment. *Geomorphology* 77: 320-334.

Crawley MJ (2007) *The R book*, Wiley, Chichester. 942 pp.

Crooks S, Pye K (2000) Sedimentological controls on the erosion and morphology of saltmarshes: implications for flood defence and habitat recreation. In: Pye K, Allen JRL (eds) *Coastal and estuarine environments: sedimentology, geomorphology and geoarchaeology*. Geological Society, Bath, p 20-222.

Dade WB, Davis JD, Nichols PD, Nowell ARM, Thistle D, Trexler MB, White DC (1990) Effects of bacterial exopolymer adhesion on the entrainment of sand. *Geomicrobiology Journal* 8: 1-16.

Dade WB, Nowell ARM, Jumars PA (1992) Predicting erosion resistance of muds. *Marine Geology* 105: 285-297.

de Brouwer JFC, Bjelic S, de Deckere E, Stal LJ (2000) Interplay between biology and sedimentology in a mudflat (Biezelingse Ham, Westerschelde, The Netherlands). *Continental Shelf Research* 20: 1159-1177.

de Brouwer JFC, Stal LJ (2001) Short-term dynamics in microphytobenthos distribution and associated extracellular carbohydrates in surface sediments of an intertidal mudflat. *Marine Ecology-Progress Series* 218: 33-44.

de Brouwer JFC, Wolfstein K, Stal LJ (2002) Physical characterization and diel dynamics of different fractions of extracellular polysaccharides in an axenic culture of a benthic diatom. *European Journal of Phycology* 37: 37-44.

de Kerchove AJ, Elimelech M (2006) Structural growth and viscoelastic properties of adsorbed alginate layers in monovalent and divalent salts. *Macromolecules* 39: 6558-6564.

Debnath K, Nikora V, Aberle J, Westrich B, Muste M (2007) Erosion of cohesive sediments: Resuspension, bed load, and erosion patterns from field experiments. *Journal of Hydraulic Engineering-ASCE* 133: 508-520.

Decho AW (2000) Microbial biofilms in intertidal systems: an overview. *Continental Shelf Research* 20: 1257-1273.

Decho AW, Moriarty DJW (1990) Bacterial exopolymer utilization by a harpacticoid copepod - A methodology and results. *Limnology and Oceanography* 35: 1039-1049.

Decho AW, Lopez GR (1993) Exopolymer microenvironments of microbial-flora - Multiple and interactive effects on trophic relationships. *Limnology and Oceanography* 38:1633-1645.

Defew EC, Tolhurst TJ, Paterson DM (2002) Site-specific features influence sediment stability of intertidal flats. *Hydrology and Earth System Sciences* 6: 971-981.

Dickhudt PJ, Friedrichs CT, Schaffner LC, Sanford LP (2009) Spatial and temporal variation in cohesive sediment erodibility in the York River estuary, eastern USA: A biologically influenced equilibrium modified by seasonal deposition. *Marine Geology* 267: 128-140.

Droppo IG (2001) Rethinking what constitutes suspended sediment. *Hydrological Processes* 15: 1551-1564.

Droppo IG, Leppard GG, Flannigan DT, Liss SN (1997) The freshwater floc: A functional relationship of water and organic and inorganic floc constituents

affecting suspended sediment properties. *Water Air and Soil Pollution* 99: 43-53.

Droppo IG, Lau YL, Mitchell C (2001) The effect of depositional history on contaminated bed sediment stability. *Science of the Total Environment* 266: 7-13.

Droppo IG, Jaskot C, Nelson T, Milne J, Charlton M (2007a) Aquaculture waste sediment stability: Implications for waste migration. *Water Air and Soil Pollution* 183: 59-68.

Droppo IG, Ross N, Skafel M, Liss SN (2007b) Biostabilization of cohesive sediment beds in a freshwater wave-dominated environment. *Limnology and Oceanography* 52: 577-589.

Droppo IG, Exall K, Stafford K (2008) Effects of chemical amendments on aquatic floc structure, settling and strength. *Water Research* 42: 169-179.

Droppo IG, Liss SN, Williams D, Nelson T, Jaskot C, Trapp B (2009) Dynamic existence of waterborne pathogens within river sediment compartments. Implications for Water Quality Regulatory Affairs. *Environmental Science & Technology* 43: 1737-1743.

Dytham C (2003) *Choosing and using statistics: a biologist's guide*, Blackwell, Malden, MA. 248 pp.

Environment Agency (2004) The state of England's chalk rivers, Environment Agency (UK), UK Biodiversity Action Plan Steering Group for Chalk Rivers, Bristol.

El Ganaoui O, Schaaff E, Boyer P, Amielh M, Anselmet F, Grenz C (2007) Erosion of the upper layer of cohesive sediments: Characterization of some properties. *Journal of Hydraulic Engineering-ASCE* 133: 1087-1091.

Emery JC, Gurnell AM, Clifford NJ, Petts GE, Morrissey IP, Soar PJ (2003) Classifying the hydraulic performance of riffle-pool bedforms for habitat assessment and river rehabilitation design. *River Research and Applications* 19: 533-549.

European Parliament (2000) Directive 2000/60/EC of the European Parliament and of the Council of 23 October 2000: Establishing a framework for Community action in the field of water policy, OJ L 327, 22.12.2000.

Fernandes S, Sobral P, Alcantara F (2009) *Nereis diversicolor* and copper contamination effect on the erosion of cohesive sediments: A flume experiment. *Estuarine Coastal and Shelf Science* 82: 443-451.

Flemming HC, Wingender J (2001) Relevance of microbial extracellular polymeric substances (EPSs) - Part I: Structural and ecological aspects. *Water Science and Technology* 43: 1-8.

Flemming HC, Wingender J (2010) The biofilm matrix. *Nature Reviews Microbiology* 8: 623-633.

Flynn NJ, Snook DL, Wade AJ, Jarvie HP (2002) Macrophyte and periphyton dynamics in a UK Cretaceous chalk stream: the River Kennet, a tributary of the Thames. *Science of the Total Environment* 282: 143-157.

Forstner U, Wittmann GTW (1981) *Metal pollution in the aquatic environment*, Springer, Berlin, 486 pp.

Fox J (2002) *An R and S-Plus companion to applied regression*, Sage, London, 311 pp

Friend PL, Ciavola P, Cappucci S, Santos R (2003) Bio-dependent bed parameters as a proxy tool for sediment stability in mixed habitat intertidal areas. *Continental Shelf Research* 23: 1899-1917.

Friend PL, Lucas CH, Rossington SK (2005) Day-night variation of cohesive sediment stability. *Estuarine Coastal and Shelf Science* 64: 407-418.

Frølund B, Palmgren R, Keiding K, Halkejaer Nielsen P (1996) Extraction of extracellular polymers from activated sludge using a cation exchange resin. *Water Research* 30: 1749-1758.

Gacia E, Granata TC, Duarte CM (1999) An approach to measurement of particle flux and sediment retention within seagrass (*Posidonia oceanica*) meadows. *Aquatic Botany* 65: 255-268.

Gebert J, Kothe H, Grongroft A (2006) Prognosis of methane formation by river sediments. *Journal of Soils and Sediments* 6: 75-83.

Gerbersdorf SU, Jancke T, Westrich B (2005) Physico-chemical and biological sediment properties determining erosion resistance of contaminated riverine sediments - Temporal and vertical pattern at the Lauffen reservoir/River Neckar, Germany. *Limnologica* 35: 132-144.

Gerbersdorf SU, Jancke T, Westrich B (2007) Sediment properties for assessing the erosion risk of contaminated riverine sites. *Journal of Soils and Sediments* 7: 25-35.

Gerbersdorf SU, Jancke T, Westrich B, Paterson DM (2008a) Microbial stabilization of riverine sediments by extracellular polymeric substances. *Geobiology* 6: 57-69.

Gerbersdorf SU, Manz W, Paterson DM (2008b) The engineering potential of natural benthic bacterial assemblages in terms of the erosion resistance of sediments. *FEMS Microbiology Ecology* 66: 282-294.

Gerbersdorf SU, Westrich B, Paterson DM (2009) Microbial extracellular polymeric substances (EPS) in fresh water sediments. *Microbial Ecology* 58: 334-349.

Gillott JE (1987) *Clay in engineering geology*, Developments in Geotechnial Engineering, Vol. 41. Elsevier, Oxford, 468 pp.

Gordon ND, McMahon TA, Finlayson BL (2004) *Stream hydrology: an introduction for ecologists*, Wiley, Chichester, 429 pp.

Gotelli NJ, Ellison AM (2004) *A primer of ecological statistics*, Sinauer, Sunderland, MA. 510 pp.

Goudie A, Lewin J (1990) *Geomorphological techniques*, Unwin Hyman, 592 pp.

Grabowski RC, Droppo IG, Wharton G (*In Press*) Estimation of critical shear stress from cohesive strength meter-derived erosion thresholds. *Limnology and Oceanography-Methods*

Grabowski RC, Droppo IG, Wharton G (*In Revision*) Erodibility of cohesive sediment: the importance of sediment properties. *Earth Science Reviews*

Green JC (2005) Velocity and turbulence distribution around lotic macrophytes. *Aquatic Ecology* 39: 1-10.

Griffiths J, Binley A, Crook N, Nutter J, Young A, Fletcher S (2006) Streamflow generation in the Pang and Lambourn catchments, Berkshire, UK. *Journal of Hydrology* 330: 71-83.

Grim R (1962) *Applied clay mineralogy*, McGraw-Hill, London, 422 pp.

Gurnell AM, Piegay H, Swanson FJ, Gregory SV (2002) Large wood and fluvial processes. *Freshwater Biology* 47: 601-619.

Gurnell AM, van Oosterhout MP, de Vlieger B, Goodson JM (2006) Reach-scale interactions between aquatic plants and physical habitat: River Frome, Dorset. *River Research and Applications* 22: 667-680.

Gurr E (1960) *Encyclopaedia of microscopic stains*, Leonard Hill, London

Gyssels G, Poesen J, Bochet E, Li Y (2005) Impact of plant roots on the resistance of soils to erosion by water: a review. *Progress in Physical Geography* 29: 189-217.

Hancock PJ (2002) Human impacts on the stream-groundwater exchange zone. *Environmental Management* 29: 763-781.

Hanson GJ, Simon A (2001) Erodibility of cohesive streambeds in the loess area of the Midwestern USA. *Hydrological Processes* 15: 23-38.

Haslam SM (2006) *River plants: the macrophytic vegetation of watercourses*, Cambridge University Press, Cambridge, 450 pp.

Heiri O, Lotter AF, Lemcke G (2001) Loss on ignition as a method for estimating organic and carbonate content in sediments: reproducibility and comparability of results. *Journal of Paleolimnology* 25: 101-110.

Heppell CM, Wharton G, Cotton JAC, Bass JAB, Roberts SE (2009) Sediment storage in the shallow hyporheic of lowland vegetated river reaches. *Hydrological Processes* 23: 2239-2251.

Heywood MJT, Walling DE (2003) Suspended sediment fluxes in chalk streams in the Hampshire Avon catchment, UK. *Hydrobiologia* 494: 111-117.

Hillel D (1982) *Introduction to soil physics*, Academic, London, 364 pp.

Horvath TG (2004) Retention of particulate matter by macrophytes in a first-order stream. *Aquatic Botany* 78:27-36.

Houwing EJ (1999) Determination of the critical erosion threshold of cohesive sediments on intertidal mudflats along the Dutch Wadden Sea Coast. *Estuarine Coastal and Shelf Science* 49: 545-555.

Imhoff JC, Stoddard A, Buchak EM (2003) Evaluation of the contaminated sediment fate and transport models. Report No. EPA/68/C-01/037, National Exposure Research Laboratory, US EPA, Washington, DC.

James WF, Barko JW, Butler MG (2004) Shear stress and sediment resuspension in relation to submersed macrophyte biomass. *Hydrobiologia* 515: 181-191.

Jarvie HP, Jurgens MD, Williams RJ, Neal C, Davies JJL, Barrett C, White J (2005a) Role of river bed sediments as sources and sinks of phosphorus across two major eutrophic UK river basins: the Hampshire Avon and Herefordshire Wye. *Journal of Hydrology* 304: 51-74.

Jarvie HP, Neal C, Withers PJA, Wescott C, Acornley RA (2005b) Nutrient hydrochemistry for a groundwater-dominated patchment: The Hampshire Avon, UK. *Science of the Total Environment* 344: 143-158.

Jepsen R, Roberts J, Lick W (1997) Effects of bulk density on sediment erosion rates. *Water Air and Soil Pollution* 99: 21-31.

Jepsen R, McNeil J, Lick W (2000) Effects of gas generation on the density and erosion of sediments from the Grand River. *Journal of Great Lakes Research* 26: 209-219.

Johnson BD, Kranck K, Muschenheim DK (1994) Physicochemical factors in particle aggregation. In: Wotton RS (ed) *The biology of particles in aquatic systems*. Lewis, London, p 75-96.

Johnson VG, Peterson RE, Olsen KB (2005) Heavy metal transport and behavior in the lower Columbia River, USA. *Environmental Monitoring and Assessment* 110: 271-289.

Joyce P, Warren LL, Wotton RS (2007) Faecal pellets in streams: their binding, breakdown and utilization. *Freshwater Biology* 52: 1868-1880.

Kandiah, A (1974) Fundamental aspects of surface erosion of cohesive soils. PhD Thesis, University of California, Davis. cited in Winterwerp and van Kesteren (2004) Winterwerp JC, Van Kesteren WGM (2004) *Introduction to the physics of cohesive sediment in the marine environment*, Elsevier, Amsterdam, 466 pp.

Keedwell MJ (1984) *Rheology and soil mechanics*, Elsevier Applied Science, London, 323 pp.

Kleeberg A, Kohler J, Sukhodolova T, Sukhodolov A (2010) Effects of aquatic macrophytes on organic matter deposition, resuspension and phosphorus entrainment in a lowland river. *Freshwater Biology* 55: 326-345.

Knighton D (1998) *Fluvial forms and processes: a new perspective*, Arnold, London, 383 pp.

Korstgens V, Flemming HC, Wingender J, Borchard W (2001) Influence of calcium ions on the mechanical properties of a model biofilm of mucoid Pseudomonas aeruginosa. *Water Science and Technology* 43: 49-57.

Kuhrts C, Fennel W, Seifert T (2004) Model studies of transport of sedimentary material in the western Baltic. *Journal of Marine Systems* 52: 167-190.

Lau YL, Droppo IG (2000) Influence of antecedent conditions on critical shear stress of bed sediments. *Water Research* 34: 663-667.

Le Hir P, Monbet Y, Orvain F (2007) Sediment erodability in sediment transport modelling: Can we account for biota effects? *Continental Shelf Research* 27: 1116-1142.

Leeder MR (1999) *Sedimentology and sedimentary basins: from turbulence to tectonics*, Blackwell, Oxford, 592 pp.

Lick W, McNeil J (2001) Effects of sediment bulk properties on erosion rates. *Science of the Total Environment* 266:41-48.

Lick W, Jin LJ, Gailani J (2004) Initiation of movement of quartz particles. *Journal of Hydraulic Engineering-ASCE* 130:755-761.

Liu H, Fang HHP (2002) Extraction of extracellular polymeric substances (EPS) of sludges. *Journal of Biotechnology* 95: 249-256.

Logan BE, Grossart HP, Simon M (1994) Direct observations of phytoplankton, TEP and aggregates on polycarbonate filters using brightfield microscopy. *Journal of Plankton Research* 16: 1811-1815.

Loring DH (1991) Normalisation of heavy-metal data from estuarine and coastal sediments. *ICES Journal of Marine Science* 48: 101-115.

Lottig NR, Stanley EH (2007) Benthic sediment influence on dissolved phosphorus concentrations in a headwater stream. *Biogeochemistry* 84: 297-309.

Luhar M, Rominger J, Nepf H (2008) Interaction between flow, transport and vegetation spatial structure. *Environmental Fluid Mechanics* 8: 423-439.

Lundkvist M, Grue M, Friend PL, Flindt MR (2007) The relative contributions of physical and microbiological factors to cohesive sediment stability. *Continental Shelf Research* 27: 1143-1152.

Luoma SN, Rainbow PS (2008) *Metal contamination in aquatic environments: science and lateral management*, Cambridge University Press, Cambridge, 573 pp.

Maa JPY (2008) Sediment erosion characteristics in the Anacostia River. *Journal of Hydraulic Engineering-ASCE* 134: 1102-1109.

Madsen JD, Chambers PA, James WF, Koch EW, Westlake DF (2001) The interaction between water movement, sediment dynamics and submersed macrophytes. *Hydrobiologia* 444:71-84.

Madsen TV, Warncke E (1983) Velocities of currents around and within submerged aquatic vegetation. *Archiv Fur Hydrobiologie* 97: 389-394.

Marshall EJP, Westlake DF (1990) Water velocities around water plants in chalk streams. *Folia Geobotanica et Phytotaxonomica* 25:279-289.

Mazik K, Elliott M (2000) The effects of chemical pollution on the bioturbation potential of estuarine intertidal mudflats. *Helgoland Marine Research* 54: 99-109.

McNeil J, Taylor C, Lick W (1996) Measurements of erosion of undisturbed bottom sediments with depth. *Journal of Hydraulic Engineering-ASCE* 122: 316-324.

McNeil J, Lick W (2004) Erosion rates and bulk properties of sediments from the Kalamazoo River. *Journal of Great Lakes Research* 30: 407-418.

Mehta AJ, Hayter EJ, Parker WR, Krone RB, Teeter AM (1989a) Cohesive sediment transport .1. Process description. *Journal of Hydraulic Engineering-ASCE* 115: 1076-1093.

Mehta AJ, Mcanally WH, Hayter EJ, Teeter AM, Schoellhamer D, Heltzel SB, Carey WP (1989b) Cohesive Sediment Transport .2. Application. *Journal of Hydraulic Engineering-ASCE* 115: 1094-1112.

Mehta AJ, Parchure TM (2000) Surface erosion of fine-grained sediment revisited. In: Flemming BW, Delafontaine MT, Liebezeit G (eds) *Muddy coast dynamics and resource management*. Proceedings in Marine Sciences, Vol. 2, Elsevier, London, p 55-74.

Mitchener H, Torfs H (1996) Erosion of mud/sand mixtures. *Coastal Engineering* 29: 1-25.

Mohle RB, Langemann T, Haesner M, Augustin W, Scholl S, Neu TR, Hempel DC, Horn H (2007) Structure and shear strength of microbial biofilms as determined with confocal laser scanning microscopy and fluid dynamic gauging using a novel rotating disc biofilm reactor. *Biotechnology and Bioengineering* 98: 747-755.

Morgan RPC (2005) *Soil erosion and conservation*, Blackwell, Oxford, 304 pp.

Morgan RPC, Rickson RJ (1995) *Slope stabilization and erosion control: a bioengineering approach*, Taylor & Francis, London, 274 pp.

Neu TR, Manz B, Volke F, Dynes JJ, Hitchcock AP, Lawrence JR (2010) Advanced imaging techniques for assessment of structure, composition and function in biofilm systems. *FEMS Microbiology Ecology* 72: 1-21.

Neumeier U, Ciavola P (2004) Flow resistance and associated sedimentary processes in a Spartina maritima salt-marsh. *Journal of Coastal Research* 20: 435-447.

Nielsen PH, Jahn A (1999) Extraction of EPS. In: Wingender J, Neu TR, Flemming H-C (eds) *Microbial extracellular polymeric substances: characterization, structure, and function*. Springer, New York p 49-72.

Old GH, Leeks GJL, Packman JC, Stokes N, Williams ND, Smith BPG, Hewitt EJ, Lewis S (2004) Dynamics of sediment-associated metals in a highly urbanised catchment: Bradford, West Yorkshire. *Water and Environment Journal* 18: 11-16.

Orvain F, Galois R, Barnard C, Sylvestre A, Blanchard G, Sauriau PG (2003) Carbohydrate production in relation to microphytobenthic biofilm development: An integrated approach in a tidal mesocosm. *Microbial Ecology* 45: 237-251.

Orvain F, Sauriau PG, Le Hir P, Guillou G, Cann P, Paillard M (2007) Spatio-temporal variations in intertidal mudflat erodability: Marennes-Oleron Bay, western France. *Continental Shelf Research* 27: 1153-1173.

Packman AI, Salehin M (2003) Relative roles of stream flow and sedimentary conditions in controlling hyporheic exchange. *Hydrobiologia* 494: 291-297.

Pamp SJ, Gjermansen M, Tolker-Nielsen T (2007) The biofilm matrix: a sticky framework. In: Kjelleberg S, Givskov M (eds) *The biofilm mode of life: mechanisms and adaptations*. Horizon Bioscience, Wymondham, p 248-244.

Panagiotopoulos I, Voulgaris G, Collins MB (1997) The influence of clay on the threshold of movement of fine sandy beds. *Coastal Engineering* 32: 19-43.

Partheniades E (1971) Erosion and deposition of cohesive materials. In: Shen HW (ed) *River Mechanics*, Vol 2. The editor, Fort Collins, CO, USA. p 25.1-91.

Partheniades E (2007) *Engineering properties and hydraulic behavior of cohesive sediments*, CRC, London, 338 pp

Passow U (2002) Transparent exopolymer particles (TEP) in aquatic environments. *Progress in Oceanography* 55:287-333.

Paterson DM (1989) Short-term changes in the erodibility of intertidal cohesive sediments related to the migratory behavior of epipelic diatoms. *Limnology and Oceanography* 34: 223-234.

Paterson DM (1997) Biological mediation of sediment erodibility, ecology and physical dynamics. In: Burt N, Parker R, Watts J (eds) *Cohesive sediments*. Wiley Interscience, Chichester, p 215-229.

Paterson DM, Black KS (2000) Temporal variability in the critical erosion threshold of saltmarsh and upper intertidal sediments. In: Sherwood BR, Gardiner BG, Harris T (eds) *British Saltmarshes*. Linnaen Society of London, Cardigan, UK, p 51-63.

Perkins RG, Paterson DM, Sun H, Watson J, Player MA (2004) Extracellular polymeric substances: quantification and use in erosion experiments. *Continental Shelf Research* 24: 1623-1635.

Pretty JL, Hildrew AG, Trimmer M (2006) Nutrient dynamics in relation to surface-subsurface hydrological exchange in a groundwater fed chalk stream. *Journal of Hydrology* 330: 84-100.

Pye K (1994) *Sediment transport and depositional processes*, Blackwell Scientific, Oxford, 397 pp.

Quinn GP, Keough MJ (2002) *Experimental design and data analysis for biologists*, Cambridge University Press, Cambridge, 537 pp.

R Core Development Team (2009) R: A language and environment for statistical computing. R Foundation for Statistical Computing. Vienna, Austria. ISBN 3-900051-07-0, URL http://www.R-project.org.

Ravisangar V, Sturm TW, Amirtharajah A (2005) Influence of sediment structure on erosional strength and density of kaolinite sediment beds. *Journal of Hydraulic Engineering-ASCE* 131: 356-365.

Righetti M, Lucarelli C (2007) May the Shields theory be extended to cohesive and adhesive benthic sediments? *Journal of Geophysical Research-Oceans* 112: C05039, doi:10.1029/2006JC003669.

Roberts J, Jepsen R, Gotthard D, Lick W (1998) Effects of particle size and bulk density on erosion of quartz particles. *Journal of Hydraulic Engineering-ASCE* 124: 1261-1267.

Rothwell JJ, Evans MG, Allott TEH (2008) In-stream processing of sediment-associated metals in peatland fluvial systems. *Water Air and Soil Pollution* 187: 53-64.

Rowell DL (1994) *Soil science: methods and applications*, Wiley, Harlow, Essex, 350 pp.

Ryan RJ, Packman AI, Kilham SS (2007) Relating phosphorus uptake to changes in transient storage and streambed sediment characteristics in headwater tributaries of Valley Creek, an urbanizing watershed. *Journal of Hydrology* 336: 444-457.

Sand-Jensen K (1998) Influence of submerged macrophytes on sediment composition and near-bed flow in lowland streams. *Freshwater Biology* 39: 663-679.

Sand-Jensen K, Mebus JR (1996) Fine-scale patterns of water velocity within macrophyte patches in streams. *Oikos* 76: 169-180.

Sand-Jensen K, Pedersen O (1999) Velocity gradients and turbulence around macrophyte stands in streams. *Freshwater Biology* 42: 315-328.

Sanders IA (2006) The source, transformation and fate of particulate organic matter in stands of the aquatic macrophyte *Ranunculus spp*., PhD Thesis, Queen Mary, University of London

Sanders IA, Heppell CM, Cotton JA, Wharton G, Hildrew AG, Flowers EJ, Trimmer M (2007) Emission of methane from chalk streams has potential implications for agricultural practices. *Freshwater Biology* 52: 1176-1186.

Sanford LP (2008) Modeling a dynamically varying mixed sediment bed with erosion, deposition, bioturbation, consolidation, and armoring. *Computers and Geosciences* 34: 1263-1283.

Sanford LP, Maa JPY (2001) A unified erosion formulation for fine sediments. *Marine Geology* 179: 9-23.

Scoles L, Faulkner H, Tapsell S, Downward s (2008) Urban rivers as pollutant sinks and sources: a public health concern for recreational river users. *Water Air and Soil Pollution: Focus* 8: 543-553.

Sear DA, Armitage PD, Dawson FH (1999) Groundwater dominated rivers. *Hydrological Processes* 13: 255-276.

Segura R, Arancibia V, Zuniga MC, Pasten P (2006) Distribution of copper, zinc, lead and cadmium concentrations in stream sediments from the Mapocho River in Santiago, Chile. *Journal of Geochemical Exploration* 91: 71-80.

Serota S, Jangle A (1972) Direct-Reading Pocket Shear Vane. *Journal of Civil Engineering - ASCE* 42: 73-74.

Simon A, Collison AJC (2001) Pore-water pressure effects on the detachment of cohesive streambeds: Seepage forces and matric suction. *Earth Surface Processes and Landforms* 26: 1421-1442.

Simon A, Pollen N, Langendoen E (2006) Influence of two woody riparian species on critical conditions for streambank stability: Upper Truckee River, California. *Journal of American Water Resources Association* 42: 99-113.

Simon M, Grossart HP, Schweitzer B, Ploug H (2002) Microbial ecology of organic aggregates in aquatic ecosystems. Aquatic Microbial Ecology 28:175-211

Smith BPG, Naden PS, Leeks GJL, Wass PD (2003) The influence of storm events on fine sediment transport, erosion and deposition within a reach of the River Swale, Yorkshire, UK. *Science of the Total Environment* 314: 451-474.

Spears BM, Saunders JE, Davidson I, Paterson DM (2008) Microalgal sediment biostabilisation along a salinity gradient in the Eden Estuary, Scotland: unravelling a paradox. *Marine and Freshwater Research* 59: 313-321.

Stoodley P, Jacobsen A, Dunsmore BC, Purevdorj B, Wilson S, Lappin-Scott HM, Costerton JW (2001) The influence of fluid shear and AlCl3 on the material properties of *Pseudomonas aeruginosa* PAO1 and *Desulfovibrio sp.* EX265 biofilms. *Water Science and Technology* 43: 113-120.

Sutherland IW (2001) Exopolysaccharides in biofilms, flocs and related structures. *Water Science and Technology* 43: 77-86.

Sutherland TF, Amos CL, Grant J (1998a) The effect of buoyant biofilms on the erodibility of sublittoral sediments of a temperate microtidal estuary. *Limnology and Oceanography* 43: 225-235.

Sutherland TF, Grant J, Amos CL (1998b) The effect of carbohydrate production by the diatom *Nitzschia curvilineata* on the erodibility of sediment. *Limnology and Oceanography* 43: 65-72.

Ternat F, Boyer P, Anselmet F, Amielh M (2008) Erosion threshold of saturated natural cohesive sediments: Modeling and experiments. *Water Resource Research* 44: W11434, doi:10.1029/2007WR006537.

Thomsen L, Gust G (2000) Sediment erosion thresholds and characteristics of resuspended aggregates on the western European continental margin. *Deep-Sea Research Pt I* 47: 1881-1897.

Thornton DCO, Fejes EM, DiMarco SF, Clancy KM (2007) Measurement of acid polysaccharides in marine and freshwater samples using alcian blue. *Limnology and Oceanography-Methods* 5: 73-87.

Tipping E, Rieuwerts J, Pan G, Ashmore MR, Lofts S, Hill MTR, Farago ME, Thornton I (2003) The solid-solution partitioning of heavy metals (Cu, Zn, Cd, Pb) in upland soils of England and Wales. *Environmental Pollution* 125: 213-225.

Tolhurst TJ, Black KS, Shayler SA, Mather S, Black I, Baker K, Paterson DM (1999) Measuring the in situ erosion shear stress of intertidal sediments with the Cohesive Strength Meter (CSM). *Estuarine Coastal and Shelf Science* 49: 281-294.

Tolhurst TJ, Black KS, Paterson DM, Mitchener HJ, Termaat GR, Shayler SA (2000a) A comparison and measurement standardisation of four in situ devices for determining the erosion shear stress of intertidal sediments. *Continental Shelf Research* 20: 1397-1418.

Tolhurst TJ, Gust G, Paterson DM (2000b) The influence of an extracellular polymeric substance (EPS) on cohesive sediment stability. In: Winterwerp JC, Kranenburg C (eds) *Fine sediment dynamics in the marine environment*. Proceedings in Marine Science, Vol. 5, Elsevier p 409-425.

Tolhurst TJ, Riethmuller R, Paterson DM (2000c) In situ versus laboratory analysis of sediment stability from intertidal mudflats. *Continental Shelf Research* 20: 1317-1334.

Tolhurst TJ, Jesus B, Brotas V, Paterson DM (2003) Diatom migration and sediment armouring - an example from the Tagus Estuary, Portugal. *Hydrobiologia* 503: 183-193.

Tolhurst TJ, Friend PL, Watts C, Wakefield R, Black KS, Paterson DM (2006) The effects of rain on the erosion threshold of intertidal cohesive sediments. *Aquatic Ecology* 40: 533-541.

Tolhurst TJ, Consalvey M, Paterson DM (2008) Changes in cohesive sediment properties associated with the growth of a diatom biofilm. *Hydrobiologia* 596: 225-239.

Tolhurst TJ, Black KS, Paterson DM (2009) Muddy Sediment Erosion: Insights from Field Studies. *Journal of Hydraulic Engineering-ASCE* 135: 73-87.

Torfs H (1995) Erosion of mud/sand mixtures. PhD Thesis. Catholieke Universiteit Leuven.

Underwood GJC, Paterson DM, Parkes RJ (1995) The measurement of microbial carbohydrate exopolymers from intertidal sediments. *Limnology and Oceanography* 40: 1243-1253.

USEPA (1997) In vitro determination of cholorphylls a, b, c1, c2 and pheopigments in marine and freshwater algae by visible spectrophotometry. National Exposure Research Laboratory, Office of Research and Development, US EPA, Cincinnati, Ohio, USA.

van Ledden M, van Kesteren WGM, Winterwerp JC (2004) A conceptual framework for the erosion behaviour of sand-mud mixtures. *Continental Shelf Research* 24: 1-11.

Vardy S, Saunders JE, Tolhurst TJ, Davies PA, Paterson DM (2007) Calibration of the high-pressure cohesive strength meter (CSM). *Continental Shelf Research* 27: 1190-1199.

Verdugo P, Alldredge AL, Azam F, Kirchman DL, Passow U, Santschi PH (2004) The oceanic gel phase: a bridge in the DOM-POM continuum. *Marine Chemistry* 92: 67-85.

Waite S (2000) *Statistical ecology in practice: a guide to analysing environmental and ecological field data*, Prentice Hall, Harlow, 414 pp.

Walling DE, Amos CM (1999) Source, storage and mobilisation of fine sediment in a chalk stream system. *Hydrological Processes* 13: 323-340.

Watts CW, Tolhurst TJ, Black KS, Whitmore AP (2003) In situ measurements of erosion shear stress and geotechnical shear strength of the intertidal sediments of the experimental managed realignment scheme at Tollesbury, Essex, UK. *Estuarine Coastal and Shelf Science* 58: 611-620.

Wetzel RG (2001) *Limnology: lake and river ecosystems*, Academic, London, 1006 pp.

Wharton G, Cotton JA, Wotton RS, Bass JAB, Heppell CM, Trimmer M, Sanders IA, Warren LL (2006) Macrophytes and suspension-feeding invertebrates modify flows and fine sediments in the Frome and Piddle catchments, Dorset (UK). *Journal of Hydrology* 330: 171-184.

Wheater HS, Peach D (2004) Developing interdisciplinary science for integrated catchment management: The UK LOwland CAtchment Research (LOCAR) Programme. *International Journal of Water Resources Development* 20: 369-385.

Whitlow R (1995*) Basic soil mechanics*, Longman Scientific & Technical, Harlow, 559 pp.

Widdows J, Brinsley MD, Bowley N, Barrett C (1998) A benthic annular flume for in situ measurement of suspension feeding/biodeposition rates and erosion potential of intertidal cohesive sediments. *Estuarine Coastal and Shelf Science* 46: 27-38

Widdows J, Brinsley MD, Salkeld PN, Lucas CH (2000) Influence of biota on spatial and temporal variation in sediment erodability and material flux on a tidal flat (Westerschelde, The Netherlands). *Marine Ecology-Progress Series* 194: 23-37.

Widdows J, Brinsley MD, Pope ND, Staff FJ, Bolam SG, Somerfield PJ (2006) Changes in biota and sediment erodability following the placement of fine dredged material on upper intertidal shores of estuaries. *Marine Ecology-Progress Series* 319: 27-41

Widdows J, Friend PL, Bale AJ, Brinsley MD, Pope ND, Thompson CEL (2007) Inter-comparison between five devices for determining erodability of intertidal sediments. *Continental Shelf Research* 27: 1174-1189.

Winterwerp JC, Van Kesteren WGM (2004) *Introduction to the physics of cohesive sediment in the marine environment*, Elsevier, Amsterdam, 466 pp.

Withers PJA, Jarvie HP (2008) Delivery and cycling of phosphorus in rivers: A review. *Science of the Total Environment* 400: 379-395.

Wood PJ, Armitage PD (1997) Biological effects of fine sediment in the lotic environment. *Environmental Management* 21: 203-217.

Wood PJ, Armitage PD (1999) Sediment deposition in a small lowland stream - Management implications. *Regulated Rivers-Research & Management* 15: 199-210.

Wotton RS (2005) The essential role of exopolymers (EPS) in aquatic systems. In: *Oceanography and Marine Biology: An Annual Review*, Vol. 42, p 57-94

Wynn T, Mostaghimi S (2006) The effects of vegetation and soil type on streambank erosion, southwestern Virginia, USA. *Journal of the American Water Resource Association* 42: 69-82.

Yallop ML, de Winder B, Paterson DM, Stal LJ (1994) Comparative structure, primary production and biogenic stabilization of cohesive and non-cohesive marine sediments inhabitated by microphytobenthos. *Estuarine Coastal and Shelf Science* 39: 565-582.

Yallop ML, Paterson DM, Wellsbury P (2000) Interrelationships between rates of microbial production, exopolymer production, microbial biomass, and sediment stability in biofilms of intertidal sediments. *Microbial Ecology* 39: 116-127.

Ziegler CK, Nisbet BS (1995) Long-term simulation of fine-grained sediment transport in large reservoir. *Journal of Hydraulic Engineering-ASCE* 121: 773-781.

Zuur AF, Ieno EN, Smith GM (2007) *Analysing ecological data*, Springer, London, 672 pp.

Zuur AF, Ieno EN, Wade AJ, Savaliev AA, Smith GM (2009) *Mixed effects models and extensions in ecology with R*, Springer, London, 574 pp.

Appendices

Appendix I - Methods

Fieldwork Equipment Checklist:

1) Personal
   - ☐ Rain Gear
   - ☐ Thermal Undies
   - ☐ Fleece
   - ☐ Rain Hat
   - ☐ Warm Gloves
   - ☐ Dry Clothes for Car
   - ☐ Water Bottles
   - ☐ Neoprene Gloves
   - ☐ Neoprene Top
   - ☐ **Camera** & Charger
   - ☐ **Laptop**

2) General Supplies
   - ☐ 30 m measuring tapes (3)
   - ☐ 1m metre stick (2)
   - ☐ Metal rods (2)
   - ☐ Nitrile Gloves – M, L, XL
   - ☐ Waders (size 8 and 11)
   - ☐ Ladder
   - ☐ Large Ziploc Bags (~100)
   - ☐ Small Ziploc Bags (~100)
   - ☐ Electrical tape
   - ☐ Coolers (3)
   - ☐ Blue Roll (2)
   - ☐ First Aid Kit

3) CSM/Coring
   - ☐ CSM – charged and memory cleared
   - ☐ Air Tank – Filled!
   - ☐ Distilled Water (1L)
   - ☐ Syringes (50ml)
   - ☐ Rinse container
   - ☐ Shear Vane
   - ☐ Scissors – Long
   - ☐ Perspex Cores
   - ☐ Milk Crate
   - ☐ 3cm core sections
   - ☐ Bungs #62 (12)
   - ☐ Plungers Bungs #57 (6)
   - ☐ Painter's Trowel
   - ☐ 1m Extension for shear vane
   - ☐ Tongs – long-necked

4) Meters
   - ☐ pH/Temp/Conductivity Meter
   - ☐ Conductivity (3)
   - ☐ Flow meter

5) Stationary
   - ☐ Field Notebook
   - ☐ Log sheets printed in "Rite in Rain" Paper
   - ☐ "Rite in the Rain" Paper
   - ☐ Permanent Markers
   - ☐ Pens/Pencils
   - ☐ Plastic Clipboard
   - ☐ Large plastic bag to cover clipboard in rain

Fieldwork Log Sheet: *(with sample data)*

Date: 23 – Sep - 10	Stream: Bere
Time: 8-11:00 am	Location: Snatford Bridge

Water Chemistry

	L	M	R
pH	8.2	8	8.2
Temp (°C)	18.6	18.4	18.7
Conductivity (mS)	654	647	645

Strength & Cores

	Transect	Distance	Substrate	M/C	Shear Vane				CSM	Notes
					S/L	Measurements				
1	0	0.5	Cress	M	L	0.6	0.3	0.3	0023	fine silt
2	2	1.5	Cress	M	L	0.8	0.2	0.6	0024	coarse silt
3	6	3.5	Ran.	C	L	1.8	2.3	2.3	0025	silt layer
4										
5										
6										
7										
8										
9										
10										
11										
12										
13										
14										
15										

Transect – Transect number, even transects only.
Distance – Distance from the right bank.
Substrate – Dominant vegetation or, if unvegetated, dominant sediment.
M/C – User-defined margin or channel
Shear Vane - Small or Large vane
- List 3 shear strength measurements
CSM – CSM run number

Particle Size Analysis for Sediment

Particle size can represented as effective or absolute size. Effective particles are the natural, unaltered, flocs and aggregates, and the analysis is conducted on fresh sediment, which has been stored in the fridge for less than 24hrs. Absolute particles are the mineralogical components of the sediment and the analysis is conducted on freeze-dried sediment, digested with H_2O_2 and dispersed with Calgon. Particle size analysis is limited to the sediment fraction that passes through a 1mm sieve, and is conducted optically using a Beckman Coulter LS 13 320 Laser Diffraction Particle Size Analyser.

Effective Particle Size

1. Mix the sediment samples gently to homogenise.
2. Place a subsample on a 1mm test sieve, placed directly over the particle sizer test chamber.
3. Rinse with tap water into the chamber.
4. Run the cycle – with pump speed sufficient to suspend the coarsest grains. Maximum speed is necessary for coarse sandy sediment.

Absolute Particle Size

Equipment:

100 ml glass beakers (40)	Spatula
50 ml Centrifuge Tubes (40)	Distilled Water Bottle
1 mm Test sieve	Fume hood

Chemicals:

- 30% Hydrogen Peroxide
  - to digest the sediment
- Octan-2-ol
  - a surfactant to prevent the sediment from foaming over during digestion
- Calgon
  - to disperse grains after digestion
  - 5g Sodium hexametaphosphate and 0.7 g of anhydrous sodium carbonate in 1l of distilled water.

Preparations:

- Clean and label glass beakers (1-40)
- Clean and label centrifuge tubes (1-40)

Method:

1) Add approximately 5 g of freeze-dried sediment to 100ml glass beakers.
2) Add 5ml of deionised (DI) water.
3) Set up a large hotplate in the H_2O_2 fume cupboard, and set beakers on top.
4) Add 5ml of H_2O_2 to each beaker. Swirl gently.
5) Monitor for several hours. If the reaction occurs too vigorously, add a drop of octan-2-ol to the beaker.
6) Once the reactions have calmed down, turn on the hotplate (90 ˚C).
7) Add more H_2O_2 when reactions begin to subside, 10ml at a time.
8) When frothing has subsided entirely and the solution is milky white, H_2O_2 digest is complete. Let the samples evaporate until *ca.* 20ml of solution remains.
9) Transfer the solution to a 50 ml centrifuge tube, and make up to 40 ml line with DI water.
10) Cap and place horizontally on the flat-bed shaker overnight.
11) Particle Size Analysis
    a. Mix sediment for 5 s on the vortex mixer.
    b. Switch the caps to the one with a hole drilled in it.
    c. Insert a disposable pipette with the tip trimmed.
    d. Vortex briefly and remove a pipetteful of sample.
    e. Add to the Lasersizer test chamber.
    f. Repeat if necessary to reach optimal obscuration (8-12%).
    g. Hit run.

Standard Operating Procedure (SOP)

Standard Operating Method (SOM):

PIDS	No
Run length	60 sec
Runs	1
Pump speed	100
Sonication b/f 1st run	No – effective particle size
	Yes – absolute particle size
	Time: 30 s
	Power – 5
Sonication during run	No
Compute sizes	Yes
Optical model	Sediment.rf780d
Save file	Yes
Export size data	No
Autorinse first	Yes
Measure offsets	Yes
Measure loading	Yes
Sampling loading	Standard obscuration
Sonicate during loading	No
Autodilution	No
Enter sample information	No
Start run	Yes
Auto rinse last run	Yes

Preferences:

Statistics Tab	Percentiles -
	μm < % - 10, 16, 25, 50, 75, 84, 90%
	% < μm - 2, 4, 63, 125, 250, 500 & 1000
	% > μm – 1000 μm
	Results to Print – all, except D(p,q)
	Statistical method – Arithmetic
Export Tab	Extension – xls
	Data Format – Tab delimited
	Export Folder – Custom Folder

Bulk Properties of Sediment

Bulk properties of the sediment refer to the solid:liquid proportions of the sediment, as well as the organic/mineral proportions of the solid fraction.

Equipment

Sieves (small diam.) - 2 mm, 1mm	Freeze-drier
Sieve brush	Balance (3 dp)
Crucible (40)	Furnace
Scoop – 25 ml plastic	

Method:

Bulk density

1. Preweigh sample cups. Label containers with the container mass, and the lid with the total (lid + container) mass
2. Collect cores, section top 3cm, and place in sample cups (see fieldwork protocol)
3. Weigh container to calculate fresh hydrated sediment mass (M_{HS})
4. Conduct effective particle size analysis (see PSA protocol).
5. Weigh container again to calculate wet mass used in PSA (M_S).
6. Immediately place sediment samples in a -20˚ C freezer until frozen.
7. Place samples in the freeze-drier. Note: samples must be frozen completely before being placed in the freeze-drier.
8. Check the freeze-drier periodically over several days to see if samples are still frozen, if they are still decreasing in mass, and if the freezer unit has excessive ice build-up. If samples are still frozen after 3 days, remove them to the freezer and thaw out the unit with warm water. Dry and reload samples.
9. After *ca.* 4 days, remove samples from the freeze-dryer and place in a dessicator until ready to re-weigh.
10. Weigh containers to calculate freeze-dried sediment mass (M_{DS}).
11. Dry sieve the sediment using a 2mm and 1mm diam, and weigh fractions using the 3 dp balance. Retain <1 mm fraction for laboratory analyses

Organic content

1. Pour freeze-dried sediment (<1 mm diam) into preweighed crucibles (M_C). Record the label on the crucible because marker pen will burn off in the furnace
2. Record mass of the crucible and sediment pre-ignition (M_{PS})

3. Load crucibles into the ashing furnace in the Sediment Prep Lab, using the rack system to accommodate all 40 samples, noting the location of each sample on the tray.
4. Start the furnace
    a. Temperature (C) = 550
    b. Routine (tnOp) = Opt.1
    c. Time (tnr) = 240 min
5. After 4 hrs of incineration, open the door and let the furnace cool to 100-300 C before removing the crucibles to the dessicator, with a heat tile to protect the acrylic shelf.
6. Weigh the crucibles and ignited sediment (M_{IS}).

Analysis:

Wet Bulk Density

$$BD_W = \frac{M_{HS}}{V_T}$$

Dry Bulk Density

$$BD_D = \frac{M_{DS} + \frac{M_{DS}}{M_{HS}} * M_S}{V_T}$$

Water content (Gravimetric)

$$WC = \frac{M_W}{M_{DS}}$$

Organic content

$$OC = \frac{M_{PS} - M_{IS}}{M_{PS} - M_{CS}}$$

Note: V_t is the volume of the sample, and for the 6.6 cm ID cores is 102.6 cm^3.

References:

Heiri O, Lotter AF, Lemcke G (2001) Loss on ignition as a method for estimating organic and carbonate content in sediments: reproducibility and comparability of results. Journal of Paleolimnology 25:101-110

Rowell DL (1994) Soil science: methods and applications. Wiley, Harlow, Essex.

Weak Acid Digest for Metal Extraction from Sediment

A weak acid is used to extract the "reactive," or "geochemically active'" pool of metals in freshwater sediment samples. Dilute HNO3 has been

Equipment

15 mL Centrifuge Tubes (40)	Balance (5dp)
Micropipettes (5mL)	Centrifuge
Spatulas	Fume hood
Syringe filters – 0.2 μm cellulose acetate	

Chemicals:

- 0.43 mol HNO_3
    - Add 27.56 ml of 69% HNO_3 to a 1L volumetric, then fill to line with Millipore ultra high purity water.
- ICP Standards (see below)

Preparations:

- Ensure at least 500ml of HNO_3.
- Acid Wash centrifuge tubes and syringes.
- Check quantity of standards – need a minimum of 10 ml of each.

Method:

1) Weigh 0.5 g of freeze-dried sediment into acid-washed centrifuge tubes. Include one blank and one reference material, if none is available use one sediment sample as a reference for all analyses.
2) Add 10 ml of weak nitric acid.
3) Vortex mix, and place on shaker for 2hrs
4) Centrifuge for 15 mins at 3000 rpm. If needed, you can let the tubes sit overnight.
5) Place a 0.2 μm cellulose acetate filter on the tip of a 10 ml syringe.
6) Filter the supernatant into a clean acid-washed ICP/centrifuge tube, using the first 1-2 ml to flush the filter.
7) Pipette out 0.5 ml of supernatant, and place in a clean acid-washed ICP/centrifuge tube. Add 4.5 ml of 0.43 M HNO_3.
8) Run on ICP.

ICP Standards:

A) Stock Solution (100 ppm multi-element, 1000 ppm Ca)
   - In a 100 ml volumetric flask, add:
     i. Multi-element standard (1000 ppm)– 10 ml
     ii. Ca (10,000 ppm) – 10 ml
   - Fill to line with 0.43 M nitric acid. This is the stock/Standard A solution.

B) Standard B (500 ppm Ca, 50 ppm others)
   - 25 ml of stock solution in 50ml vol. flask, fill with nitric acid

C) Standard C (250 ppm Ca, 25 ppm others)
   - 12.5 ml of stock solution in 50ml vol. flask, fill with nitric acid

D) Standard D (100 ppm Ca, 10 ppm others)
   - 5 ml of stock solution in 50ml vol. flask, fill with nitric acid

E) Standard E (50 ppm Ca, 5 ppm others)
   - 5 ml of stock solution in **100ml vol. flask**, fill with nitric acid

F) Standard F (25 ppm Ca, 2.5 ppm others)
   - 2.5 ml of stock solution in **100ml vol. flask**, fill with nitric acid

G) Standard G (10 ppm Ca, 1 ppm others)
   - 0.5 ml of stock solution in 50ml vol. flask, fill with nitric acid

H) Standard H (1 ppm Ca, 0.1 ppm others)
   - 5ml of **Standard G** in 50ml vol. flask, fill with nitric acid

I) Blank

J) Quality Control (QC)
   - Standard E, or
   - Standard F

K) Transfer to plastic containers, as metals bind less readily to plastics than glass. Store in fridge.

References:

Tipping, E. et al. 2003. The solid-solution partitioning of heavy metals (Cu, Zn, Cd,Pb) in upland soils of England and Wales. Enviromental Polution. 125: 213-225

Groenberg, J.E. et al. In Prep. Transfer functions for solid solution partitioning of cadmium, copper, nickel, lead and zinc.

Extraction and analysis of water-soluble proteins and carbohydrates

Extracellular polymeric substances (EPS) are composed of a variety of organic compounds, including carbohydrates, proteins and nucleic acids. Several techniques are available for the extraction and quantification of specific fractions of EPS. The simplest and most commonly-used are based on a water extraction. This fraction is often referred to as the colloidal fraction.

Carbohydrates: Phenol-sulphuric acid assay for the determination of neutral and acidic polysaccharides. Sulphuric acid hydrolyses the sample, and hexoses are converted to derivatives that react with the phenol to give a yellow colour. The extinction of the yellow solution is measured in a spectrophotometer, against a glucose calibration curve

Proteins: A spectrophotometric technique that measures colour development with $CuSO_4$ to determine protein and humic acid concentrations, and without to measure solely humic compounds and chromogenic amino acids.

Equipment

10mL Centrifuge Tubes
Mortar and Pestle
Micropipettes (500 µl, 1000 µl)
Erlenmeyer Flasks (250mL)
Spatulas/
Test Tube Rack
Freeze-drier
Balance (5dp)
Centrifuge
Fume hood
Spectrophotometer

Chemicals

- 5% (w/v) phenol
- Sulphuric Acid (concentrated ~95.5%)
- Standards – Glucose and Albumin (separately)
    - Stock (1mg/ml) – 1 g in 1 L volumetric, fill with distilled water (DW).
    - Place the following amount in a 50ml volumetric, and fill with DW.
        - Standard 1 (500 µg ml^{-1}) – 25 ml
        - Standard 2 (200 µg ml^{-1}) – 10 ml
        - Standard 3 (100 µg ml^{-1}) – 5 ml
        - Standard 4 (50 µg ml^{-1}) – 2.5 ml

- Standard 5 (20 μg ml^{-1}) – 1 ml
- Standard 6 (10 μg ml^{-1}) – 0.5 ml

- Freeze in 5ml portions in centrifuge tubes.
- Thaw in fridge 1 day in advance.

Extraction

1. Place 0.100 g of sediment into 15ml acid-washed centrifuge tubes.
2. Add 5 ml of distilled water.
3. Place horizontally on the flat bed shaker for 15min at room temp.
4. While samples are incubating, prepare 1x acid-washed centrifuge tubes, and 3x disposable, semi-micro cuvettes.
5. Centrifuge the samples 3500g for 15 min.

Carbohydrates

1. In fume cupboard, pipette 200 μl of supernatant (and standards) to a clean tube.
2. Add 1 ml concentrated sulphuric acid and 200 μl 5% (w/v) phenol. Add to **standards AND samples**.
3. Incubate for 15 min, and read absorbance at 485 nm.
4. Calibration curve run with glucose standards, so results expressed as glucose equivalents.

Underwood GJC, Paterson DM, Parkes RJ (1995) The measurement of microbial carbohydrate exopolymers from intertidal sediments. Limnology and Oceanography 40:1243-1253

Chlorophyll-a Extraction from Sediment using Acetone

Chlorophyll-a is commonly used to quantify the autotrophic microbial community biomass. The chlorophyll is extacted with acetone and quantify calorimetrically.

Equipment

Freeze-drier
Balance (4dp)
10mL Centrifuge Tubes PP (40)
Spatulas
250ml Conical Flask
Aluminium Foil
Micropipettes (100 µL and 5mL)
Syringe filters – 0.2 µm PP diam?
10ml syringes (40)
Fume hood
Centrifuge
Glass/quartz cuvettes (min. 7)
Spectrophotometer

Chemicals

- Acetone, HPLC Grade
  - Make a 90% solution with distilled water
- Hydrochloric Acid (HCL) - 0.1 N HCL Solution
  - - 0.980 mL HCL (32%) in 100ml volumetric flask

Method:

1. Freeze-dry sediment and store in the dark.
2. Transfer 0.100 g of sediment to a 10ml centrifuge tube. Use the 5dp balance in the sediment room.
3. In the solvents fume cupboard, add 4.5 mL 90% acetone to each tube.
4. Seal and place horizontally on a flatbed shaker for 1 hr at 120 rpm, room temperature.
5. Place in fridge overnight (4˚ C).
6. Centrifuge samples at 3000 rpm for 10 min.
7. In a fume cupboard, decant the supernatant into quartz cuvettes.
8. Supernatant read spectrophometrically. Insert cuvette of distilled water into blank position. Position 1 is reference (90% acetone). Positions 2-7 for samples. EPA Method 446 – read at 750 first to measure turbidity, then 664, 647 and 630 for Chl *A*, Chl *B*, and Chl C_1+C_2, respectively.

9. For pheopigment. Add 0.09ml 0.1 N HCl. Pippete just below surface to minimize air bubbles and wait 90 seconds. Measure absorbance at 750 and 665 nm.
10. Use Lorenzen's Pheopigment-corrected formulae.

****Always keep tubes in the dark! Wrap tubes in foil!!****

Lorenzen's Pheopigment-corrected Chl *a* and Pheo *a*

Subtract the absorbance values at 750 nm from the absorbance values at 664 and 665 nm. Calculate the concentrations (mg/L) in the extract solution, C_E, by inserting the 750 nm *corrected* absorbance values into the following equations:

$C_{E,a} = 26.7(A_{664} - A_{665})$

$P_{E,a} = 26.7\ [1.7(A_{665}) - (A_{664})]$

where,

$C_{E,a}$ = concentration (mg/L) of chlorophyll *a* in the extract solution measured,

$P_{E,a}$ = concentration (mg/L) of pheophytin *a* in the E,a extraction measured.

A_{664} = sample absorbance at 664 nm (minus absorbance at 750 nm) measured before acidification, and

A_{665} = sample absorbance at 665 nm (minus absorbance at 750 nm) measured after acidification.

References:

de Brouwer JFC, Stal LJ (2001) Short-term dynamics in microphytobenthos distribution and associated extracellular carbohydrates in surface sediments of an intertidal mudflat. Marine Ecology-Progress Series 218:33-44

de Brouwer JFC, Wolfstein K, Ruddy GK, Jones TER, Stal LJ (2005) Biogenic stabilization of intertidal sediments: The importance of extracellular polymeric substances produced by benthic diatoms. Microbial Ecology 49:501-512

USEPA (1997) In vitro determination of chlorophylls a, b, c_1, c_2 and pheopigments in marine and freshwater algae by visible spectrophotometry. National Exposure Research Laboratory, Office of Research and Development, US EPA, Cincinnati, Ohio

Appendix II – Stream cross-sections

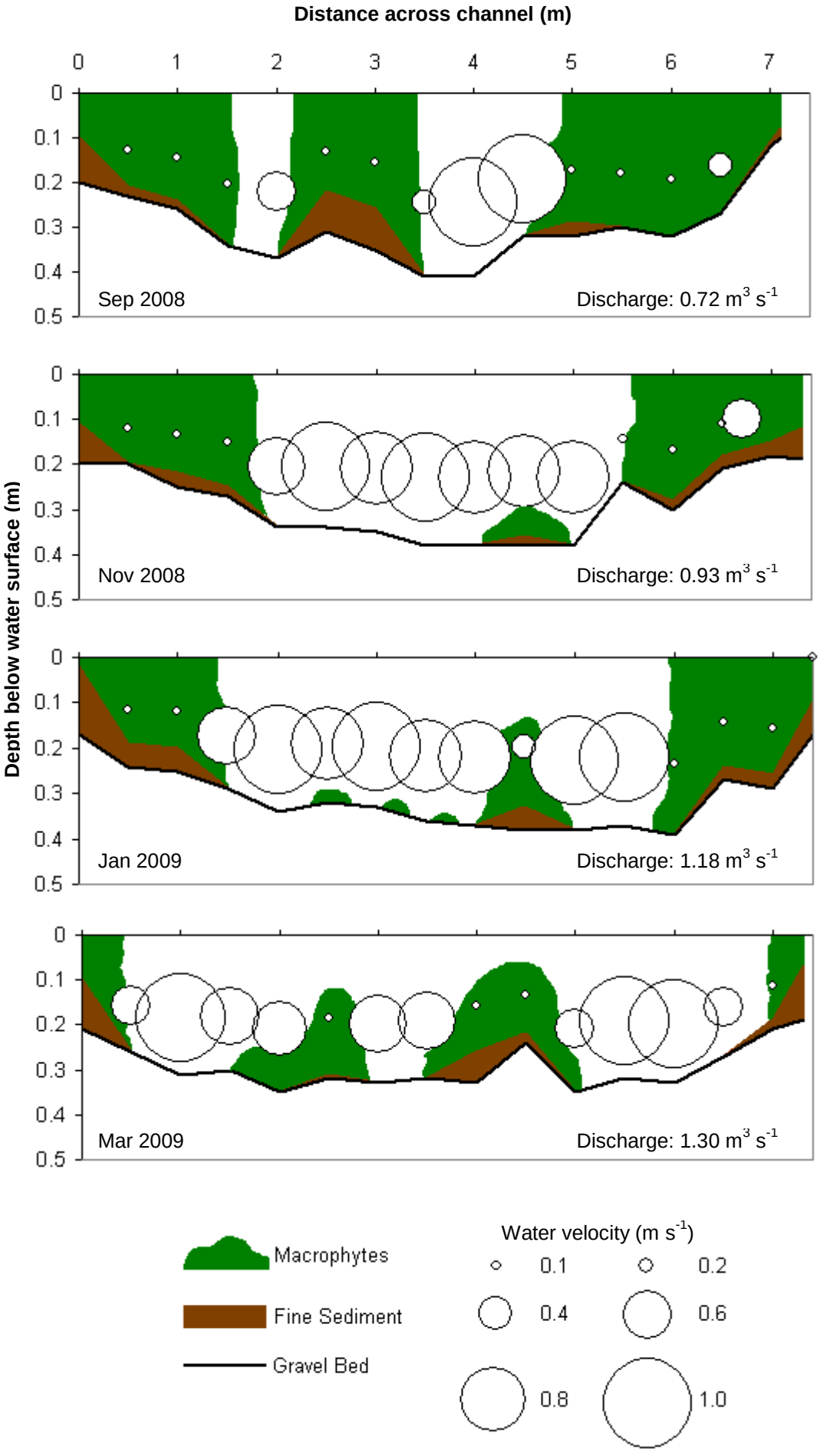
Distance across channel (m)
0
1
2
3
4
5
6
7
Depth below water surface (m)
0
0.1
0.2
0.3
0.4
0.5
Sep 2008
Discharge: 0.72 m3 s-1
Nov 2008
Discharge: 0.93 m3 s-1
Jan 2009
Discharge: 1.18 m3 s-1
Mar 2009
Discharge: 1.30 m3 s-1
Macrophytes
Fine Sediment
Gravel Bed
Water velocity (m s-1)
0.1
0.2
0.4
0.6
0.8
1.0

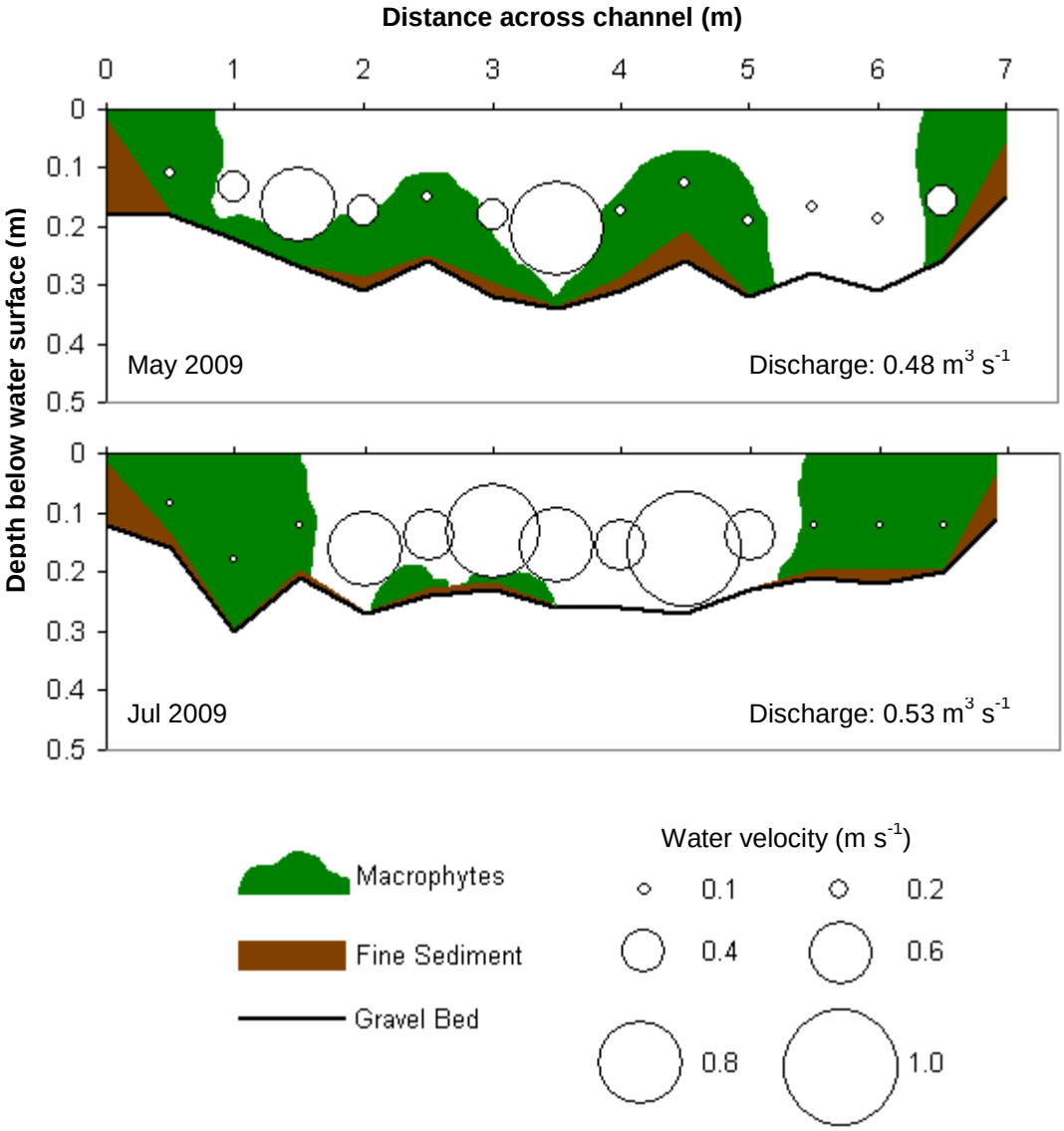

Figure AII.1. Cross-section of the Bere Stream (Transect #10), showing water depth, fine sediment accumulation, the presence of macrophytes, water velocity at 60% depth, and discharge.

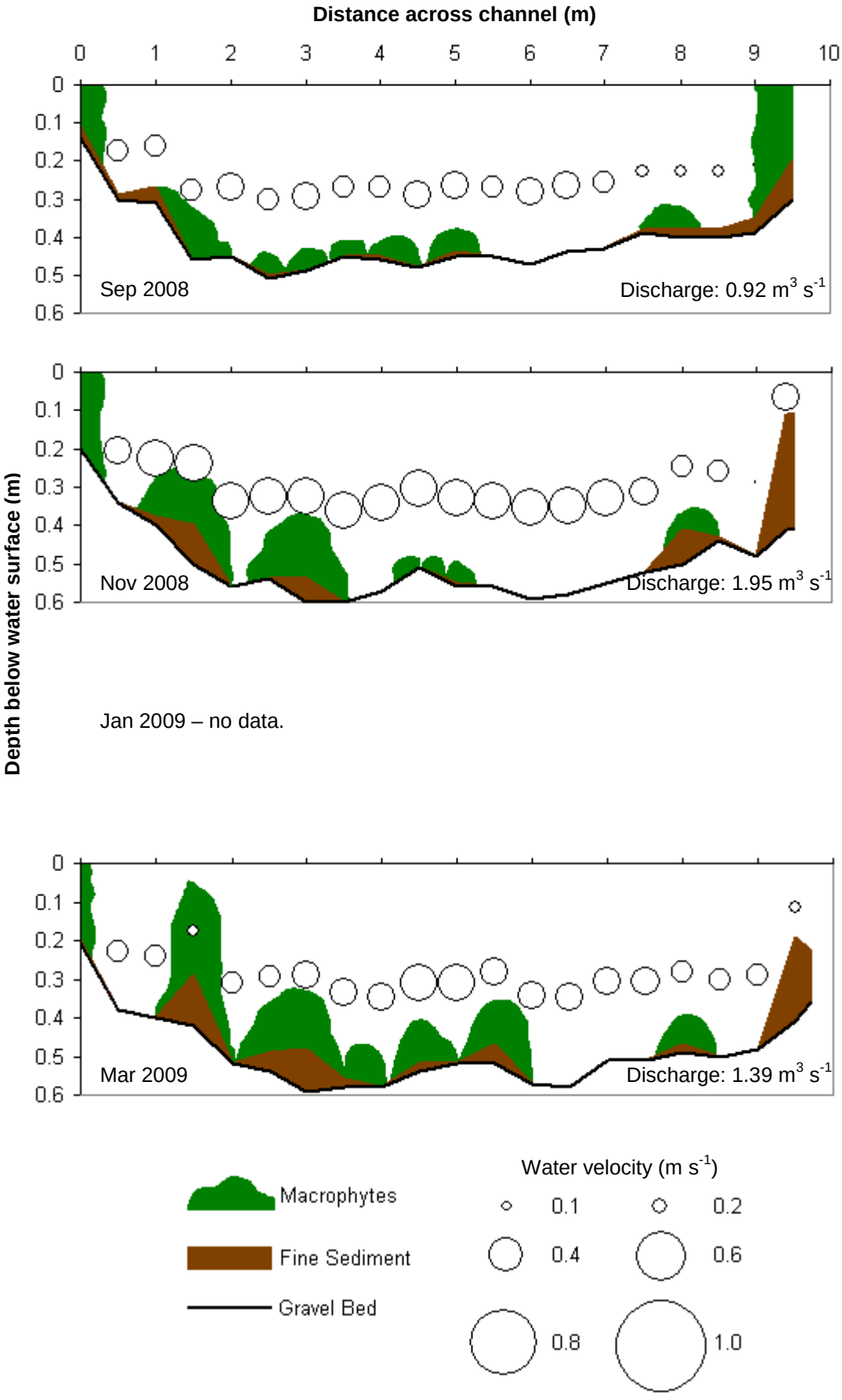
Distance across channel (m)
0 1 2 3 4 5 6 7 8 9 10
Depth below water surface (m)
0 0.1 0.2 0.3 0.4 0.5 0.6
Sep 2008
Discharge: 0.92 m3 s-1
Nov 2008
Discharge: 1.95 m3 s-1
Jan 2009 – no data.
Mar 2009
Discharge: 1.39 m3 s-1
Macrophytes
Fine Sediment
Gravel Bed
Water velocity (m s-1)
0.1
0.2
0.4
0.6
0.8
1.0

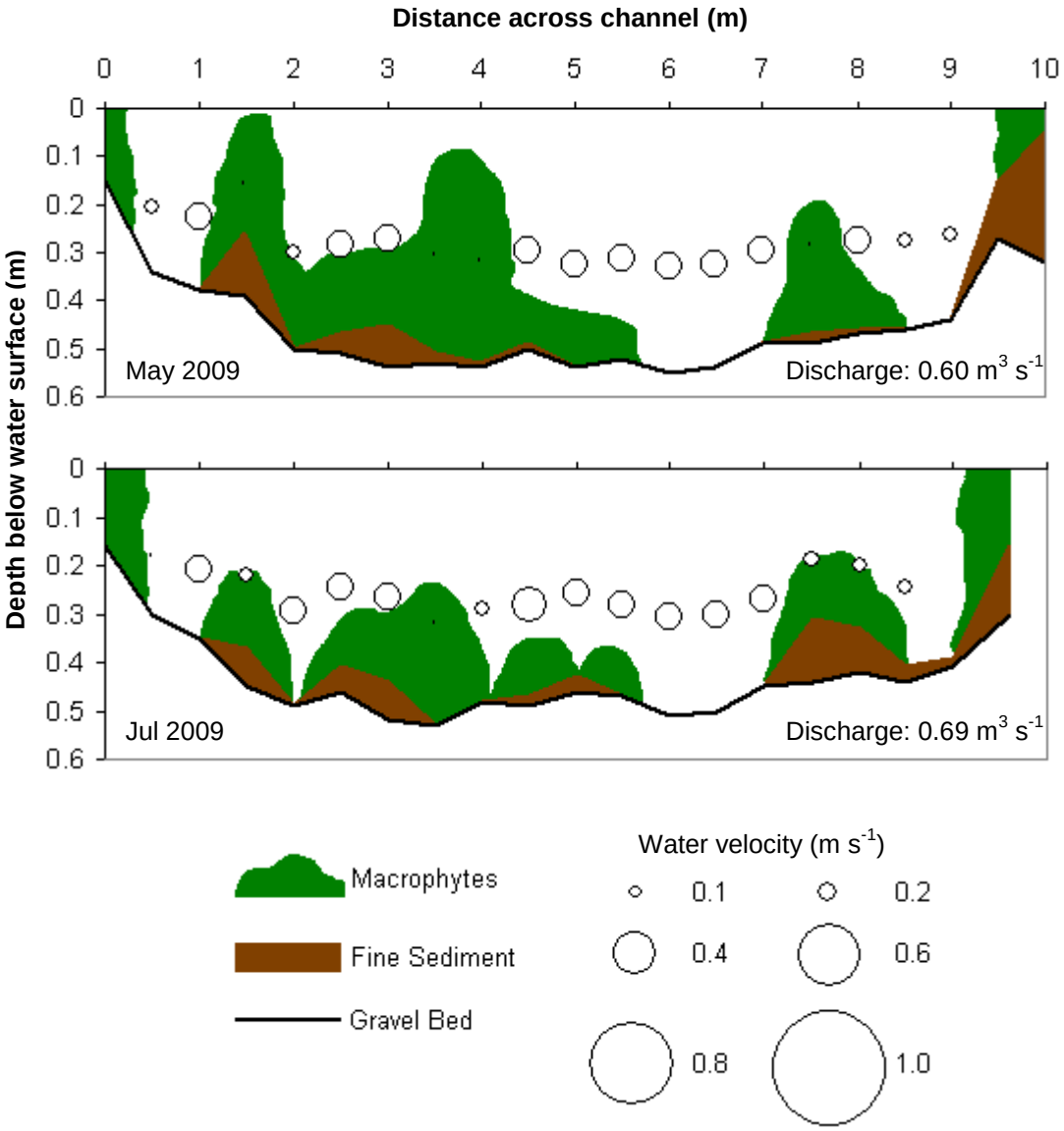

Figure AII.2. Cross-section of the River Frome (Transect #26), showing water depth, fine sediment accumulation, the presence of macrophytes, water velocity at 60% depth, and discharge.

Appendix III - Generalised linear (GLM) and additive modelling (GAM)

Advanced linear regression techniques are not bound to the assumptions of normality, homogeneity or even linear responses. Generalised linear modelling (GLM) is an extension of linear regression that allows the user to specify a non-normal error structure and account for a non-constant variance. Generalised additive modelling (GAM) replaces linear responses with curves generated by smoothing functions. As a result, GLMs and GAMs are often better suited to modelling ecological data than traditional linear regression analysis (Zuur et al. 2009).

GLM

Generalised linear modelling is essentially a linear regression with a few added features. GLM has three components: 1) a distribution of the response variable, 2) a linear predictor composed of the explanatory variables, and 3) a function that links the linear predictor to the response variable (Crawley 2007, Zuur et al. 2009). The nature of the dataset will dictate the form taken by each of the components. First, several distributions are available for the response variable, and many are ideally suited for specific types of data, such as Poisson for count data and binomial for proportions. Erosion threshold is a continuous variable with a non-normal distribution truncated at zero. The most suitable distribution for this dataset is a gamma distribution, which is used for a continuous response variable that is non-negative. Gamma distributions are particularly useful when the variance of the response variable increases with its mean (i.e. constant coefficient of variation) (Crawley 2007). Second, the linear predictor is a formula containing the explanatory variables, which may be transformed if necessary, and is similar to a linear regression formula. Finally, the link function sets the type of transformation that will be applied to the results of the linear predictor to predict erosion threshold. There are several link functions to choose from, including log, logit, square root, and the correct link should minimise the residual deviance of the model, which is an estimator of goodness of fit.

The optimal model was selected using a similar procedure as in linear regression, with hypothesis testing and information criteria. The gamma distribution was used and a log link function minimised residual deviance. The optimal model contained only two

explanatory variables, effective median particle size and month (Table 5.8). The model accounted for 25% of the variation in the dataset, according to null and residual deviance (Table AII.1). Overdispersion can be a problem with GLM, however dispersion is well below 1, indicating that residual variance is less than the mean erosion threshold (Table AII.1). Model validation plots show residuals are predominately homogeneous, but deviate from normal at the lower end of the distribution (Fig. AII.1).

Whilst the GLM does an adequate job of modelling the dataset, there does not appear to be an incentive to use it instead of the one generated by LR. The optimal LR model explains more of the variation in the dataset (35%), and conforms to the three major assumptions of normality, homogeneity, and independence. Furthermore, LR is more widely used in the field and the results more easily applied, which make it more directly useful to other researchers.

Table AIII.1. Summary statistics for the optimal model generated by GLM, gamma distribution with a log link. eff_median = median effective particle size, month = ordinal variable (1-6, bimonthly)

	Estimate	Std. Error	t value	Pr(>|t|)
(Intercept)	4.68	0.15	32.03	< 2e-16
eff_median	0.0032	0.00075	4.26	3.61e-05
Month	-0.16	0.024	-6.63	5.53e-10

Dispersion: 0.30, AIC: 1656.8

Null deviance: 76.59 on 154 degrees of freedom

Residual deviance: 57.08 on 152 degrees of freedom

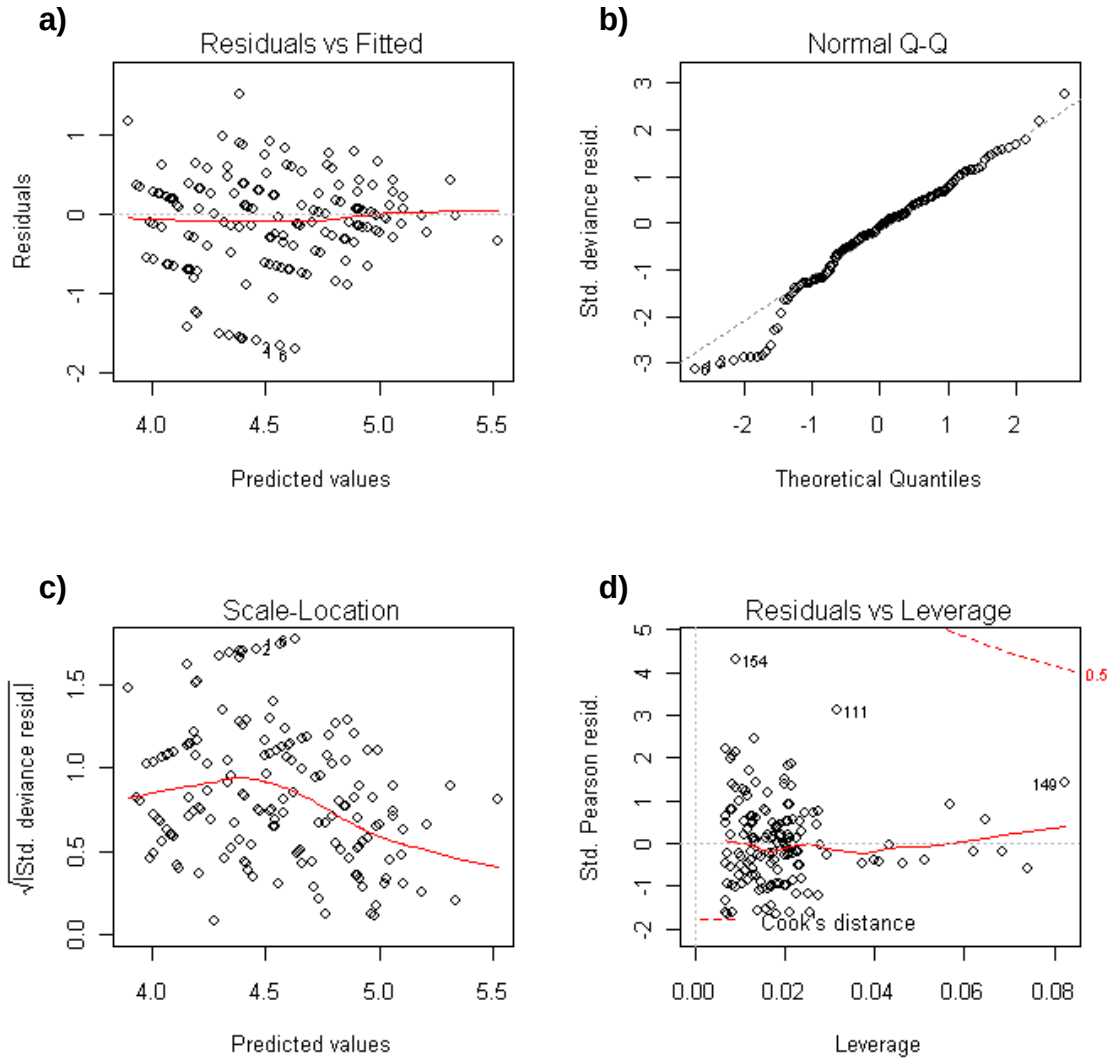

Figure AIII.1. Validation plots for the optimal GLM for the dataset without 0.15 PSI values, using a gamma distribution with a log link, (a) model residuals plotted against fitted values, (b) Q-Q plot of standardised residuals, (c) standardised residuals plotted against fitted values, and (d) standardised residuals plotted against Cook's leverage, a measure of the disproportionate impact of a data point on the model regression.

GAM

Generalised additive models are a useful tool for modelling environmental datasets which show nonlinear response curves. In the approach, a smoothing function is used to describe the relationship between the explanatory and response variables. The smoothing function is typically a cubic regression spline, in which cubic polynomials are fitted to subsections of the response curve and their ends joined together to form the smoothing function (Zuur et al. 2009). As a result, GAMs use up more degrees of freedom than a linear regression or GLM.

Effective particle size has a clear positive linear correlation with erosion threshold (Fig. 5.2). Chlorophyll-a and month, though, potentially have non-linear relationships with erosion threshold (Figs. 5.3 & 4.37). An optimal GAM was created using $P_{stag}^{0.5}$ as the response variable, and systematically replacing linear parameters with smoothing functions. The smoothing functions did not significantly increase the model fit (ANOVA, $p > 0.05$), which suggests that linear regression or GLM was sufficient for the erosion threshold dataset.